Vol. 56 APRIL, 1952 No. 4

THE JOURNAL OF PHYSICAL CHEMISTRY

(Registered in U. S. Patent Office)

Founded by Wilder D. Bancroft

CONTENTS

Founded by Wilder D. Bancroft

THE JOURNAL OF PHYSICAL CHEMISTRY

(Registered in U. S. Patent Office)

Published monthly (except July, August and September) by the American Chemical Society at 20th and Northampton Sts., Easton, Pa.

Entered as second-class matter at the Post Office at Easton, Pennsylvania.

The *Journal of Physical Chemistry* is devoted to the publication of selected symposia in the broad field of physical chemistry and to other contributed papers.

Manuscripts originating in the British Isles, Europe and Africa should be sent to F. C. Tompkins, The Faraday Society, 6 Gray's Inn Square, London W. C. 1, England.

Manuscripts originating elsewhere should be sent to W. Albert Noyes, Jr., Department of Chemistry, University of Rochester, Rochester 3, N. Y.

Correspondence regarding accepted copy, proofs and reprints should be directed to Assistant Editor, Allen D. Bliss, Department of Chemistry, Simmons College, 300 The Fenway, Boston 15, Mass.

Business Office: American Chemical Society, 1155 Sixteenth St., N. W., Washington 6, D. C.

Advertising Office: American Chemical Society, 332 West 42nd St., New York 18, N. Y.

Articles must be submitted in duplicate, typed and double spaced. They should have at the beginning a brief Abstract, in no case exceeding 300 words. Original drawings should accompany the manuscript. Lettering at the sides of graphs (black on white or blue) may be pencilled in, and will be typeset. Figures and tables should be held to a minimum consistent with adequate presentation of information. Photographs will not be printed on glossy paper except by special arrangement. All footnotes and references to the literature should be numbered consecutively and placed on the manuscript at the proper places. Initials of authors referred to in citations should be given. Nomenclature should conform to that used in *Chemical Abstracts*, mathematical characters marked for italic, Greek letters carefully made or annotated, and subscripts and superscripts clearly shown. Articles should be written as briefly as possible consistent with clarity and should avoid historical background unnecessary for specialists.

Symposium papers should be sent in all cases to Secretaries of Divisions sponsoring the symposium, who will be responsible for their transmittal to the Editor. The Secretary of the Division by agreement with the Editor will specify a time after which symposium papers cannot be accepted. The Editor reserves the right to refuse to publish symposium articles, for valid scientific reasons. Each symposium paper may not exceed four printed pages (about sixteen double spaced typewritten pages) in length except by prior arrangement with the Editor.

Remittances and orders for subscriptions and for single copies, notices of changes of address and new professional connections, and claims for missing numbers should be sent to the American Chemical Society, 1155 Sixteenth St., N. W., Washington 6, D. C. Changes of address for the *Journal of Physical Chemistry* must be received on or before the 30th of the preceding month.

Claims for missing numbers will not be allowed (1) if received more than sixty days from date of issue (because of delivery hazards, no claims can be honored from subscribers in Central Europe, Asia, or Pacific Islands other than Hawaii), (2) if loss was due to failure of notice of change of address to be received before the date specified in the preceding paragraph, or (3) if the reason for the claim is "missing from files."

Annual Subscription: $8.00 to members of the American Chemical Society, $10.00 to non-members. Postage free to countries in the Pan American Union; Canada, $0.40; all other countries, $1.20. Single copies, $1.25; foreign postage, $0.15; Canadian postage, $0.05.

The American Chemical Society and the Editors of the *Journal of Physical Chemistry* assume no responsibility for the statements and opinions advanced by contributors to THIS JOURNAL.

The American Chemical Society also publishes *Journal of the American Chemical Society, Chemical Abstracts, Industrial and Engineering Chemistry, Chemical and Engineering News* and *Analytical Chemistry*. Rates on request.

* * * (*Continued from first page of cover*) * * *

THE JOURNAL OF PHYSICAL CHEMISTRY

(Registered in U. S. Patent Office) (Copyright, 1952, by the American Chemical Society)

Founded by Wilder D. Bancroft

VOLUME 56 APRIL 15, 1952 NUMBER 4

CONSTITUTION AND STABILITY OF COMPLEX IONS FROM SOLUBILITY MINIMA

BY C. A. REYNOLDS AND WILLIAM J. ARGERSINGER, JR.

Department of Chemistry, University of Kansas, Lawrence, Kansas

Received March 2, 1951

A simple new method of determining both the constitution and stability of certain complex ions from measurements of solubility minima is presented. Applications of the method are discussed and calculations of stability using literature data are given.

The use of solubility data in the determination of the formula and dissociation constant of complex ions has been described in several reports in the literature.[1-12] In this paper an alternative direct method of treating such data, based on the position of the minimum in the solubility curves, will be developed and applied to data from the literature. Minima in the solubility curves of slightly soluble salts, curves in which the solubility of the salt is plotted as a function of the stoichiometric concentration of the added anion common to the salt, were first reported in 1911 by W. D. Harkins[9] and Maurice Barre.[13] The general shape of such solubility curves is similar to that shown in Fig. 1.[10] The initial decrease in the solubility of the salt is caused by the common-ion effect, but the minimum and subsequent increase can be the result of two independent causes. A decrease in the mean activity coefficient at high total concentrations will increase the solubility of the salt, but if the minimum occurs at a concentration of the anion such that activity effects are negligible, the only phenomenon which will cause an increase in the solubility of the salt is complex-ion formation.

A great number of examples of solubility minima have been reported since 1911,[1-8,10-12,14-24] but in none of these reports was any special significance attached to the actual position of the minimum in the solubility curve. The position of the minimum determines two experimental data, the solubility of the salt at the minimum and the stoichiometric concentration of the added anion at this point. From these two data and the solubility product of the salt, it is possible to calculate for the complex ion the number of complexing anions per central atom, and the dissociation constant.

Garrett and his co-workers made a number of very reliable solubility studies[4-8] in an attempt to

(1) W. Erber and A. Schuhly, *J. prakt. Chem.*, **158**, 176 (1941).
(2) G. S. Forbes, *J. Am. Chem. Soc.*, **33**, 1937 (1911).
(3) A. B. Garrett, *ibid.*, **61**, 2744 (1939).
(4) A. B. Garrett and R. E. Heiks, *ibid.*, **63**, 562 (1941).
(5) A. B. Garrett and A. E. Hirschler, *ibid.*, **60**, 299 (1938).
(6) A. B. Garrett, O. Homes and A. Laube, *ibid.*, **62**, 2024 (1940).
(7) A. B. Garrett, M. V. Noble and S. Miller, *J. Chem. Ed.*, **19**, 485 (1942).
(8) A. B. Garrett, S. Vellenga and C. M. Fontana, *J. Am. Chem. Soc.*, **61**, 367 (1939).
(9) W. D. Harkins, *ibid.*, **33**, 1807 (1911).
(10) H. L. Johnston, F. Cuta and A. B. Garrett, *ibid.*, **55**, 2311 (1933).
(11) J. Kendall and C. H. Sloan, *ibid.*, **47**, 2306 (1925).
(12) H. Topelmann, *J. prakt. Chem.*, **121**, 320 (1929).
(13) Maurice Barre, *Anal. Chem. Phys.*, **24**, 145 (1911).
(14) J. B. Chloupek and Vl. Z. Danes, *Collection Czechoslov. Chem. Commun.*, **4**, 8 (1932).
(15) H. D. Crockford and D. J. Brawley, *J. Am. Chem. Soc.*, **56**, 2600 (1934).
(16) D. N. Craig, G. W. Vinal and F. E. Vinal, *J. Research, U. S. Bureau of Stand.*, **17**, 709 (1936).
(17) A. E. Hill and J. H. Wills, *J. Am. Chem. Soc.*, **60**, 1647 (1938).
(18) M. Huybrechts and Andrault de Langeron, *Bull. soc. chim Belg.*, **39**, 43 (1930).
(19) M. Huybrechts and H. Romelot, *ibid.*, **35**, 239 (1926).
(20) J. Piater, *Z. anorg. allgem. Chem.*, **174**, 321 (1928).
(21) A. Pinkus and N. Berkolaiko, *J. Chim. Phys.*, **27**, 364 (1930).
(22) A. Pinkus and A. M. Timmermans, *Bull. soc. chim. Belg.*, **46**, 46 (1937).
(23) A. Pinkus and M. Haugen, *ibid.*, **45**, 693 (1936).
(24) Seidell, "Solubility of Inorganic and Metallic Compounds," Vol I, 3rd Ed., D. Van Nostrand, New York, N. Y., 1940.

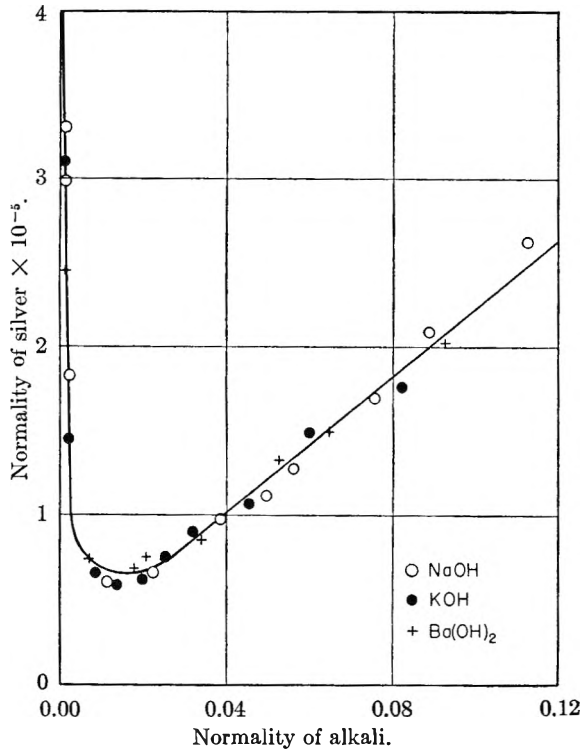

Fig. 1.—The solubility of silver oxide in solutions of alkali.[10]

ascertain the stabilities of the complex ions present in the systems investigated. Their method of attack, in at least one investigation,[10] was to measure the slope of the ascending branch of the solubility curve and from this to calculate the dissociation constant of the postulated complex ion. In other reports, *e.g.*,[7] the formula and dissociation constant of the complex ion were determined from a linear plot of the logarithm of the solubility *versus* the logarithm of the concentration of added salt, the usually justifiable assumptions being made that all dissolved salt is present as complex ion, and the actual concentration of anion is equal to the concentration of added salt.

The alternative method of calculation herewith presented requires no assumption as to the formula of the complex ion or the nature of the related equilibrium, nor need any approximation be made for the various equilibrium concentrations. The only assumptions necessary are that activity effects are negligible in the concentration range in which the solubility minimum occurs, that the dissolved salt is completely dissociated and that one particular complex ion predominates in causing the minimum. The particular complex ion thus identified is normally that with the smallest number of coördinated anions. The experimental data required for the application of this method consist of an accurate determination of the position of the minimum in the solubility curve, an equally accurate determination of the solubility in pure water from which the solubility product is determined, and analysis of the composition of the solid phase in equilibrium with the solutions. A method of correcting for incomplete ionization of the saturating salt is also suggested.

Derivation of Relationships.—The salt A_mB_n dissolves in a solution of B ion to form the complex ion AB_q; let us assume that the dissolved A_mB_n is completely dissociated, and that all activity coefficients are unity. Let S be the solubility of A_mB_n in moles per liter in a solution of B ion containing C moles per liter. For the sake of simplicity and clarity, all charge notation on ions will be omitted.

In the system at equilibrium the fact that both species, A and B, must be conserved leads to the equations

$$(A) + (AB_q) = mS \tag{1}$$

and

$$(B) + q(AB_q) = nS + C \tag{2}$$

Furthermore since the solution is in equilibrium with excess A_mB_n, we have the expression for the solubility product K_s

$$(A)^m(B)^n = K_S \tag{3}$$

Finally, the dissociation constant expression for the complex ion is given by

$$(A)(B)^q/(AB_q) = K_D \tag{4}$$

In Equations 1–4 parentheses are used to indicate molar concentration. For the sake of simplicity, let

$$(B) = x$$
$$(A) = y$$
$$(AB_q) = z$$

With these substitutions, Equations (3) and (4) may be solved for y and z as functions of x; when the results are substituted in Equations (1) and (2) we obtain

$$S = \frac{1}{m}\left(K_S^{1/m}x^{-n/m} + \frac{K_S^{1/m}}{K_D}x^{q-n/m}\right) \tag{5}$$

$$C = x - \frac{n}{m}K_S^{1/m}x^{-n/m} + \left(q - \frac{n}{m}\right)\frac{K_S}{K_D}x^{q-n/m} \tag{6}$$

Equations (5) and (6) may be regarded as the parametric equations of the usual solubility curves in which S is plotted as a function of C. In most cases it is impossible to eliminate the parameter x from these equations, but for our purpose such elimination is not necessary. We need only recognize that at the minimum in such a solubility curve $dS/dC = 0$.

Differentiating Equations (5) and (6) with respect to C, and setting $dS/dC = 0$, we obtain

$$\left[-\frac{n}{m}K_S^{\frac{1}{m}}x_m^{-\frac{n}{m}-1} + \left(q - \frac{n}{m}\right)\frac{K_S^{1/m}}{K_D}x_m^{q-\frac{n}{m}-1}\right]\left(\frac{dx}{dC}\right)_{C=C_m} = 0 \tag{7}$$

and

$$\left[1 + \left(\frac{n}{m}\right)^2 K_S^{\frac{1}{m}}x_m^{-\frac{n}{m}-1} + \left(q - \frac{n}{m}\right)^2\frac{K_S^{1/m}}{K_D}x_m^{q-\frac{n}{m}-1}\right]\left(\frac{dx}{dC}\right)_{C=C_m} = 1 \tag{8}$$

where x_m and C_m are the values of x and C at the minimum.

Since the quantity in brackets in Equation (8) is certainly not infinite, then $(dx/dc)_{C=C_m}$ is not equal to zero, and, therefore, the quantity in brackets in Equation (7) must vanish. Hence, we have

$$\frac{K_S^{1/m}}{K_D}x_m^{q-n/m} = \frac{nK_S^{1/m}x_m^{-n/m}}{m\left(q - \frac{n}{m}\right)} \tag{9}$$

Substituting this result back into Equations (5) and (6) we find

$$S_m = \frac{1}{m}\left(1 + \frac{n}{mq - n}\right) K_S^{1/m} x_m^{-n/m} \qquad (10)$$

and

$$C_m = x_m \qquad (11)$$

With this relationship Equation (10) may now be solved for q, the number of anions coördinated to the cation

$$q = \frac{nS_m C_m^{n/m}}{mS_m C_m^{n/m} - K_S^{1/m}} \qquad (12)$$

The same substitution for x_m in Equation (9) leads to the result

$$K_D = \left(\frac{m}{n} q - 1\right) C_m^q \qquad (13)$$

For a simple 1–1 salt Equations (12) and (13) reduce, of course, to

$$q = \frac{S_m C_m}{S_m C_m - K_S} \qquad (14)$$

and

$$K_D = (q - 1) C_m^q \qquad (15)$$

The results of many accurate solubility determinations are reported in the literature. Unfortunately, however, most of these fail to satisfy one or another of the previously discussed requirements for data to which this method is applicable; in many cases the composition of the solid phase was not indicated, and in many others the solubility in pure water was not reported. Work is now in progress in this Laboratory on several systems for which the requisite data will be obtained.

The data of Johnston, Cuta and Garrett[10] on the solubility of AgOH in OH^- solutions show the position of the solubility minimum very accurately, as is seen in Fig. 1. The solubility minimum occurs at 0.015 M alkali, and the solubility at that concentration is 6.0×10^{-6} M; the solubility in pure water is 2.22×10^{-4} M. With these data the value of q calculated from equation (14) is 2.20, indicating the complex ion $Ag(OH)_2^-$. The value of the dissociation constant for the equilibrium

$$Ag(OH)_2^- \rightleftharpoons Ag^+ + 2OH^-$$

is found from Equation (15) to be 2.3×10^{-4}. Johnston, Cuta and Garrett reported 3.80×10^{-8} as the value of the constant for the equilibrium

$$Ag_2O + 2OH^- \rightleftharpoons 2AgO^- + H_2O$$

It may be shown that the two equilibrium constants are related by the expression

$$K_D = \frac{K_S}{\sqrt{K_G}}$$

in which K_G is the constant reported by Johnston, Cuta and Garrett. If K_D is calculated from the reported value of K_G, the result 2.5×10^{-4} is obtained.

Similar calculations have been made with the data of Chloupek and Danes[14] on the solubility of Ag_2SO_4 in Na_2SO_4 solution. The calculated value of q is 1.05, indicating the complex ion $AgSO_4^-$, and the dissociation constant is 1.2×10^{-1}.

The extensive data of Garrett, Vellenga and Fontana[8] on the solubility of the several lead oxides in solutions of alkali indicate a minimum solubility, but it is not possible to fix the position of the minimum with sufficient accuracy to apply the present method of calculation.

It is well known that certain systems may form more than one complex ion, such as $PbCl_2$ in solutions of Cl^- ion, for example, where the complex ions $PbCl_3^-$ and $PbCl_4^=$ have been found and studied. If no one of the several complex ions predominates strongly in the region of the minimum, the present method is incapable of determining both the constitution and dissociation constant of the complex ions; this limitation follows naturally from the fact that the experimental data consist essentially of only two numbers, the solubility of the salt and the concentration of added ion, both at the minimum point in the solubility curve. The fact that the curve is known experimentally to exhibit a minimum, not a maximum, constitutes a third (but only qualitative) factor which has been found of very little use in the analysis. If one of the complex ions does predominate strongly, however, the present method gives the properties of this one ion.

In some cases where two complex ions exist, the formula and dissociation constant of one may be known from independent sources. It is then possible to determine the formula and dissociation constant of the other complex ion by a simple extension of the solubility minimum method. By the use of essentially the same method as before it is easily shown that at the position of the solubility minimum, the actual concentration of the complexing ion is equal to the stoichiometric concentration of the anion solution which has been saturated with the salt. In the notation previously defined, with the addition of K_r and r as the dissociation constant and number of complexing anions, respectively, for one of the complex ions, presumed known from independent sources, the treatment leads to the following results for the other complex ion

$$q = \frac{nS_m C_m^{n/m} - r\, C_m^r \dfrac{K_S^{1/m}}{K_r}}{mS_m C_m^{n/m} - K_S^{1/m} - C_m^r \dfrac{K_S^{1/m}}{K_r}} \qquad (16)$$

$$K_q = \frac{\left(\dfrac{m}{n} q - 1\right) C_m^q}{1 - \left(\dfrac{m}{n} r - 1\right) \dfrac{C_m^r}{K_r}} \qquad (17)$$

Thus if r and K_r are known, it is possible to calculate q and K_q from the experimental values of S_m and C_m. It is interesting to note that if one complex ion is extremely unstable, so that K_r becomes very large, these expressions approach those derived earlier for q and K_q for systems containing no second complex ion.

In a number of instances strong indication of incomplete ionization of the saturating salt may be observed, and the assumption of complete ionization, therefore, becomes untenable. At every concentration of added anion the solubility exceeds that previously calculated by an amount equal to the concentration of un-ionized solute. Now, if the activity coefficient of the weak electrolyte may be assumed constant over the concentration range considered, then the concentration of un-ionized solute is also constant over this range. The previously de-

rived relations for q and K_D are corrected merely by subtracting this concentration of un-ionized electrolyte from every solubility value.

If independent data exist from which the solubility product may be determined, then the concentration of un-ionized saturating salt is easily calculated. In the absence of such data, it must be obtained from the solubility results. It may be shown that in general if the ascending branch of the curve of solubility *versus* concentration of added anion be extrapolated to zero concentration, the intercept is just the concentration of un-ionized solute. When $q - n/m = 1$, the ascending branch is very nearly linear, and the extrapolation is extremely simple; in other cases, the ascending branch is not linear, and the extrapolation is more difficult and uncertain. When the contribution of the complex ion to the solubility in very dilute solutions of added anion may be neglected, the appropriate modifications of Equations (5) and (6) may be solved either numerically or graphically with experimentally determined solubility data to determine both the solubility product and the concentration of un-ionized electrolyte.

THE ENERGY OF VAPORIZATION OF NON-IONIC, NON-ASSOCIATED SUBSTANCES

BY J. H. SIMONS[1a] AND J. B. HICKMAN[1b]

School of Chemistry and Physics, The Pennsylvania State College, State College, Pa.

Received March 12, 1951

It has been possible to correlate the energy of vaporization per molecule of the gas of non-polar substances at 298.2°K. on the basis of polarizability, interpenetration and entropy of fusion. The resulting expressions have been generalized as to temperature. Energy of vaporization of a limited number of polar substances can also be correlated by means of a similar expression; however, in this case the dipole moment must also be taken into consideration.

I. Introduction

The energy of vaporization of a pure substance can be used directly to calculate its vapor pressure at a given temperature, and is involved in expressions permitting estimation of the viscosity and surface tension. More importantly, energy of vaporization is a measure of the forces acting between molecules of the same species, and as such is intimately concerned with solubility behavior.

If energy of vaporization could be independently related to measurable physical properties and structural features of a substance, it should be possible to consider mutual effects on energy of vaporization in a binary mixture, and hence to predict the escaping tendency of each component. This article is concerned with seeking such a relationship.

The Clapeyron equation, Trouton's rule and Hildebrand's modification thereof for pure substances and Raoult's law and the Hildebrand solubility equation for the components of a binary mixture superficially appear to represent the desired type of relationship. However, the data upon which they operate are themselves derived from experiments involving the vaporization process, hence these expressions, very useful in furnishing numerical approximations, are powerless to indicate why a particular material has a given energy of vaporization.

The concept of interpenetration, recently formulated by Simons and Dunlap[2] furnishes a picture of the vaporization process which has been used herein as a basis for the empirical development of expressions connecting energy of vaporization and other physical properties, free from the limitations mentioned above.

Simons and Dunlap[2] found that pentane and pentforane, although similar in those physical properties (such as energy of vaporization, polarizability and molar volume) considered to be critical in determining solubility behavior, formed mixtures deviating widely from Raoult's law. The deviations from Raoult's law were explained by assuming that pairs of hydrocarbon molecules intermesh or interpenetrate, while fluorocarbon molecules interpenetrate in a relatively negligible amount, either with one another or with hydrocarbon molecules. A quantitative evaluation of the distance of interpenetration, entirely consistent with the dimensions of the molecules, was shown to account for the observed deviations from Raoult's law.

As applied to the vaporization of pure substances, the concept of interpenetration indicates that the total energy of vaporization of a significantly interpenetrated material such as a hydrocarbon must involve both the energy required to transport the molecule permanently into the vapor, and an initial expenditure of energy to extract the molecule from its interpenetrated condition. Since only the former quantity is involved in the vaporization of non-interpenetrated materials such as rare gases, fluorocarbons and symmetrical halides, they should represent the simplest cases for application of a theory of energy of vaporization. Thus the first service of the interpenetration concept was to indicate a method of approach to the problem.

No attempt is made herein to derive equations from a fundamental law of forces between molecules. Rather, the data are examined empirically in the order suggested by the concept of interpenetration. In order to limit the number of variables

(1) (a) J. H. Simons, College of Engineering, University of Florida, Gainesville, Fla.; (b) J. B. Hickman, Dept. of Chemistry, University of West Virginia, Morgantown, W. Va.

(2) J. H. Simons and R. D. Dunlap, *J. Chem. Phys.*, **18**, 335 (1950).

being considered, equations were first developed for 298.2° K., then extended to other temperatures.

The equations developed relate energy of vaporization, polarizability, interpenetration, entropy of fusion and, in the case of certain polar substances, dipole moment. Mass is not involved. This contradicts a strong intuition which connects high molecular mass, high boiling point and consequent large energy of vaporization. This feeling probably arises from consideration of organic homologous series; no equation involving mass could be found to apply to the energies of vaporization of molecules made up of atoms of different sorts, hence held together by forces of different magnitude. For example, sulfur hexafluoride,[2a] molecular weight 146, has an energy of vaporization considerably lower than that of butane,[3] molecular weight 58.

The availability of physical properties of the fluorocarbons[4] aided the study greatly. The fluorocarbons are a large group of essentially non-interpenetrating substances to which the equations developed could be applied. Explanation of the anomalous behavior of the fluorocarbons (very low energy of vaporization relative to molecular weight, and almost identical energy of vaporization for structural isomers) was a stimulating challenge.

II. Energy of Vaporization at 298.2° K., Essentially Non-interpenetrating Substances

The energy of vaporization[5] at 298.2°K. of nonpolar, essentially non-interpenetrating substances can be represented by the empirical equation

$$e_v^{298.2} = A(\alpha_{total} - B) \qquad (1)$$

in which α_{total} is the total polarizability in cubic centimeters per molecule, and A and B are constants, having values, respectively, of 3.98×10^{10} and 2.55×10^{-24}. α_{total} is written to emphasize the fact that both electronic and atomic polarizability must be included. Experimentally, α_{total} may be derived from molecular polarization values computed from dielectric constant and density using the Mosotti–Clausius equation, or from molecular refractions at infinite wave length, cognizance being taken of the infrared contributions.

Figure 1 and Table I show the applicability of equation (1). The significance of the circles numbered 14 to 19 will be explained in Section III.

Polarizability has the dimensions of volume. Unlike molar volume, the polarizability of a nonpolar substance is practically independent of temperature.[6] Its size depends upon two factors: the inherent deformability of the molecule in an electric field, and how much material there is to deform.

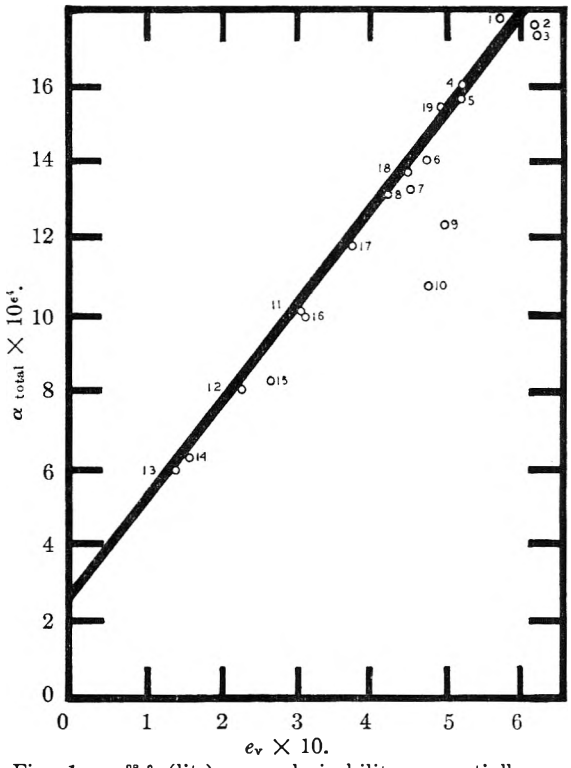

Fig. 1.—$e_v^{298.2}$ (lit.) *vs.* polarizability, essentially non-interpenetrating substances: 1, octforane; 2, stannic chloride; 3, titanium tetrachloride; 4, heptforane; 5, germanium tetrachloride; 6, hexforane; 7, silicon tetrachloride; 8, pentforane; 9, carbon tetrachloride; 10, uranium hexafluoride; 11, butforane; 12, propforane; 13, ethforane. Hydrocarbons, corrected for interpenetration: 14, propane; 15, butane; 16, pentane; 17, hexane; 18, heptane; 19, octane.

Thus, polarizability will increase with increasing molar volume in a series of related compounds, but a given ratio of molar volume to polarizability will not be duplicated in molecules held together by forces of different magnitudes.

The principal force against which a molecule leaving the surface of a liquid acts is certainly not gravity, otherwise mass would enter the energy of vaporization equation. Once a force whose effect depends upon the area over which it acts is admitted, a physical picture of a possible relationship between e_v and polarizability can be imagined. The larger a molecule is, and the more readily it is deformed in the presence of a force field, the greater its effective area will be, and the larger the amount of energy required to remove it some critical distance above the surface of the liquid, beyond which it will continue into the vapor rather than returning to the surface. Polarizability is a combined measure of molecular size and deformability.

Relating polarizability volume to energy of vaporization has a historical precedent in the work of Henglein[7] who demonstrated a proportionality between molar volume and heat of vaporization for the halogens. Such a linear dependence is not generally applicable; in fact, in some cases the situation is reversed: silicon tetrachloride, whose molar volume at 25° is 115.4 cm.^{3}/mole[8] has an energy of

(2a) W. A. Roth and K. Scheel, editors, "Landolt-Börnstein Physikalisch-chemische Tabellen," Vol. III, Verlag Julius Springer, Berlin, 1936, p. 2709.

(3) F. D. Rossini, K. S. Pitzer, W. J. Taylor, J. P. Ebert, J. E. Kilpatrick, C. W. Beckett, M. G. Williams and H. G. Werner, "Selected Values of Properties of Hydrocarbons," U. S. Govt. Printing Office, Washington, 1947.

(4) J. H. Simons (editor), "Fluorine Chemistry," Academic Press, Inc., New York, N. Y., 1950.

(5) By energy of vaporization is meant energy of vaporization in ergs per molecule, to be represented throughout this paper by the symbol e_v. It is related to ΔE_v, cal./mole, by the equation

$$e_v = \Delta E_v \times 4.184 \times 10^7/6.02 \times 10^{23}$$

Within the accuracy of this work, ΔE_v is considered equal to $\Delta H_v - RT$.

(6) R. Schmidt, *Physik. Z.*, **39**, 574 (1938).

(7) F. A. Henglein, *Z. anorg. Chem.*, **118**, 166 (1921).

(8) J. H. Hildebrand, "Solubility," Reinhold Publishing Corp., New York, N. Y., 1936.

TABLE I

CALCULATED AND OBSERVED VALUES, $e_v^{298.2}$, SUBSTANCES NOT EXHIBITING SIGNIFICANT INTERPENETRATION

Formula	α_{total} $\times 10^{24}$	$e_v^{298.2}$ $\times 10^{13}$ (lit.)	$e_v^{298.2}$ $\times 10^{13}$ (calcd.)
CCl_4	12.4[a]	5.02[b]	3.93
$SiCl_4$	13.4[c]	4.58[b]	4.32
$TiCl_4$	17.4[d]	6.26[b]	5.91
$GeCl_4$	14.7[e]	5.21[b]	4.85
$SnCl_4$	17.7[d]	6.21[b]	6.03
UF_6	10.8[f]	4.68[g]	3.30
C_2F_6	6.0[h]	1.41[i]	1.38
C_3F_8	8.1[h]	2.24[j]	2.21
C_4F_{10}	10.2[h]	3.07[j]	3.05
C_5F_{12}	13.1[h]	4.22[j]	4.20
C_6F_{14}	14.0[h]	4.74[j]	4.57
C_7F_{16}	16.1[h]	5.25[j]	5.41
C_8F_{18}	17.9[h]	5.77[j]	6.12

[a] A. Eucken and K. L. Wolf (editors), "Hand- und Jahrbuch der chemischen Physik," Vol. VI (1), Akademische Verlagsgesellschaft, Leipzig, 1935, pp. 262–263. [b] Reference 9. [c] Calculated from $\alpha_{electronic}$ given in: J. H. Hildebrand, *J. Chem. Phys.*, **15**, 727 (1947), and average per cent. contribution (21) of α_{atomic} for tetrahalides. [d] H. Ulich, E. Hertel and W. Nespital, *Z. physik. Chem.*, **17B**, 370 (1932). [e] J. G. Miller, *J. Am. Chem. Soc.*, **56**, 2360 (1934). [f] C. P. Smyth and N. B. Hannay, *Abs. Unclassified Documents*, **1**, 263 (1947) (Document MDDC-441). [g] J. F. Masi, *J. Chem. Phys.*, **17**, 765 (1949). [h] Calculated from values of $\alpha_{electronic}$ given in Reference 4, and values of α_{total} from the following sources: H. E. Watson, K. L. Ramaswamy and G. P. Kane, *Proc. Roy. Soc. (London)*, **156A**, 130 (1936); J. H. Simons and W. A. Wilson, private communication. [i] E. L. Pace, Ph.D. Dissertation, The Pennsylvania State College, 1946. [j] Calculated from values given in reference *i*, Table I, reference 1 and reference 4.

vaporization of 4.58×10^{-13} ergs/molecule,[9] while titanium tetrachloride with a 25° molar volume of 110.5 cm.^{3}/mole[8] has an energy of vaporization of 6.26×10^{-13} ergs/molecule,[9] both e_v values being measured at 298.2°K.

Debye[10] has related polarizability to van der Waals a. Since the a in the van der Waals equation represents an effective addition to pressure occasioned by cohesive interaction of the molecules, the analogy to the present application is evident.

Reasonable agreement between calculated and observed e_v values was found for the substances listed in Table I with the exception of carbon tetrachloride and uranium hexafluoride.

The observed e_v of carbon tetrachloride is 1.09×10^{-13} ergs/molecule higher than the calculated value; however, carbon tetrachloride is known to have a strained structure, making it doubtful that it can be considered in the same class as other symmetrical halides.

The fact that the calculated e_v for uranium hexafluoride is only 70% of the observed value is in accord with the electron-diffraction work of Bauer,[11] who suggested that the uranium hexafluoride molecule is not a regular octahedron. A non-symmetrical structure would be attracted more vigorously.

The two instances of large deviations between calculated and observed values of e_v appear to correspond to physical realities in the structures of the compounds concerned, suggesting that equation (1) may be used in conjunction with other data in determining molecular structure.

III. The Energy of Vaporization of Materials Exhibiting Significant Interpenetration

Alkanes.—Equation (1) cannot be applied directly to alkanes; the predicted energies of vaporization are too low, and the variations in polarizability between isomers are too small to account for the variations in energy of vaporization.

Both of these discrepancies can be explained in terms of the interpenetration concepts of Simons and Dunlap.[1] According to this concept, the molecules of hydrocarbons intermesh, in contrast to the compact molecules of fluorocarbons, rare gases and symmetrical halides. The vaporization process in a hydrocarbon must consist of first unmeshing the molecules, then giving them sufficient energy to remain in the vapor state.

Equation (1) represents the energy required to remove a non-interpenetrated molecule of given polarizability permanently to the vapor. If interpenetration is present, an additional expenditure of energy will be required to bring the molecule into a condition from which it can be vaporized.

The magnitude of this extra energy is assumed to depend upon two factors: the distance to which the molecules interpenetrate, and the total area interpenetrated. As a reasonable approximation, the distance interpenetrated will be assumed to be constant for the hydrocarbon series and independent of temperature.

The area interpenetrated must depend upon the structure of the hydrocarbon; one need only imagine interpenetration to the same distance of two perfect spheres and of two elongated, highly-branched rods to envision the variations possible.

Incorporating these statements into an equation gives

$$e_v^{298.2} = A(\alpha_{total} - B) + k'I(\text{area interpenetrated}) \quad (2)$$

in which k' is a constant, like I, the distance interpenetrated, assumed to be independent of temperature. For non-interpenetrating substances, $I = 0$, and equation (2) automatically resolves into equation (1), the constants A and B being identical.

As written, equation (2) is useless in the absence of any physical measure of area interpenetrated. Ideally, the ratio of surface to volume of the molecule would serve, but this is equally incapable of being measured directly. As an admitted rough and inadequate substitute, molecular symmetry as reflected[12,13] in entropy of fusion will be adopted.

Symmetry at best can only approximately measure the desired quantity, and solids certainly exist showing wide divergence in the relationship between symmetry and surface–volume ratio. Doubtless some of the failures of equation (5) properly to represent the data spring from this approximation.

In relating symmetry to entropy of fusion, it will be considered that entropy of fusion is made up of two additive terms: the necessary energy to disrupt the crystal lattice divided by the fusion temperature, and a symmetry term measuring the difference

(9) K. K. Kelley, *Bur. Mines Bull.* (U. S. Dept. Interior), **383** (1935).

(10) P. Debye, *Physik. Z.*, **22**, 302 (1921).

(11) S. H. Bauer, *J. Chem. Phys.*, **18**, 27 (1950)

(12) J. Pirsch, *Ber.*, **70B**, 12 (1937)

(13) E. van de Vloed, *Bull. soc. chim. Belg.*, **48**, 229 (1939).

in probability between a preferred spatial orientation in the crystal, and randomness in the liquid.

$$\Delta S_f = \Delta S_{\text{lattice-disruption}} + \Delta S_{\text{symmetry}} \qquad (3)$$

The entropy of lattice-disruption must of course vary with the type of crystal, and the species of molecules involved. Again as an approximation, it will be assumed to be constant. The approximations here made can be justified only by the utility of the resulting expression.

The second right-hand member of (3) should certainly be zero for the perfectly spherical atom-molecules of the rare gases. This is borne out by the facts; the entropies of fusion of neon, argon, krypton, xenon and radon being essentially constant, respectively, being equal to 3.26,[14] 3.35,[14] 3.36,[14] 3.40[14] and 3.43.[15] The average of these values, 3.3 e.u., has been taken as an approximation for $\Delta S_{\text{lattice-disruption}}$. Equation (3) can be rewritten

$$\Delta S_{\text{symmetry}} = (\Delta S_f - 3.3) \qquad (4)$$

Since $\Delta S_{\text{symmetry}}$ has been adopted as an approximation for a value proportionate to area interpenetrated, equation (2) and equation (4) can be combined

$$e_v^{298.2} = A(\alpha_{\text{total}} - B) + k''I(\Delta S_f - 3.3) \qquad (5)$$

The constants A and B are identical with those of equation (1); k'' is not necessarily equal to k', since $\Delta S_{\text{symmetry}}$ is only assumed to be proportionate, not equal, to area interpenetrated. Equation (5) is the equation actually used in correlating alkane energies of vaporization.

The product of constants $k''I$ was evaluated empirically and arbitrarily from the single case of *n*-octane and 2,2,3-trimethylpentane, whose α values are essentially equal,[3] whose energies of vaporization differ by 0.76×10^{-13} ergs/molecule,[3] and whose energy of fusion values differ by exactly 10 e.u.[3] The consequent value of $k''I$, 0.076×10^{-13}, is used throughout this paper. It is realized that $k''I$ is not completely constant; it is felt that it is sufficiently so for the uses to which it is put.

Table II compares literature values of e_v with those calculated using equation (5). In Fig. 1, the circles numbered 14 to 19 represent a plot against polarizability of the quantity

$$e_v^{298.2}\,(\text{lit.}) - k''I(\Delta S_f - 3.3)$$

According to the theory here presented, this quantity represents the energy required to remove a molecule of the listed normal alkane to the vapor, the interpenetration energy having been accounted for in $k''I$ $(\Delta S_f - 3.3)$. It will be noted that these plotted points fall close to the graph of equation (1), which relates e_v and polarizability for essentially non-interpenetrating substances.

Isomers omitted from Table II are those for which all requisite data could not be located.

In substituting in equation (5) for 2,2- and 2,3-dimethylbutane the ΔS value used was $\Delta S_f + \Delta S_{\text{transition}}$. These two substances belong to the class characterized by van de Vloed[13] as forming soft crystals. Transition to hard crystals similar to those of other hydrocarbons is accompanied by a heat of transition often greater than the heat of fusion. Since the soft crystals formed at first permit considerable randomness in the orientation of the molecules, it is felt that no true measure of ΔS symmetry can be obtained unless both the heat of fusion and the heat of transition to hard crystals similar to those of other hydrocarbons are included.

The fact that equation (1) rather than equation (5) applies to fluorocarbons explains the low energy of vaporization, and the fact that isomers have almost identical e_v values. Since interpenetration energy makes no significant contribution, total e_v is low; difference in e_v between isomers arises largely from differences in interpenetration energy, therefore the fluorocarbon isomers have almost identical energies of vaporization.

Cyclic Compounds.—If equation (5) is applied to cyclic compounds under the assumptions that A, B and $k''I$ have the values determined for the alkanes, the calculated energies of vaporization are generally much too low, as indicated in Table III (in which the quantity $e_v^{298.2}$ (lit.) $- e_v^{298.2}$ (calcd.) has been listed under the column heading "Difference."

While there is no direct evidence as to the physical significance of these "Difference" values, a possible explanation in accord with experimental evidence may be suggested. Bell and Davey,[16] using an X-ray diffraction technique, have shown the existence of a layer structure in liquid benzene and cyclohexane. The observed energies of vaporization of cyclic compounds may consist of terms corresponding to normal vaporization, to removing the molecules from their interpenetrated condition,

TABLE II

CALCULATED AND OBSERVED VALUES OF $e_v^{298.2}$ FOR ALKANES

Name	α_{total}[a] $\times 10^{24}$	ΔS_f	$e_v^{298.2} \times 10^{13}$ (lit.)	$e_v^{298.2} \times 10^{13}$ (calcd.)	Error, %
Propane	6.31	9.8	2.09	2.00	− 4.5
Butane	8.30	8.3	3.08	2.67	−10.0
n-Pentane	10.00	14.0	3.98	3.77	− 5.8
2-Methylbutane	10.04	10.9	3.67	3.55	− 3.4
Neopentane	10	3.4	3.15	2.96	− 6.0
n-Hexane	11.81	17.5	4.83	4.76	− 1.4
2-Methylpentane	11.84	12.6	4.54	4.41	− 2.9
2,2-Dimethylbutane	11.82	11.0[b]	4.17	4.27	+ 2.4
2,3-Dimethylbutane	11.80	12.8[b]	4.42	4.39	− 0.7
n-Heptane	13.69	18.4	5.66	5.57	− 1.6
2-Methylhexane	13.70	13.7	5.44	5.23	− 3.9
3-Ethylpentane	13.69	14.6	5.44	5.30	− 2.6
2,2-Dimethylpentane	13.69	9.4	4.98	4.90	− 1.6
2,4-Dimethylpentane	13.70	10.4	5.05	4.99	− 1.2
3,3-Dimethylpentane	13.69	12.2	5.07	5.12	+ 1.0
n-Octane	15.50	22.8	6.47	6.63	+ 2.5
2-Methylheptane	15.52	14.9	6.16	6.04	− 1.9
3-Methylheptane	15.50	17.8	6.19	6.25	+ 1.0
4-Methylheptane	15.50	17.0	6.17	6.19	+ 0.3
2,2-Dimethylhexane	15.51	10.7	5.76	5.72	− 0.7
2,5-Dimethylhexane	15.51	16.9	5.87	6.17	+ 5.1
3,3-Dimethylhexane	15.49	12.0	5.81	5.70	− 1.9
2-Methyl-3-ethylpentane	15.40	17.1	5.98	6.16	+ 3.0
3-Methyl-3-ethylpentane	15.35	14.2	5.88	5.92	+ 0.7
2,2,3-Trimethylpentane	15.50	12.8	5.71	5.87	+ 2.8
2,3,3-Trimethylpentane	15.50	2.1[c]	6.17	5.12	−16.5
2,3,4-Trimethylpentane	15.40	13.5	5.84	5.90	+ 2.7
2,2,4-Trimethylpentane	15.40	13.3	5.44	5.88	+ 8.1

[a] All data from reference 3 unless otherwise indicated. [b] Includes entropy of transition: D. R. Douslin and H. M. Huffman, *J. Am. Chem. Soc.*, 68, 1704 (1946). [c] Interpenetration energy assumed = 0.

(14) K. Clusius and L. Riccoboni, *Z. physik. Chem.*, **38B**, 81 (1938).

(15) United States National Bureau of Standards, "Selected Values of Chemical Thermodynamic Properties," U. S. Govt. Printing Office, Washington, 1947, Series II

(16) P. H. Bell and W. P. Davey, *J. Chem. Phys.*, **9**, 441 (1941).

TABLE III

CALCULATED AND OBSERVED VALUES OF $e_v^{298.2}$, CYCLIC COMPOUNDS AND ALKENES

Name	α_{total}[a] × 10^{24}	ΔS_f	$e_v^{298.2}$ × 10^{13} (lit.)	$e_v^{298.2}$ × 10^{13} (calcd.)	Difference × 10^{13}
Cyclopentane	9.16	0.8[b]	4.26	2.63	1.63
Methylcyclopentane	11.02	12.7	4.78	4.18	0.60
Ethylcyclopentane	12.82	12.2	5.56	4.90	0.66
1,1-Dimethylcyclopentane	12.88	2.0[b]	5.15	4.12	1.03
Cyclohexane	10.98	2.3[b]	5.02	3.36	1.66
Methylcyclohexane	12.89	11.0	5.40	4.70	0.70
Ethylcyclohexane	14.68	12.3	6.23	5.52	0.71
1,1-Dimethylcyclohexane	14.64	2.0[c]	5.81	4.81	1.00
Benzene	10.51[c]	8.4	5.12	3.56	1.56
Toluene	12.69[c]	8.8	5.80	4.46	1.34
Ethylbenzene	14.08	12.3	6.51	5.18	1.33
o-Xylene	14.40	13.1	6.69	5.46	1.23
m-Xylene	14.45	12.3	6.57	5.42	1.15
p-Xylene	14.50	14.3	6.65	5.60	1.05
Mesitylene	16.40	27.5[d]	7.36	7.30	0.06
p-Dichlorobenzene	15.01[e]	11.7[e]	7.50[f]	5.59	1.91
Benzene-d_6	10.34[g]	8.4[g]	5.10[g]	3.49	1.61
Cyclopentforane	11.50[h]	...	3.69	3.56	0.13
1-Butene	7.96	10.5	2.97	2.73	.24
cis-2-Butene	8	13.0	3.28	2.89	.39
trans-2-Butene	8	13.9	3.17	2.96	.18
2-Methylpropene	8	10.7	2.97	2.73	.24

[a] All data from reference 3 unless otherwise indicated. [b] Interpenetration energy assumed = 0. [c] Reference *a*, Table I. [d] Includes entropy of transition. [e] F. Richter, "Beilsteins Handbuch der organischen Chemie," 2nd suppl., Vol. V, Verlag Julius Springer, Berlin, 1946. [f] Reference 2. [g] C. K. Ingold, C. G. Raisin and C. L. Wilson, *J. Chem. Soc.*, 915 (1936). [h] Reference 4.

and to breaking up the layer structure. Equation (4) would represent only the first two of these, hence the large "Difference."

Some other observations are compatible with this viewpoint. Benzene, cyclohexane and cyclopentane show about the same difference between observed and calculated e_v, suggesting the presence of a similar type of layering in each compound. Invariably, substitution in the ring decreases the amount of difference; this would correspond to partial disruption of layer formation.

Substitution of a methyl or ethyl on an alicyclic ring lowers the "Difference" value much more than corresponding substitution in the benzene nucleus. Again this corresponds with a picture of the formation of layers in the liquid; substitution in the alicyclic ring, in which the substituent does not lie in the plane of the ring, should have a stronger effect in disrupting the orderly formation of layers than corresponding substitution in benzene, where the carbon of the substituent methyl lies in the plane of the ring.[17]

If entropy of transition is included in substituting for ΔS_f in equation (5) for mesitylene, the calculated and observed e_v values are essentially identical, suggesting that three methyl groups completely block off layer formation.

(17) An alternative explanation would be to regard the reported[18] 0.4 debye unit dipole moment of toluene as possessing physical reality. Calculating toluene's e_v as a substance containing a dipole, according to the method of section V of this paper, gives a "Difference" value of 0.88 × 10. This could be interpreted as meaning that toluene, a weakly polar substance, has the same type of layering characteristics as methylcyclohexane, methylcyclopentane and the like.

(18) A. Eucken and K. L. Wolf, "Hand- und Jahrbuch der Chemischen Physik," Akademische Verlagsgesellschaft, Leipzig, 1936. Appendix: Dipolmomente.

p-Dichlorobenzene, although it possesses no overall dipole moment, certainly has an unbalanced electric field effective at distances of a few Å. from the molecule. This is reflected in the large difference value, to which only qualitative significance can be attached, however, since the unbalanced field undoubtedly affects the interpenetration characteristics as well as the e_v value directly.

The fact that benzene-d_6 has a lower e_v than benzene itself is reflected in the lower polarizability of the compound. No significance can be attached to the slightly larger difference value for benzene-d_6, since the increment is smaller than, for example, the uncertainty in the entropy of fusion.

If the behavior of cyclopentforane is typical, it appears that if interpenetration is absent, layering also disappears. This is in accord with the picture of interpenetration presented by Simons and Dunlap.[1] The compact fluorocarbon molecules, not intermeshing to any significant extent, could scarcely be expected to participate in even a transient liquid layer-structure.

The energy of vaporization of the alkenes is discussed in section IV.

IV. Temperature Dependence of the e_v-Polarizability Function

Empirical consideration of the available energy of vaporization data at temperatures other than 298.2 indicates that equation (6) correlates the e_v values for substances not exhibiting significant interpenetration, equation (7), for interpenetrating substances.

$$e_v^T = (T_0/T)^{1/2} A[\alpha_{total} - (T/T_0)^2 B] \quad (6)$$

$$e_v^T = (T_0/T)^{1/2} A[\alpha_{total} - (T/T_0)^2 B] + k''I(\Delta S_f - 3.3) \quad (7)$$

If $T_0 = 298.2$, A and B have the values given in connection with equation (1). The constants $k''I$ have the values previously given at all temperatures; it was stated earlier that distance interpenetrated was assumed as an approximation to be independent of temperature. For the special case of $e_v^{298.2}$ equations (6) and (7) are identical, respectively, with equations (1) and (5).

Figure 2 and Table IV represent application of equations (6) and (7) to energies of vaporization in the temperature range 24–491°K. Plotted hydrocarbon values are corrected to zero interpenetration as in section III.

Equations (6) and (7) are approximate, and can be applied to a particular substance only in a limited range of temperature, at best from the melting point to somewhat above the normal boiling point. As the critical temperature of a substance is approached, the rate of change of e_v with temperature becomes much higher; equations (6) and (7) are not meant to apply to this situation.

No physical significance should be attached to the increase of temperature coefficient of e_v with lowering of temperature for a given substance implied by equations (6) and (7). As stated before, they are meant only as empirical approximations; doubtless part of the difficulty arises from the fact that the variation of two different types of functions must be approximated in one equation: the temperature variation of e_v, and the inherent tem-

TABLE IV

CALCULATED AND OBSERVED VALUES, e_v^T

Substance	α total $\times 10^{24}$	ΔS_f	$e_v^T \times 10^{13}$ (lit.)	$e_v^T \times 10^{13}$ (calcd.)	T
Neon	0.394[a]	[g]	0.270[b]	0.520	24.6
Argon	1.635[a]	..	0.950[b]	1.040	87.3
Krypton	2.46[a]	..	1.320[b]	1.275	119.9
Xenon	4.02[a]	..	1.849[b]	1.730	165.1
Oxygen	1.50[c]	..	0.996[b]	0.920	90.2
Nitrogen	1.71[c]	..	0.826[b]	1.17	80.2
Ethene	4.25[c]	7.70[d]	2.04[d]	2.14	169.5
Propene	6.22[c]	8.20[d]	2.76[d]	2.53	225.5
Silicon tetrachloride	13.4[e]	..	4.13[f]	3.90	329.9
Germanium tetrachloride	14.7	..	4.40[f]	4.00	357
Titanium tetrachloride	17.4	..	5.24[f]	4.34	409
Tin tetrachloride	17.7	..	5.26[f]	4.64	386
Sulfur hexafluoride	6.52[c]	..	2.83[f]	2.56	205
Tin tetraiodide	33.6[h]	..	8.90[i]	9.00	450
Methforane	4.02[j]	..	1.95[f]	1.68	145
Ethforane	6.0[k]	..	2.70[l]	2.79	165
Ethane	4.4[c]	7.6[d]	2.40[f]	2.07	183
Ethane	4.4[c]	7.6[d]	1.70[f]	1.78	233
Propane	6.31[d]	9.8[d]	2.60[d]	2.64	231
Butane	8.30[m]	8.3	3.35	2.92	272.7
Pentane	10.00	14.0	3.85	3.65	309.3
2-Methylbutane	10.04	10.9	3.67	3.52	301.0
Neopentane	10	3.4	3.35	3.11	282.7
Hexane	11.8	17.5	4.32	4.32	341.9
2-Methylpentane	11.84	12.6	4.15	3.92	333.5
2,2-Dimethylbutane	11.80	11.0[o]	3.87	3.92	322.9
2,3-Dimethylbutane	11.80	12.8	4.07	4.00	330.7
Heptane	13.7	18.4	4.75	4.61	371.6
2-Methylhexane	13.70	13.7	4.59	4.36	363.2
3-Ethylpentane	13.69	14.6	4.63	4.38	366.7
2,2-Dimethylpentane	13.69	9.4	4.35	4.32	352.4
2,4-Dimethylpentane	13.70	10.4	4.40	4.26	353.7
3,3-Dimethylpentane	13.69	12.2	4.42	4.31	359.3
Dichloromethforane	7.96[p]	..	2.44[f]	2.16	296.2
Naphthalene	17.5[c]	12.8[q]	6.05[f]	4.02	491

[a] H. E. Watson, G. G. Rao and K. L. Ramaswamy, *Proc. Roy. Soc.* (*London*), 132A, 569 (1931). [b] Reference 15. [c] H. E. Watson, G. G. Rao and K. L. Ramaswamy, *Proc. Roy. Soc.* (*London*), 146A, 558 (1934). [d] Reference 3. [e] Polarizabilities of $SiCl_4$, $GeCl_4$, $TiCl_4$ and $SnCl_4$ identical with those listed in Table I, *q. v.* [f] Reference 2. [g] A dash in the entropy of fusion column indicates that interpenetration energy is regarded as zero. [h] Calculated as in Table I, note *c*. [i] J. H. Hildebrand, *J. Chem. Phys.*, 15, 727 (1947). [j] Watson, Ramaswamy and Kane, *Proc. Roy. Soc.* (*London*), 156A, 130 (1936). [k] Table I, reference *i*. [m] Unless otherwise indicated, all data on alkanes from reference 3. [o] Note *b*, Table II. [p] Note *a*, Table I. [q] Note *e*, Table III.

perature dependence of the e_v-polarizability function.

Reasonable agreement between calculated and observed values of e_v is evidenced in Table IV.

Rare Gases.—The fact that the rare gases' e_v values are correlated assuming no interpenetration indicates the possibilities of generalizing the Simons–Dunlap interpenetration concept.

Symmetrical Halides.—Two more symmetrical halides, stannic iodide and sulfur hexafluoride, for which $e_v^{298.2}$ data were unavailable, show good agreement between observed and calculated e_v values, zero interpenetration being assumed.

Alkanes.—A comparison of e_v (lit.) and e_v (calcd.) for a number of alkanes at their normal boiling points is included. The isomeric octanes are omitted in order to conserve space; in general, the branched-chain isomers show reasonable agreement between observed and calculated values, not so good agreement, however, as the normal hydrocarbons.

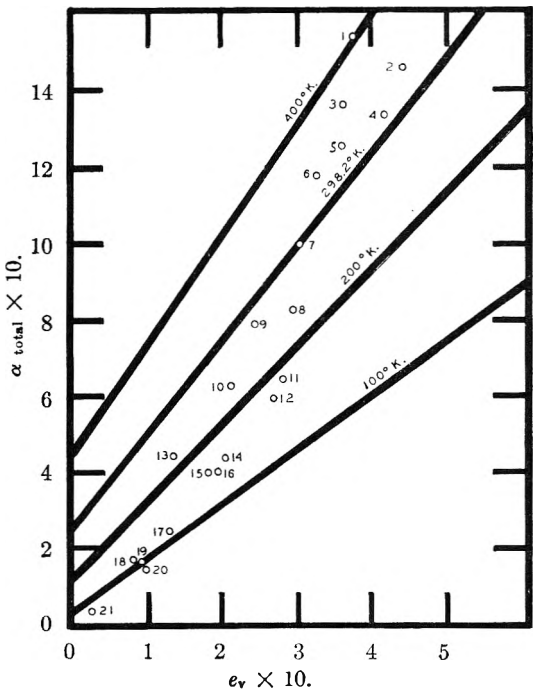

Fig. 2.—Temperature dependence, e_v *vs.* polarizability function (name of substance and temperature, ° K.): 1, octane, 398.9; 2, germanium tetrachloride, 356; 3, heptane, 371.6; 4, silicon tetrachloride, 329.9; 5, silicon tetramethyl, 299.8; 6, hexane, 341.9; 7, pentane, 309.3; 8, butane, 272.7; 9, dichloromethforane, 296.2; 10, propane, 231; 11, sulfur hexafluoride, 205; 12, ethforane, 165; 13, ethane, 233; 14, ethane, 183; 15, xenon, 165.1; 16, methforane, 145; 17, krypton, 119.9; 18, nitrogen, 80.0; 19, argon, 87.3; 20, oxygen, 90.2; 21, neon, 24.6.

Alkenes.—Within the accuracy of this work, ethylene (ethene) has the same energy of vaporization characteristics as an alkane of the same polarizability and entropy of fusion; propylene and α-butylene require significantly more energy for their vaporization than predicted by equation (7). A possible interpretation is that the unsymmetrical alkenes possess a small but existent dipole moment, as reported in the literature.[18] The two compounds for which dipole moment values are available are included in Table V. Although no dipole moment data for *cis*- or *trans*-2-butene are available, the smaller difference between observed and calculated $e_v^{298.2}$ (Table III) for the *trans*-isomer is in accord with the viewpoint that the unsymmetrical alkenes possess a definite dipole moment reflected in the e_v values.

Naphthalene.—Naphthalene, for which no $e_v^{298.2}$ value was available, shows a difference of 2.03×10^{-13} ergs/molecule between e_v (lit.) and e_v (calcd.), to be compared with 1.56×10^{-13} ergs/molecule for benzene. Partly, the increase may be attributed to the approximate nature of equation (7); it is reasonable to suppose that the greater area of the naphthalene ring system would enhance the effect of layering.

V. Energy of Vaporization of Substances Containing a Dipole

A few of the simplest compounds containing dipoles—alkyl halides, ethers and olefins—will be considered. No attempt will be made to correlate

data for such associated compounds as water, ammonia and hydrogen fluoride.

The presence of a dipole in a compound can affect the energy of vaporization directly, by increasing the amount of energy required to lift the molecule beyond some critical distance of no return, and indirectly, by changing the interpenetration characteristics of the compound. The latter effect will be considered first, the alkyl halides being used as a particularly simple example.

Substitution of one hydrogen atom of an alkane by a halogen atom will change the entire charge distribution of the molecule. In terms of a naive but useful picture, each electron pair will shift slightly toward the halogen atom, resulting in a small residue of positive charge on each carbon atom. A picture of this sort is used to explain the fact that chloroacetic acid is stronger as an acid than acetic acid—the shift of electron pairs toward the substituted chlorine atom allowing easier escape of the solvated proton.

A slight excess of positive charge on each carbon atom would reduce interpenetration because of mutual repulsion of like charges. No direct measure of the extent to which this is effective is available, so once more an approximate and indirect approach must be used.

Table V lists the entropies of fusion of some of the lower alkyl halides, together with the ΔS_f values for the corresponding hydrocarbons.

TABLE V

ENTROPY OF FUSION OF SOME ALKYL HALIDES

Substance	ΔS_f, halide	ΔS_f, corresponding hydrocarbon
Methyl chloride	8.91[a]	2.2[b]
Ethyl chloride	7.85[a]	7.6[b]
Ethyl bromide	9.03[a]	7.6[b]
Propyl bromide	9.56[a]	9.8[b]
Butyl bromide	13.5[a]	8.3[b]
Amyl bromide	18.6[a]	14.0[b]

[a] C. P. Smyth and W. O. Baker, *J. Am. Chem. Soc.*, **61**, 1644 (1939). [b] Reference 3.

The methyl, ethyl and propyl halides have essentially the same ΔS_f value. This can be interpreted to mean that dipole–dipole interaction is sufficient to orient the molecules completely before the fusion process, no $\Delta S_{symmetry}$ being involved. The entropy of fusion would therefore represent only the energy necessary to separate the dipoles, divided by the fusion temperature. As an approximation, this dipole-separation entropy will be assumed to be proportional to the dipole moment, or approximately for the halides considered, $\Delta S_{dipole\text{-}separation} = 4.5\ \mu$ (μ being the dipole moment in Debye units, e. s. u. $\times 10^{-18}$).

The butyl and amyl bromides represent a situation in which the dipole alone is not completely effective in bringing about orientation before freezing, and symmetry must enter again. This $\Delta S_{symmetry}$ will be assumed to be equal to $\Delta S_f - \Delta S_{dipole\text{-}separation}$, and will be used in calculating the effect of interpenetration. Obviously, what is really wanted is a measure of the extent to which interpenetration has been disrupted by the substituted halogen atom; at best, the quantity here suggested as an approximation has only an extremely indirect connection with the one wanted. In the absence of a better physical measure it must serve.

The direct effect of the dipole moment on energy of vaporization was estimated empirically to be equal to $0.85 \times 10^{-13} \times \mu$ ergs/molecule.

Equation (8) combines the assumptions and approximations listed in regard to the effect of the dipole with the over-all assumption that, in general, compounds containing a dipole have the essential energy of vaporization characteristics of non-polar substances, the effect of the dipole being separable and in addition to the normal energy of vaporization.

$$e_v^T = (T_0/T)^{1/3} A\,[\alpha_{total} - (T/T_0)^2 B] + k''I(\Delta S_f - 4.5\mu) + (0.85 \times 10^{-13})\mu \quad (8)$$

The constants A, B and $k''I$ are identical with those in equation (7). The dipole moment in debye units is represented by the symbol μ. α_{total} designates the polarizability, derived from the distortion polarization. The distortion polarization of a dipole substance can be determined experimentally as the $1/T = 0$ intercept of a plot of total polarization *vs.* $1/T$ for the gas, or from the molar refraction, indices of refraction in the infrared being taken into account.

Table VI compares calculated and literature values for a few substances containing a dipole.

TABLE VI

CALCULATED AND OBSERVED VALUES OF e_v, SUBSTANCES CONTAINING A DIPOLE

Substance	$\alpha_{total} \times 10^{24}$	ΔS_f	$e_v^T \times 10$ (lit.)	$e_v^T \times 10$ (calcd.)	T	μ[d]
Methyl chloride	6.09[a]	8.91[b]	2.97[c]	2.97	298.2	1.86
Methyl iodide	8.57[a]	...	4.56[c]	3.76	298.2	1.60
Ethyl chloride	7.87[a]	7.85[b]	3.67[c]	3.85	298.2	2.03
Ethyl bromide	9.35[a]	9.03[b]	4.45[c]	4.26	311.6	2.00
Ethyl iodide	10.58[a]	...	4.91[c]	4.77	298.2	1.85
Butyl iodide	11.5[a]	13.5[b]	4.64[e]	4.96	341.0	1.9
Amyl chloride	13.0[a]	18.5[b]	4.93[e]	5.47	381.6	1.9
Methyl ether	6.16[f]	8.96[g]	3.22[e]	3.27	248.3	1.3
Ethyl ether	10.21[f]	10.1[e]	4.21[e]	4.34	298.2	1.14
Propylene	6.22[g]	8.2[h]	2.76[h]	2.99	225.5	0.4
α-Butylene	7.96[g]	10.5[h]	2.97[h]	3.17	298.2	0.4

[a] A. Audsley and F. R. Goss, *J. Chem. Soc.*, 498 (1942). [b] C. P. Smyth and W. O. Baker, *J. Am. Chem. Soc.*, **61**, 1644 (1939). [c] Reference 15. [d] All values from Reference 18. [e] Reference 2a. [f] Table I, note *a*. [g] Table IV, note *c*. [h] Reference 3.

ON THE CALCULATION OF ENTROPY AND ENTHALPY CHANGES FROM FREE-ENERGY DATA

BY REINO W. HAKALA

Department of Chemistry, Syracuse University, Syracuse, New York

Received March 21, 1951

Klotz and Fiess[1] employed the function $(\partial\Delta F/\partial T)_P = -\Delta S$ to determine the entropy of formation of copper(II)–albumin complexes using measurements made at two temperatures 25° apart. With ΔS thus found they then calculated the enthalpy of formation. It is here pointed out that this procedure leads to exact results only if ΔH is sensibly constant in the temperature interval under consideration. To ascertain this, measurements at more than two temperatures are needed. However, the data of Klotz and Fiess, though insufficient for the exact calculation of ΔS and ΔH, provide ample support for their major conclusion that electrostatic factors play a dominant role in the copper(II)–albumin interaction. Formulas are derived which are convenient in the determination of ΔS and ΔH from ΔF data at various temperatures.

In their very interesting work on copper(II)–albumin complexes, Irving M. Klotz and Harold A. Fiess[1] employed the general thermodynamic function

$$\left(\frac{\partial\Delta F}{\partial T}\right)_P = -\Delta S \qquad (1)$$

apparently taking a ratio of differences instead of the true derivative—or using the integrated form, assuming ΔS to be constant—to determine the entropy of formation of the complexes at a given *p*H over a temperature range of 25°, and then calculated the enthalpy of formation from this value of ΔS and the general relationship

$$\Delta F = \Delta H - T\Delta S \qquad (2)$$

At first glance, it would appear that this procedure can lead only to approximate results, because the temperature range that was taken is far from infinitesimal or because ΔS may not be temperature independent. It therefore seems pertinent to inquire, under what conditions, if any, does this procedure lead to exact rather than merely approximate results; *i.e.*, when is ΔS actually constant over the temperature range taken, and when is the calculated value of ΔS only an average value? It will be shown in what follows that the procedure of Klotz and Fiess leads to exact results if, and only if, the enthalpy of formation is sensibly constant in the temperature range under consideration; *i.e.*, that the expression

$$\left(\frac{\Delta F_{T_2} - \Delta F_{T_1}}{T_2 - T_1}\right)_{P,\Delta H} = -\Delta S \qquad (3)$$

where ΔF_{T1} and ΔF_{T2} are the free energies of formation at the temperatures T_1 and T_2, respectively, is exactly true. This is an important point which, though readily derived, is rather likely to be overlooked and so is presented here. A convenient test for the constancy of ΔH and a convenient procedure for calculating ΔH and ΔS at various temperatures when ΔH is not sensibly constant, will also be given.

Integration of the Gibbs-Helmholtz equation

$$\left(\frac{\partial(\Delta F/T)}{\partial T}\right)_P = -\frac{\Delta H}{T^2} \qquad (4)$$

assuming ΔH to be temperature independent, gives

$$\frac{\Delta F}{T} = \frac{\Delta H}{T} + \text{constant} \qquad (5)$$

Comparison of this result with equation 2 shows that the constant of integration is the negative of the entropy change, whence the entropy change is also independent of temperature. Integration of equation 1 then leads directly to equation 3.

Klotz and Fiess made measurements at just two temperatures, whence there is no way of determining whether the enthalpy of formation of the complexes is actually constant over the temperature range taken. If the exact values of the entropies and enthalpies of formation are desired, it is necessary to repeat the measurements at a minimum of one additional temperature. However, their major conclusion, that electrostatic factors play a dominant part in the copper(II)–albumin interaction, receives adequate support from their present data.

Should measurements be made at other temperatures, it would be necessary to calculate ΔH, to determine whether it is constant over the temperature range taken, before calculating ΔS, for, should ΔH prove to be appreciably temperature dependent, ΔS might be. Values of ΔS at the various temperatures would then be most conveniently calculated using equation 2. If it is known that ΔH is appreciably temperature dependent but it is not desired to calculate ΔH for every temperature at which ΔS is to be calculated, average values of ΔS should be calculated using equation 3, employing the smallest possible temperature intervals, and the values of the true derivative (equation 1) at the various temperatures can then be found by the chord-area method.

Integration of equation 4 between limits, assuming that ΔH is constant over the temperature interval of the integration, leads to the expression

$$\left(\frac{T_2\Delta F_{T_1} - T_1\Delta F_{T_2}}{T_2 - T_1}\right)_P = \Delta H \qquad (6)$$

which is more convenient to use than the van't Hoff isochore in those cases where the free energy of formation is found more directly than the equilibrium constant. If ΔH is sensibly constant for the two extreme temperature intervals in the temperature range under consideration (preferably employing small temperature intervals), then ΔH is sensibly constant over the entire temperature range. Otherwise it is not, and the chord-area method, employing average values of ΔH calculated with equation 6, found with the smallest possible temperature intervals, or the van't Hoff isochore, must be

(1) I. M. Klotz and H. A. Fiess, THIS JOURNAL **55**, 108 (1951).

used to determine ΔH at the various temperatures if these values are desired.

(Equation 6 can obviously also be derived by integrating the van't Hoff isochore between limits and solving the result simultaneously with

$$\Delta F^\circ = -RT \ln K \qquad (7)$$

The derivation from the Gibbs-Helmholtz equation, however, is the most fundamental.)

RACEMIZATION RATE STUDIES ON POTASSIUM TRIS-(OXALATO)-CHROMATE(III)

BY GEORGE K. SCHWEITZER AND JOHN L. ROSE, JR.

Department of Chemistry, University of Tennessee, Knoxville,[1] *Tennessee*

Received March 22, 1951

A study has been made of the effect of a number of mixed solvents on the racemization rate of the optically active inorganic complex, potassium dextro-tris-(oxalato)-chromate(III). The solvents used were aqueous solutions of methanol, ethanol, 1-propanol, 2-propanol, acetone and 1,4-dioxane. In all the solvent mixtures the racemization rate decreases with an increase in the concentration of the organic component; however, no definite relationships between the solvent systems could be established. It is believed that the nature of the effect is specific for the complex involved.

The effect of increased temperature on the reaction rate was studied in the cases of the methanol, ethanol and 1-propanol systems. An increase in the reaction rate was noted, as would be expected. However, in the case of the latter two solvent systems, at 35°, little change in the half-time was found over the entire concentration range investigated.

A value of 13,300 cal./mole was found for the energy of activation of the inversion reaction. This is close to an average of the values found by other investigators. The observed molecular rotation of the complex was 4447 degrees as measured at the sodium D line.

Introduction

Until quite recently, no exhaustive studies of the effect that organic solvents have on the racemization of optically active inorganic complex salts had been made. Werner,[2] Bushra and Johnson,[3] and Rideal and Thomas[4] report that the addition of acetone to the water solutions of optically active potassium tris-(oxalato)-chromate(III) has a decelerating effect on the racemization rate, but their experiments were carried out at only a few concentrations of the non-aqueous solvent. Rideal and Thomas[4] attempted to express the action of acetone as a function of its concentration, and they developed an exponential type of equation to represent their data. However, this work was based only on the racemization rates in pure water and in three concentrations of acetone in water.

Schweitzer and Lee[5] turned their attention to the complex tris-(2,2′-dipyridyl)-nickel(II) chloride, and have reported the effects of a number of aqueous organic solvents over a wide range of concentrations.

The purpose of this investigation was to extend the work of previous investigators on the effects of mixed solvents on racemization rates of inorganic complexes. Aqueous solutions of methyl, ethyl, 1-propyl, 2-propyl alcohols, acetone and 1,4-dioxane were chosen as the solvent systems to be used.

Preparation and Resolution

Potassium tris-(oxalato)-chromate(III) was prepared according to the method of Croft[6] from C.P. potassium dichromate, potassium oxalate and oxalic acid. The crystals were dried in a vacuum desiccator over sulfuric acid and subsequently used as the anhydrous salt.

The complex compound was resolved by precipitation of the dextro-isomer with levo-strychnine sulfate. An almost saturated solution of the strychnine sulfate was prepared by dissolving 2.7 g. of l-$(Str)_2{\cdot}H_2SO_4{\cdot}5H_2O$ in 100 ml. of water at room temperature. To this was added 1.0 g. of $K[Cr(C_2O_4)_3]$ in 15 ml. of water. The less soluble l-$(Str)_3d$-$[Cr(C_2O_4)_3]$ formed an immediate precipitate. Three fractions of crystals were collected: those which formed immediately (I), those which formed after standing for 18 hours at 22° (II), and those which formed after standing 24 hours longer at 10° (III). All three fractions can be converted into the active complex, however, the activity of fraction (II) was the greatest followed in order by (III) and (I).

Trituration of the precipitate with an excess of potassium iodide removed the strychnine by precipitation of the very insoluble strychnine iodide. This was removed by filtration, and potassium dextro-tris-(oxalato)-chromate(III) was precipitated from the filtrate by the addition of a large excess of ethyl alcohol. After filtration, the material was dried in a vacuum desiccator over sulfuric acid, and could be preserved under these conditions for several weeks without appreciable loss of activity.

Solvents.—The organic solvents employed were of Eastman White Label or C.P. quality. They were fractionated through a 12-foot Vigreux column at a reflux ratio of approximately 8:1. The following boiling points were observed: methyl alcohol 64.7°, ethyl alcohol 78.3°, 1-propyl alcohol 97.8°, 2-propyl alcohol 82.6°, acetone 56.5° and 1,4-dioxane 101.0°. The organic solvents and the water were measured from burets into glass-stoppered flasks and equilibrated in a constant temperature bath before the active complex was added. In most cases, it was found that the complex dissolved slowly in the mixed solvent, so 1 ml. of water was withheld from the mixture and used to effect initial solution.

Apparatus.—Rotations were observed with a Fric and Fric half shadow polarimeter. The scale of the polarimeter was graduated in quarter degrees, and was read to 0.01 degree with a vernier. A sodium vapor lamp was used to give the predominant sodium doublet at 5890 and 5896 Å.

Measurements were made in a 2-dm. water-jacketed polarimeter tube of approximately 14-ml. capacity. Water was circulated through the jacket at the rate of 2 liters per minute from a water-bath equipped with a mercury thermostat, heater and a zero current relay. The temperature of the water was maintained constant within 0.1°.

Racemization in Water.—Figure 1 shows three typical examples of the quality of data obtained in these experiments. The best line through any set of points was calculated using the method of least squares. These three curves

(1) Contribution No. 100.
(2) Werner, *Ber.*, **45**, 3061 (1912).
(3) Bushra and Johnson, *J. Chem. Soc.*, 1937 (1939).
(4) Rideal and Thomas, *ibid.*, **121**, 196 (1922).
(5) Schweitzer and Lee, THIS JOURNAL, **56**, 195 (1952).
(6) Croft, *Phil. Mag.*, **21**, 197 (1842).

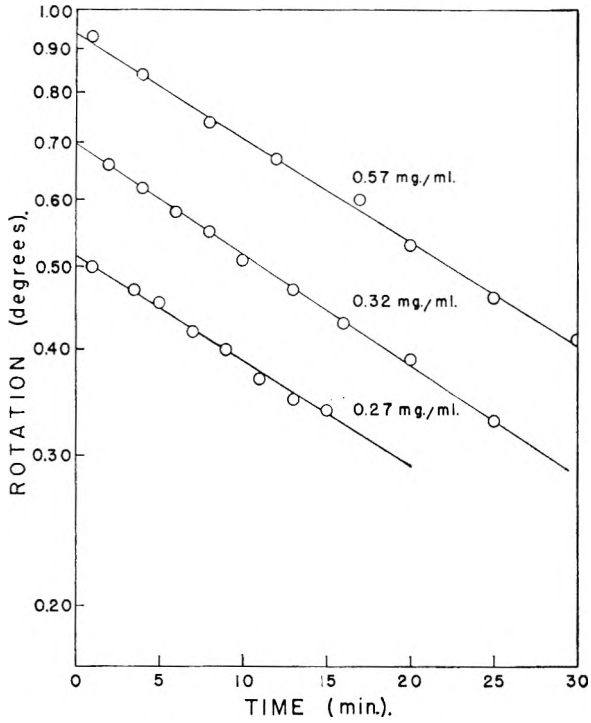

Fig. 1.—Racemization rate of the complex in water at 20°.

also indicate, as would be expected, that the rate of racemization is not affected by the concentration of the complex.

The energy of activation for the conversion of K_3d-[Cr-$(C_2O_4)_3$] to the levo-isomer has been reported as 9650 cal./mole[4] and as 15,750 cal./mole.[3] Figure 2 is a composite of the data from these two investigations along with the results of this work. The line was drawn by the method of least squares and from it the activation energy was calculated to be 12,800 cal./mole. This compares favorably with the value of 13,300 cal./mole calculated from the present data alone.

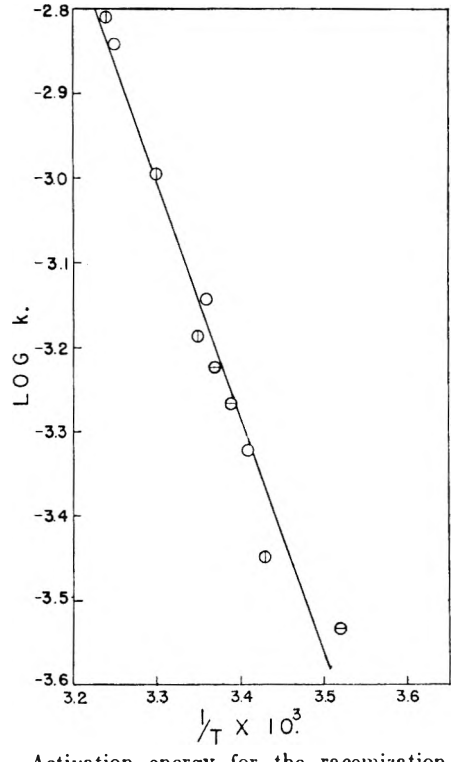

Fig. 2.—Activation energy for the racemization of the complex: ⊕, ref. 3; ⊖, ref. 4; ○, present work.

A check on the molecular rotation was desired, but the very low concentration of complex employed made analysis of the solutions on a weight basis impractical. Since colored solutions of low concentrations usually follow Beer's law, a spectrophotometric analysis seemed applicable. A sample of the complex was purified by repeated recrystallization from aqueous alcohol solution and was dried in a vacuum desiccator over concentrated sulfuric acid. It was used as

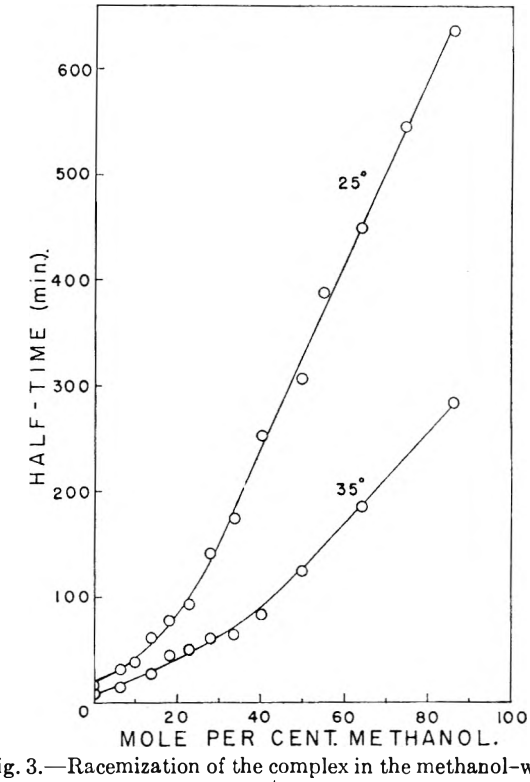

Fig. 3.—Racemization of the complex in the methanol-water system.

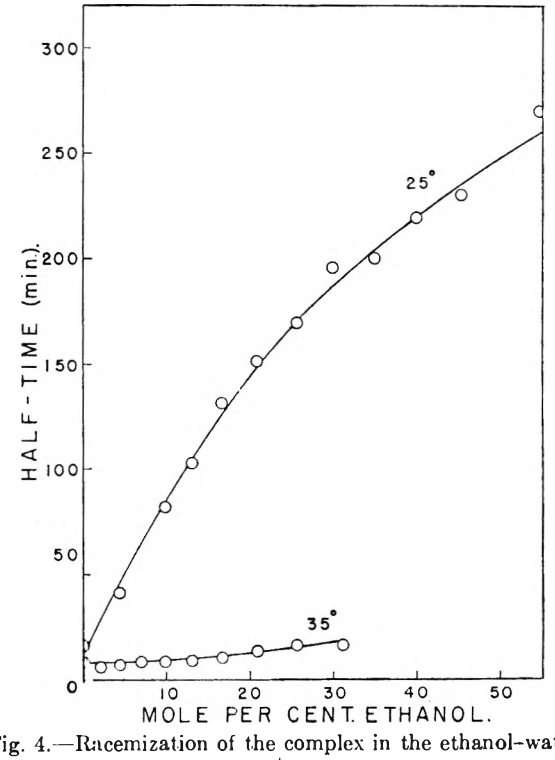

Fig. 4.—Racemization of the complex in the ethanol-water system.

the anhydrous salt to make up a series of solutions of known composition. These solutions were analyzed with a Beckman model DU quartz spectrophotometer, and a calibration curve drawn over the concentration range from 0 to 0.4 mg./ml.

The initial rotations of six solutions were determined by extrapolation of the half-time lines (similar to those in Fig. 1) back to zero time. The concentrations of these solutions were then determined spectrophotometrically. From these data, a solution containing 0.365 mg./ml. of the complex was found to have an initial rotation of 0.76 degree. In terms of molecular rotation, this gives a value of 4447 degrees at the wave length of the sodium doublet. This value was calculated using the convention that molecular rotation equals specific rotation times the molecular weight divided by one hundred.

Racemization in Mixed Solvents.—The effects of aqueous organic solvents on the racemization of the complex are shown graphically in Figs. 3, 4, 5, 6, 7 and 8. In most cases the reaction was run at 25°, this temperature being most convenient to maintain constant.

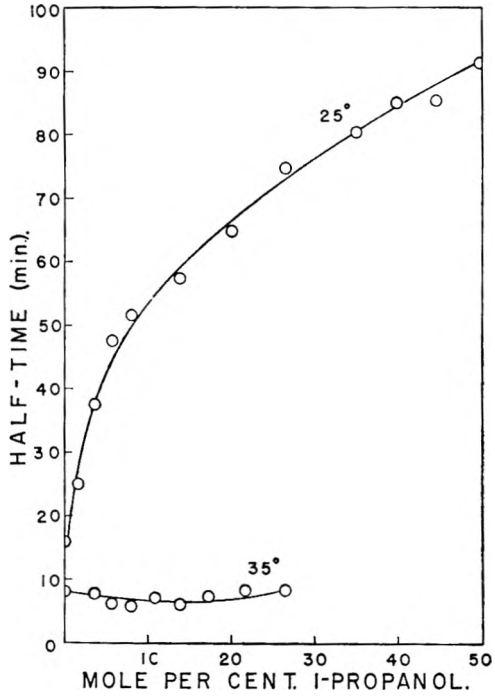

Fig. 5.—Racemization of the complex in the 1-propanol–water system.

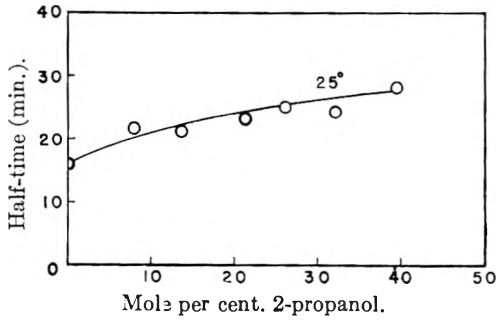

Fig. 6.—Racemization of the complex in the 2-propanol–water system.

The solvents may be divided roughly into three groups according to their action on the reaction. Methanol and acetone have comparatively slight effect at low concentrations, but the effect is markedly increased as the concentration increases. Ethanol and 1-propanol show an action just opposite to this; the increase in the reaction half-time with concentration is large in dilute solutions, but becomes less as the solutions become more concentrated with respect to the organic component. The third group, 2-propanol and 1,4-dioxane, seems to have only a slight decelerating effect on the racemization at all of the concentrations studied.

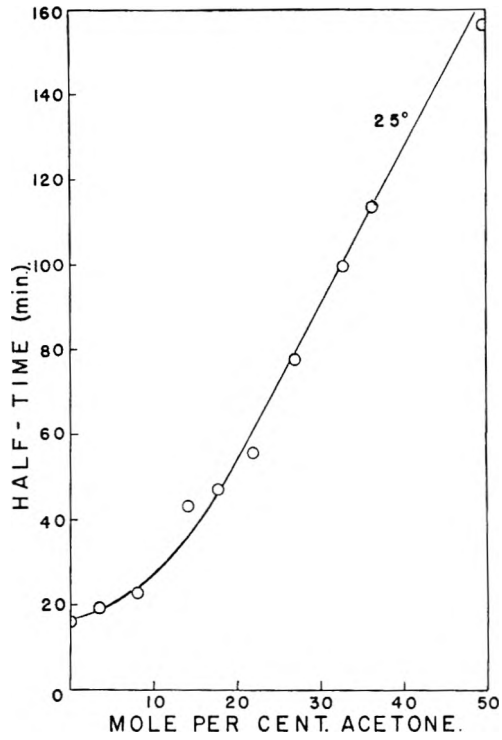

Fig. 7.—Racemization of the complex in the acetone–water system.

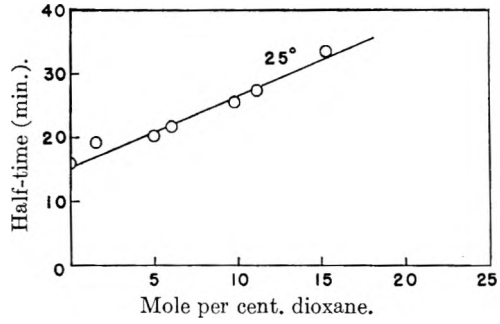

Fig. 8.—Racemization of the complex in the 1,4-dioxane–water system.

As might be expected, the complex was more soluble in the more water-like solvent, *i.e.*, the solubility decreases through the alcohol series from methanol to propanol; also the complex was more soluble in acetone than dioxane. The effect of the solvent on the racemization rate does not follow this trend, in fact at 40 per cent. the reaction proceeds the slowest in methanol and the fastest in 2-propanol. It is interesting to note that the relative decelerating power of the six organic solvents varies at different concentrations. For instance two lists might be developed showing the solvents in order of their decreasing effect at two different concentrations:

10 mole per cent. organic solvent	40 mole per cent. organic solvent
Ethanol	Methanol
1-Propanol	Ethanol
Methanol	Acetone
Acetone	1-Propanol
Dioxane	Dioxane (by extrapolation)
2-Propanol	2-Propanol

Thus it is seen that 2-propanol and dioxane are the only solvents that do not change position on the lists.

As a result of these variations, it is found that the half-time is the same for equal concentrations of different solvents in at least four cases:

Organic component	Concn. (mole %)
Methanol or ethanol	36
Methanol or 1-propanol	15
Acetone or 1-propanol	35
Dioxane or 2-propanol	8

A literature survey of the physical properties of the various pure solvents fails to show any reason for their relative effectiveness in decelerating the racemization to follow the order that was found. However, an extensive study of the aqueous solutions of these solvents might clarify the results.

In the cases of methanol, ethanol and 1-propanol, some work was done at a temperature of 35°. In the methanol system the results were as might have been suspected; the temperature coefficient for the reaction was a little more than two for a 10° rise at all concentrations studied. However, with the other two systems at this temperature, very little change in the reaction rate was noted over the entire concentration range studied. It was confirmed by investigation of the absorption spectra of these solutions that the complex was not decomposing and no other explanation can be offered for the phenomena. It was also noted that the complex seemed to be less soluble in the aqueous solvents at this higher temperature.

Conclusions

The general decelerating effect of organic solvents on the racemization rate of potassium dextro-tris-(oxalato)-chromate(III) is in accord with the findings of previous investigators. Also the activation energy and the molecular rotation value as found in this study show that the reaction studied was identical with that described by other authors. The important fact noted was that the effect of mixed solvents on the racemization rate of an inorganic complex is apparently more specific for the complex than for the solvent system.

Although several accounts are given of the effect of aqueous organic solvents on the racemization of inorganic complexes, the work of Schweitzer and Lee[5] is the only one that is entirely analogous to this. However, comparison of the results of the two investigations shows little similarity. They invariably found one or more maxima in the half-time *versus* mole per cent. organic solvent curves, while in every case the curves were smooth in this instance. This points out the fact that the nature of the complex is probably of prime importance.

The structural relationships between the organic compounds used gives no basis for the formulation of any empirical rules as to what effect a particular solvent will have on a given complex. Assuming there is no interaction between solvent and complex, it would seem that the answer lies in the nature of the solvent in aqueous solution.

Acknowledgment.—The authors wish to express their appreciation to the Research Corporation for the grant which made this work possible.

VISCOSITIES OF 0.25 TO 90% GR-S RUBBER SOLUTIONS[1,2]

BY A. B. BESTUL, H. V. BELCHER, F. A. QUINN, JR., AND C. B. BRYANT

National Bureau of Standards, Washington 25, D. C.

Received April 5, 1951

Solutions of from 0.25 to 90 per cent. of X-518 GR-S rubber (polymerized at 50°) and of X-558 GR-S rubber (polymerized at 5°) in α-methylnaphthalene have been prepared for flow measurements with Bingham viscometers and with the McKee worker-consistometer. A less extensive range of solutions of X-518 GR-S rubber in cetane were also prepared. The higher concentrations were prepared by forced mixing in a helium atmosphere in an internal mixer. Preliminary measurements on the solutions in cetane indicated that any molecular degradation of the rubber by this internal mixer is no greater than that produced by shearing in the worker-consistometer, and that the solutions do not change in viscosity with aging. Bingham viscometers were used for flow measurements on solutions of 10% and less rubber in α-methylnaphthalene at 30 and at 40°. These measurements covered shearing stresses at the capillary wall from 50 to 3,000 dynes/cm.^{2}, and nominal rates of shear at the capillary wall from 35 to 30,000 sec.$^{-1}$. The McKee worker-consistometer was used for measurements on solutions of 10% and more rubber in α-methylnaphthalene at 40 and at 50°. The bulk rubbers were also investigated similarly. These measurements covered shearing stresses at the capillary wall from 2,400 to 6,500,000 dynes/cm.^{2} and nominal rates of shear at the capillary wall from 2.8 to 122,000 sec.$^{-1}$.

The differentiation method was used to reduce the observed data to values for actual rate of shear as a function of shearing stress. Logarithmic plots of rate of shear *versus* shearing stress show that as the concentration of the solutions increases they become increasingly non-Newtonian. Such plots do not show much difference between the behavior of X-518 GR-S solutions and that of X-558 GR-S solutions up to concentrations of about 70%. At higher concentrations, however, the increase of non-Newtonian character with increasing concentration is greater for the X-558 GR-S solutions than for the X-518 GR-S solutions.

Although the concentration variation of the experimentally measured viscosities (ratios of shearing stress to rate of shear) did not follow the relation: viscosity = $(\text{Const}_1)\exp(\text{Const}_2)(\text{conc.})^{1/2}$, the data indicate strongly that this expression would correctly express the viscosity *versus* concentration relation in the limit of zero shearing stress. The variation of viscosity with temperature at fixed shearing stress is of the same magnitude as the variation expressed by the usually quoted values for flow activation energy. The variation at fixed rate of shear is smaller than this by an amount which increases with increasing non-Newtonian character in the flow.

A more sensitive examination of the data at concentrations of 10% and below by plotting apparent fluidity *versus* shearing stress at the capillary wall indicates that the flow of the present solutions does not follow the quadratic flow relation: rate of shear = (Const_1)(shearing stress) + (Const_2)(shearing stress)^2, as do many other high polymer solutions under the same conditions. These plots also support recent observations that as the temperature of polymerization of a rubber is lowered, the flow of its solutions at low concentrations becomes more nearly Newtonian.

Introduction

Existing literature on the flow behavior of solutions of linear amorphous high polymers provides extensive data up to concentrations of several per cent., some data for concentrations up to about 10%,[3] a few data for concentrations up to about 50%,[4-6] but, as far as we have found, no data for the entire concentration range for a given system including a high molecular weight (>100,000) polymer. There have been two principal reasons for this deficiency: (1) lack of adequate flow measuring instruments, and (2) the difficulty of preparing solutions at very high concentrations, where they are extremely viscous.

The development of the McKee worker-consistometer[7] provides an instrument capable of being used for flow measurements over the entire concentration range for such systems except at low concentrations. The problem of preparing highly concentrated, extremely viscous, solutions has been overcome by the use of an internal mixer with counter-rotating sigma-shaped blades.

This paper presents the results of flow measurements with the McKee worker-consistometer, and with Bingham viscometers at low concentrations, over the entire concentration range for solutions of two GR-S rubbers in α-methylnaphthalene, as well as over a less complete concentration range for one of them in cetane. These measurements cover a range of rates of shear, and several different temperatures.

Experimental

Materials.—The two rubbers investigated are one reference lot of ordinary GR-S (designated as X-518 GR-S); and one of "cold" GR-S (designated as X-558 GR-S). Some of their properties are listed in Table I.

TABLE I

PROPERTIES OF RUBBERS INVESTIGATED

Property	GR-S Rubber X-518	X-558
Polymerization temperature, °C.	50	5
Raw Mooney number, ML-4	49	59
Reduced viscosity of 0.25 g./dl. solution in benzene at 25°, dl./g.[a]	2.02	1.89
Approximate styrene content, %	24	24

[a] Measured by June Duke, University of Akron Government Laboratories.[8]

Two solvents were used: α-methylnaphthalene and cetane. The α-methylnaphthalene was obtained by removing most of the impurities from a crude commercial material by passing it through a silica gel column. Mass spectrographic analysis by the Mass Spectrometry Section[9] of this Bureau indicated that the purified material contained 96% methylnaphthalene and 4% of a $C_{11}H_{16}$ hydrocarbon, which is probably hexahydromethylnaphthalene. The cetane was a commercial product sold as a primary reference standard for the determinaion of ignition quality of Diesel fuels.

(1) The work reported herein was sponsored by the Reconstruction Finance Corporation, Office of Rubber Reserve.

(2) Presented at the 58th Meeting of the American Chemical Society Division of Rubber Chemistry, Washington, D. C., February 28, March 1 and 2, 1951.

(3) *Cf., e.g.*, W. Philippoff, "Viskosität der Kolloide," Steinkopff, Dresden and Leipzig, 1942.

(4) C. L. Abernethy, *India-Rubber J.*, **70**, 775 (1925).

(5) L. H. Cragg, L. M. Faichney and H. F. Olds, *Can. J. Research*, **B26**, 551 (1948).

(6) J. D. Ferry, *J. Am. Chem. Soc.*, **64**, 1330 (1942).

(7) S. A. McKee and H. S. White, ASTM Bull. No. 153, 90 (1948); also *J. Research NBS*, **46**, 18 (1951).

(8) June Duke, letter to J. W. Schade, January 30, 1950.

(9) F. L. Mohler, report to attention of L. A. Wood, August 14, 1950.

Solutions of 0.25, 1, 5 and 10% of the two rubbers in α-methylnaphthalene were prepared by placing weighed quantities of rubber and solvent in cylindrical glass jars and rolling them slowly until the charges appeared homogeneous. In addition, solutions of 10, 30 and 50% X-518 GR-S in cetane were prepared by this method, with the modification that when the contents of the jars became so viscous that rolling no longer produced agitation the jars were removed from the roller and inverted every day until the charges appeared homogeneous.

An internal mixer was used to prepare 10, 30, 50, 70 and 90% solutions of both rubbers in α-methylnaphthalene and of X-518 GR-S in cetane. This mixer consists of a stainless steel, water-cooled chamber, in which two motor-driven sigma-shaped blades rotate in opposite directions, thereby thoroughly masticating and blending the components placed in the chamber. The chamber was closed and continuously swept with helium before and during the mixing, so that the only oxygen present for oxidative breakdown during mixing was that which remained adsorbed on the rubber. In preparing the solutions the chamber was first charged with 90% rubber and 10% solvent; this charge was mixed; a weighed quantity of 90% solution was removed; additional solvent was added to the chamber in the proper amount to give a 70% solution; this charge was mixed, and the removal of solution–addition of solvent procedure was repeated successively to produce the 50, 30 and 10% solutions. In order to prevent leakage of the solvent through the packing surrounding the shafts of the mixing blades, this packing was saturated with a neutral silicone lubricant. It was apparent that a small amount of this lubricant worked into the mixing chamber and became dispersed in the blends. It is not thought that this small amount appreciably affected the flow characteristics of the solutions.

Upon standing, the 10% solution in cetane separated into two phases, one containing most of the cetane and the other containing most of the rubber. Obviously this mixture was an unstable suspension rather than a solution. The relative quantities of the two phases from this suspension suggest that the higher concentrations of this system, which appear to be stable solutions, may actually be only suspensions which appear stable over long periods of time because their high viscosities prevent their separation into two phases. Nevertheless, this system was used for the preliminary measurements reported later in this paper. None of the solutions in α-methylnaphthalene showed any indication of separation into more than one phase.

All stocks of solutions were stored in darkness at all times when they were not in use.

Apparatus.—The McKee worker-consistometer and its operation are described in reference 7. In it the experimental material is forced through one of three shearing elements each consisting of 1, 10 and 50 parallel holes, respectively, of about 0.015″ diameter in a 0.25″ thick steel disk. The disk is clamped between flanges on the ends of two steel cylinders, each of which is equipped with a close-fitting piston which is used to force the experimental material through the holes. The shearing is actuated by, and the rate of flow and corresponding pressure drop are measured with, any one of three different driving mechanisms, which are based upon dead-weights, a cam and a reversing-screw, respectively, as described in the above reference.

Three Bingham viscometers having capillary lengths of 12 cm. and radii of 0.0363, 0.0187 and 0.0109 cm., respectively, were used according to the general techniques described by Swindells.[10]

Preliminary Measurements.—To investigate possible molecular degradation of the rubbers during preparation of solutions in the internal mixer, comparisons were made between 10, 30 and 50% solutions of X-518 GR-S in cetane prepared by rolling and therefore presumed not to have suffered any molecular degradation in preparation, and like solutions prepared in the mixer. In the cam-driven worker-consistometer at 100°F. these solutions were repeatedly forced back and forth through the shearing element at a given nominal rate of shear (D), and the driving load recorded as a function of the number of times a sample had been passed through the capillaries. These records are shown in Fig. 1. The nominal rate of shear (D) used for each solution was the highest value the instrument could accommodate for the concentration (viscosity) concerned. These values (shown in Fig. 1) were different for the three concentrations since a 1-hole shearing element was used with the 10% solutions, a 10-hole with the 30% and a 50-hole with the 50%.

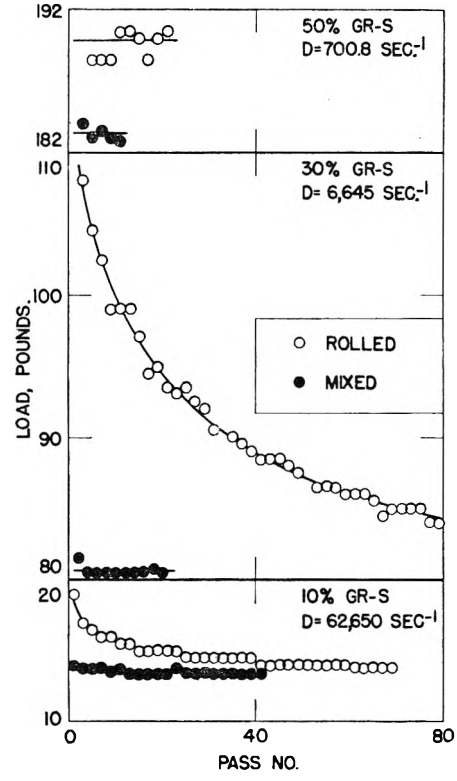

Fig. 1.—Comparison of rolled and mixed solutions in cetane.

The above-mentioned data provide some indication of the properties of the rubber solutions during shearing. Figure 1 shows that the 10 and 30% rolled solutions suffered degradation when they were sheared in the worker-consistometer, whereas the mixed solutions did not, but that the (constant) apparent viscosities indicated for the mixed solutions have about the same values that would be reached by the rolled solutions at the completion of their degradation. This implies that a degradation similar to that occurring in the rolled solutions during shearing in the worker-consistometer had occurred previously, presumably during preparation, in the mixed solutions. Therefore, at 10 and and at 30% concentrations, the preparation of solutions in the internal mixer does result in some molecular degradation of the rubbers; however, this degradation is no more than would occur during shearing in the worker-consistometer, so its effects cannot be avoided in the results of worker-consistometer measurements and there is no disadvantage to its occurring during the preparation of the solutions.

In contrast to the behavior for the 10 and the 30% solutions, the apparent viscosities indicated in Fig. 1 for the two 50% solutions are both constant and are not very different. It is assumed that the rolled solution was not degraded during preparation, and Fig. 1 shows that it is not degraded by shearing in the worker-consistometer. Therefore, Fig. 1 implies that at concentrations as high as 50%, solutions are not degraded very much by preparation in the internal mixer. To examine this implication, a sample of bulk X-518 GR-S which had been masticated for four hours in the internal mixer, and a second sample which had not been so masticated, were placed in the worker-consistometer and forced back and forth through the shearing element for a number of passes at a fixed nominal rate of shear. Figure 2 shows the load as a function of the number of passes for these two samples. The behavior shown by the bulk rubber is very similar to that of the 50% solution. Neither the masticated nor the unmasticated rubber is degraded by shearing in the worker-consistometer, and a comparison with the unmasticated sample indicates that the masticated sample was not degraded very much by mastication in the internal mixer.

(10) J. F. Swindells, *J. Colloid Sci.*, **2**, 177 (1947).

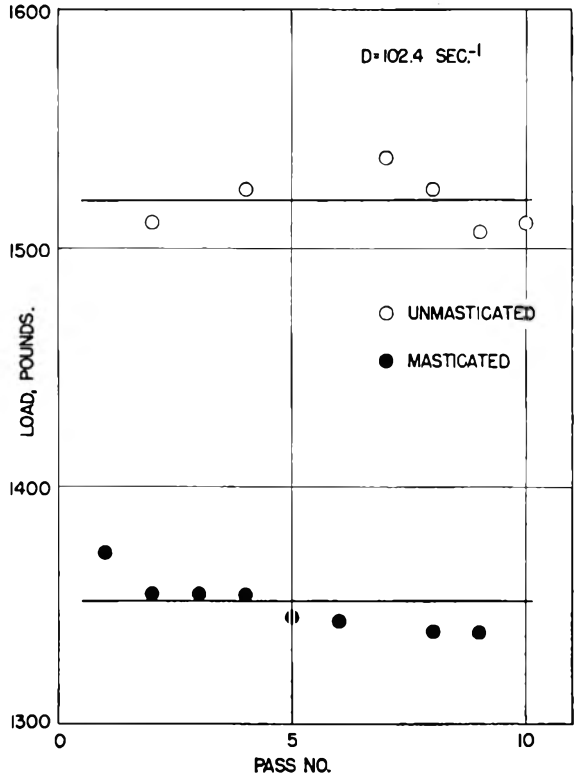

Fig. 2.—Comparison of masticated and unmasticated X-518. GR-S.

To demonstrate that the results on mixed solutions and on rolled solutions which have undergone any degradation produced by the worker-consistometer are similar at all nominal rates of shear investigated, and not only at those in Fig. 1,

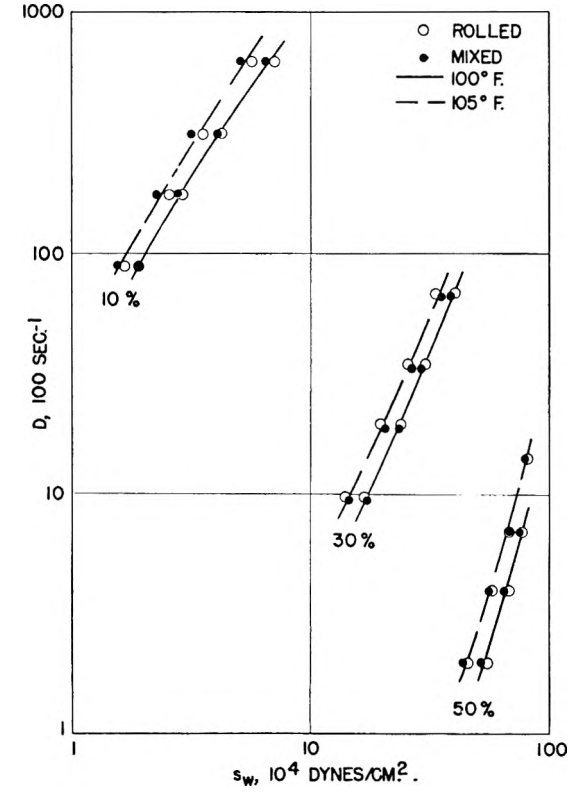

Fig. 3.—Flow curves: rolled *versus* mixed solutions, in cetane.

flow curves were determined for the above 10, 30 and 50% solutions over a range of nominal rates of shear at 100 and at 125°F. These results are shown in Fig. 3 as plots of nominal rate of shear (D) *versus* shearing stress at the capillary wall (s_w). Reasonable agreement is shown between the results for the mixed solutions and those for the rolled solutions.

Since many instances have been observed, in this and other laboratories,[11] where the viscosities of polymer solutions changed markedly on aging of the solutions, a test was made for the presence of such an effect in the 70% solution of X-518 GR-S in cetane. This concentration was selected as being the most likely to show this effect because during the first few days after it was prepared it underwent a change in appearance, now thought to have been only a slow flowing together of lumps formed by the mixer. Four days after the solution was prepared a flow curve was determined for it over a range of nominal rates of shear at 100°F. Sixty days later these measurements were repeated. The results of both sets of measurements are shown in Fig. 4 as plots of nominal rate of shear (D) *versus* shearing stress at the capillary wall (s_w). The results for the fresh and for the aged solutions were identical within the uncertainty of the measurements. It is concluded that the viscosities of the solutions reported herein did not change with aging over the duration of the investigation reported.

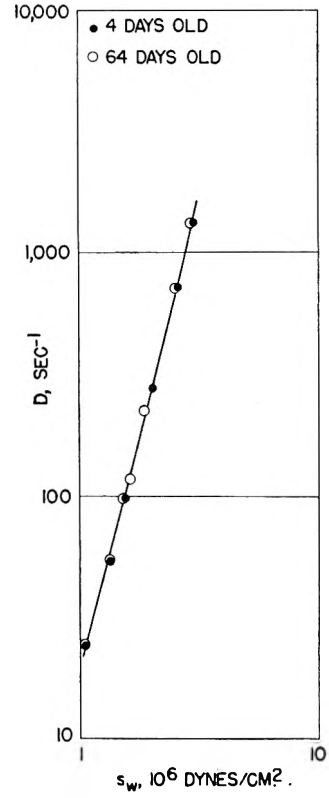

Fig. 4.—Effect of aging: 70% solution in cetane.

Principal Measurements.—Flow measurements were made on the 30, 50, 70 and 90% solutions of X-518 GR-S and X-558 GR-S rubbers in α-methylnaphthalene, and on the rubbers themselves (which will hereafter be referred to as 100% solutions) with a screw-driven McKee worker-consistometer. These measurements were made at 40 and at 50°, the accuracy of the thermostating in the worker-consistometer usually being about ±0.5°. The measurements covered nominal rates of shear (D) from 2.8 to 4,700 sec.$^{-1}$ and shearing stresses at the capillary wall (s_w) from 28,000 to 6,500,000 dynes/cm.^{2}; however, this total range was not covered for each solution.

Worker-consistometer measurements on the (mixed) 10% solutions in α-methylnaphthalene were made with the dead

(11) *Cf.*, *e.g.*, H. Campbell and P. Johnson, *J. Polymer Sci.*, **4**, 443 (1950).

weight-driven apparatus at 40 and at 50°, with nominal rates of shear from 190 to 122,000 sec.$^{-1}$ and shearing stresses at the capillary walls from 2,400 to 190,000 dynes/cm.^{2}. Flow measurements were also made with Bingham viscometers on these 10% solutions as well as on 0.25, 1, 5 and 10% rolled solutions in α-methylnaphthalene. These measurements were made at 30 ± 0.1° and 40 ± 0.1°, and covered nominal rates of shear from 30 to 30,000 sec.$^{-1}$ and shearing stresses at the capillary walls from 50 to 3,000 dynes/cm.^{2}.

The quantities which are directly observed in measurements with any of the instruments used are the time required for a given amount of flow through a capillary and the pressure drop, or the load, across the capillary. These are readily converted into volume rate of flow through the capillary (Q) and pressure drop across it (P), which in turn are converted into nominal rate of shear (D) and shearing stress at the capillary wall (s_w) by the usual expressions

$$D = 4Q/\pi R^3 \quad \text{and} \quad s_w = PR/2L \qquad (1)$$

where R and L are the radius and the length, respectively, of the capillary. The actual rate of shear at the capillary wall ($\dot{\gamma}_w$) is obtained from D and s_w by the relation

$$\dot{\gamma}_w = (D/4)(3 + \text{d log } D/\text{d log } s_w) \qquad (2)$$

which is obtained by the differentiation method for reducing observed data to fundamental rheological quantities.[12] The term d log D/d log s_w is evaluated by plotting the observed values for log D *versus* log s_w and measuring the slope of this plot at the value of s_w concerned.

The results of all the flow measurements on the α-methylnaphthalene solutions are given in Fig. 5 as logarithmic plots of $\dot{\gamma}_w$ *versus* s_w. The fact that we dealt with conditions existing at the capillary walls has no significance after the data have been reduced to the fundamental quantities shearing stress and rate of shear. Therefore, the plots in Fig. 5 are the general log $\dot{\gamma}$ *versus* log s plots for the solutions.

Discussion

A desirable way of studying the effect of concentration on the flow properties of the solutions would be to find analytical representations for the flow curves in Fig. 5, and to observe the effect of concentration on these analytical expressions. Since no one has yet succeeded in finding generally successful tractable analytical representations for such curves, this approach cannot be followed. A less adequate, but still informative, approach is to observe the effect of concentration on certain specific properties of the flow curves. Two properties of the curves which are convenient for this purpose are the slope (which gives a measure of the deviation of the flow from Newtonian) and the ratio of shearing stress to rate of shear.

For Newtonian flow, log $\dot{\gamma}$ *versus* log s plots are straight lines having a slope of unity. For such plots the above ratio is constant. Any deviation of the log $\dot{\gamma}$ *versus* log s plot for a material from a slope of unity is a demonstration of the presence of non-Newtonian flow. The magnitude of the deviation of the slope from unity is some measure of the magnitude of the deviation of the flow from Newtonian. None of the curves in Fig. 5, except those for the pure solvent, are straight lines with slopes of unity. Therefore, non-Newtonian flow occurs in these solutions at all concentrations. Furthermore, in general, the slopes of the curves (deviations from Newtonian flow) increase with concentration.

(12) *Cf., e.g.*, Turner Alfrey, Jr., "Mechanical Behavior of High Polymers," Interscience Publishers, Inc., New York, N. Y., 1948, p. 41.

When the slope of the log $\dot{\gamma}$ *versus* log s plot is different from unity, the ratio of shearing stress to rate of shear is not constant for a given material. Therefore, a numerical value of this ratio must be accompanied by a specification of the point on the curve to which it applies. Many authors[13] call this variable ratio the viscosity, η, which is the same designation applied to the same (constant) ratio in Newtonian flow. This nomenclature is adopted in this paper. When a plot of log $\dot{\gamma}$ *versus* log s is non-linear, as are those for the higher concentrations in Fig. 5, the slope is also not constant for a given material, and numerical values of the slope must also be accompanied by a specification of the points on the curve to which they apply.

The points on the flow curves for which values of the viscosity and of the slope are to be given could be specified in various ways, but two obvious ways are at fixed $\dot{\gamma}$ and at fixed s. Both of these ways are used in this paper, though it is obvious from inspection of Fig. 5 that larger ranges of concentration may be studied at constant $\dot{\gamma}$ than at constant s.

(1) **Deviation from Newtonian Flow.**—Figure 6 shows plots of the slopes of the log $\dot{\gamma}$ *versus* log s plots (d log $\dot{\gamma}$/d log s) against concentration at several given values of $\dot{\gamma}$ at 40°. These plots demonstrate clearly that the slopes of the log $\dot{\gamma}$ *versus* log s plots (deviations from Newtonian flow) do indeed increase with concentration. The plots also show an increase of slope with increasing rate of shear at a given concentration. This would also be expected from the general shape of the log $\dot{\gamma}$ *versus* log s curves as long as one restricts one's considerations to rates of shear below those at which inflections, such as those shown for the 10% solutions in Fig. 5, occur. Such inflections are usually found for polymer solutions at sufficiently high

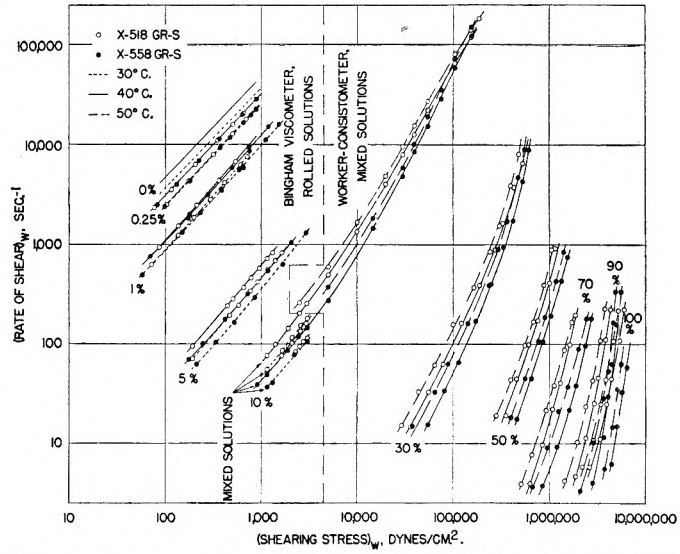

Fig. 5.—Flow curves for solutions of X-518 GR-S and X-558 GR-S in α-methylnaphthalene.

(13) *Cf., e.g.*, J. M. Burgers and G. W. Scott-Blair, *Proceedings of the International Congress of Rheology, Holland, 1948*, North-Holland Publishing Co. (Amsterdam), 1949, p. V-1.

rates of shear,[14] but they have never been observed in experimentally determined flow curves for bulk polymers.

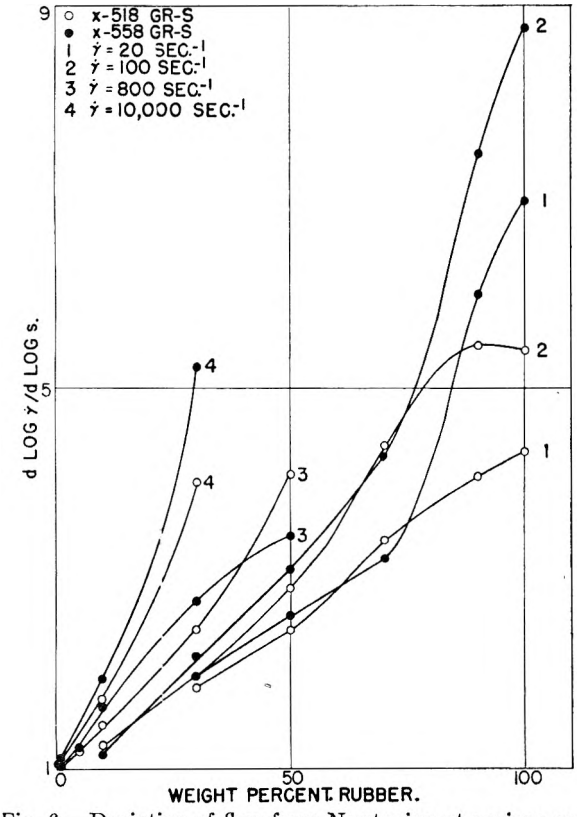

Fig. 6.—Deviation of flow from Newtonian at various concentrations, fixed γ, in α-methylnaphthalene.

From the plots in Fig. 6 it is difficult to detect any marked differences in the behaviors of the solutions of X-518 GR-S and of X-558 GR-S at low concentrations. It is very noticeable, however, that, at the temperature concerned here, at concentrations above 70% rubber the slopes (deviations from Newtonian flow) increase much more rapidly with concentration for the X-558 GR-S solutions than for the X-518 GR-S solutions. This situation is in agreement with the fact that at 100° bulk X-558 GR-S is markedly more non-Newtonian than bulk X-518 GR-S at rates of shear of about 20 sec.$^{-1}$ or above.[15] This difference in the behaviors of the two rubbers is probably not generally applicable to "cold" and regular GR-S's in general since another GR-S polymerized at 5°, X-478 GR-S, shows deviations from Newtonian flow which are about equal to those of X-518 GR-S.[15] Figure 7 shows plots of d log $\dot{\gamma}$/d log s *versus* concentration at several given values of s at 40°. Because of the limited concentration range which can be observed at a given shearing stress it is impossible to draw any wide-spread conclusions from these plots. The fact that over most of the narrow ranges considered, the slope decreases with increasing concentration cannot be true over the entire concentration range. It is merely a result of the fact that the spread of the flow curves with

(14) Ref. 3, pp. 113–129.

(15) A. B. Bestul G. E. Decker, and H. S. White, *J. Research NBS*, to be published April, 1951, Vol. 46.

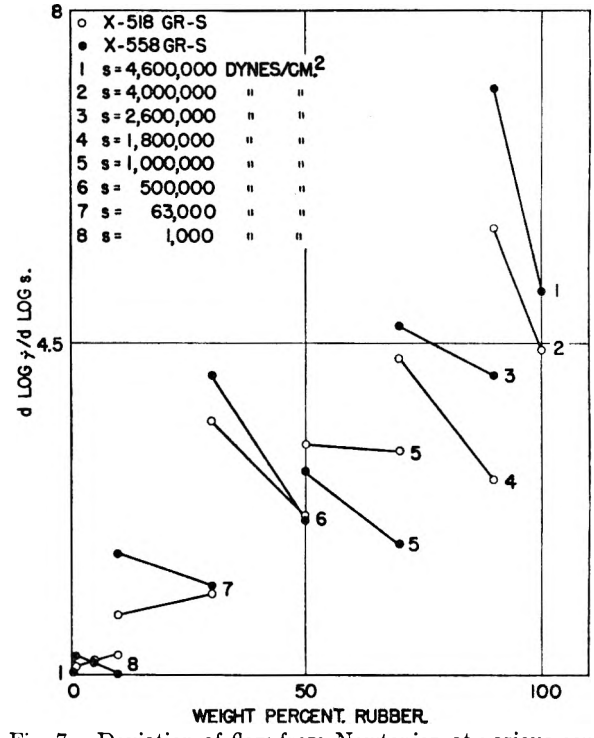

Fig. 7.—Deviation of flow from Newtonian at various concentrations, fixed s, in α-methylnaphthalene.

concentration is greater normal to the s-axis than to the $\dot{\gamma}$-axis. This situation is generally true for a family of flow curves for different concentrations (*cf.*, *e.g.*,[14]).

(2) **Viscosities.**—Figure 8 shows plots of viscosity on logarithmic coördinates *versus* concentra-

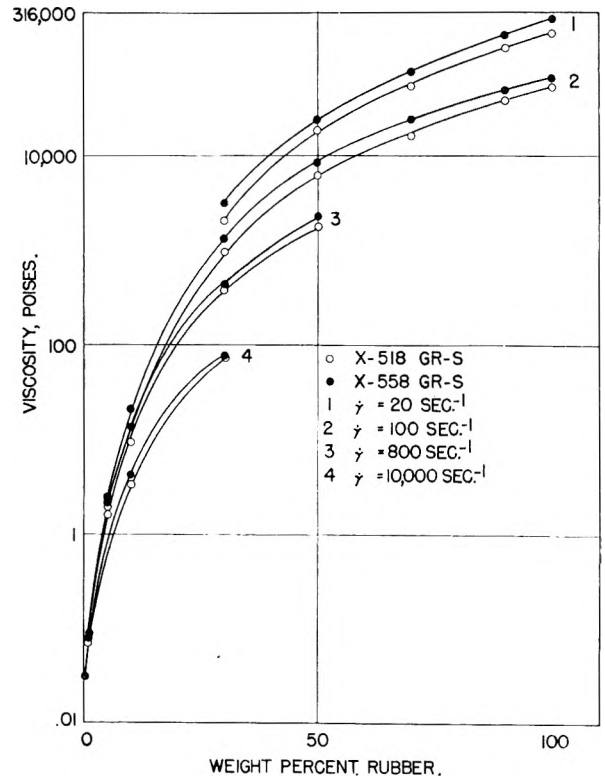

Fig. 8.—Viscosity *versus* concentration at several fixed values of γ, in α-methylnaphthalene.

tion for several given values of $\dot{\gamma}$ at 40°. These plots look very similar to those given by Abernethy[4] for concentrations up to about 50% of natural rubber in benzene and in toluene. Abernethy's data for concentrations above about 1% rubber gave straight lines for plots of log viscosity *versus* square root of concentration. Cragg,[5] Flory,[16] and Spencer and Williams[17] have also found such a relation applicable to concentrated polymer solutions. The present data at 100 sec.$^{-1}$ and 40° are shown plotted in this manner in Fig. 9. For concentrations up through 10% the points fit straight lines reasonably well, but above that the points form lines which are markedly concave toward the concentration axis. It should be pointed out that in the above cited cases where the relation

$$\eta = (\text{Const}_1) \exp (\text{Const}_2)(\text{conc.})^{1/2} \qquad (3)$$

did hold the viscosities were presumably those at low rates of shear; whereas the data in Fig. 9 are for a relatively high rate of shear. Since as the rate of shear decreases the viscosity increases proportionately more rapidly for higher concentrations than for lower, the plots in Fig. 9 would tend to straighten out as the rate of shear decreases. This raises the possibility that the present systems may follow equation (3) for all higher concentrations at the limit of zero rate of shear. If the straight lines in Fig. 9 are extrapolated to the bulk rubber, they give viscosity values of the order of 10^8 poises. Recent measurements[18] show that certain GR-I rubbers, which have about the same viscosities as the present GR-S's at rates of shear around 1 sec.$^{-1}$ have indeed viscosities as high or higher than 10^8 poises at very low rates of shear (*e.g.*, η = 400,000,000 poises at $\dot{\gamma}$ = 0.001 sec.$^{-1}$). Therefore although the present data do not fit equation (3), they indicate that, except at low concentrations, the flow behaviors of the present systems do follow this relationship at the limit of zero rate of shear.

It may be mentioned in passing that at a rate of shear of 100 sec.$^{-1}$ the present data for concentrations above about 5% rubber form nearly straight lines when plotted as log η *versus* log concentration. However, from the discussion of the preceding paragraph it is clear that this linearity can exist only at a certain value of $\dot{\gamma}$, and that at lower $\dot{\gamma}$'s such a plot will be concave toward the viscosity axis. Since the linearity for the present data applies only under such limited conditions, it is not treated further here.

No significant difference between the behaviors of X-518 GR-S and of X-558 GR-S can be detected from the relation between viscosity and concentration in concentrated solutions.

Inspection of Fig. 5 shows immediately that the variation of viscosity with concentration is much greater at fixed s than at fixed $\dot{\gamma}$. This is a necessary consequence of the slopes of the log $\dot{\gamma}$ *versus* log s plots being greater than unity. Since the range of concentration which can be observed at a given value of s is so limited, and since the situation

(16) P. J. Flory, THIS JOURNAL, **46**, 870 (1942).
(17) R. S. Spencer and J. L. Williams, *J. Colloid Sci.*, **2**, 117 (1947).
(18) G. E. Decker, to be published.

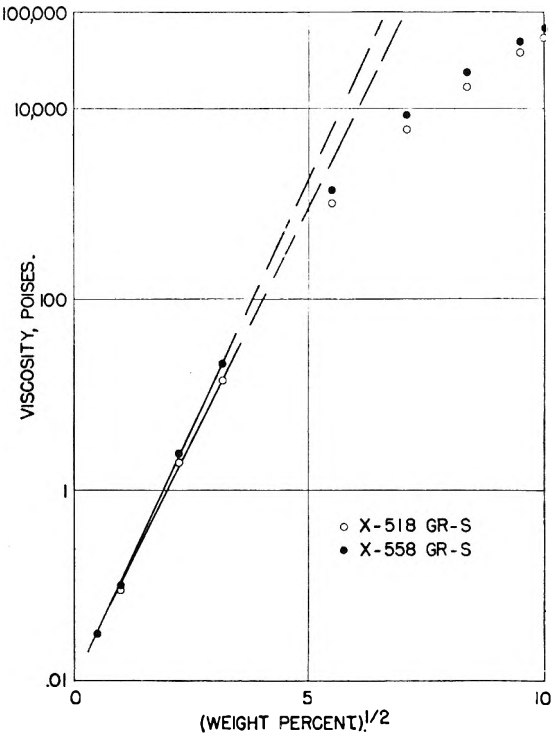

Fig. 9.—Log viscosity *versus* square root of concentration, γ = 100 sec.$^{-1}$, in α-methylnaphthalene.

is shown so clearly in Fig. 5, no plots at fixed s are given here.

(3) Variation of Viscosity with Temperature.—It is seen from Fig. 5 that the variation of the viscosity of concentrated solutions with temperature is greater at fixed s than at fixed $\dot{\gamma}$. This is also necessarily coexistent with log $\dot{\gamma}$ *versus* log s slopes greater than unity. One inquires whether either the variation at fixed $\dot{\gamma}$ or that at fixed s is of approximately equal magnitude with that variation expressed by the statement that the energy of activation of flow (E_{vis}) of the bulk polymer is about 13.0 kcal./mole around room temperature.[5]

E_{vis} is a complete measure of the temperature variation of viscosity in Newtonian flow. It arises from the relation

$$\eta = (\text{Const}) \exp E_{vis}/RT \qquad (4)$$

where R is the gas constant and T is the absolute temperature. E_{vis} is evaluated as R times the measured slope of a plot of ln η *versus* $1/T$(°K.). For non-Newtonian flow the relation (4) does not hold; there is not necessarily a complete correspondence between E_{vis} and the temperature variation of viscosity, and the above simple method of evaluating E_{vis} cannot correctly be used.

Stating a value of E_{vis} for a material constitutes an implication that the flow concerned is Newtonian. When a value of E_{vis} is given for a material such as a bulk polymer, the flow of which is known to be in general non-Newtonian, it is usually considered that the measurements were made at rates of shear low enough so that the flow is only negligibly different from Newtonian, or that the results have been extrapolated to zero rate of shear, where the flow is considered to be Newtonian. Since neither of these conditions are met by the present

TABLE II

VARIATION OF VISCOSITY WITH TEMPERATURE

Material	Δ^a from E_{vis}	E_{vis},[a] kcal./mole monomer	Δ^a at const $\dot{\gamma}$	const $\dot{\gamma}$, sec.$^{-1}$	Δ^a at const s	const s, dynes/cm.^{2}
100%	0.281	13.0	0.08	6.3	0.24	2,500,000
X-518 GR-S			.06	160	.30	4,600,000
50%	.199	9.2	.09	20	.19	320,000
X-518 GR-S			.05	630	.23	1,100,000
10%	.0886	4.1	.08	250	.09	2,500
X-518 GR-S			.05	4,000	.08	20,000
			.05	126,000	.08	160,000

[a] $\Delta = -10\ (\Delta \log \eta/\Delta T)$; ΔT = 40 to 50°.

data, the temperature dependence for it cannot be represented by values for E_{vis}. However, literature values for E_{vis} can be converted to values of $\Delta \log \eta/\Delta T$ and these compared with the present experimental values.

Table II gives values of $\Delta \log \eta/\Delta T$ obtained from the present data for the X-518 GR-S solutions and like values calculated from values of E_{vis} estimated by Cragg[5] for a GR-S system. It is clearly indicated that in different regions of the flow curves the temperature variation of viscosity at constant s remains roughly the same as that calculated from the energy of activation, whereas the variation at constant $\dot{\gamma}$ deviates widely from such a value. This can probably be interpreted as evidence that as the temperature is varied for a given material the nature of the flow remains the same if s is held constant and $\dot{\gamma}$ allowed to vary, but changes if $\dot{\gamma}$ is held constant and s allowed to vary. This picture of shearing stress, rather than rate of shear, as the determining factor in non-Newtonian flow (or at least as the more determining factor of the two) is in agreement with the fact that the onset of a marked non-Newtonian character in the flow of materials of different viscosities occurs at rates of shear which are different by amounts which cannot be explained by the differences in the molecular weights of the materials alone, but at shearing stresses which are different by amounts no greater than can be explained by the molecular weight differences alone. This situation is also found in the theoretical equations for non-Newtonian flow such as those developed by Eyring, *et al.*,[19] Bondi,[20] and Grunberg and Nissan[21]; a marked non-Newtonian character of the flow sets in at a critical shearing stress, which does not vary with the viscosity of the material concerned (except through molecular weight), although the corresponding rate of shear does then necessarily vary directly with the viscosity.

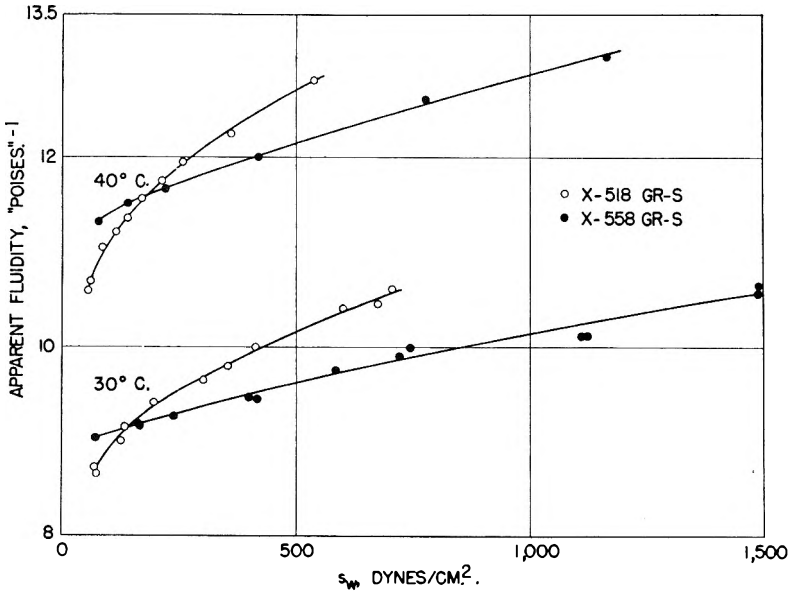

Fig. 10.—Comparison of 1% solutions of X-518 GR-S and X-558 GR-S rubbers in α-methylnaphthalene.

(4) **Low Concentrations.**—Flow data for solutions of lower concentrations have sometimes been analysed with greater sensitivity than above by using the quadratic flow equation

$$\dot{\gamma} = as + bs^2 \qquad (5)$$

where a and b are constants, which was suggested by Ferry,[6] and has recently found a number of instances of application.[22,23]

If the flow of a material follows this relation, a plot of D/s_w (the apparent fluidity) *versus* s_w will be a straight line. For a Newtonian material the plot will be a horizontal straight line ($b = 0$). The intercept of such a straight line will give a (an inverse measure of the viscosity of the material at zero shearing stress) and the slope will give b, which measures the deviation of the flow from Newtonian. The flow of many high polymer solutions at lower concentrations has been found to follow equation (5) except above inflections such as those shown for the 10% solutions in Fig. 5.[6,22,23] Equation (5) cannot describe such an inflection, nor can it hold at concentrations for which the slopes in Fig. 5 are greater than two.

Figure 10 shows plots of apparent fluidity *versus* s_w for the 1% solutions of X-518 GR-S and of X-558 GR-S in α-methylnaphthalene at 30 and at 40°. The data shown here are those at comparatively low s_w's, obtained in a Bingham viscome-

(19) S. Glasstone, K. J. Laidler, and H. Eyring, "The Theory of Rate Processes," McGraw-Hill Book Co., Inc., New York, 1941.

(20) A. Bondi, *J. App. Phys.*, **16**, 539 (1945).

(21) L. Grundberg and A. H. Nissan, *Nature*, **156**, 241 (1945).

(22) H. Leaderman, R. G. Smith, and R. W. Jones, to be published.

(23) A. B. Bestul and H. V. Belcher, *J. Colloid Sci.*, **5**, 303 (1950).

ter. It is immediately obvious that the plots are not straight lines, and that therefore these solutions do not follow equation (5). The data at concentrations of 0.25, 5 and 10% are not shown here, but also indicate the same situation. Solutions of X-518 GR-S in *o*-dichlorobenzene at low concentrations are known to follow equation (5).[23] The failure of the present systems to follow this relation suggests that the interaction of the rubber with α-methylnaphthalene is different from that with *o*-dichlorobenzene and other, more common, solvents.

A second noticeable feature in Fig. 10 is that the plots for the two different rubbers intersect. This is also shown by the data for the 0.25% solutions (not shown here), but not for any higher concentrations, although those for the 5% solutions suggest a possible intersection at shearing stresses lower than used here. These results are in agreement with the reduced viscosity values given in Table I, which show that at low shearing stresses, dilute solutions of X-558 GR-S are less viscous than corresponding solutions of X-518 GR-S, although under most other conditions X-558 GR-S systems are more viscous than corresponding X-518 GR-S systems. Figure 10 is also in agreement with unreported previous measurements of this and other laboratories which indicate that, in general, as the polymerization temperature of a polymer is lowered, other things remaining equal, the flow of the polymer's dilute solutions becomes more nearly Newtonian, and the solutions become less viscous. Although X-558 GR-S is polymerized to a higher raw Mooney number than X-518 GR-S its polymerization temperature is lower, and the effect of this shows up over the effect of the higher raw Mooney number. The comparatively small slopes for the X-558 GR-S solutions in Fig. 10 show that they are more nearly Newtonian than those of X-518 GR-S, and the larger non-Newtonian effect in the X-518 GR-S solutions finally brings their viscosities up (fluidities down) beyond those of the X-558 GR-S solutions. It seems likely that this effect is associated with the relatively greater content of *trans*-1,4-adducts in the lower temperature polymerizate,[24] although a specific explanation has not yet been developed.

(24) E. J. Hart and A. W. Meyer, *J. Amer. Chem. Soc.*, **71**, 1980 (1949); also Hampton, *Anal. Chem.*, **21**, 923 (1949).

VIBRATING MICRO-ELECTRODES IN POLAROGRAPHY. THE RELATIONSHIP BETWEEN DIFFUSION CURRENT AND FREQUENCY AND AMPLITUDE OF VIBRATION

By A. J. Lindsey

Sir John Cass College, London, England

Received March 28, 1951

The relationship between diffusion curent and frequency and amplitude of vibration of platinum micro-electrodes has been studied and it has been shown that at low speed the diffusion current is proportional to both amplitude and frequency. At higher speeds (> 16 cm./sec.) there is no appreciable increase in current with increase in frequency or amplitude. It is therefore recommended that vibrating micro-electrodes be used with amplitude and frequency sufficient to ensure a constant average relative speed of about 25–30 cm. per second. The apparatus employed for testing vibrating electrodes is described and a method of using them in polarography and amperometric titration is given.

Introduction

In a previous publication,[1] it was announced that reproducible polarograms may be obtained with platinum micro-electrodes vibrating at a constant frequency. A more complete study of the behavior of these electrodes has now been made and their application in polarography has been studied.

Diffusion at stationary electrodes has been studied by a number of workers,[2–5] who have shown the diffusion currents to be proportional to concentrations. The accuracy with which this relationship holds depends upon the constancy of the thickness of the diffusion layer. The thickness is considerable (*e.g.*, 0.3 mm.) with stationary electrodes in unstirred solutions and those factors which hinder the establishment of a diffusion layer of constant thickness or which tend to vary its thickness will affect the current produced. It is well known that at constant temperature the current due to an electrode process at a stationary electrode is given by the equation

$$i = (AD/l)nF(C - C_0) \qquad (1)$$

where

A is the electrode area,
D is the diffusion coefficient of the substance reacting,
l is the effective thickness of the diffusion layer,
n is the number of electrons reacting in the process,
C is the concentration of the electro-active species in the solution,
C_0 is the concentration of the species at the electrode surface, and
F is the Faraday constant.

When the diffusion current is established, C_0 is very small and equation (1) becomes

$$i_d = (AD/l)nFC \qquad (2)$$

where i_d is the diffusion current.

Diffusion currents at stationary electrodes may be measured with an accuracy within 1% if the temperature is kept constant (±0.01°) and if external vibration is prevented.[5] The main dis-

(1) E. D. Harris and A. J. Lindsey, *Nature*, **162**, 413 (1948).
(2) S. Glasstone, *Trans. Am. Electrochem. Soc.*, **59**, 277 (1931).
(3) S. Glasstone and G. D. Reynolds, *Trans. Faraday Soc.*, **29**, 399 (1933).
(4) R. E. Wilson and M. A. Youtz, *Ind. Eng. Chem.*, **15**, 603 (1923).
(5) H. A. Laitinen and I. M. Kolthoff, *J. Phys. Chem.*, **45**, 1061 (1941).

advantages of stationary electrodes in polarography are (i) that it is necessary to await for at least two minutes for constant diffusion conditions and thus for a steady value of the current to be attained and (ii) that external vibration affects the thickness of the diffusion layer and therefore the diffusion current.

Kolthoff and Laitinen eliminated these disadvantages by employing rapidly rotating micro-electrodes.[5] Such electrodes had been studied previously, but less exhaustively, by other workers.[6,7,8] The main advantage of the rotating electrode is that the diffusion layer is much thinner than with a stationary electrode. As a result of this, the diffusion current is larger and attains constant value sooner. In addition a rotating electrode is less sensitive to external vibration and the effective thickness of the diffusion layer does not vary appreciably with temperature. The change of diffusion coefficient with temperature then becomes the significant effect. However, the main disadvantage of the rotating electrode is that the speed of rotation must be very constant. Kolthoff and Laitinen have described an elaborate synchronous motor to achieve the necessary constant speed, and thus ensure a constant diffusion current.

Müller[9] has obtained constant diffusion conditions by using a fixed micro-electrode and passing the electrolyte steadily by it at a constant rate. This technique is not suitable for the more ordinary methods of polarographic measurement.

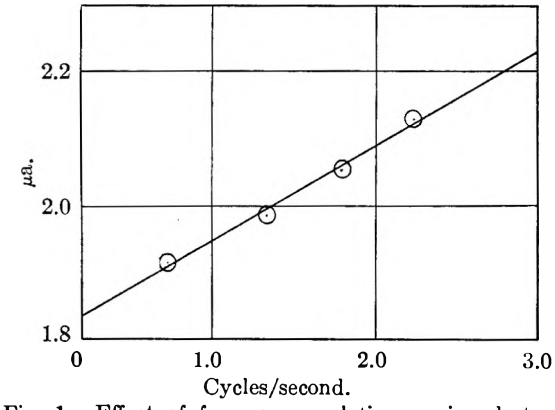

Fig. 1.—Effect of frequency: platinum wire electrode area 0.0460 sq. cm.; temp. 14°, bromate–bromide equivalent to 0.00297 g. equiv./l. in $N/5$ KCl + HCl supporting electrolyte; amplitude 0.58 cm.

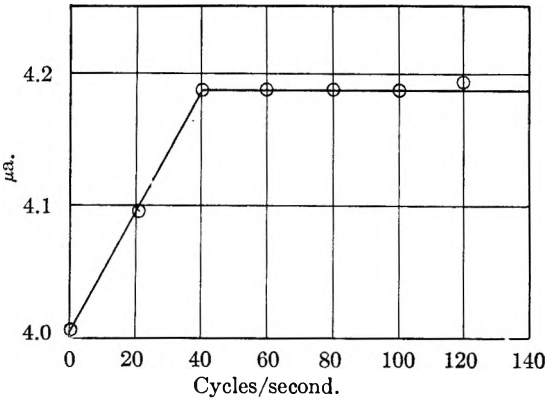

Fig. 2.—Effect of frequency: platinum wire electrode area 0.0490 sq. cm.; temp. 14°; bromate–bromide equivalent to 0.00910 g. equiv./l. in $N/5$ KCl + HCl supporting electrolyte; amplitude 0.09 cm. approx.

(6) L. R. Fresenius, *Z. physik. Chem.*, **80**, 481 (1912).

(7) W. Nernst and E. S. Merriam, *ibid.*, **62**, 235 (1905).

(8) R. Rosenthal, A. E. Lorch and L. P. Hammett, *J. Am. Chem. Soc.*, **59**, 1795 (1937).

Methods

The vibrating micro-electrode[1] has been in use in this and other laboratories since 1948, and, provided it is properly adjusted, it is capable of giving reproducible diffusion currents. If a platinum micro-electrode is vibrated at a constant frequency with constant amplitude the diffusion layer is reduced in effective thickness to a constant value. It was considered necessary to measure the effect of changes of frequency and amplitude upon the magnitude of the current, and for this purpose two types of apparatus were employed.

The first apparatus for measurements at lower frequencies of vibration consisted of an electric motor connected through reduction gears to a cam which moved a lever up and down. The micro-electrode was held in a clamp which could slide along the lever and be fixed at any distance from the pivot. Frequency of oscillation was adjusted by controlling the voltage applied to the motor and amplitude was controlled by alteration of the length of the lever.

The other machine consisted of a laminated E-shaped core of soft iron upon the center portion of which was wound a coil of wire through which an alterating current could be passed. An armature held by a strong spring across the open end of the E, carried a threaded socket into which the electrode could be screwed and thus vibrated at a frequency controlled by that of the alternating current. This device was found satisfactory for measurements with current at frequencies between a few cycles per second to about 60 cycles per second.

The range of amplitudes and frequencies thus available for study were from 0.5 to 1.8 cm. at from 0.158 to 1.28 cycles per second on the lever machine, to from 0.005 to 0.08 cm. at from 1 or 2 to 120 cycles per second on the vibrating armature machine.

Results

Effect of Frequency of Vibration.—At low frequencies (up to about 40 cycles per second) and at constant amplitude it was found that the diffusion current was proportional to the frequency. At higher frequencies of vibration (from 40 cycles to 120 cycles per second) the diffusion current was independent of frequency variation. This is a result similar to that discovered for the rotating electrode by Kolthoff and Laitinen and by Rosenthal, Lorch and Hammett. The former authors[5] found it was important to keep the speed of rotation very constant to ensure a constant current whilst the latter authors[8] discovered that at a very rapidly rotating electrode, the current was not increased by further increase in rotation speed.

The general results quoted above have been found for a variety of electrode reactions; it was, however, found very convenient to employ a bromine solution as the electrode reactant because with such a solution the diffusion current is attained at a potential before that corresponding to the reduction of oxygen. No de-aeration is therefore necessary,[5] and the electrode suffers no permanent polarization.

Figure 1 shows the effect of frequency variation upon the diffusion current of a bromine solution at low vibration frequencies while Fig. 2 shows the effect at higher frequencies. Very similar results

(9) O. H. Müller, *ibid.*, **69**, 2992 (1947)

are given for other electrode reactions and the change from linear proportionality to invariance occurred at about 40 cycles per second with all reactions studied. At a sufficiently high frequency therefore the effective diffusion current is independent of frequency. For analytical purposes it is recommended that with an amplitude of 0.5 to 1 mm. a frequency of 100 cycles per second be used, *i.e.*, that the electromagnetic vibrator be connected to the 50 cycle a.c. mains.

The Effect of Amplitude of Vibration.—With large amplitude of vibrations at a constant low frequency using the lever machine, it was found that the diffusion current was proportional to amplitude. Figure 3 shows the relationship between amplitude and diffusion current for a solution of bromine.

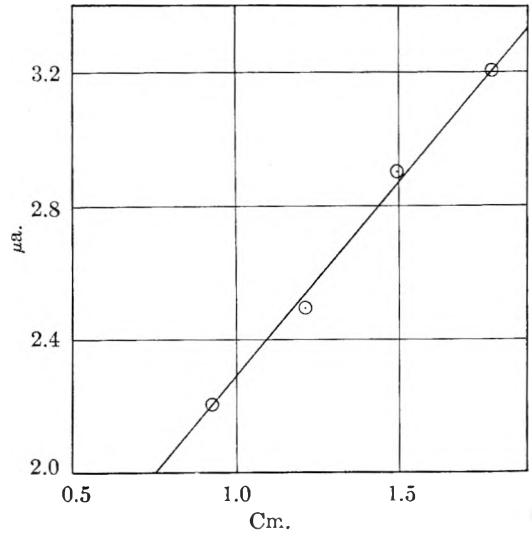

Fig. 3.—Effect of amplitude: platinum wire electrode area 0.0460 sq. cm.; temp. 14°; bromate–bromide equivalent to 0.00477 g. equiv./l. in $N/5$ KCl + HCl supporting electrolyte; frequency 1.24 cycles/sec.

At a constant higher frequency the linear relationship still holds for small amplitudes but for higher values the diffusion current becomes independent of amplitude. This is shown in Fig. 4. The results are thus similar to those obtained with frequency variation and indeed are considered to be due to the same fundamental cause: the velocity of the electrode with reference to the solution.

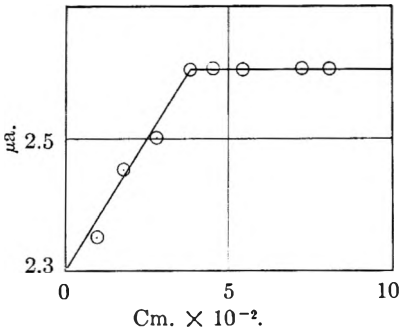

Fig. 4.—Effect of amplitude: platinum wire electrode area 0.0490 sq. cm.; temp. 18°; bromate–bromide soln. equivalent to 0.00477 g. equiv./l. in $N/5$ KCl + HCl supporting electrolyte; frequency 100 cycles/second.

With increase in the velocity of an electrode the diffusion layer becomes thinner and the thickness reaches a limiting value for very high speeds. The velocity thus has a maximum value = $2\pi fa$.

The average velocity may then be assumed to be $1.414\ \pi fa$ or $4.44\ fa$ cm. per sec. if the amplitude is measured in cm. In Fig. 2 the maximum current is attained at a frequency of 40 cycles per second and the amplitude of about 0.9 millimeter corresponds to an average velocity of about 16 cm./sec. In Fig. 4 the maximum current is attained at an amplitude of 3.6×10^{-2} cm. which gives a velocity at 100 cycles per second of 15.9 cm./sec. This limiting velocity is in good agreement with the previous approximate calculation. The mean velocity (velocity of the center of the electrode) of Kolthoff and Laitinen's rotating electrode at the recommended speed (600 r.p.m.) is 44 cm./sec. This is considerably greater than the average limiting value found by the vibrating experiments, and agrees with the reproducible diffusion currents obtained by these workers at high rotation speeds.

In practice for polarographic determinations it is recommended that the amplitude be well over the limiting value, *i.e.*, about 0.7 mm. at 100 cycles per second, which corresponds to a mean velocity of about 30 cm./sec.

Experimental Details

A simple manual polarizing circuit was employed for these investigations. Figure 5 shows the connections. The current was supplied from an accumulator B and two radio rheostats C and D. V was a "Unipivot" voltmeter of 50,000 ohms resistance and readable to 2 mv., and A was a microammeter with full scale deflection of 15 microamperes and readable to 0.02 μa. The circuit could be closed for a short time by means of the key thus minimizing permanent polarization. The electrode vessel, developed from a hydrogen electrode previously described,[10] was designed for easy washing and refilling and could be de-aerated by means of a stream of hydrogen. The gas was swept over the surface of the solution to prevent entry of oxygen during an experiment. As a reference electrode a normal or decinormal calomel electrode F was employed.

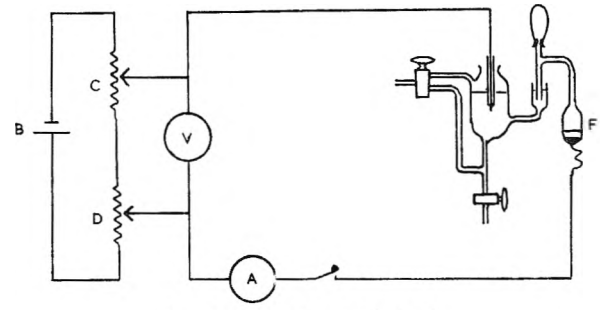

Fig. 5.—Experimental circuit.

The electro-magnetic vibrating apparatus was a commercial massage vibrator marketed for use on 50 cycle a.c. mains. For experiments upon the effect of frequency on diffusion current the vibrator was driven by a calibrated heterodyne beat oscillator through a power amplifier. In the frequency band 0–140 vibrations per minute there were two frequencies which caused mechanical resonance in the vibrating system. These frequencies were avoided in all measurements. Measurements of amplitude were made by focusing a reading microscope with a micrometer eye-piece on the electrode stem. It was found convenient to select a small bubble of air in the glass and to observe the image

(10) A. J. Lindsey, *Analyst*, **57**, 573 (1932).

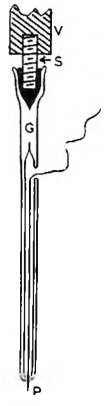

Fig. 6.—Construction of electrodes: V = stem of vibrator, S = screw cemented into electrode, G = glass tubing support for P = platinum wire electrode.

of this when brightly illuminated against the eyepiece scale. Amplitude was controlled by means of a Variac transformer when the a.c. mains were used to drive this vibrator.

In order to use vibrating electrodes for polarographic determinations it is recommended that an electromagnetic vibrator be used. Commercially available massage machines are readily adapted for holding electrodes and Fig. 6 which is self-explanatory shows a method of attaching an electrode to such a machine. As is common practice with other electrode systems, calibration of the electrode with standard solutions and thermostatic control are recommended.

For amperometric titrations the electrode is polarized to the voltage corresponding to the electro-active species and the diffusion current is plotted against the quantity of reagent added. The end-point is given by an abrupt change of direction of the current-volume curve. Practical details will be described elsewhere.

The author wishes to thank Mr. J. V. Westwood, M.Sc., F.R.I.C, for helpful criticism, Mr. R. H. Humphry, M.Sc., F. Inst.P., for the loan of a low frequency oscillator and Messrs. I. C. I. Ltd., for a grant used to purchase chemicals.

THE LOGARITHMICO-NORMAL DISTRIBUTION OF PARTICLE SIZES: HOMOGENEITY AND HETEROGENEITY

BY F. KOTTLER

Communication No. 1401 from the Kodak Research Laboratories, Eastman Kodak Company, Rochester, New York

Received April 19, 1951

It is well known that the distribution of particle sizes, in many processes of growth as well as of breakage, obeys the logarithmico-normal law. An analytical method of dealing with such cases was developed in two previous papers of the author's. These cases were simple cases where the particles belonged to a *homogeneous* population. In the present paper, more complex cases are discussed where the particles belong to a *heterogeneous* population. Examples of such cases are encountered with photographic emulsions. The method for dealing with them is expounded briefly here. Some information about the growth of silver halide grains can be derived from the results of this method.

(1) The Log-Normal Distribution

The logarithmico-normal (shorter, log-normal) distribution is well known from mathematical statistics and also from the popular log-probability charts which are used for graphical analysis in practice. It will be recalled that, on such a chart, the cumulated frequencies of the data are expressed as percentages and are plotted along one axis *versus* the logarithms of the independent variable on the other axis. If the data are distributed log-normally, they fit a *straight* line

$$a + b \log x \qquad (1)$$

where a, b are the two *parameters* of the distribution. Of them, a is the *intercept* of that line with the midline of the chart, and b is the slope of the line. Statistically speaking, the reciprocal value of b is a measure of dispersion of the distribution and is (approximately) related to Pearson's coefficient of variation, which is the ratio of the standard deviation by the arithmetic mean. The parameter, a, on the other hand, is connected with the *median* by the formula

$$\log \text{nat median} = -a/b \qquad (2)$$

More details of these well-known properties of the log-normal distribution will be found in the appendices of an earlier paper.[1]

(2) Application of the Distribution to Particle Sizes

The log-normal distribution has been applied to the distribution of sizes of small particles such as are observed and measured under the microscope. The method of analysis used nearly exclusively was graphical, by means of the log-probability chart. The first to apply it was Loveland[2] in 1924. He used it for the distribution of the silver halide grains such as are used in photographic emulsions. He was followed by Drinker[3] in 1925, who applied it to dust particles. Since then, numerous authors have applied the log-normal distribution to various particles which were produced either by a process of crystallization or by a process of breakage. We mention only recent papers by Austin,[4] written in 1939, and by Epstein,[5] in 1947 and 1948.

(3) Replacing the Graphical Analysis by an Algebraic Analysis

The author has recently published two papers,[1,6] pointing out that the graphical analysis of a distribution is not sufficiently accurate to yield reliable information, and that, in many cases, it is even misleading. It was shown how an algebraic method of greater reliability can replace the graphical analysis. The algebraic method has, moreover, the advantage of permitting the application of statis-

(1) Kottler, *J. Franklin Inst.*, **250**, 339, 419 (1950).

(2) Sheppard, Trivelli and Wightman, THIS JOURNAL, **28**, 529 (1924). In this paper, the log-normal distribution is first applied to the problem of grain-size frequency and is called the "Loveland Equation."

(3) Drinker, *J. Ind. Hyg. Tox.*, **7**, 305 (1925).

(4) Austin, *Ind. Eng. Chem., Anal. Ed.*, **11**, 334 (1939).

(5) Epstein, *J. Franklin Inst.*, **244**, 471 (1947); *J. Appl. Phys.*, **19**, 140 (1948); *Ind. Eng. Chem.*, **40**, 2289 (1948).

(6) Kottler, *J. Franklin Inst.*, **251**, 499, 617 (1951).

tical tests, which yield important information about the "goodness of the fit." It is not sufficient to draw a curve which fits the data more or less approximately. Another curve might fit them still better. This can be decided only by a statistical test, and such a test can only be applied if an algebraic method is used. The theory of these tests involves some recent achievements in mathematical statistics. Readers who are not familiar with such tests and want more information are referred to the textbooks of statistics, *e.g.*, Cramér,[7] or to the writer's second paper.[6]

(4) The Normal Distribution Should Not Be Applied to Particle-Size Distributions

Before passing to the main subject of this paper, we should like to mention briefly an important point. Before the log-normal distribution was introduced into the analysis of particle-size distributions, the Gaussian or Normal distribution was widely used. This distribution also permits a graphical analysis by means of the arithmetic probability charts and is, therefore, easy to apply in practice. Even now, it is still in use. The author[1] pointed out why the distribution of particle sizes cannot be Normal. There are, sometimes, cases where the data seem to fit a Normal distribution. The author[6] suggests that, in such cases, also a log-normal distribution be tried according to the rules given and that the criterion of the goodness of fit be applied to both representations. It is very likely that the goodness of fit will prove to be much better for the log-normal distribution than for the Normal distribution.

(5) Homogeneity and Heterogeneity

There are, however, cases where the simple log-normal distribution does not seem to fit the observations. Such cases were encountered in the study of photographic emulsions by Loveland and Trivelli[8,9] and were also studied by Sheppard and Lambert.[10]

The explanation of these cases, which is given in the present paper, introduces the well-known concepts of statistics: homogeneity and heterogeneity of the population. A sample is said to be homogeneous when all its members belong to the same population. If they belong to two or several different populations, the sample is said to be heterogeneous. The population is characterized, in the case of a log-normal distribution, by the two parameters, a, b. Populations are said to be different if they differ in one or in both of these parameters.

(6) Physico-Chemical Interpretation of the Parameters

It was explained[1] that the two parameters differ in their respective physico-chemical natures. It was pointed out that the log-normal distribution is founded on the simple exponential (Malthusian) law of growth (or decay), and it was shown that the parameter, a, is in the nature of an integration constant and, therefore, completely arbitrary or random. The parameter, b, on the other hand, is inversely proportional to the velocity constant of the process of growth (or decay) regarded as a chemical reaction of the first order and is, therefore, a fundamental constant of that process as long as the physico-chemical conditions do not change.

Now, there can be heterogeneity with respect to a, or with respect to b, or both. The first case[6] arises frequently in the process of growth of a photographic emulsion, especially in large samples. If one does not restrict oneself, locally, to a close vicinity inside the sample, one will find that the growth in different vicinities has started at different times, owing to random differences which cannot be controlled. This causes the parameter, a, to differ for different vicinities and entails a heterogeneity in a, which is, by no means, always negligible. It is often larger than the experimental error permits. It was for this reason that the author advised against the pooling of several samples, which were taken from a large sample and from different localities inside this sample. If such pooling is done, statistical analysis of the size distribution is made difficult and even impossible. It should be noted, however, that, in all these cases, the other parameter, b, remains constant throughout the entire large sample, the reason being, of course, that the physico-chemical conditions prevailing are everywhere the same.

Other cases are encountered, however, in which, even in a close vicinity in a sample, heterogeneity occurs with respect to the parameter, b. According to what has gone before, this indicates the presence of at least two different populations, *of which one grows faster than the other*. As a rule, two populations which differ in the parameter, b, will also differ in the parameter, a, which is easily understood from the random nature of a. It would be a rare coincidence if samples differing in b would *not* differ in a.

(7) Analysis of a Heterogeneous Sample

It was shown[6] how to analyze algebraically a homogeneous sample. To recapitulate briefly, the method is as follows: Let there be $i = 1, 2, \ldots, n$ classes of size. Let the class frequencies be f_i and the cumulated frequencies be $F_1 = f_1$, $F_2 = f_1 + f_2$, etc. Let

$$N = \sum_{i=1}^{n} f_i$$

be the "size" of the sample, that is, the total number of grains counted. The percentages, or probabilities, are then

$$P_i = F_i/N \qquad i = 1, 2, \ldots, n$$

The statistical problem is, then, to represent these probabilities in the form

$$P_i = \int_{-\infty}^{t} z\, dt \tag{3}$$

where $z = \exp(-t^2/2)/\sqrt{2\pi}$ is the ordinate of the Gaussian or Normal probability curve and

$$t_i = a + b \ln x_i$$

x_i being the size corresponding to the end of the class, i.[11]

(7) Cramér, "Mathematical Methods of Statistics," Princeton University Press, Princeton, N. J., 1946.

(8) Loveland and Trivelli, *J. Franklin Inst.*, **204**, 193, 377 (1927).

(9) Loveland and Trivelli, THIS JOURNAL, **51**, 1004 (1947).

(10) Sheppard and Lambert, *Colloid Symp. Monograph*, **6**, 265 (1928).

(11) The size, x, is measured in square microns of the projected area.[1]

To solve that problem, we start with a first "guess" or first approximation derived, for instance, from a plot of the data, P_i, on a log-probability chart. Let the values of the parameters for the first approximation be denoted by one prime, a', b', and the corresponding quantities, similarly. This first approximation will not be, in general, a good fit. To find the best fit, better values for a and b than a' and b' are required and these are given by a second approximation, a'', b'', or a third approximation, a''', and b''', and so on, as the case may be. To find such values, a method is used which is similar to, but not identical with, the method of least squares. It is the method of Chi-Square Minimum.[12] For certain reasons, it is performed not on the cumulative curve but on the non-cumulative frequency curve or, rather, frequency polygon. For further mathematical details, the reader is referred to ref. 6.

This method is easily generalized to a heterogeneous sample. Let us assume that the sample is made up of members of two different populations, their parameters being denoted by the subscripts I and II, respectively. For instance, let the parameters be a_I, b_I, and a_{II}, b_{II}, for the two populations. Let the total numbers of members of the two populations present in the sample be N_I and N_{II}, respectively, so that

$$N_I + N_{II} = N$$

where N is the total "size" of the sample. We introduce a new parameter, c, called the "composition," which is defined as

$$N_I = cN \quad , \quad N_{II} = (1 - c)N$$

Obviously, c is a fraction contained between 0 and 1. If c were zero or 1, the sample would no longer be heterogeneous but would be homogeneous. With these notations, the problem is reformulated as

$$P_i = c \int_{-\infty}^{t_{I,i}} z\, dt + (1 - c) \int_{-\infty}^{t_{II,i}} z\, dt \qquad (4)$$

where

$$t_{I,i} = a_I + b_I \ln x_i$$
$$t_{II,i} = a_{II} + b_{II} \ln x_i$$

Obviously, we now have a representation of the data, P_i, by means of five parameters, a_I, b_I, a_{II}, b_{II}, c. The procedure for finding these five parameters is similar to, but more complicated than, that described in the case of homogeneity. Again, we start with a first "guess" or approximation, denoted by one prime. The value c' is a pure guess which has to be repeated if it does not lead to a successful termination of the computation. The other values, a_I', b_I', a_{II}', b_{II}', can be found by means of a log-probability chart in a manner which will not be described here in detail. Suffice it to say that the computation is similar to a problem of least squares with five unknowns.

(8) First Example

We shall illustrate the method by two examples. The first example is taken from an experimental series of pure silver bromide emulsions called L-1. By volume precipitation, lasting through different periods of time, a number of emulsions were produced and described by Loveland and Trivelli.[9] Our example is their number 8 and the volume precipitation lasted for six minutes.

The sizes of the grains were classified and counted by the aforementioned authors. Their data were subjected by the present author to an algebraic analysis, as described before, and formulated in Equation (4). The best fit was obtained after only two approximations, and the parameter, c, which gives the composition of the resultant distribution, was found to be very nearly equal to 0.60. If the two components of the distribution are designated as I and II, and the resultant as III, the resultant can be written

$$\text{III} = 0.60\,\text{I} + 0.40\,\text{II} \qquad (5)$$

In Table I, in the second column, are shown the class frequencies observed by Loveland and Trivelli. In Column 3 are shown the class frequencies computed according to Equation (4), by our method. In Column 4 are shown the deviations between observation and computation, and in Column 5, the corresponding contributions to the Chi Square. (See the formula at the head of the column.) The sum of the fifth column is the value of the Chi Square which is used in the Chi-Square test. The purpose of this test is to show whether the unavoidable discrepancies between observation and computation can be ascribed to random errors of observation or not. To each value of Chi Square, there corresponds, by the general laws of statistics, a certain probability *that the discrepancies are random*. It is generally agreed that this probability should be not smaller than 5%. If it is smaller, the discrepancies

TABLE I

ANALYSIS OF THE EMULSION L-1 No. 8

The class intervals for the sizes are 0.1 square micron, and the first class covers the interval 0.0–0.1 square micron, the other classes covering successive intervals.

Class number, i	Observed class frequency, f	Computed class frequency, f_c	δf $f - f_c$	Chi-square test, $\delta f^2/f_c$
1	571	570.88	+0.12	0.000
2	402	402.32	−0.32	.000
3	222	219.95	+2.05	.019
4	143	148.66	−5.66	.215
5	120	119.30	+0.70	.004
6	111	105.40	+5.60	.298
7	103	95.99	+7.01	.512
8	81	88.18	−7.18	.585
9	74	80.77	−6.77	.567
10	74	73.51	+0.49	.003
11	70	66.48	+3.52	.186
12	63	59.78	+3.22	.173
13	55	53.56	+1.44	.039
14	56	47.84	+8.16	1.392!
15	36	42.53	−6.53	1.003
16	35	37.80	−2.80	0.207
17	29	33.63	−4.63	.638
18	28	29.81	−1.81	.110
19	23	26.45	−3.45	.450
20	19	23.49	−4.49	.858
21	19	20.86	−1.86	.166
22	20	18.54	+1.46	.115
23	17	16.46	+0.54	.018
24	15	14.67	+0.33	.007
25	16	13.05	+2.95	.667
26	11	11.61	−0.61	.032
27	13	10.39	+2.61	.656
28–63	98	92.11	+5.89	.378
	2524	2524.02	−0.02	$\chi^2 = 9.298$
				$P_{[22]} = 99.9\%$

(12) This method is equivalent to the method of Maximum Likelihood, as developed by R. A. Fisher and widely used in mathematical statistics. See Cramér (ref. 7, p. 426).

cannot be regarded as merely random, and the hypothesis underlying the computation, in our case Equation (4), should be rejected.

It is quite obvious that the Chi Square must be small if the probability of the random nature of the discrepancies is to be large, and conversely.

It will be noted that Classes 28–63 have been pooled corresponding to the well-known procedure that *small* class frequencies below ten should be pooled in the Chi-Square test. (See Cramér, ref. 7, p. 420.)

The probability for the random nature of the discrepancies between observation and computation is given at the lower right end of the table as $P_{[22]}$. The subscript signifies that there are 22 degrees of freedom left when the necessary corrections are applied to the number, 63, of observed classes. It will be seen that this probability is 99.9%, which is excellent and shows that our hypothesis expressed in Equation (4) is acceptable for the example studied.

These results are illustrated in three charts. Figure 1 is a log-probability chart such as is explained in ref. 1. At the bottom, the size, x, is plotted in square microns according to a logarithmic scale. (It has been found more convenient to use natural logarithms in the algebraic work.) Vertically upwards are plotted the percentages. The data are denoted by crosses, and it is seen that they do *not* fit a *straight* line as the data with an ordinary homogeneous log-normal distribution would do. (Compare, for instance, the Seed Lantern Emulsion shown in ref. 1.) Actually, they fit a *curved* line denoted by III, and they fit it very well except for the last points. This deviation, which concerns only small class frequencies, need not concern us here.[13]

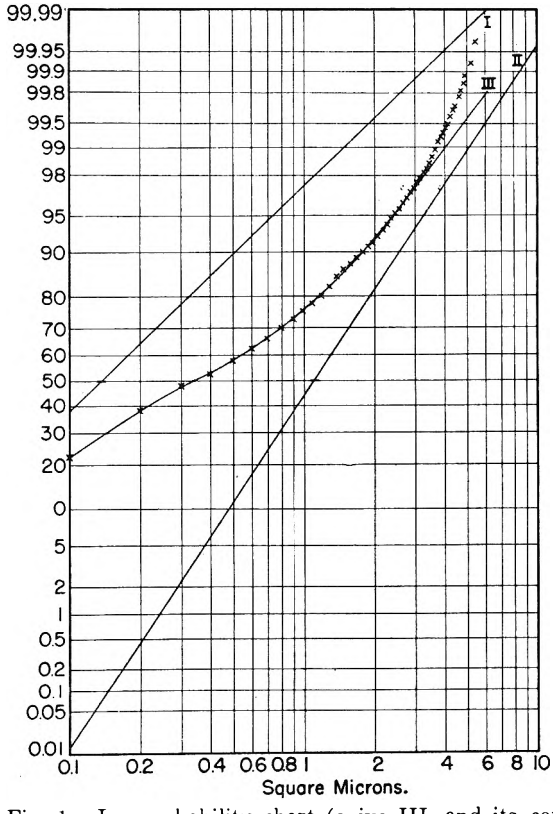

Fig. 1.—Log-probability chart (ogive III, and its components, I, II); pure silver bromide emulsion L-1 No. 8 (6 minutes volume precipitation).

This curved line, according to what has gone before, is the resultant of two simple and homogeneous components, I and II, which are distributed log-normally and are represented by the straight lines, I and II, in Fig. 1. The curved line, III, is the sum already expressed in Equation (5).

$$\text{III} = 0.60\,\text{I} + 0.40\,\text{II}$$

It will be seen that the slope, b_{I}, of the first component is smaller than the slope, b_{II}, of the second component. Hence, by ref. 1, the component I grows at a faster rate than II. It will also be seen that the median (intersection with the 50% line) of I is about 0.4 square micron and is smaller than the median of II, which is 1.1 square microns. Hence, the faster-growing component, I, contains, on the average, finer grains than the slower-growing component, II.

Figure 2 is a logarithmic curve such as was introduced into the study of log-normal distributions by Loveland and Trivelli.[8] At the bottom, there are, again, the sizes according to a logarithmic scale. Vertically upwards are now the logarithms of the ratios of the class frequencies to the class interval. A simple homogeneous log-normal distribution would be represented on such a chart by a *parabola*. It is seen that the data, denoted by crosses, do *not* fit a parabola. Hence, this logarithmic chart cannot be used for a graphical analysis of the data. It can only serve as an illustration of the results of the computation. As such, it is quite useful. First, we note the broken lines which represent the "error band," which accompanies the curve on both sides. It is a strip of the width of ± one standard error; the standard error is given in this case, according to Karl Pearson's Chi Square, by the square root of the computed class frequency.[6] The width of this strip varies from point to point and decreases with decreasing frequencies, and hence with increasing sizes. The contrary appearance on the chart (Fig. 2) is merely due to the distortion by the logarithmic scale. The error band provides a good illustration of the nature of the Chi-Square test. Consider, for instance, the point, number 14, which is marked by an exclamation point. It is outside the error band, and this agrees with Table I, according to which number 14 contributes a comparatively large amount, 1.392, to the Chi Square. It will be recalled that a large Chi Square means a bad fit. Hence, if many points are found outside the error band, the resulting fit must be judged as poor. Actually,

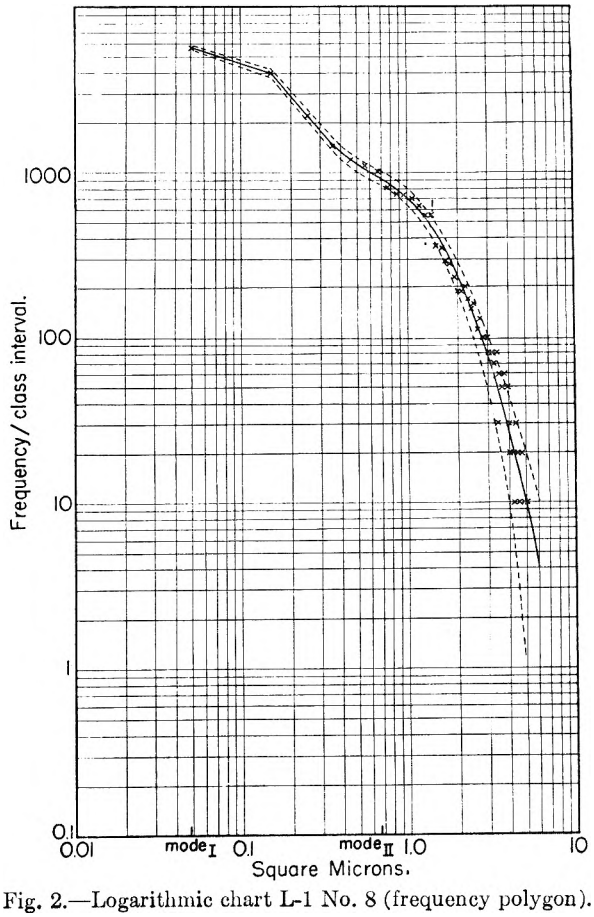

Fig. 2.—Logarithmic chart L-1 No. 8 (frequency polygon).

(13) It is due to the fact that the data actually fit a *limited* distribution, whereas the log-normal distribution is *unlimited*. In other words, the unlimited exponential, or Malthusian, law of growth should be replaced by the limited law of growth which is similar to the logistic law of Verhulst, and of Pearl–Reed (see ref. 1)

it will be seen from Fig. 2 that most of the other points are inside the error band and, hence, the fit is good. How good it is can, of course, be judged only by computing the Chi Square.

Next, we note that, as a consequence of the heterogeneity, there are two modes, that is, two different peaks or maxima. The first mode is due to Component I and is situated at 0.045 square micron, which is outside the range of observations, which begins at 0.1 square micron. The second is at 0.724 square micron and is due to Component II. Between the two values, there will be noted a kind of *indentation* in the curve. It should be stated, however, that this is not a genuine case of "bi-modality," because the two modes belong to two different curves by whose superposition the resultant curve is produced. This will become clearer, later, when we discuss Fig. 3.

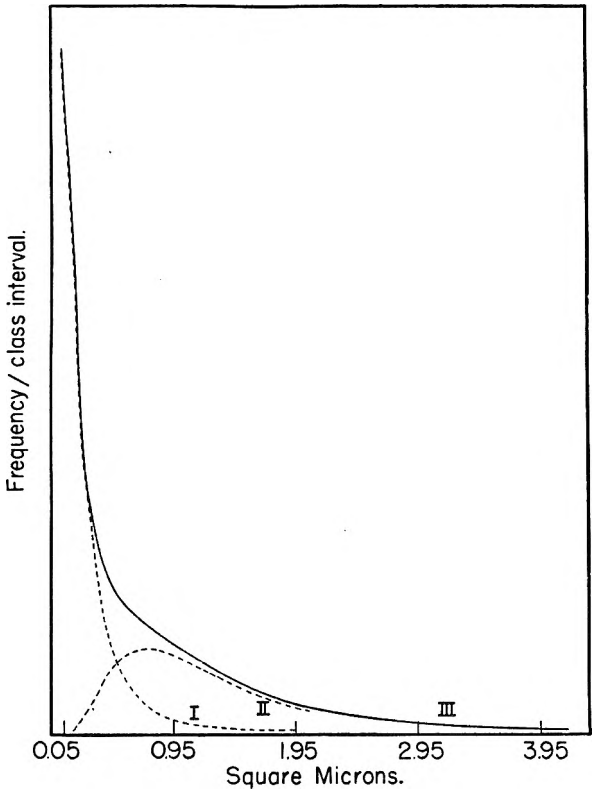

Fig. 3.—Arithmetic chart L-1 No. 8 (frequency polygon, III, and its components, I, II).

Lastly, the figure shows clearly the irregular fluctuations of the small frequencies corresponding to large sizes. This is a well-known phenomenon and illustrates that the laws of statistics and probability must always be applied with great caution to events which happen only once or twice.

Consider, now, Fig. 3. It is an ordinary "arithmetic" chart. The sizes are plotted along the bottom on a regular arithmetic scale, and vertically upwards are plotted the class frequencies divided by the class interval, again on an arithmetic scale. The two components, I and II, are indicated by broken lines. They are drawn so that their respective areas are proportional to $N_{\mathrm{I}} = cN$ and $N_{\mathrm{II}} = (1 - c)N$. Hence, they can simply be added or superimposed upon each other and so give the resultant curve, III, which has an area proportional to the total "size" of the sample, N.

The reader will easily distinguish, in Fig. 3, the two modes corresponding to I and II and the elongation of the tail of the resultant curve, III, which is due to the existence of the mode, II. It will also be noted that the range of Curve I and the range of Curve II overlap. This is a characteristic feature of all the heterogeneous log-normal distributions of photographic grains analyzed so far.

(9) Second Example

The second example is taken from an experimental series of photographic emulsions, L-α, produced by "stream precipitation." It was studied by Loveland and Trivelli (ref. 8, Part II), Sheppard and Lambert,[10] and Loveland and Trivelli (ref. 9, especially pp. 1004–1005 and Figs. 1–6).

We have selected an emulsion denoted by the authors as L-α6c, of which three samples were taken and averaged. For the reasons given in Section 6 of this paper, we do not accept here the averages, but select sample No. 3.

It should be noted that the emulsion was prepared by adding six parts of potassium bromide to forty parts of silver bromide and allowing it to ripen for 345 minutes before the analysis was taken.

The algebraic analysis performed in the manner described in the foregoing sections confirms again the heterogeneity of the sample and shows it to consist of two components. Figure 4 illustrates the resultant curve, III, and its components, I and II. In the present case, using the same symbols as in Equation (5), we have

$$\mathrm{III} = 0.80\,\mathrm{I} + 0.20\,\mathrm{II} \qquad (6)$$

Hence, the L-α series obeys the same law of heterogeneity as the L-1 series; more specifically, both series can be explained as the resultants of two simple, homogeneous, log-normal distributions.

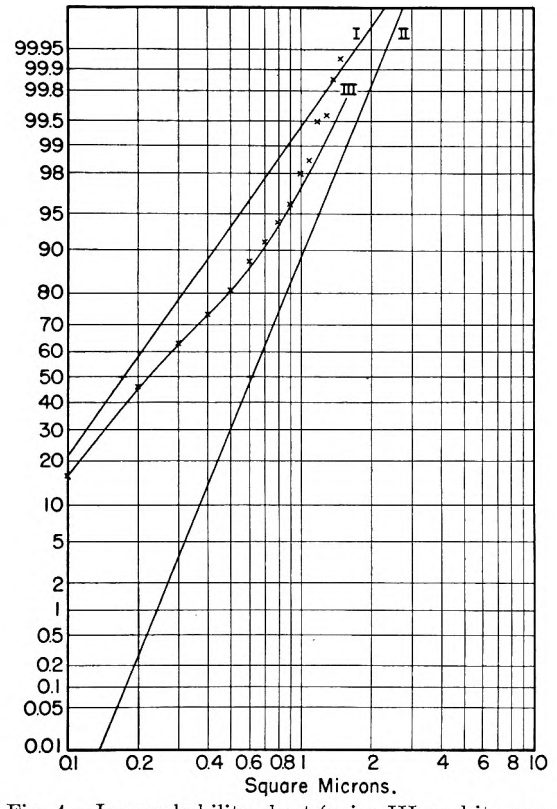

Fig. 4.—Log-probability chart (ogive III, and its components, I, II) L-α-6c, No. 3 (stream precipitation) (6 parts KBr added to 40 AgBr; ripening time, 345 min.)

Again, a table similar to Table I can be compiled and the hypothesis (6) can be tested by means of the Chi-Square test. The outcome is a probability of 75.4% in favor of the hypothesis. This result is nearly as good as that obtained in Table I for L-1 number 8, especially if it is considered that, in the present case, owing to the few classes observed, we have only five degrees of freedom, whereas before we had twenty-two degrees of freedom.

Note that there is a difference in the composition of the two series

$$\text{L-1} \quad c/(1 - c) = 0.60/0.40$$
$$\text{L-}\alpha c \quad c/(1 - c) = 0.80/0.20$$

It should be noted that Loveland and Trivelli have given a different explanation of such curves as those in Fig. 4 (they did not apply this explanation to the curves such as those in Fig. 1). According to these authors, the curve in

Fig. 4 is explained by "breaks" or "discontinuities in the distribution." From their hypothesis it would follow that the curve III in Fig. 4 consists of two segments of straight lines, one comprising the points Numbers 1 to 7, and the other comprising the remaining points, Numbers 8 to 15. For more details, we refer to the quotations given before, and, also, for a physico-chemical explanation of these "breaks," to the paper by Sheppard and Lambert.[10]

However, if the Chi-Square test is applied to this hypothesis, as formulated above, the resulting probability is

$$P_{[5]} << 0.1\%$$

and this signifies that the hypothesis tested must be *rejected.*

(10) Testing the Entire L-1 Series

In order to test our own hypothesis, as expressed by Equation (4), we have analyzed the full L-1 series, comprising eleven emulsions. In Table II, there are listed the results of the Chi-Square test obtained by applying the hypothesis, (4), to the data observed by the experimenters.

TABLE II

SURVEY OF THE L-1 SERIES OF EMULSIONS

Time of precipitation, min.	Time of digestion, min.	Number of classes observed	Degrees of freedom	Probability in favor of the hypothesis (in %)
1	..	13	6	15.9
1½	..	23	13	0
2	..	23	13	77.7
2½	..	33	12	72.6
3	..	29	13	70.2
4	..	40	17	95.2
6	..	63	22	99.9
8	..	70	22	96.7
10	1	53	25	99.9
10	6	53	24	99.9
10	25	45	14	76.0

Since the rejection level of a hypothesis is commonly regarded as 5% or less, our hypothesis can, therefore, be regarded as acceptable in ten out of the eleven cases examined. In most of the cases, the probability in favor of this hypothesis is so overwhelming that there can be hardly any doubt about its validity. Only in one case is the hypothesis rejected by the Chi-Square test. This can be due to mere chance. If the rejection level is 5%, for instance, rejection must occur once in twenty times by mere chance.[14] Or, it could be the result of the entering of some agent into the experiments in an unknown way and producing a systematic error of the observations in that special emulsion (1.5 minutes precipitation).

(11) The Composition, c, of the L-1 Series

In view of the fact that the hypothesis (4) is verified by Table II for the entire series of emulsions, L-1, it is interesting to investigate whether the composition, c, of these emulsions changes with time.

In Fig. 5, we have plotted the parameter, c, for each of the eleven emulsions *versus* time. It goes without saying that c marks the fraction of the entire number of grains which belong to Component I and $(1 - c)$ marks the remaining fraction, which belongs to Component II. In preparing Fig. 5, we have omitted from the computation the emulsion corresponding to 1.5 minutes precipitation for reasons which will be obvious by an inspection of the probability column in Table II. Nevertheless, the corresponding point for c of that emulsion is entered on the chart and marked by enclosing it in parentheses.

(14) Brownlee, "Industrial Experimentation," His Majesty's Stationery Office, London, 1947, p. 113.

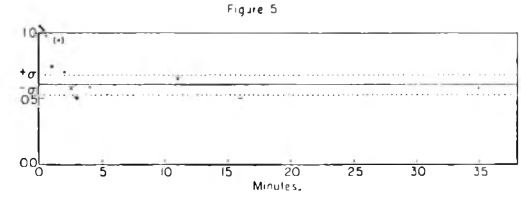

Fig. 5.—The composition (parameter c) *versus* time; L-1 series.

Figure 5 is a so-called "control chart," which shows the mean of all the c values except the aforementioned one. It is denoted by a solid line. It shows, also, by two broken lines, control limits of ± one standard error. *It will be seen that, within these very strict and narrow control limits, the composition, c, can be regarded as constant for the entire L-1 series throughout the process of precipitation and digestion.*

We can formulate this result, differently, in the following manner: The L-1 series is composed of two components having grain numbers N_I, N_{II}, and, throughout the entire series, we have the ratio

$$N_I/N_{II} = 3/2 \qquad (7)$$

(12) The Velocity Constants of the Two Components

We next consider the two parameters b_I and b_{II}, or rather, their reciprocal values, $1/b_I$ and $1/b_{II}$, which, by ref. 1, are proportional to the velocity constants of growth, assuming the validity of an exponential law of growth and treating it as if it were a chemical reaction of the first order.

In Fig. 6, we have plotted the two values *versus* the corresponding times. Again, the value for the precipitation, 1.5 minutes, has been excluded from the computations for the reasons evident from Table II. The corresponding values, $1/b_I$ and $1/b_{II}$, have, however, been entered on the figure and denoted by enclosing them in parentheses. Again, control charts were set up for the two quantities, means denoted by solid lines and control limits of ± one standard error denoted by broken lines. The

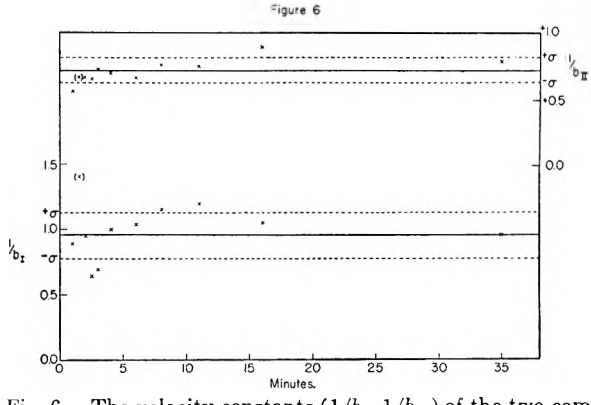

Fig. 6.—The velocity constants ($1/b_I$, $1/b_{II}$) of the two components *versus* time; L-1 series.

upper part of the figure presents the values $1/b_{II}$, which are proportional to the velocity constants of growth of Component II. There can be no doubt that, within the very narrow and strict limits of control, this velocity constant can be regarded as constant throughout the entire process of precipitation and digestion.

The lower part of the figure refers to Component I. Here, we encounter a larger standard error and, consequently, larger fluctuations of the values, $1/b_I$, appear. By taking into consideration this larger yardstick of the standard error, it can safely be stated that, statistically, there is no objection to treating $1/b_I$ also as a constant during the entire process.

Why are the fluctuations and, consequently, the standard error, larger for Component I than for Component II? We offer the following explanation: Most of the grains belonging to Component I are fine, and, therefore, near to or perhaps below the limits of the resolving power of the microscope. This may introduce a larger error into the measurement of these grains.

(13) The Parameters, a_I, a_{II}

We do not discuss the remaining two of the five parameters, a_I, a_{II}, because of their completely random nature, as has been explained in Section 6. No additional information could be obtained by plotting these parameters, or functions of them, *versus* time. They just depend on the chance moments when the precipitation was begun and when the crystallization started.

(14) A Possible Explanation of the Difference in the Velocity Constants of Growth

It remains to say a few words about the difference in the two velocity constants of Components I and II. We can only give a guess about that difference, since the ground covered by the preceding investigation is not extensive enough. One might be inclined to ascribe this difference to the existence of two different types of crystals or of crystalline nuclei.[9] Our guess would be, rather, that this difference in growth velocity is to be ascribed to the anisotropy which exists in a crystal. It is a well-established fact that the different faces of a crystal grow at different rates.[15] It appears that the face which has a larger number of inhabitant ions grows faster than any other face, which has a smaller number of inhabitant ions, the area of both faces being assumed to be equal.

However that may be, it is interesting to note the following regularity which seems to govern some of the emulsions of the L-1 series. In Table III, we have listed the data for emulsions which have had three minutes or more time of precipitation or precipitation plus digestion. We find that the velocity constants are directly proportional to the relative numbers, N_I, N_{II}, of the components present, as can be seen from the last column of Table III.

TABLE III

EMULSIONS OF THE L-1 SERIES WITH MORE THAN 3 MINUTES OF PRECIPITATION

Precipitation, min.	Digestion, min.	Total time, min.	$cb_I/(1-c)b_{II}$
3	0	3	0.9
4	0	4	1.0
6	0	6	1.0
8	0	8	1.0
10	1	11	1.2
10	6	16	0.9
10	25	35	1.2

(15) Conclusions

(1) Previous papers by the present author have dealt with the log-normal distribution of particle sizes observed by many authors working with photographic emulsion and similar grains. This distribution has been found to hold if the sample analyzed belongs to a homogeneous population.

(2) In the present paper, it has been established with sufficient statistical evidence that, in cases where the simple log-normal distribution does not hold, one is faced with a heterogeneous population.

Such is the case with the eleven emulsions of the series L-1, which are composed of two components bearing the constant ratio

$$N_I/N_{II} = 3/2$$

(3) It has been shown in another case (an example of the L-αc series of emulsions) that a similar law holds and that the components obey the law

$$N_I/N_{II} = 4/1$$

(4) It has not been found necessary in the cases examined so far to introduce more than two components. It is, however, possible that with more complex emulsions it might be necessary to consider three or more components.

(15) Dr. C. R. Berry, of these Laboratories, has pointed out to me that, in this case, one might expect to find particles of two distinct shapes, for example, triangles and cubes. According to him, other causes of a possible heterogeneity can be differences in the number or in the pattern of imperfection in the crystals which affect the growth rates. Also, the same faces may not develop to the same extent. Thus, one may have crystals which are nearly flat and others which are more nearly spherical.

THE DISSOLUTION OF METALS OVER THE TEMPERATURE RANGE OF 25 TO −60°. II.[1] THE DISSOLUTION OF CADMIUM IN HYDROCHLORIC ACID-METHYL ALCOHOL-WATER SOLUTIONS[2]

BY A. B. GARRETT AND J. R. HEIKS[3]

The Department of Chemistry, The Ohio State University, Columbus, Ohio

Received April 16, 1951

Data have been obtained for the rate of dissolution of cadmium in methanol–water–hydrochloric acid solutions under static and dynamic conditions, in the presence and absence of a depolarizer over the temperature range of 25 to −60°. The energy of activation of the static depolarized process is in the order of 4000 cal./mole and of the non-depolarized process is about 10,000 cal /mole. The non-depolarized dissolution process is first order with respect to the acid concentration.

Purpose of the Investigation

The purpose of this research was to obtain the rate of dissolution of cadmium in an acid medium over the temperature range of 25 to −60°. These data were necessary in a study of cadmium as a possible anode in cells for low temperature operation. We have chosen 90% methanol–0.1 *N* hydrochloric acid solution as a solvent medium because of the desirable physical properties of this system over the above temperature range. This system[4,5] has a low freezing point; it also has a low viscosity and a relatively good electrical conductivity at −65°.

The dissolution of cadmium in acid media (undepolarized) has been studied recently by McDonald and Zimmerman[6] who have also reviewed the earlier work. Their data show that, after an initial transient period, the rate of dissolution is independent of the acid concentration. They found, however, that if dissolved oxygen is removed from the solution the reaction is first order. The variation of reaction rate with ionic strength was also studied. They were not able to obtain the actual energy of activation by the method of temperature variation.

Experimental

Apparatus.—The apparatus employed was described in Paper No. I of this series, except that a single hook was used to support the metal plates, instead of two as shown in Paper No. I, Fig. 1.

Materials.—Chemically pure cold rolled cadmium sheet (analysis: 99.9% cadmium, major impurity zinc) 0.041 cm. thick, obtained from Belmont Smelting and Refining Company was used in this investigation. The cadmium sheet was cut into plates 2.41 by 1.91 cm. The hydrochloric acid solution used contained 90% methyl alcohol and 10% water by weight. The acid concentration of the solution was approximately 0.05 *N* and was standardized with sodium hydroxide using phenolphthalein as the indicator. The nitroethane used was repurified by treatment with anhydrous aluminum chloride followed by distillation from boric acid.

Procedure

The Solution.—Four hundred milliliters of the prepared hydrochloric acid solution, measured at 25°, was placed in the reaction vessel. To this solution 1.5 ml. of nitroethane was added as a depolarizer. The solution was precooled to the desired temperature in an acetone–Dry Ice-bath and brought to thermal equilibrium with the cryostat.

The Atmosphere.—All dissolution experiments were carried out in an atmosphere of dry nitrogen.

The Cadmium.—The cadmium plates were polished with fine emery paper, and carefully weighed on an analytical balance before installing on the stirrers for a determination. At the end of a pre-determined time interval the cadmium plates were removed from the solution and rinsed with distilled water, dried and weighed in order to determine the weight lost during the reaction. Area measurements were made before and after each run with a micrometer.

In general, determinations were run in duplicate by using two stirrers driven by the same stirring motor.

Errors.—The analysis of the errors involved is given in Paper No. I. The reproducibility involved in this investigation is somewhat lower than that reported for magnesium. At 25° the individual values for the reaction velocity constant deviate from the mean of two determinations by an average of 1.2%, the maximum deviation being 2.1%. Corresponding values at 0°, −30° and −60° are, respectively: 2.1% and 4.9%; 2.7% and 4.2%; 2.1% and 5.6%.

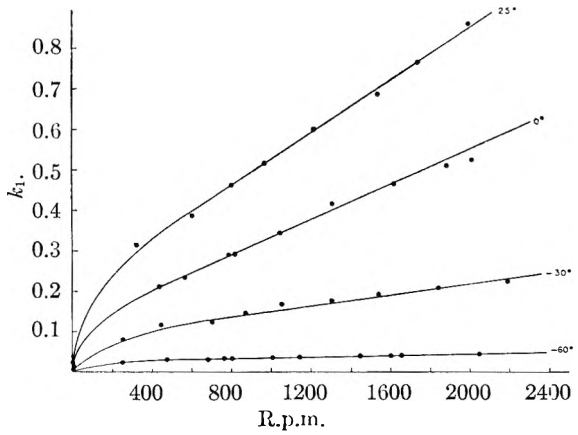

Fig. 1.—Dissolution of cadmium in 90% methyl alcohol-10% water containing hydrochloric acid solutions. Reaction velocity constants for several temperatures plotted against stirring speeds.

Data

Measurements Obtained.—The dissolution rate of cadmium was first determined as a function of depolarizer (nitroethane) concentration and as a result a concentration of 0.05 molar nitroethane was used in these studies.

Static data were obtained over the temperature range −20 to −50° for cadmium plates in eutectic hydrochloric acid containing no depolarizer (Table II).

In the main investigation the dissolution characteristics of cadmium in the presence of a depolarizer were evaluated by determining its dissolution

(1) Paper I, Garrett and Cooper, THIS JOURNAL, **54**, 437 (1950).

(2) This work was initiated and is supported by the Battery Branch of the Signal Corps Engineering Laboratories at Fort Monmouth, New Jersey.

(3) Mound Laboratory, Monsanto Chemical Co., Miamisburg, Ohio.

(4) A. B. Garrett, Robert Cooper, John Heiks and Samuel Woodruff, THIS JOURNAL, **53**, 505 (1949).

(5) A. B. Garrett and Samuel Woodruff, *ibid.*, **55**, 477 (1951).

rate as a function of the following variables: (1) acid concentration (other factors constant). The acid concentration and/or the time of reaction were varied over rather wide limits at 25° and −60°, respectively. (2) Stirring speeds (other factors constant): dynamic dissolution data were obtained at numerous rotational speeds over the range 0 to 2,200 r.p.m. at 25, 0, −30 and −60°, respectively. By measuring from the center of the stirrers to the center of the plates it is possible to approximate the linear speed. On this basis the linear speed varies from 0 to 27,600 cm./min. (3) Temperature, under static conditions, at ten degree intervals over the temperature range 25° to −60°.

Treatment.—The dissolution data obtained are correlated and compared on the basis of a first order reaction. The existence of a first order reaction is indicated by the fact that the calculated value of the first order reaction velocity constant, k_1

$$dx/dt = k_1A(a - x)/V \qquad (1)$$

remains constant, within experimental error, as shown in Table I, even though the original acid concentration and/or the time of the runs are varied. Since a first order reaction holds for both extremes of temperature, it was assumed to hold over the entire temperature range investigated.

Plots of the first order reaction velocity constant, k_1, *vs.* stirring speed on the rate of dissolution are given (Fig. 1). Up to about 500 r.p.m. the velocity constant does not vary linearly with stirring speed, but above this speed the variation seems to be almost linear. A plot of $-\log k_1$ *vs.* $1/T$ has been drawn for the depolarized static dissolution process and the activation energy of the process (Fig. 2) determined to be 3770 cal./mole. Also a plot of −log (wt. loss)/(area × time) *vs.* $1/T$ was drawn of the data

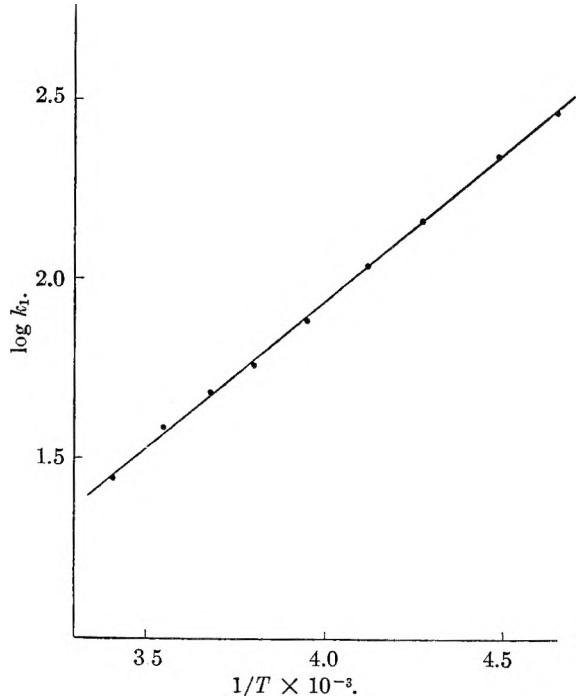

Fig. 2.—Dissolution of cadmium in 90% methyl alcohol–10% water containing hydrochloric acid solutions: log k_1 *vs.* $1/T$, static conditions, activation energy 3770 cal./mole.

TABLE I

DETERMINATION OF ORDER OF REACTION OF CADMIUM IN METHANOL–WATER–HYDROCHLORIC ACID

R.p.m.	Milliequiv. of metal used (x in Eq. 1)	Original quantity of acid in milliequivalents (a in Eq. 1)	Surface area in cm.²	Time in min.	k_1 (average)
Temperature −60°; volume of solution 369 ml.					
600	0.68	20.62	18.71	25.0	0.0265
600	.70	20.60	18.58	25.0	.0275
600	.81	19.92	18.71	30.0	.0273
600	.85	19.90	18.58	30.0	.0289
600	.92	20.60	18.46	35.0	.0261
600	.94	20.60	18.30	35.0	.0270
Temperature 25°; volume of solution 386 ml.					
680	1.16	20.60	18.39	3.0	0.416
680	1.22	20.60	18.42	3.0	.438
680	1.50	19.94	18.48	4.0	.430
680	1.52	19.38	18.35	4.0	.441
680	1.90	20.60	18.38	5.0	.417
680	2.11	18.78	18.35	6.0	.429

TABLE II

DETERMINATION OF (WEIGHT LOSS/HOURS × CM.²) OF CADMIUM IN EUTECTIC HYDROCHLORIC ACID SOLUTION

Static data; no depolarizer; from a plot of −log (wt. lost)/(cm.² × hr.) *vs.* $1/T$ the activation energy of 9600 cal./mole is calculated.

Temp. in °C.	Wt. loss in grams	Surface area in cm.²	Time in min.	Wt. loss in g./min./cm.²	Wt. loss in m.d.d
−20.0	0.0084	16.37	780.0	3.95×10^{-5}	5.69×10^{2}
−30.0	.3532	23.46	1020.0	1.4×10^{-5}	2.02×10^{3}
−40.0	.1823	23.46	1200.0	6.47×10^{-6}	9.32×10^{2}
−50.0	.0749	23.46	1320.0	2.35×10^{-6}	3.39×10^{2}

in Table III for the non-depolarized dissolution process in eutectic hydrochloric acid, and the activation energy of that process was determined to be 9600 cal./mole. The reaction rate in this case can be expressed in terms of weight loss per (area × time) since the percentage change in acid concentration before and after reaction is very small. A simple plot of k_1 *vs.* T was made of the static depolarized dissolution process and used to prepare Table III showing the temperature coefficient for ten degree intervals over the temperature range covered.

TABLE III

DETERMINATION OF TEMPERATURE COEFFICIENT OF DISSOLUTION OF CADMIUM IN METHANOL–WATER–HYDROCHLORIC ACID

Depolarizer, nitroethane, 0.05 *M*; static conditions

Temperature, °C.	$(k_1)_T$	$(k_1)_{T+10°}$	Temp. coeff. per 10° interval
10 to 20	0.6270	0.0345	1.28
0 to 10	.0210	.0270	1.29
−10 to 0	.0161	.0210	1.30
−20 to −10	.0123	.0161	1.31
−30 to −20	.0093	.0123	1.32
−40 to −30	.0067	.0092	1.38
−50 to −40	.0046	.0067	1.45
−60 to −50	.0031	.0046	1.53

Discussion.—The following generalizations can be made from the data obtained: (1) The depolarized dissolution process appears to be first order with respect to the acid concentration. (2) The rate of stirring has a profound effect on the dis-

solution rate. This is an indication that diffusion is an important factor in determining the rate of reaction. (3) The energy of the activation of the static depolarized dissolution process is in the order of 4000 cal./mole. This low energy of activation is further evidence that a mechanical process, probably diffusion, is the principal factor in determining the rate of reaction. (4) The non-depolarized dissolution process shows a higher energy of activation, in the order of 10,000 cal./mole, which indicates that some chemical process is probably involved in the process.

A black film on the cadmium, reported by McDonald and Zimmerman,[6] was noticed at 0° only. However, this did not have any apparent effect on the value of the velocity constant.

(6) H. J. McDonald and J. F. Zimmerman, THIS JOURNAL, **51**, 857 (1947).

AN ELECTRON DIFFRACTION STUDY OF FILMS FORMED BY SODIUM NITRITE SOLUTION ON IRON

BY M. COHEN

National Research Council, Ottawa, Canada

Received April 16, 1951

The passive film formed by sodium nitrite is γ-Fe_2O_3 with a small amount of γ-$Fe_2O_3 \cdot H_2O$. The oxide film is formed by a reaction between the nitrite (and oxygen) and the metal at the liquid–metal interface, with adsorption of the inhibitor as a probable intermediate step.

Sodium nitrite is one of several oxidizing agents which can prevent the corrosion of iron in aqueous solutions. An understanding of the mechanism by which sodium nitrite inhibits the corrosion of iron might assist in the formation of a general picture of the mechanism by which the passivity of iron is produced by other oxidizing inhibitors.

In previous papers on the inhibition of the corrosion of iron by solutions of sodium nitrite[1,2,3] the following observations were made: (1) The concentration of sodium nitrite required for inhibition increases with increasing temperature and electrolyte content and decreases with movement of the solution and an increase in oxygen concentration. (2) Sodium nitrite does not decompose in the absence of corroding iron, but does decompose in the presence of corroding iron. Ammonia was isolated from a nitrite solution in which iron was corroding. (3) Under non-inhibiting conditions nitrite stimulates corrosion. (4) The potential of iron is "ennobled" in solutions of sodium nitrite of sufficient concentration to give inhibition. This noble potential and lack of corrosion are maintained for a considerable period of time if the solution conditions are then changed to the corroding range. (5) It was noted that as the solution was varied from the corroding to the inhibiting range, the form of corrosion passed from general corrosion through pitting and interference colors to no apparent attack.

On the basis of these experiments it was concluded that sodium nitrite inhibits the corrosion of iron by producing a protective oxide film on the metal surface. It was proposed that this oxide film was produced by a heterogeneous reaction, and that the first steps in the reaction were the adsorption of nitrite ion on anodic areas, and that these adsorbed ions subsequently reacted with atomic hydrogen adsorbed on adjacent cathodic areas to give iron oxide and reduction products of nitrite. It was also suggested that inhibition by nitrite was enhanced by the similarity of the O–O distance in the nitrite ion to the Fe–Fe distance in the α-iron lattice.

An attempt was made to identify the oxide film on the metal by X-ray diffraction. Unfortunately only films of interference colors could be examined, although the film was tentatively identified as γ-Fe_2O_3 or magnetite. In view of the uncertainty of these measurements it was felt that a study by electron diffraction of the thinner films probably necessary for inhibition should be made. This work is reported in this paper.

Experimental

Materials.—The iron used was sheet iron which was kindly supplied by the British Iron and Steel Research Association. It had the following analysis: C, 0.005; Si, 0.0075; S, 0.013; P, 0.003; Mn, 0.007; Ni, 0.018; Cr, 0.02; Cu, 0.003; O, 0.12; N, 0.008; H, 0.00009. The specimens used in the film stripping experiments were 0.2 mm. thick and 4 × 1.5 cm. in area. The specimens used in the reflection experiments were discs 1.9 cm. in diameter and 1 mm. thick. All chemicals were C.P. grade.

Films Studied by Stripping from the Iron.—The specimens were degreased with xylene, abraded with 3/0 emery paper, swabbed with C.P. acetone, and dried. They were then immersed in 60 cc. of *N*/5 hydrochloric acid for 15–30 seconds; this acid was then rapidly displaced upwards by 1,000 ml. of molar sodium nitrite solution. The specimens were left in contact with 60 cc. of this passivating solution for 48 hours. They were then washed in distilled water, acetone, and dried on filter paper.

The films on the passivated specimens were stripped from the iron with a solution of iodine in anhydrous methyl alcohol by the method of Vernon, Wormwell and Nurse[4] as modified by Mayne and Pryor.[5] After washing, the specimen was transferred to a dish of methyl alcohol and the film detached by gently stroking the surface with a brush.

Some of the separated film was floated onto a fine copper gauze and examined by electron diffraction.

A Finch Electron Diffraction Camera was used. The

(1) M. Cohen, *Trans. Electrochem. Soc.*, **93**, 26 (1948).

(2) M. Cohen, R. Pyke and P. Marier, *J. Electrochem. Soc.*, **96**, 254 (1949).

(3) R. Pyke and M. Cohen, *Trans. Electrochem. Soc.*, **93**, 63 (1948).

(4) W. H. J. Vernon, F. Wormwell, and T. T. Nurse, *J. Chem. Soc.*, **621** (1939).

(5) J. E. O. Mayne and M. J. Pryor, *ibid.*, 1831 (1949).

measurements were made by taking alternate pictures of the stripped film and gold leaf in order to obtain the absolute spacings. The size of the unit cell for gold was taken as 4.06 Å.[6] A typical pattern is shown in Table I. The comparison patterns for this and the following tables are taken from the A.S.T.M. Index of X-ray Diffraction Patterns.

TABLE I

TRANSMISSION PICTURE OF STRIPPED FILM

S, strong; M, medium; W, weak; strongest line, 2.51; the lattice parameter was calculated to be 8.30 ± 0.05; it was found that the stripped film dissolved only very slowly in 3 *N* HCl. The solution gave a test for ferric iron only. The film was feebly magnetic.

Ring radius *R*, cm.	Spacing *d*, Å.	Intensity *I*	*hkl*	γ-Fe_2O_3 (X-Ray) *d*, Å.	Intensity *I*
1.34	2.92	M	220	2.93	0.4
1.56	2.51	V.S.	311	2.51	1.0
1.88	2.08	M	400	2.07	0.7
2.28	1.71	W	422	1.71	0.6
2.42	1.61	M	511, 333	1.60	0.9
2.63	1.48	S	440	1.48	1.0
3.58	1.09	W	642	1.09	

Films Studied on the Metal by Reflection.—The specimens were degreased with xylene, washed with running hot water and dried. They were then abraded down to 4/0 paper and finally polished lightly with a dispersion of MgO in water on selvyt cloth. They were then washed under running hot water, rinsed in acetone and dried on filter paper. The specimens were etched lightly with 0.2*N* HCl for 20 seconds and transferred to 1 molar sodium nitrite solution in a manner similar to the specimens treated for the transmission work. After passivating for a minimum of 48 hours they were washed and dried and put into the electron diffraction camera within 30 minutes. The patterns obtained by reflection were not as sharp as those obtained by transmission. A typical pattern obtained using the above procedure is given in Table II. This pattern

TABLE II

REFLECTION PATTERN OF IRON EXPOSED TO 1 *M* $NaNO_2$—72 HR.

d, Å.	*I*	γ-Fe_2O_3	γ-$Fe_2O_3 \cdot H_2O$	*I*
3.32	S		3.29	0.9
2.50	S	2.51	2.46	.7
2.12	W	2.07	2.08	.2
1.89	M		1.93	.7
1.73	W	1.71	1.73	.4
1.50	S	1.48	1.52	.4
1.37	W	1.33	1.37	.4
1.20	W	1.21	1.22	.3

appears to be a mixture of those for γ-Fe_2O_3 and γ-$Fe_2O_3 \cdot H_2O$.

Using the same procedure as above some specimens were exposed to *M*/50 sodium nitrite for 30 days. Others were exposed to *M*/100 sodium nitrite for thirty days and then transferred to *M*/1000 sodium nitrite plus *M*/1000 potassium chloride for a further 60 days. Reflection patterns for these are shown in Table III.

TABLE III

LONG EXPOSURES TO WEAKER NITRITE SOLUTIONS

M/50 $NaNO_2$ *d*, Å.	*I*	*M*/1000 $NaNO_2$ + Cl^- *d*, Å.	*I*
		3.42	Diffuse
2.54	S	2.52	S
1.92	W	1.95	S
1.75	W	1.71	W
1.52	S	1.53	S
		1.38	W
1.22	M	1.20	M

The lepidocrocite shows up more strongly in the solution which is close to the corroding range.

Two sets of specimens were polished and etched in *N*/5 HCl. In one set they were washed and dried and a diffraction picture taken. In the second set they were given a 30-second dip in *N*/50 sodium nitrite solution before washing and drying. The diffraction patterns are shown in Table IV.

TABLE IV

Etched *d*	*I*	γ-Fe *d*	*I*	Etched + nitrite *d*	*I*	γ-Fe_2O_3 *d*
2.53	M			2.54	S	2.51
				2.28	M	2.28[a]
2.01	S	2.05	1.00			
				1.66	W	1.60
1.47	M	1.43	0.46	1.51	S	1.48
				1.28	W	1.28
1.17	M	1.16	.54			
				0.88	W	0.88
0.77	W	0.76	.22			

[a] Observed by Haul and Schoon[7] on γ-Fe_2O_3.

The surface of the acid-treated specimen is mainly iron with some γ-Fe_2O_3 while that with the nitrite dip shows γ-Fe_2O_3 only.

Attempts were made to prepare some specimens for reflection by electropolishing with the perchloric–acetic anhydride bath. These showed iron with faint γ-Fe_2O_3 lines. On exposure to nitrite there was no change in the diffraction pattern.

Lepidocrocite was prepared by corroding iron in a dilute chloride solution for two months. The corrosion product was filtered, washed and air-dried. Some of it was treated with an alcohol-iodine solution for 48 hours. X-Ray diffraction patterns of both the treated and untreated powders were the same and agreed with that of lepidocrocite (γ-$Fe_2O_3 \cdot H_2O$). The washed and air-dried lepidocrocite was only slowly attacked by 1 *N* HCl.

Discussion

The film stripped from originally film-free iron passivated in a sodium nitrite solution exposed to air gives a diffraction pattern which agrees very closely with that of γ-Fe_2O_3 (Table I). The chemical tests and the poor magnetic properties indicate that it is γ-Fe_2O_3 and not magnetite.

The patterns obtained by reflection are not as sharp as those obtained by transmission. The reflection patterns also show lines which are not usually attributable to γ-Fe_2O_3 but which fit γ-$Fe_2O_3 \cdot H_2O$ (Tables II and III). The diffraction patterns of γ-Fe_2O_3 and its hydrate overlap and it is sometimes difficult to determine if there is γ-$Fe_2O_3 \cdot H_2O$ in the film. However, the diffraction pattern obtained by a very short exposure to nitrite (Table IV) was purely that of γ-Fe_2O_3. This indicates that γ-Fe_2O_3 is the first part of the film that is formed while the lepidocrocite is formed later as the film is being completed. During this time some ferrous ions are escaping which react to form lepidocrocite and are adsorbed on or occluded in the film. This would account for the lepidocrocite showing up in the patterns obtained by reflection but not by transmission. Specimens which were etched with acid and washed gave a diffraction pattern of iron with a small amount of γ-Fe_2O_3. This indicates that most of the film is produced by the passivating solution. It is interesting to note that the patterns obtained with nitrite are almost

(6) G. P. Thompson and W. Cochran, "Theory and Practice of Electron Diffraction," Macmillan, London, 1933.

(7) R. Haul and Th. Schoon, *Z. physik. Chem.*, **B44**, 216 (1939).

identical to those obtained with chromate and aerated sodium hydroxide solutions.[5,8,9]

The film on the metal is probably in a constrained state and relaxes when stripped from the surface. This accounts for the sharper pattern obtained by transmission. An anhydrous oxide film is most probably produced by a heterogeneous reaction of oxygen and nitrite with the metal and starts to grow as a continuation of the metal surface. This reaction most probably is preceded by adsorption of the nitrite ion on the surface. The film thickens by migration of iron ions outward through the originally thin film, which iron ions then react to give more oxide. Some of the ferrous ions escaping through the originally imperfect film react homogeneously to form γ-$Fe_2O_3 \cdot H_2O$. The oxide film is formed very rapidly and when sufficiently thick and continuous reduces the further corrosion of the iron.

(8) I. Iitaka, S. Miyake and T. Iimori, *Nature*, **139**, 156 (1937).

(9) J. E. O. Mayne, J. W. Menter and M. J. Pryor, *J. Chem. Soc.*, 3229 (1950).

Acknowledgment.—This work was done while the author was on leave of absence in the laboratory of Dr. U. R. Evans at Cambridge University. The author wishes to thank Dr. U. R. Evans, Dr. J. E. O. Mayne and Dr. M. J. Pryor for helpful discussion and Dr. J. Sanders and Dr. J. W. Menter for help with some of the electron diffraction work.

HYSTERESIS OF CONTACT ANGLES. A STUDY OF INTERFACIAL CONTACT ANGLES IN THE MERCURY–BENZENE–WATER SYSTEM[1]

BY F. E. BARTELL AND CARL W. BJORKLUND

Department of Chemistry, University of Michigan, Ann Arbor, Michigan

Received April 16, 1951

It was found that in this liquid–liquid–liquid (mercury–benzene–water) system "hysteresis" of the contact angle does occur. This effect can be of considerable magnitude. Values for advancing and for receding angles may be dependent upon a number of different factors, one of the most predominant of which relates to the time that the interfaces have aged before a drop is formed or before measurement of the angle is made. A water drop at a mercury–benzene interface may expand, or contract, spontaneously as the tensions of the system tend to attain conditions of equilibrium. The magnitude of the contact angle is dependent upon the relative magnitudes of the interfacial tensions operating within the system. A change in value of one or more of the interfacial tensions within the system is usually accompanied by a change in value of the contact angle. Evidence has been obtained indicating that an alteration of the effective tensions such as might result from movement, or attempted movement of the line of contact (*i.e.*, the periphery) of the drop would result in the hysteresis effect.

If truly reliable contact angle data were available, it would be possible to calculate the approximate magnitudes of the free energy changes which occur when liquids come in contact with solids. Justifiable predictions based on this information could then be made regarding the probable behavior of the different systems in numerous processes which are dependent upon surface properties. Although considerable work has been done on the measurement of contact angles, only a very small fraction of the available data can be accepted as being more than qualitative in nature. In most of the earlier work insufficient consideration was given to the effects of hysteresis of contact angles and to the factors responsible for these effects. While some investigators have been cognizant of the existence of hysteresis and have taken it into consideration, many others have entirely ignored its effects.

It has too often been tacitly assumed that the contact angles formed by almost any solid–liquid–gas or solid–liquid–liquid system should be stable, reproducible and of definite value for the given system. Furthermore, the angles as initially formed have too often been assumed to be representative of the system in true equilibrium. It happens, however, that for almost any system one can obtain apparently stable angles with values ranging between two fairly wide but definite limits. The angles representing these two limits are referred to as advancing and receding angles. An *advancing* angle is defined in this paper as the maximum angle that is formed when a liquid is caused to advance over a solid surface, while a *receding* angle is the minimum angle that is formed when a liquid is caused to recede over a solid surface. The intermediate angles have been given no definite designation, and it is one of these angles that often is measured in the mistaken belief that it is the "equilibrium," or representative, angle of the system.

In this paper, when a specific value is given for a contact angle, reference is made to the angle as measured through the liquid phase if the third phase is a gas or a vapor, and as measured through the water phase whenever a water phase is present.

A number of different theories have been proposed to account for hysteresis of contact angles. Evidence presented by Shuttleworth and Bailey,[2] Coghill and Anderson,[3] Wenzel[4,5] and others support the theory that hysteresis is caused by surface roughness. Adam and Jessop[6] attributed the variation in contact angle values to "friction" of the liquid on the solid. The value of the equilibrium angle for the system was considered to be represented by the mean of the maximum and minimum values. Ablett[7] believed that "hysteresis" is

(1) The data in this paper were taken from a portion of the thesis of Carl W. Bjorklund, submitted to the School of Graduate Studies of the University of Michigan in partial fulfillment of the requirements for the Ph.D. degree, August, 1950.

(2) R. Shuttleworth and G. L. J. Bailey, Discussions, Faraday Soc. No. 3, 16 (1948).

(3) Coghill and Anderson, U. S. Bur. Mines Tech. Paper, **262**, 47 (1923).

(4) R. N. Wenzel, *Ind. and Eng. Chem.*, **28**, 988 (1936).

(5) R. N. Wenzel, THIS JOURNAL, **53**, 1466 (1949).

(6) N. K. Adam and G. Jessop, *J. Chem. Soc.*, **127**, 1863 (1925).

(7) R. Ablett, *Phil. Mag.*, **46**, 244 (1923).

caused by the adsorbed liquid remaining on the solid when a drop is caused to recede. Edser,[8] MacDougall and Ockrent,[9] and Bartell and Cardwell[10] have also expressed the opinion that adsorbed liquid layers or films at the surface of the solid are largely responsible for hysteresis effects.

Space does not permit discussion of these and of other theories. It may be sufficient to state that probably every theory that has been presented possesses elements that must be taken into consideration in the development of a generally acceptable, truly comprehensive, theory. No one theory so far presented can account for all behaviors observed in different contact angle systems.

The Mercury–Benzene–Water System

A mercury–benzene–water system was selected for the present study. With mercury as a substrate the question of surface roughness and of polar heterogeneity was eliminated, while the fluidity and mobility of mercury appeared to offer good conditions for the attainment of equilibrium. Of most importance, since each of the phases in contact was fluid, the interfacial tensions existing between each fluid pair could be determined directly. Knowing the values of these tensions it would then be possible to calculate the values of the interfacial angles which should be expected.

Young's equation[11] relating interfacial tensions and contact angles has been generally accepted. For solid–liquid–air systems it may be written[12]

$$S_1 - S_{12} = S_2 \cos \theta_{12} \qquad (1)$$

or for solid–liquid–liquid systems

$$S_{12} - S_{13} = S_{23} \cos \theta_{23} \qquad (2)$$

Materials and Methods for Contact Angle Measurement

The liquids used were all carefully purified (though in the majority of experiments were not air free).

The controlled drop method was used for the measurement of contact angles. Water drops were added at the mercury–benzene interface with a hypodermic syringe pipet. The tip of the pipet was a very fine glass capillary of approximately 0.05 mm. inner diameter. Attached to the syringe was a mechanism by means of which liquid could be extruded from or drawn into the tip very slowly and at a uniform rate. It was found that the value of the contact angle was unaltered by the presence of this fine tip within the drop. At the time of measurement the drops were usually between 1 and 2 mm. in diameter.

The drop was placed in the light beam from a concentrated arc lamp. The beam was passed through a lens, and the drop image was brought to a focus upon a ground glass plate where the angle could be measured directly or could be photographed. The temperature of the system was held at 25.0 ± 0.1°.

Interfacial Tension Measurements.—The pendent drop method was used for measurement of interfacial tensions. The results obtained with this method, as now developed, have a high degree of precision. Inasmuch as measurements can be made over almost any time interval, changes in interfacial tension which may occur with time can be detected and measured. Such changes were determined for each of the three interfaces in the system under study.

Initial[13] Advancing Interfacial Contact Angles

The Mercury–Water–Benzene System.[14]—In preliminary measurements progressively larger angles were observed as water drops were introduced at mercury–benzene interfaces which had been standing for progressively longer periods of time. Studies were then planned[7] to determine whether the value of the initial water advancing angle was directly proportional to the time that the mercury and benzene had been in contact prior to the introduction of the water drop, and[6] to determine whether the interfacial tension at the mercury–benzene interface likewise changed with time.

Relation between Time of Exposure of Benzene on Mercury and the Initial Interfacial Water Advancing Angle.—As soon as possible (about six minutes) after the formation of a mercury–benzene interface, a water drop was introduced, and the value of the initial advancing angle was recorded. After this drop had been allowed to stand for some time it was caused to advance still further, whereupon the angle was found to be larger than before. A new drop was then formed at a different location at the mercury–benzene interface and the procedure was repeated. The results are given in Table I. It will be noted that the value of the initial advancing angle increased as the age of the mercury–benzene interface increased. After the mercury and benzene had been in contact for as long as 23 hours, the water drop did not tend to break through to the mercury and displace the benzene with the result that angles of 180° were formed.

TABLE I

EFFECT OF THE TIME OF EXPOSURE OF MERCURY TO BENZENE (SATURATED WITH WATER) ON INITIAL WATER ADVANCING ANGLES (OBSERVED VALUES)

Time of Exposure	Initial Water Advancing Angle, Degrees
6 minutes	118
25 minutes	119
1 hour	122
2.5 hours	138
5 hours	144
19 hours	159
21 hours	164
23 hours	(drop would not 180 break through)

Interfacial Tension between Mercury and Benzene (Saturated with Water) as a Function of Time.—Since the values of the initial advancing angles were found to depend upon the time that the mercury had been in contact with benzene, a study was made of the interfacial tension between

(8) E. Edser, Brit. Assoc. Advancement Sci., Report 4 of Reports on Colloid Chem., 292 (1922).

(9) G. MacDougall and C. Ockrent, *Proc. Roy. Soc.* (*London*), **A180**, 151 (1942).

(10) F. E. Bartell and P. H. Cardwell, *J. Am Chem. Soc.*, **64**, 1530 (1942).

(11) T. Young, *Phil. Trans.*, **95**, 65 (1805).

(12) The letter S will be used to designate surface or interfacial tensions, and subscripts 1, 2 and 3 will define the phases as solid, organic liquid and water, respectively. For example, S_1 represents the surface tension of a solid of air, S_2, the tension of organic liquid in its own vapor or in air, and S_3, that of water in its vapor or in air. Similarly, S_{12} represents the interfacial tension of solid against organic liquid, S_{13} of solid against water, and S_{23}, of organic liquid against water. θ used with the same subscripts represents contact angle values for the different contiguous phases. A superscript (′) indicates mutual saturation of the fluid phases; thus S_{12}' represents the interfacial tension between mercury and benzene saturated with water, while S_{13}' represents that between mercury and water saturated with benzene. θ^a refers to an advancing angle, and θ^r refers to a receding angle. Young's equation, in terms of the mutually saturated liquids, may then be written as

$$S_{12}' - S_{13}' = S_{23}' \cos \theta_{23} \qquad (3)$$

(13) The interfacial advancing angle measured two minutes after a water drop was caused to advance at a given interface will be referred to hereinafter as an "initial" advancing angle.

(14) Wherever reference is made to water and to benzene in this paper, the mutually saturated liquids are intended since they were used in all experiments.

mercury and benzene saturated with water as a function of time.

The combined results of two independent series of determinations are shown by the curve in Fig. 1. The interfacial tension between mercury and benzene saturated with water decreased rapidly from a value of 365 dynes/cm. to a value of 360 dynes/cm. within the first 20 minutes. The tension values then decreased more slowly until after one hour the rate of decrease was practically constant. A low value of 336 dynes/cm. was recorded after 13 hours.

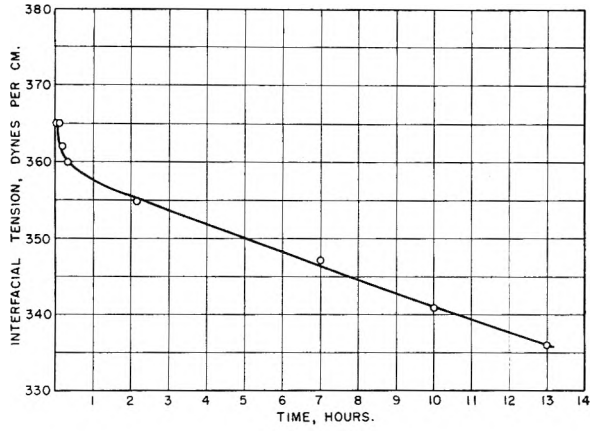

Fig. 1.

Correlation of Initial Advancing Angle and Interfacial Tension Data.—Equation (3) was used to correlate the contact angle and interfacial tension data which had been obtained. As a first approximation the values of S_{13}' and S_{23}' were considered to be constant for each of the water drops referred to in Table I because the ages of the interfaces represented by these terms were essentially the same throughout the series. With this assumption, the only variable terms in equation (3) were the contact angle, θ_{23}, and the interfacial tension, S_{12}', at the different mercury–benzene interfaces. The value of S_{13}' (interfacial tension between mercury and water) at the end of two minutes was found to be 379.5 dynes/cm., while the value of S_{23}' (interfacial tension between benzene and water) was 34.0 dynes/cm. The values of the variable term, S_{12}', in equation (3) at different time intervals were obtained from the curve in Fig. 1. (For the purpose of calculation and because more quantitative data were not available, it was assumed that the tension at a given mercury–benzene interface was not appreciably changed by the introduction of a water drop at the interface.) These values were then substituted in equation (3) to calculate the values of the contact angle, θ_{23}, which would be expected at given time intervals. The results summarized in Table II indicate that the value of the initial advancing angle would be expected to increase with the time that the mercury and benzene had been in contact before the water drop was formed. The calculated angle for time intervals greater than 7 hours is approximately 180°.

TABLE II

EFFECTS OF THE TIME OF EXPOSURE OF MERCURY TO BENZENE (SATURATED WITH WATER) ON INITIAL WATER ADVANCING ANGLES (CALCULATED VALUES)

Time of exposure	S_{12}', dynes/cm.	S_{13}', dynes/cm.	S_{23}', dynes/cm.	$\frac{S_{12}' - S_{13}'}{S_{23}'}$	θ_{23} (calculated value), degrees
2 min.	364.5	379.5	34.0	−0.44	116
6 min.	363.0	379.5	34.0	− .49	119
10 min.	362.0	379.5	34.0	− .52	121
18 min.	360.5	379.5	34.0	− .56	124
25 min.	359.5	379.5	34.0	− .59	126
1 hr.	358.0	379.5	34.0	− .63	129
2.5 hr.	354.5	379.5	34.0	− .74	138
5 hr.	350.0	379.5	34.0	− .82	145
7 hr.	346.0	379.5	34.0	− .99	172
13 hr.	336.0	379.5	34.0	−1.3	180

The tendency for the observed values of the initial advancing angles to increase (see Table I) can, therefore, be attributed to the steady decrease in the interfacial tension which occurs when mercury and benzene are allowed to stand in contact. When the results in Tables I and II are compared, fair agreement is noted between the experimental and the calculated interfacial contact angle values. The somewhat different rate at which the calculated angles increase with time is not unreasonable in view of the assumptions required for the calculations.

Spontaneous Changes in Water Advancing Angles

Variation of the Water Advancing Angle, with Time, at Undisturbed Mercury-Benzene Interfaces.—The data in Table III illustrate the extent to which the contact angle formed by a water drop at a mercury–benzene interface changed spontaneously as the system was allowed to stand undisturbed. In this particular experiment the mercury had been in contact with benzene for 2.5 hours before the water drop was introduced at the interface. The initial advancing angle was 138°. The diameter of the base of the drop was observed to increase very slowly as the drop was allowed to stand, while the value of the advancing angle gradually decreased. A number of similar experiments were made with such systems, and the same trend was always noted.

Interfacial Tension between Mercury and Water (Saturated with Benzene) as a Function of Time.—The combined results of three independent series of determinations of the interfacial tension between mercury and water (saturated with benzene) are represented in Fig. 2. The interfacial tension decreased rapidly from a high value of 381 dynes/cm. to a much lower value of 366 dynes/cm. within the first 30 minutes. The tension values then decreased more slowly until after one hour the rate of decrease was practically constant. A low value of 351 dynes/cm. was recorded after 11 hours.

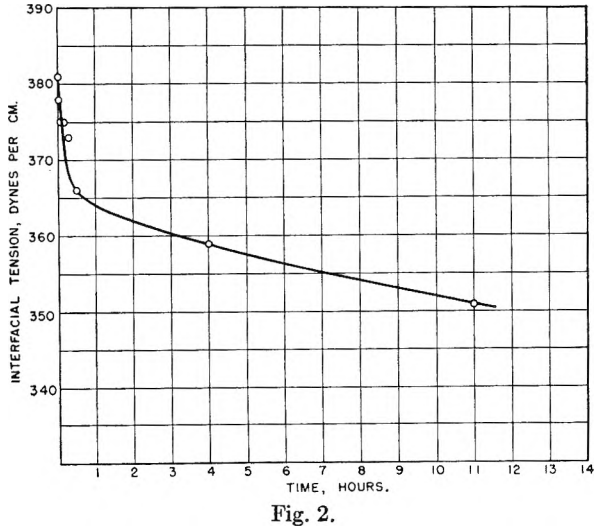

Fig. 2.

Upon comparing Figs. 1 and 2 the similarity between the two interfacial tension–time curves is readily apparent. Both exhibit the same sharp initial decrease, after which the slopes become linear and very nearly the same for both curves. It is interesting to note that the initial sharp decrease in both curves occurs within the first 20 to 30 minutes despite the fact that the decrease for the mercury–water tension is three times as great as that for the mercury–benzene tension in this time interval.

Interfacial Tension between Mutually Saturated Water and Benzene.—The interfacial tension between water and benzene was measured by forming both pendent-up drops of benzene in water and pendent-down drops of water in ben-

zene. In both cases the liquids were mutually saturated, and measurements were made over time intervals ranging from one minute to six hours at a temperature of 25.0 ± 0.1°. No time effect could be detected in this system. The average value for 10 determinations by the two procedures was 34.0 ± 0.1 dynes/cm., taking 0.9969 g./cc. as the density of water saturated with benzene and 0.8725 g./cc. as the density of benzene saturated with water.

Explanation of Spontaneous Changes in Water Advancing Angles.—Equation (3) was used to correlate the contact angle data reported in Table III with the observed interfacial tension data. As in the previous calculations, it was necessary to assume that the tension at the mercury–benzene interface was not appreciably altered by the introduction of a water drop. The value of the mercury–water interfacial tension could then be obtained from the curve in Fig. 2 for the selected time interval. Thus, the system reported in Table III was one in which the mercury–benzene interfacial tension remained practically constant while the mercury–water interfacial tension changed; *i.e.*, variations in θ_{23} in equation (3) were directly related to the changes in the value of S_{13}', the values of S_{12}' and S_{23}' being relatively constant. By using the difference between these two values ($S_{12}' - S_{13}'$) as obtained from Figs. 1 and 2 and substituting in equation (3) it was then possible to calculate the value of the contact angle which should be expected at any specified time interval. For example, the value of S_{12}' (mercury–benzene interfacial tension) at the end of 2.5 hours was found from Fig. 1 to be 354.5 dynes/cm. If a water drop were introduced at this mercury–benzene interface and allowed to stand for two minutes, the resultant value of S_{13}' (mercury–water interfacial tension) obtained from Fig. 2 would be 379.5 dynes/cm. Taking the value of S_{23}' as 34.0 dynes/cm. and substituting in equation (3) the value of the angle which would be expected is found to be one of 138°. Similar calculations were made for drops which had been standing for progressively longer time intervals (corresponding to those reported in Table III) and the results are given in Table IV. They indicate that interfacial contact angles in this system could be expected to decrease from a value of 138° at the end of two minutes to a value of 108° after the system had been allowed to stand for 3 hours. The drop would be expected to spread spontaneously, fairly rapidly at first, and then more slowly as a result of the relatively large change in the tension at the mercury–water interface.

When the results in Tables III and IV are compared, it is noted that the initial values of the calculated and observed contact angles do agree, but that the values of the *calculated* angles decrease more rapidly with time. A large part of this discrepancy may be attributed to the necessarily inadequate assumptions which were required in the calculations for the ideal case. For example, it is highly unlikely that the tension at the mercury–benzene interface was not altered somewhat by the introduction of the water drop, nor is it likely that the benzene would be completely swept back from the mercury surface when the water drop was introduced. Quantitative estimates of the effect of such factors, however, were not possible, although a qualitative consideration of their effect indicated a tendency toward better agreement between the calculated values and the observed results.

TABLE III

SPONTANEOUS VARIATION OF ADVANCING ANGLES OF A WATER DROP AT AN UNDISTURBED MERCURY–BENZENE INTERFACE[a] (OBSERVED VALUES)

Time elapsed after formation of water drop	Water advancing angle, degrees
2 min.	138
4 min.	137
6 min.	136
8 min.	135
10 min.	134
19 min.	132
25 min.	131
2 hr.	128

[a] The mercury had been exposed to benzene saturated with water for 2.5 hours prior to the introduction of the water drop.

TABLE IV

SPONTANEOUS VARIATION OF ADVANCING ANGLES OF A WATER DROP AT AN UNDISTURBED MERCURY–BENZENE INTERFACE[a] (CALCULATED VALUES)

Time elapsed after formation of the water drop	S_{12}', dynes/cm.	S_{13}', dynes/cm.	S_{23}', dynes/cm.	$\frac{S_{12}' - S_{13}'}{S_{23}}$	θ_{23} (calculated values), degrees
2 min.	354.5	379.5	34.0	−0.74	138
4 min.	354.5	377.5	34.0	− .68	133
6 min.	354.5	376.0	34.0	− .63	129
8 min.	354.5	375.0	34.0	− .60	127
10 min.	354.5	373.5	34.0	− .56	124
14 min.	354.5	371.5	34.0	− .50	120
19 min.	354.0	369.0	34.0	− .44	116
25 min.	354.0	367.0	34.0	− .38	112
2 hr.	351.0	362.0	34.0	− .32	109
3 hr.	349.5	360.0	34.0	− .31	108

[a] Calculations were made for a system which would correspond to that referred to in Table III, *i.e.*, one in which the mercury had been exposed to benzene saturated with water for 2.5 hours prior to the introduction of the water drop.

The fact that a drop of water placed at a mercury–benzene interface tended to spontaneously spread, giving a smaller interfacial angle, indicates quite definitely that in a system in which all phases are fluid and mobile the system will adjust itself so as to approach closely true equilibrium conditions. Spontaneous readjustment within a solid–liquid–liquid system would normally not take place so quickly and, in some cases, would probably require very long periods of time in order even to approach equilibrium conditions.

Interfacial Water Receding Angles in the Mercury–Water–Benzene System

Interfacial Water Receding Angles Equal to the Water Advancing Angles.—It was found that advancing and receding angles of equal value could be obtained for systems in which the advancing angle had a value of 118 ± 2° (*i.e.*, systems in which the mercury and benzene had been in contact for less than an hour prior to introduction of the water drop). In order to obtain the same value for the receding angle as for the advancing angle it was only necessary to cause the drop to recede very slowly; the extent to which it was caused to recede had no effect. Under this condition, receding angle values which were equal to the advancing angle values were obtained even if the water drops were allowed to stand at the mercury–benzene interface for periods up to 30 minutes before they were caused to recede. Equal values for these angles were not obtained under any conditions for systems in which the water drops were formed after the mercury and benzene had been in contact for periods longer than one hour.

Interfacial Water Receding Angles not Equal to the Water Advancing Angles.—The value of the receding angle was found to depend upon the rate at which the drop was caused to recede before the angle was measured. Thus, for the system described above in which the initial advancing angle was 118°, the receding angle after the drop had been partially withdrawn *very slowly* was also 118°. Receding angles having values between 118° and approximately 108° could, however, be obtained in the same system if the drop was caused to recede more rapidly. The magnitude of the angle depended upon the rate of withdrawal.

It was found subsequently that advancing and receding angles having the same, and constant, values could be observed for the systems in which the contact angles were 118 ± 2° even though the drops were being slowly expanded or contracted while the contact angle measurements were being made. It was necessary, however, that the rate of movement of the drop periphery did not exceed about 0.02 mm. per minute.

Interfacial Contact Angles on Mercury Substrates Previously Exposed to Water Drops.—Evidence has been presented to indicate that the tensions at both mercury–benzene and at mercury–water interfaces slowly change with

time. The effect of these slow changes upon the contact angle may be further illustrated by the following typical experiment.

A drop of water was allowed to stand for $1^1/_2$ hours at a given mercury–benzene interface, at the end of which time the advancing angle was 120°. The drop was then caused to recede rapidly, and when it was caused to readvance three minutes later the contact angle was found to have a low value of 111°. After 4 minutes the drop was caused to advance further and the value of the angle was found to be 114°. Again after the drop had stood for another 6 minutes and was then caused to advance still further, the value of the advancing angle was 119°. At no time in the above experiment was the periphery of the drop caused to advance over surface which had not been covered by the original drop. Later, when the drop was advanced beyond the area covered by the original drop, the value of the advancing angle was found to be equal to the value of the angle formed by a fresh drop at any portion of the interface which had not been previously exposed to water. It was subsequently found that if sufficient time elapsed after the drop had been receded and before it was caused to readvance, the value of the readvancing angle equaled or exceeded that of the original angle even though the drop was not caused to advance beyond the area which had been covered by the original drop.

Conclusions

It is believed that the results described in this paper furnish sufficient evidence to establish the existence of hysteresis effects in the mercury–water–benzene system.

It is evident that hysteresis is not dependent entirely upon surface roughness, nor upon polar heterogeneity, nor yet upon frictional effects as has heretofore been postulated.

It is believed that the results of the contact angle measurements obtained in this investigation furnish conclusive evidence that hysteresis of the contact angle in the mercury–water–benzene system does exist. It is believed further that the hysteresis effects observed in this system can be logically explained by a consideration of the alteration with time of the interfacial tensions existing at the mercury–water and the mercury–benzene interfaces.

No attempt has been made in this paper to discuss the probable cause for the decrease in tension values with time at either the mercury–benzene or the mercury–water interfaces.[15] Whether an adsorption process or a chemical reaction be responsible is immaterial in order to prove that hysteresis effects *do* occur, that the magnitudes of the angles *do* change with time, and that the magnitudes of the angles *are* dependent upon the relation of the interfacial tension values within the system.

(15) Evidence bearing upon this point will appear in an early paper from this laboratory (THIS JOURNAL in press).

PRODUCTION OF THE JOSHI EFFECT UNDER DIRECT CURRENT EXCITATION

BY H. J. ARNIKAR

Chemical Laboratories, Banaras University, Banaras, India

Received April 30, 1951

Joshi effect was studied in (i) hydrogen, (ii) mercury vapor, (iii) chlorine, (iv) argon–alcohol mixture and (v) iodine vapor contained (i) and (iii) in full ozonizer, (ii) and (iii) in semi-ozonizer, (iv) in a GM counter and (v) in a tube with external sleeves; both in the positive and negative coronas due to steady d.c .potentials in the range 1–4 kv. The glow due to discharge was found throbbing. Besides the much larger d.c. (stable) component, an appreciable a.c. (pulsating) component was observed. The former showed a maximum of 20% negative Joshi effect; the latter 100%; both with but ordinary light. Iodine vapor gave a maximum of 40% positive Joshi effect which diminished with increased potential. Argon–10% alcohol mixture (appropriate for "counter" action) showed a very much larger positive Joshi effect. The oscillograms revealed complete suppression under light of the H.F. pulses corresponding to 100% negative Joshi effect.

Introduction

Except for early observations by Joshi[1] using unsmoothed unidirectional potential pulses, work on the above phenomenon refers to a.c. excitation. Warburg's theory[2] for a glass ozonizer postulates an accumulation of electrons and positive ions on the appropriate electrode walls; this induces a field reverse to the one applied. With the waning of the applied potential during a given cycle, the primary discharge practically stops and the reverse field acts on the gas producing a number of local discharges; these correspond to the discrete pulses observed on the cathode ray oscillograph (C.R.O.). This series of events recurs in the other half of the potential cycle. The reverse oriented surface charges being thus considered essential to the ozonizer discharge, it was argued by Klemenc, Hintenberger and Höfer[3] that d.c. potentials would be ineffective in exciting such a tube. In support of this deduction is cited the failure to produce a glow in the gas in an ozonizer even at 15 kv. (d.c.).[3]

The successful working, on the other hand, of a GM counter with a glass cathode (first introduced by Maze[4] and identical with semi-ozonizer[5]), as also the recent experiments of English[6] on d.c. discharges between dielectric and semi-conducting points and metal plate, negate the above view. Hence, it appeared desirable to study the behavior under smooth d.c. potentials of an ozonizer from the point of its discharge characteristic and the associated Joshi effect.

Experimental

Carefully purified samples of hydrogen, chlorine, mercury vapor, iodine and argon were employed. The first three were excited in semi- or/and full ozonizers (Tables I–II). In the case of argon a GM counter was used containing

(1) S. S. Joshi, *Proc. Ind. Acad. Sci.*, **22**, 389 (1945).

(2) E. Warburg, *Ann. Phys.*, **28**, 1 (1909).

(3) A. Klemenc, H. Hintenberger and H. Höfer, *Z. Elektrochem.*, **47**, 708 (1937).

(4) R. Maze, *J. Phys. Radium*, **7**, 164 (1946).

(5) S. S. Joshi, Presidential Address to the Chemistry Section, Indian Science Congress, 1943.

(6) W. N. English, *Phys. Rev.*, **74**, 170, 179 (1948).

TABLE I

THE JOSHI EFFECT IN HYDROGEN UNDER D.C. EXCITATION

Full-ozonizer: length = 10 cm.; internal diameters: inner tube = 8 mm.; outer tube = 12 mm.; pressure = 18 mm. (30°)

Potential, kv.	(i) Steady current component: (a) Positive corona i_D	i_L	$-\Delta i$	$-\%\Delta i$	(b) Negative corona i_D	i_L	$-\Delta i$	$-\%\Delta i$	(ii) Pulsating current component: (a) Positive corona i_D	i_L	$-\Delta i$	$-\%\Delta i$	(b) Negative corona i_D	i_L	$-\Delta i$	$-\%\Delta i$
1	2	3	4	5	6	7	8	9	10	11	12	13	14	15	16	17
1.76	12	12	0	0	14	14	0	0	..	..	..	..	0	0	..	..
2.00	15	13	2	13	18	17	1	6	3	0	3	100	6	0	6	100
2.20	17	15	2	12	20	19	1	5	3	0	3	100	7	0	7	100
2.40	21	18	3	14	23	22	1	4	4	0	4	100	8	0	8	100
2.56	23	20	3	13	25	24	1	4	..	..	..	..	..	..	..	..
2.60	25	22	3	12	26	24	2	8	5	0	5	100	10	0	10	100
2.80	26	24	2	7	29	27	2	7	5	0	5	100	12	6	6	50
3.20	33	31	2	6	36	34	2	6	7	0	7	100	15	10	5	30
3.36	37	34	3	8	38	36	2	5	7	0	7	100	16	11	5	30
3.60	41	38	3	7	42	39	3	7	8	3	5	60	17	11	5	30

TABLE II

THE JOSHI EFFECT IN MERCURY VAPOR UNDER D.C. EXCITATION

Pt wire-glass semi-ozonizer: length = 10.5 cm.; diameters: Pt wire = 0.3 mm.; glass tube = 9 mm.; pressure = 0.0028 mm. (30°)

1	2	3	4	5	6	7	8	9	10	11	12	13	14	15	16	17
1.20	4	3.5	0.5	13	7	7	0	0	..	..	..	..	..	..	..	..
1.60	9	7	2	22	13	13	0	0	..	..	..	..	..	..	..	..
2.00	16	13	3	19	21	21	0	0	2	0	2	100	..	..	..	..
2.20	21	17	4	19	24	24	0	0	3	0	3	100	1	0	1	100
2.40	25	21	4	16	28	28	0	0	4	0	4	100	2	0	2	100
2.60	29	25	4	14	33	33	0	0	5	0	5	100	2	1	1	50
2.80	37	30	7	19	39	38	1	3	7	0	7	100	3	2	1	30
3.00	43	35	8	19	49	47	2	4	9	0	9	100	3	2	1	30
3.20	51	43	8	16	55	53	2	4	11	0	11	100	5	4	1	20
3.40	57	48	9	16	66	62	4	6	13	3	10	80	8	6	2	25
3.52	60	53	7	12	72	69	3	4	14	4	10	70	10	8	2	20
3.60	75	66	9	12	93	91	2	2	15	5	10	70	12	10	2	17

TABLE III

THE JOSHI EFFECT IN CHLORINE UNDER D.C. EXCITATION

Ag wire-glass semi-ozonizer: length = 15 cm.; diameters: Ag wire = 0.5 mm.; glass tube = 7 mm.; pressure = 170 mm. (30°)

Potential, kv.	In the pulsating current component: (a) Positive corona i_D	i_L	$-\Delta i$	$-\%\Delta i$	(b) Negative corona i_D	i_L	$-\Delta i$	$-\%\Delta i$
1.12	6	1	5	80	2	0.5	1.5	75
1.25	8	1	7	90	2	0.5	1.5	75
1.40	10	2	8	80	2	0.5	1.5	75
1.60	13	2	11	85	2	1	1	50
1.80	15	3	12	80	2	1	1	50
2.00	20	9	11	55	2	1	1	50
2.20	25	17	8	30	3	2	1	30
2.40	30	25	5	15	3	2	1	30
2.60	34	31	3	10	4	3	1	25
2.80	41	39	2	5	4	3	1	25
3.00	48	45	3	6	4	4	0	0
3.20	53	50	3	6	4	4	0	0
3.40	59	57	2	3	4	4	0	0

spectroscopically pure samples of the gas at a pressure of 90 mm., and admixed with 10% alcohol vapor as a "quencher" in proportion appropriate for "counter" action (Table IV). Iodine–iodine vapor was excited in a glass tube with external sleeves (Table V). The systems were excited by smooth rectified and stabilized potentials obtained from an "E.H.T." unit of the Dynatron Radio make, which also included a polarity reversing switch and a potential indicator. In the accessible potential range the glow was found to be throbbing. This as well as the oscillographic pattern of the current suggested the presence of two groups in the discharge current, one *steady* and the other *pulsating*. The steady component was measured using a reflection galvanometer introduced directly between the ozonizer L.T. and earth, while the pulsating component was measured by the same

TABLE IV

THE JOSHI EFFECT IN ARGON (+ ALCOHOL) GM COUNTER

Counter length = 6 inches; diameters: W wire = 0.006 inch; brass cylinder = 1 inch; p_{argon} = 90 mm.; $p_{ethyl\ alcohol}$ = 10 mm. (30°)

Potential, kv.	In the positive corona: (i) Steady current component i_D	i_L	$+\Delta i$	$+\%\Delta i$	(ii) Pulsating current component i_D	i_L	$+\Delta i$	$+\%\Delta i$
1.16	1	1	0	0	0	0	..	..
1.20	3	6	3	100	0	0	..	..
1.22	7	11	4	60	2	3	1	50
1.24	9	23	14	160	2	3	1	50
1.26	11	33	22	200	2	4	2	100
1.28	19	42	23	120	2	5	3	150
1.30	24	58	34	140	3	7	4	130
1.32	29	64	35	120	3	8	5	170
1.34	38	93	55	150	4	10	6	150
1.38	38	105	67	180	6	15	9	150
1.40	48	106	58	120	6	16	10	170
1.42	55	135	80	150	7	21	14	200
1.44	62	150	88	140	11	215	204	1900
1.46	92	>300	>200	>300	..	..	..	..

galvanometer actuated by a diode coupled inductively with the L.T. line.

Light from a 200-watt incandescent (glass) bulb run at a constant potential was used for irradiating the system provided with a simple shutter arrangement. Results are obtained for *net Joshi effect* ($\Delta i = i_{light} - i_{dark}$), and *relative Joshi effect* ($\%\Delta i = 100\Delta i/i_D$) at potentials varied in the range 1–4 kv. for (i) steady and (ii) pulsating component, and each for (a) positive and (b) negative polarity for the inner electrode (Tables I–III). Some of the typical wave forms of the discharge current in dark and in light corresponding to (i)(a), (i)(b), (ii)(a), and (ii)(b) obtained with Philips C.R.O. connected across a megohm resistance in the ozonizer L.T. line are given in Fig. 4.

TABLE V

THE JOSHI EFFECT IN IODINE VAPOR UNDER D.C. SLEEVE EXCITATION

Tube length, 10 cm., diameter, 11 mm.; sleeves, 12 mm. wide and 20 mm. apart; pressure, 0.47 mm. (30°): in the steady current component

Potential, kv.	i_D	i_L	$+\Delta i$	$+\%\Delta i$
2.00	1	1	0	0
2.96	3	4	1	30
3.20	5	7	2	40
3.36	6	8	2	30
3.52	8	10	2	25

Discussion of Results

The V–i Characteristic of the d.c. Ozonizer Discharge.—Contrary to the findings of Klemenc, *et al.*,[3] the present work shows that gases contained in ozonizers with one or both glass electrodes can be excited by smooth continuous potentials. These experiments revealed that a part of the discharge current consists of a pulsating component which is significant to the Joshi effect. Results of Tables I and II indicate that in the case of the steady component the current is less in the positive corona than in the negative at a given potential. This is consistent with the slightly higher threshold potential V_m^+ observed for the positive than V_m^- for the negative corona. A like difference in the breakdown values for discharges from points and wires has been attributed to mechanisms distinctive of coronas of the two polarities. Secondary liberation of electrons from the cathode by photons (γ-mechanism) and by positive ions (β-mechanism) are known to be the factors mainly operative in the positive and negative coronas, respectively (Loeb[7]). The contribution of γ depends on the effective area of the cathode, *ceteris paribus*, while that of β depends on the potential gradient close to the cathode. Hence, whether γ or β will be relatively more pronounced will depend on whether the inner electrode is positive or negative. However, the known lower efficiency of γ compared with β leads to the threshold potential being slightly higher for the positive than for negative corona, as observed. This difference should be much less in full ozonizers specially of the dimensions used (*viz.*, the two radii differing but little) than in point or wire coronas. In discharges from semi-conducting points of CuO and FeS to metal plate, the breakdown value for the point positive was found by English[6] to be 0.7 to 0.9 kv. above that for the point negative.

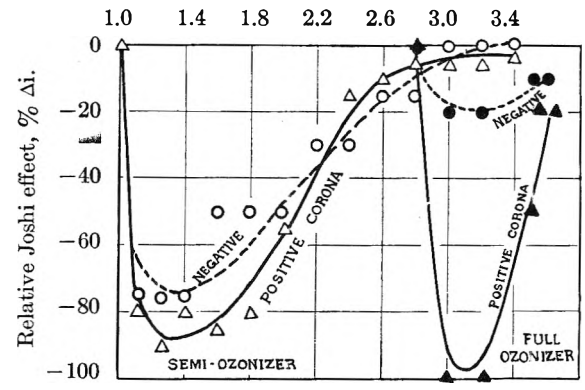

Fig. 3.—Joshi effect in Cl_2 under positive and negative corona, in semi- and full ozonizer, in the pulsating current component (*cf.* Table III).

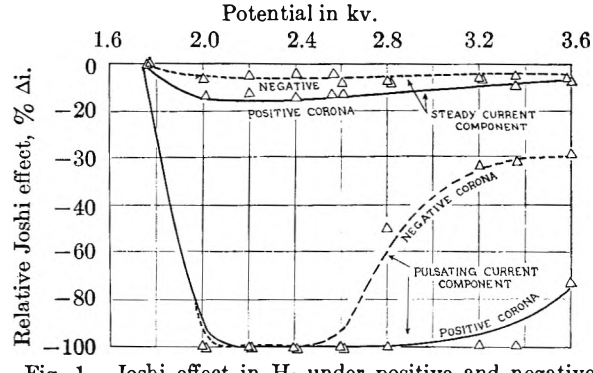

Fig. 1.—Joshi effect in H_2 under positive and negative corona in the steady and pulsating current components (*cf.* Table I).

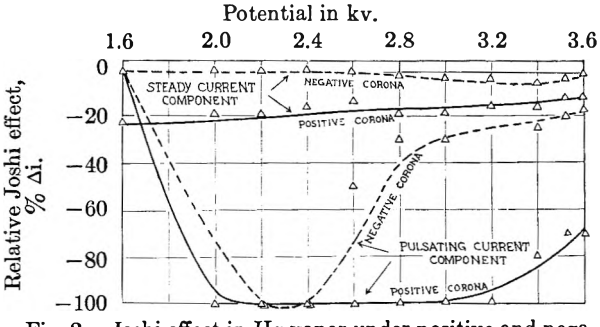

Fig. 2.—Joshi effect in Hg vapor under positive and negative corona in the steady and pulsating current components (*cf.* Table II).

The pulsating component amounted to 5–30% of the steady one and became measurable at potentials well above V_m for the latter (*cf.* columns 2 and 10; 6 and 14 of Tables I and II). There appears, however, no regularity in the corresponding values of the pulsating component in coronas of the two polarities, unlike in the case of the steady component described above. Thus, while in hydrogen the pulsating current is less in the positive corona than in

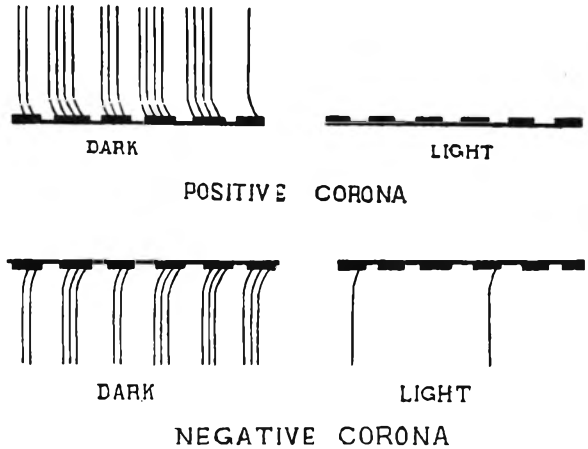

Fig. 4.—Joshi effect in H_2 under d.c. excitation: change of wave form.

(7) L. B. Loeb, "Fundamental Processes of Electrical Discharge in Gases," John Wiley and Sons, Inc., New York, N. Y., 1939, pp. 507–513.

the negative (Table I), the reverse is the case in mercury vapor (Table II) and in chlorine (Table III). These systems show negative Joshi effect on irradiation (*vide infra*).

The Nature of the Current Oscillograms.—The wave forms for the full-ozonizer discharge through hydrogen (p = 18 mm.) were practically straight lines with regularly spaced L.F. segments (50–100 p.s.) to one side (Fig. 4). These were of very short amplitude and corresponded to the observed throbbing of the glow. Superimposed on these were similarly directed H.F. pulses (10^3–10^4 p.s.) of much longer and practically constant amplitude (Fig. 4). These latter represent the descending branches of sharp ionization maxima on analogy with the well known Trichel pulses[8] for the negative point corona, which they resemble except in the order of frequency. Such a structure accounts for the co-occurrence of two groups of current components observed in the discharge; the H.F. pulses are associated with the pulsating and the rest with the steady component.

Irradiation of the system resulted, remarkably enough, in the instantaneous and total suppression of the H.F. pulses both in number and in amplitude, the action being reversible, light $\rightleftarrows$ dark. This complete elimination of the H.F. pulses under light corresponds to the 100% negative Joshi effect in the pulsating component (*vide infra*).

The oscillograms for the negative corona were essentially similar, except for about 20% reduction in the number as well as the amplitude of the H.F. pulses (Fig. 4). The total current was, however, greater in the negative discharge and hence the ratio $i_{H.F.}/i_{Total}$ was less in this than in the positive. This and the other finding that the ratio (as observed on the C.R.O.) diminished with increasing potential under either polarity agree with the view of Warburg,[9] Joshi,[1] and Prasad.[10] That the magnitude of the Joshi effect ($-\%\Delta i$) follows changes in this ratio due to polarity reversal or/and potential variation corroborates Joshi's suggestion that the H.F.'s are the principal determinant of the phenomenon.[1,5]

The Negative Joshi Effect.—Results for hydrogen, mercury vapor and chlorine (Tables I, II and III) showed that the Joshi effect producible in these systems excited in fields due to smooth continuous potentials had the following features. (1) Only the negative Joshi effect ($-\Delta i$) was observed up to a potential of 4 kv. under either polarity. (2) In the *steady component* $-\Delta i$ set in at a potential close to V_m, increased to a maximum of about 10–20% at a slightly higher potential and diminished thereafter (Figs. 1 and 2). In the case of chlorine, however, $-\Delta i$ was immeasurably small in this current component. (3) In the positive corona, $-\%\Delta i$ was markedly higher than in the negative at a given potential (Figs. 1 and 2). For example, in hydrogen at 2.6 kv. it was 12 and 8% in the steady component in the positive and negative discharges, respectively (Table I). (4) The *pulsating component* (regarded due to H.F. pulses), on the other hand, showed 100% negative Joshi effect, being completely and reversibly suppressed on irradiation *ad libitum*. (5) The potential range for the occurrence of the total or 100% negative Joshi effect was wider under the positive than under the negative corona. These ranges in hydrogen, for instance, are 2–3.6 kv. under the former and 2–2.6 kv. under the latter (Table I, Fig. 1); results for the other two systems were similar. (6) For potentials above this range, the Joshi effect diminished precipitously to about 50% and slowly thereafter. Thus, while the *magnitude* of the negative Joshi effect in the pulsating component under d.c. excitation is comparable with that producible under a.c., the *nature of the potential variation* is distinctive.

The Positive Joshi Effect.—One fact conspicuous in these experiments has been the limited occurrence of the positive Joshi effect ($+\Delta i$) in argon–alcohol mixture excited in a wire-in-cylinder (metal) GM counter and in iodine vapor with external sleeves. In the case of argon–alcohol mixture it was observed that in the rather narrow range of 1.2–1.4 kv., the positive Joshi effect varied between 100 and 200% due presumably to the low and the comparatively unsteady current regime (Table IV). At only a slightly higher potential, the $\%\Delta i$ rose very rapidly to several hundred per cent. till a steady discharge set in the counter at 1.8 kv. The system iodine–iodine vapor showed a maximum of 40% positive Joshi effect at 3.2 kv. (Table V).

These studies of the Joshi effect under d.c. excitation in systems of coaxial cylinders, either or both of glass (semi- and full ozonizer), or both metallic (GM counter), are the first to be reported.

The Mechanism of the Joshi Effect.—The production of practically 100% negative Joshi effect in numerous excited media has been established over a range of operative conditions, for irradiation by light of varying intensities and frequencies both within and *outside* the selective absorption region of the gas.[5,11,12] This complete blocking of current by but visible light, that has not been reported before, has obviously a bearing on the mechanism of gas discharge. Being producible in a variety of gases and vapors both elemental and compound, its theory should be physical and explain the reversible transition from positive to negative Joshi effect ($+\Delta i \rightleftarrows -\Delta i$), the latter reaching practically a 100% suppression. Joshi suggested,[1,13] that there are three stages in the development of the effect. (i) An adsorption-like layer is formed on the electrode walls under excitation. This layer consists partly of electrons and ions and excited particles produced in the discharge, and is characterized by a low work function. (ii) Photoelectric emission is assumed to occur from (i) on irradiation. This *per se* should cause a photoincrease of conductivity or the positive Joshi effect. (iii) As a further stage, a secondary reaction is postulated whereby the electrons released in (ii) are captured by the gas atoms, free radicals and molecules in an excited state due to their appreciable electron affinity. The negative ions that result from such captures

(8) G. W. Trichel, *Phys. Rev.*, **54**, 1078 (1938).

(9) E. Warburg, *Z. tech. Phys.*, **4**, 450 (1923); **5**, 165 (1924).

(10) B. N. Prasad and T. C. Jain, *Proc. Ind. Acad. Sci.*, **25**, 515 (1947).

(11) H. J. Arnikar, *Current Sci.*, **19**, 377 (1950).

(12) D. V. R. Rao and B. K. Sarma, THIS JOURNAL, **53**, 753 (1949).

(13) S. S. Joshi, *Current Sci.*, **16**, 19 (1947).

lower the potential gradient as a space charge effect, and thus the net current is reduced under light.

While the space charge effect due to negative ions may be anticipated in chlorine due to the high electron affinity of the gas, literature on the subject provides evidence of negative ions in other systems showing large negative Joshi effect. The presence of H^- ions in a hydrogen beam due to a glow discharge has been confirmed by Tüxen (*cf.* Massey[14]). Besides H^-, the formation of H_2^- ions is also inferred corresponding to an electron affinity of -2.4 e.v. In the case of mercury vapor, Arnot showed the conversion of Hg^+ into Hg^- occurs following the capture of two electrons successively from the cathode (Massey[14]).

(14) H. S. W. Massey, "Negative Ions," Cambridge Physical Tracts, Cambridge, 1938, pp. 1-2, 26-27, 68

The third postulate of Joshi's theory that these negative ions build into a space charge which has the effect of quenching the discharge receives additional support in the recent experiment of Weissler and Mohr.[15] They found that the corona discharge in freon-12 and air mixture is suppressed by negative ions.

Grateful thanks are due to Prof. S. S. Joshi, University Professor of Physical Chemistry and Principal College of Science, Banaras, for his valuable advice and guidance; and to Prof. P. S. Gill, Chairman of the Physics Department, Aligarh, for facilities for carrying out a part of this work in his department.

(15) G. L. Weissler and H. I. Mohr, *Phys. Rev.*, **72**, 289 (1947).

THE RATE OF SAPONIFICATION OF ACETATES OF UNSATURATED ALCOHOLS[1]

By R. Thomas Myers,[2] A. R. Collett and C. L. Lazzell

Chemistry Department, West Virginia University, Morgantown, West Virginia

Received April 30, 1951

The following new esters were prepared and characterized: 3-methyl-1-pentyn-3-ol acetate and 3-methyl-1-penten-3-ol acetate. In addition 3-methyl-1-penten-3-ol was characterized. Using a conductometric method the rate of saponification of the following acetates with 0.01 *N* NaOH at 25° was determined: ethyl, *n*-propyl, allyl, *s*-butyl, 2-propyn-1-ol, 3-buten-2-ol, 3-butyn-2-ol, 3-methyl-1-pentyn-3-ol and 3-methyl-1-penten-3-ol. For each ester, runs of two kinds were made: ester and base of the same concentration, and ester of higher concentration than the base. Trials using base of higher concentration than ester gave unsatisfactory values for the velocity constants.

According to many investigators in this field the mechanism of the saponification of carboxylic esters is considered to be[3,4]

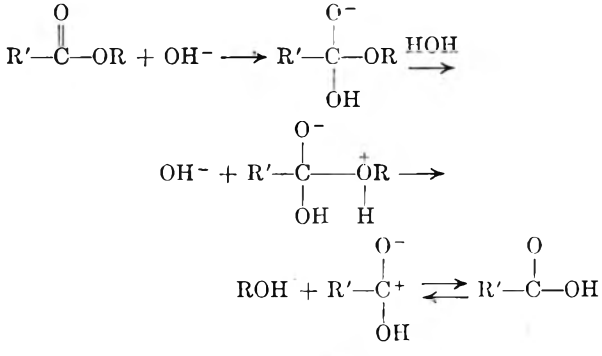

It is assumed that most of the energy of activation is involved in the fixation of the hydroxyl ion on the carbonyl carbon.[4] Therefore any group which increases the positive charge on the carbonyl carbon will accelerate the hydrolysis. An unsaturated carbon-to-carbon linkage near the carbonyl carbon in carboxylic esters always speeds the rate of hydrolysis compared to that of the saturated ester. For this and other reasons it has been assumed that an unsaturated group is electronegative with respect to hydrogen.[5,6] Much of this work has been done with esters of unsaturated acids. In this case the interpretation of results has been obscured by electromeric shifts (A) and possible chelate ring structures (B).[7]

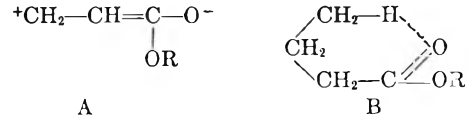

A B

The following work was carried out to extend the information on ester saponification, and to supply some of the information necessary to determine the reason for the acceleration of the saponification of esters caused by unsaturation. No previous work has been reported on the rate of saponification of esters of acetylenic alcohols.

In order to compare and relate the effect of various structures, ten esters were used, of which six were prepared by the authors. The alcoholic components contained saturated, ethylenic and acetylenic linkages connected to primary, secondary and tertiary carbinol groups. The physical properties of the esters used are listed in Table I.

The saponifications were done with sodium hydroxide, using a conductometric method.[3] This was used for three reasons. The first was the ease of manipulation, since no samples need be taken for analysis. The second reason was that errors due

(1) Adapted from a dissertation by R. Thomas Myers, submitted in partial fulfillment of the requirements for the degree of Doctor of Philosophy at West Virginia University.

(2) Chemistry Department, Colorado School of Mines, Golden, Colo.

(3) Fuson, "Advanced Organic Chemistry," John Wiley and Sons, Inc., New York, N. Y., 1950, p. 82.

(4) Mumm, *Ber.* **72B**, 1874 (1939).

(5) Dippy, *Chem. Rev.*, **25**, 151 (1939).

(6) Olsson, *Z. phys. Chem.*, **133**, 233 (1928).

(7) Smith and McReynolds, *J. Am. Chem. Soc.*, **61**, 1963 (1939).

(8) Walker, *Proc. Royal Soc. (London)*, **78A**, 157 (1906).

TABLE I

PHYSICAL PROPERTIES OF COMPOUNDS

	Acetate of:	Boiling point, °C. (cor.)	Pressure, mm.	$n^{25}D$	d^{25}_4
I	Ethanol	75.7–75.9	730	1.3701	0.8942
II	*n*-Propyl alcohol	101.0 (const.)	742	1.3822	0.8833
III	Allyl alcohol	102.9–03.7	736	1.4009	0.9222
IV	2-Propyn-1-ol	122.4–23.6	738	1.4151	0.9943
V	*s*-Butyl alcohol	111.3–11.9	747	1.3863	0.8647
VI	3-Buten-2-ol	111.7 (const.)	727	1.4016	0.8939
VII	3-Butyn-2-ol	124.4–25.4	738	1.4112	0.9437
VIII	3-Methyl-3-pentanol	142.0–43.5	744	1.4070	0.8768
IX	3-Methyl-1-penten-3-ol	146.9	730	....	....
X	3-Methyl-1-pentyn-3-ol	151.4–52.4	739	1.4238	0.9256
Free alcohol:					
	3-Methyl-1-penten-3-ol	114.0–16.6	735	1.4262	0.8334
		115.4–15.5	730	....	....

to evaporation were eliminated. Preliminary experiments showed that these errors were rather large, even for the higher-boiling esters. Lastly, the simplicity was greatly enhanced by the fact that the same ions were present in all cases.

$$CH_3{-}\overset{\overset{O}{\|}}{C}{-}OR + Na^+ + OH^- \longrightarrow CH_3COO^- + Na^+ + ROH$$

The fraction of material reacted at any time t was assumed to be $C_0 - C_t/C_0 - C_\infty$ where C is the conductivity. (In practice 1000/resistance was used instead of conductivity.) If we note that the concentration of base corresponding to this fraction is $b(C_0 - C_t)/(C_0 - C_\infty)$, the following formula is applicable when the initial concentration of reactants is the same

$$k = \frac{C_0 - C_\infty}{b(t_2 - t_1)} \frac{C_1 - C_2}{(C_2 - C_\infty)(C_1 - C_\infty)}$$

When the concentration of base and ester are not the same the following formula applies

$$k = \frac{2.303}{(a - b)(t_2 - t_1)} \log \frac{a(C_0 - C_\infty)/b - (C_0 - C_2)(C_1 - C_\infty)}{a(C_0 - C_\infty)/b - (C_0 - C_1)(C_2 - C_\infty)} = \frac{2.303}{(a - b)(t_2 - t_1)} \log Y$$

In these equations a is the concentration of ester and b the concentration of base. The former was determined by weighing out a definite amount of ester and diluting with carbon-dioxide-free conductivity water in a volumetric flask, the latter by standardization against sulfamic acid. The conductivity water was prepared by redistilling water from alkaline permanganate, using a block-tin condenser. It will be noted that this method of preparing the ester solutions was a check on their purity. Impurities, either saponifiable or not, will cause unsatisfactory values for the rate constant.

The concentration of ester was always equal to or greater than that of the base. Determinations using base stronger than ester did not give satisfactory results for the rate constant. Values of the constant from the first and last quarter were not used.

In order to illustrate the procedure, data for a typical run are included in Table II.

TABLE II

SAPONIFICATION OF 2-PROPYN-1-OL ACETATE

Initial Concentrations: ester 0.01200 *N*, base 0.0100 *N*.

R	1000/*R* (*C*)	$C_0 - C$	$\frac{a(C_0 - C_\infty)}{(C_0 - C)} - (C_0 - C)$	$C - C_\infty$	log *Y*	$t_2 - t_1$	*k*(l./mole-min.)
(726)	(1.377)		(1.064)	(0.887)	.....	...	..
920	1.087	0.290	0.774	0.597	.....	...	..
960	1.042	.335	.729	.552	0.00802	0.200	46.1
1000	1.000	.377	.687	.510	.00860	.217	45.6
1050	0.952	.425	.639	.462	.0015	.32	41.4
1100	.909	.468	.596	.419	.0122	.31	45.3
1150	.870	.507	.557	.380	.0130	.35	42.8
1200	.833	.544	.520	.343	.0146	.39	43.1
1250	.800	.577	.487	.310	.0155	.40	44.6
1300	.769	.608	.456	.279	.0173	.45	44.2
1350	.741	.636	.428	.251	.0184	.51	41.5
1400	.714	.663	.401	.224	.0211	.52	46.7
(2041)	(.490)	(.887)	(.177)	0	.....	...	..

The experimental results for all esters are summarized in Table III. The acetate of 3-methyl-3-pentanol is too insoluble to be determined with 0.01 *N* base. The units of the saponification constants are liters × mole^{-1} × min.$^{-1}$. The base is 0.01 *N* sodium hydroxide.

TABLE III

SAPONIFICATION RATE CONSTANTS FOR ESTERS AT 25.0°

Acetate of:	Init. concn. of ester	Trial 1	Trial 2	Trial 3	Av. *k*
Ethanol	0.0100	6.69			
	.0200	6.62			6.66
2-Propyn-1-ol	.0100	43.7	43.9		
	.0120	44.1			43.9
Allyl alcohol	.0100	12.48	12.64		
	.0150	12.55			12.56
n-Propyl alcohol	.0100	5.85	5.90		
	.0200	5.76	5.75		5.82
3-Butyn-2-ol	.0100	22.1	21.9		
	.0150	21.9	21.6		21.9
3-Buten-2-ol	.0100	4.33	4.36	4.27	
	.0200	4.23	4.23		4.30
s-Butyl alcohol	.0100	1.039			
	.0200	1.023	1.046	1.063	1.043
3-Methyl-1-pentyn-3-ol	.0100	1.291	1.342		
	.0150	1.322			1.318
3-Methyl-1-penten-3-ol	.0100	0.24			0.24
3-Methyl-3-pentanol[9]	....	(0.025)			(0.025)

(9) Calculated from *k* at 20° (6), assuming the same temperature coefficient as for *t*-butyl acetate.

Experimental

Preparation of Esters.—I, II, III and V (Table I) were purchased from Eastman Kodak Company and redistilled before use. Esters IV, VI, VII, VIII, IX and X were prepared by the action of acetyl chloride on the alcohol in the presence of pyridine or dimethylaniline.

The alcohols were obtained as follows. 2-Propyn-1-ol and 3-methyl-1-pentyn-3-ol were purchased from Farchan Research Laboratories, Cleveland, Ohio. 3-Butyn-2-ol was supplied by the Electrochemicals Division, E. I. du Pont de Nemours and Co. 3-Buten-2-ol was prepared by a Grignard reaction with acrolein and methylmagnesium iodide. The yield was rather low. 3-Methyl-1-penten-3-ol was prepared by the reduction of the corresponding alkynol using coppered zinc dust.[10,11] Since this alcohol has not been sufficiently characterized in the literature, its physical properties are included in Table I. An attempt was made to prepare this alcohol by the following series of reactions[12]

$$CH_3—CO—CH_3 + (CH_2O)_n \xrightarrow{OH^-}$$

$$CH_3—CO—CH_2—CH_2OH \xrightarrow{H_3PO_4} H_2O +$$

$$CH_3—CO—CH=CH_2 \xrightarrow[HOH]{C_2H_5MgBr} CH_3—\underset{\displaystyle C_2H_5}{\overset{\displaystyle OH}{\underset{|}{\overset{|}{C}}}}—CH=CH_2$$

The result was a mixture of methyl *n*-butyl ketone and the alcohol, so the procedure was abandoned. The esterification of 3-methyl-1-penten-3-ol proved very difficult; the ester was never obtained free from combined chlorine. This was further evidenced by the unsatisfactory value obtained for the rate constant. 3-Methyl-3-pentanol was obtained from 3-methyl-1-pentyn-3-ol by the complete hydrogenation with Raney nickel catalyst.

Apparatus.—The conductance cell was constructed similarly to those of Jones and Bollinger,[13] except that only one opening for filling was provided. The conductivity bridge was assembled from Leeds and Northrup apparatus: audiofrequency oscillator, audiofrequency amplifier, shielded ratio box (with Wagner earthing device) and resistance box (non-inductively wound). As is usual in such measurements, the internal series capacitance of the cell, due both to geometry and polarization, was corrected for by a variable capacitor connected in parallel with the resistance box. It was estimated that the accuracy of any resistance reading was about 0.1%.

Saponification Technique.—From saturated aqueous C.P. sodium hydroxide, 0.0601 molar sodium hydroxide was prepared by diluting with conductivity water. This was standardized against sulfamic acid using phenolphthalein as indicator. A flask of the base was placed in the constant temperature bath. The latter was set at 25.0°, using a thermometer calibrated by the National Bureau of Standards. Ester solutions of a definite concentration were prepared by weighing out the requisite amount of ester in small thin-walled glass bulbs. Each bulb was placed in a volumetric flask and the necessary amount of conductivity water added to bring the solution to the mark. The flask was closed with a rubber stopper through which a glass rod extended almost to the bottom. The bulb was broken, the flask shaken until the ester dissolved and the flask then placed in the constant temperature bath. By means of a pipet 9.97 cc. of ester solution was delivered into the conductivity cell, and 1.99 cc. of sodium hydroxide solution added. Timing was started when one-half of the base was added.

The value of the conductivity at zero time was obtained by diluting the base with conductivity water to the desired normality. The value of the conductance at infinite time (C_∞) was obtained from experimental measurements of a 0.01 *N* solution of sodium acetate. This method was satisfactory for those reactions which go to completion in a reasonable time.

(10) Rupe and Vonaesch, *Ann.*, **442**, 81 (1925).

(11) Strauss, *Ber.*, **26**, 284 (1893); *ibid.*, **342**, 190, 238 (1905).

(12) White and Haward, *C. A.*, **37**, 1989 (1943); *J. Chem. Soc.*, 2531 (1943).

(13) Jones and Bollinger, *J. Am. Chem. Soc.*, **53**, 411 (1931).

Discussion

Inspection of the results in Table III shows that unsaturation speeds the rate of saponification in all cases. It also shows the following: (1) as regards branching in the alkyl group, the rate of saponification is in the order primary > secondary > tertiary, (2) the ethynyl group changes the rate more than the vinyl group (as compared to the ethyl group), (3) the relative amount of this change is in the order tertiary > secondary > primary.

Models of these ester molecules made with Fisher–Hirshfelder–Taylor atom models show that replacing an ethyl group by a vinyl group, and that in turn by an ethynyl group, causes a decrease in the purely steric blocking of the carbonyl carbon. The relative decrease in steric hindrance of the carbonyl carbon caused by exchanging ethyl for vinyl is greatest in tertiary, less in secondary and least in primary esters. The same is true for the exchange of vinyl for ethynyl. This indicates that the increase in rate of saponification in passing from propyl to allyl to 2-propyn-1-ol acetate may be due to steric factors, and not to changes in energy of activation. This is true in increasing amount in the other two series of secondary and tertiary esters. This is corroborated by data for allyl and *n*-propyl acetate. Olsson has found that the energy of activation for the saponification of allyl acetate is greater than that of propyl acetate, even though the former hydrolyzes more rapidly.[6] This increase in the energy of activation contradicts the supposed electron-attracting powers of the carbon-to-carbon unsaturated bonds, and could be explained by chelate structures C and D of the type postulated by Smith and McReynolds[7] and by Dippy.[5]

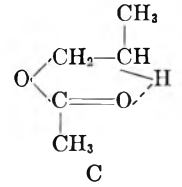

C

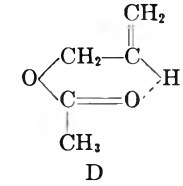

D

Since the ethylenic hydrogen is more labile, it seems probable that it would form a more stable hydrogen bond than the alkyl hydrogen, stabilizing D more than C. This stabilization would raise the activation energy for the hydrolysis. The increased rate of hydrolysis is then due to an increase in the probability of reactive collisions.

Models show that the lone acetylenic hydrogen of 2-propyn-1-ol acetate cannot approach the carbonyl oxygen, thus barring the chelate ring structure. Therefore if the ethynyl group is actually electronegative compared to the ethyl group, then the activation energy of 2-propyn-1-ol acetate should be significantly lower than for ethyl and allyl acetate.

HYDRODYNAMIC FACTORS IN MOVING BOUNDARY ELECTROPHORESIS.[1,2] AN INTRODUCTION TO THE ELECTROPHORETIC STUDY OF LIPOPROTEINS

BY RODES TRAUTMAN AND J. W. GOFMAN

Division of Medical Physics, Donner Laboratory and the Radiation Laboratory, University of California, Berkeley

Received May 9, 1951

1. Modifications of a schlieren optical system are described which enable detection of deflections of light in any direction, thus aiding in the study of non-planar boundaries. 2. Movement of a boundary from one position in a cell to another by hydrodynamic flow leads to a non-planar boundary region. The convective flow is a resultant of the velocity distribution of fluid above and below and the tendency to remain horizontal due to its hydrostatic stability. 3. Various factors involved in sharpening a boundary by means of suction on an inserted capillary are described. A practical method of sharpening satisfactorily two boundaries simultaneously in the usual electrophoretic cells is given. 4. Electro-osmosis is present in moving boundary electrophoresis of proteins and tends to disrupt a planar boundary in a manner similar to that of compensation. By opposing the disrupting forces of electro-osmosis with those of compensation, a horizontally plane boundary can be maintained. 5. The low density gradient of certain of the lipoprotein boundaries necessitates very careful attention to select the proper compensation rate. The best compensation seems to be the value for which the boundary in question remains stationary with respect to the cell.

The lipoproteins of human sera have received especial significance at this Laboratory as a result of the work of Gofman, *et al.*,[3] on the atherosclerosis problem. The electrophoresis of these numerous lipoprotein species isolatable by ultracentrifugal means[4] has not been without serious difficulties which have necessitated queries into very basic electrophoretic principles. Horizontally plane

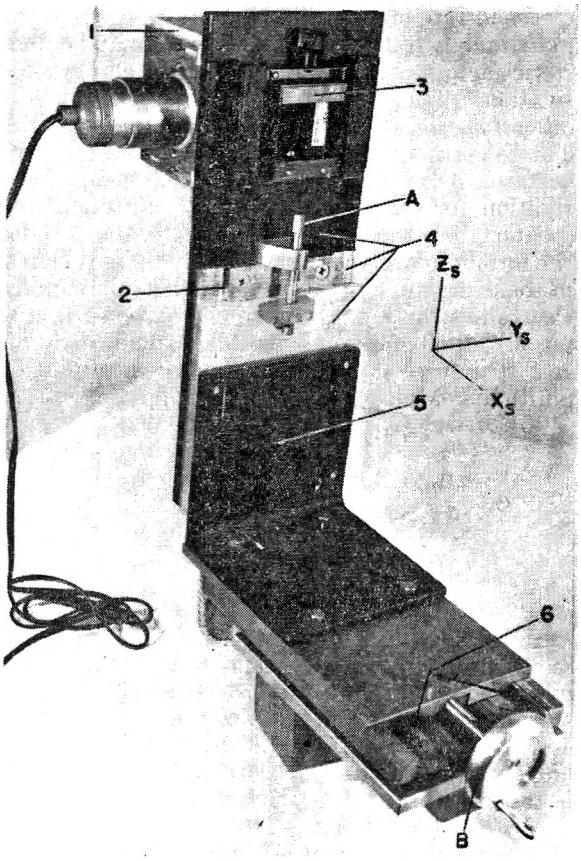

Fig. 1.—Light source assembly (as seen from schlieren camera): 1, light source mount; 2, vertical ways; 3, filter holder; 4, light source mount support; 5, 90° angle brace; 6, horizontal ways; A, light source height adjustment (z axis); B, light source focus adjustment (x axis).

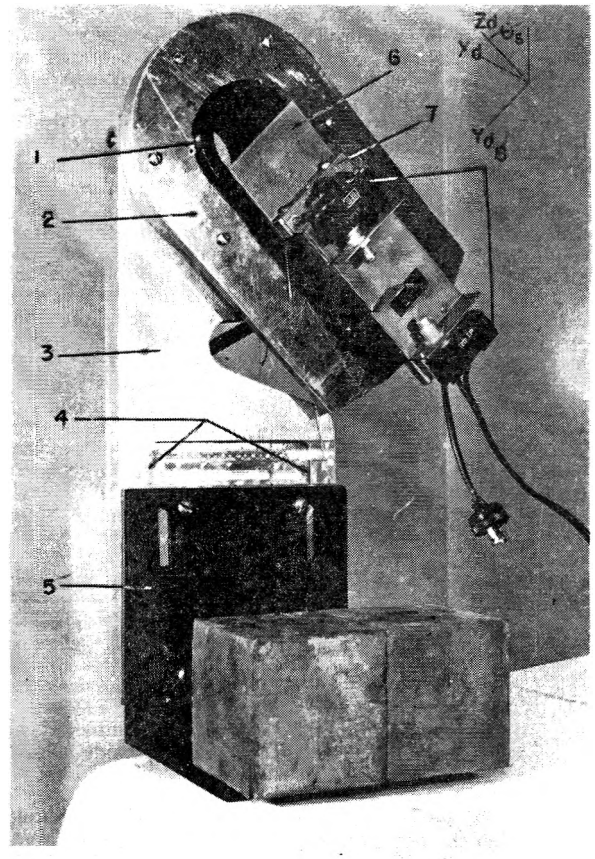

Fig. 2.—Objective end of schlieren camera (as seen from the light source): 1, camera objective holder; 2, objective-diaphragm mount; 3, objective-diaphragm mount support; 4, vertical ways; 5, 90° angle brace; 6, schlieren blade; 7, schlieren diaphragm holder; 8, schlieren diaphragm travel limit switches; θ_s, schlieren optical system detection angle.

(1) This work was supported (in part) by the Atomic Energy Commission and the United States Public Health Service.

(2) This paper is taken from the doctorate thesis of Rodes Trautman, submitted in partial satisfaction of the requirements to the University of California, September, 1950.

(3) J. W. Gofman, *et al.*, *Circulation*, **2**, 161 (1950)

(4) F. T. Lindgren, H. A. Elliott and J. W. Gofman, THIS JOURNAL, **55**, 80 (1951).

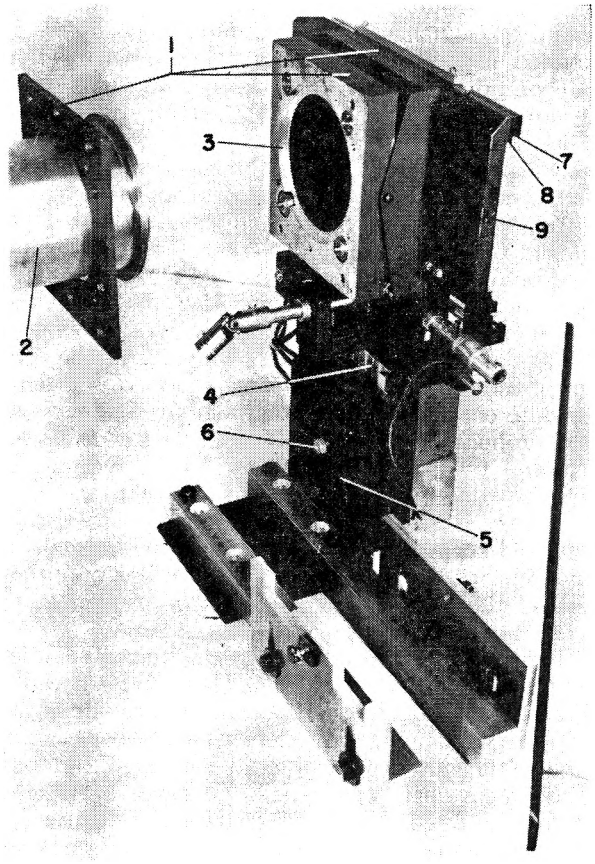

Fig. 3.—Plate end of schlieren camera (looking from light source): 1, plate and camera bellows tube mount; 2, camera bellows tube; 3, circular track for rotatable camera bellows tube; 4, vertical ways; 5, 90° angle brace; 6, clamp screw for vertical ways; 7, ways for plate carriage; 8, ways for plate mask; 9, plate carriage—mask mount.

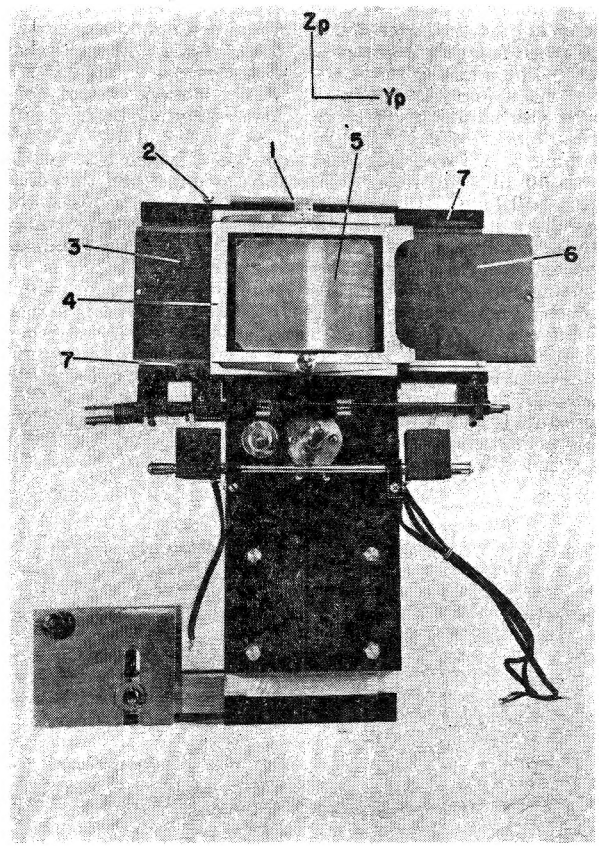

Fig. 4.—Plate end of schlieren camera (looking toward light source): 1, plate carriage scale; 2, clamp screw for 3; 3, left plate mask; 4, Graflex 4″ × 5″ adapter back as plate carriage; 5, ground glass; 6, right plate mask; 7, plate carriage-mask mount.

boundaries do not always result in the classical techniques, especially with lipoprotein boundaries for which the stabilizing density gradient[5] is orders of magnitude smaller than for the 1.3 density proteins. This paper is a report of the investigations here into the classical problems of (a) boundary formation technique, especially compensated boundaries[6] and the capillary sharpening procedure of Polson[7] and (b) electro-osmosis.[8] All these problems are hydrodynamic in nature.

Experimental

Optical System.—The following major modifications were made on a Klett Manufacturing Co. (New York) electrophoresis apparatus to give a versatile schlieren optical tool. (Figs. 1, 2, 3 and 4 show the modified components before attaching to the optical beam.) (a) The light source intensity was increased twenty-fold by using an AH-6 mercury arc lamp instead of the AH-4. (AH-4 mount shown in Fig. 1.) (b) The camera mounts were made with vertical ways so that the camera may be placed at any vertical position with respect to the axis of the schlieren lens. (c) The light source mount was made with both vertical and horizontal ways, the former permitting adjustment to the axis of the schlieren lens, and the latter enabling quick focusing, which was found to be necessary not only from cell to cell, but even from channel to channel in a particular cell, because an optical flat changes the focus of converging light (only one schlieren lens). (d) Two slides with ground jaws were incorporated behind the plate holder carriage (which was changed to a Graflex 4″ × 5″ adapter back) so that any vertical portion of the camera image may be selected, masking the remainder. (e) The axis of travel of the schlieren diaphragm, the cylindrical lens axis and the light source were made rotatable through 90°, so that deflections of light in the cell in directions other than vertical can be detected. The conventional system,[9] using a horizontal schlieren diaphragm in the Longsworth scanning, or a cylindrical lens with axis vertical in the Philpot–Svensson arrangement, will be termed the "horizontal" position ($\theta_s = 0$) of the rotatable system. And 90° from that, namely with the schlieren diaphragm of the scanning method vertical, will be called the "vertical" position ($\theta_s = 90°$) of the camera. (f) The schlieren diaphragm holder was made so that rapid change to different diaphragms is possible (bar, slit, blade, etc.).

Cell.—Rectangular Tiselius electrophoresis micro cells (2 cc.) were used. In the study of the factors involved in capillary sharpening, a special top piece was constructed, equipped with standard socket joints (18/9), one of which is directly over one slot so that a capillary can be passed into the center section. Various diameter glass tubes ("standpipes") could be attached to these standard joints to provide both a reservoir for material and a barrier to keep the thermostat water out (see Figs. 10 and 11). In some experiments greater length cells were assembled using several center sections. For electrophoresis another special top piece, made by Pyrocell Manufacturing Co. (New York), is shown in Fig. 13.

(5) D. R. Briggs, "Biophysical Research Methods," F. M. Uber, ed., Interscience Publ., Inc., New York, N. Y., 1950, p. 297.

(6) A. Tiselius, *Trans. Faraday Soc.*, **33**, 524 (1937).

(7) A. Polson, *Onderstepoort J. Vet. Sci. Animal Ind.*, **20**, 159 (1945); D. S. Kahn and A. Polson, THIS JOURNAL, **51**, 816 (1947).

(8) L. G. Longsworth, *J. Am. Chem. Soc.*, **65**, 1755 (1943) (footnote 23); T. Shedlovsky and J. E. Smadel, *J. Exptl. Med.*, **72**, 511 (1940); A. S. McFarlane, *Trans. Faraday Soc.*, **36**, 257 (1940).

(9) L. G. Longsworth, *Ind. Eng. Chem., Anal. Ed.*, **18**, 219 (1946).

Capillary System.—A "capillary unit" consists of a glass capillary (of the order of 0.5 mm. diameter and long enough to reach from the top piece to the bottom of the cell) connected by a rubber sleeve to a small stopcock equipped with a socket joint (see Fig. 5). The suction system consists of a motor driven screw which can either push or pull the plunger of a syringe which is connected by pressure tubing to a 3-way stopcock, one side of which is attached to a 40-ml. centrifuge tube used as a funnel and the other to a ball joint. It is much more satisfactory to insert the capillary unit by hand and then connect the suction assembly by means of the spherical joint than to lower the capillary mechanically. This enables more care to be taken in inserting the capillary and makes the suction system mount much easier to construct and operate since the spherical joint can take even gross mal-alignments. The stopcock in the capillary unit is of value in keeping the capillary unit full when handled separately and, even more, in allowing the suction to be terminated sharply when necessary. The pressure tubing contracts a little under suction and when the motor is turned off, expands to its normal size, continuing suction at a slower, non-uniform rate.

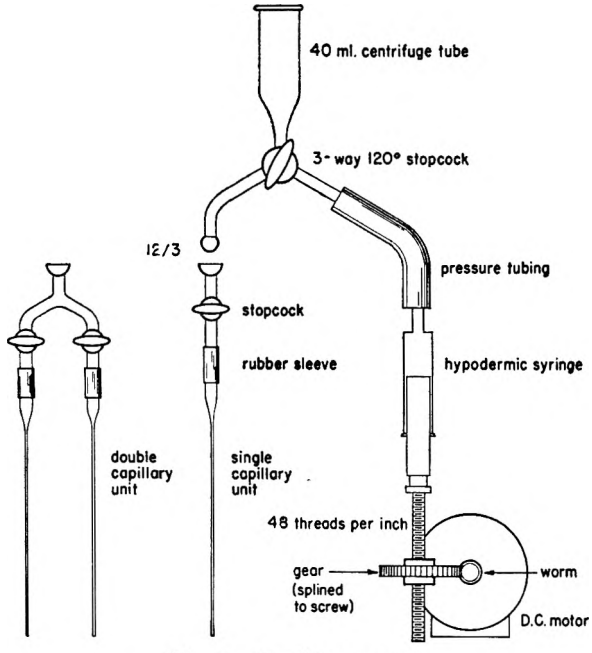

Fig. 5.—Capillary system.

The motor is a Bodine NSH-12R 115V D-C with 35:1 speed reducer (60 r.p.m. output at full voltage) geared 10:1, 20:1 or 100:1 to the Klett compensator, which has a 48 threads per inch screw and can accommodate a hypodermic syringe in the range of 5 to 100 ml. capacity. With the Bodine motor, remote control at the camera end of direction and selected speed range is possible (over-all with the gear changes: 0.1–50 microliters/sec.).

Material.—Sucrose solutions were made from C.P. sucrose in distilled water.

Bovine albumin solutions were made from crystalline bovine serum albumin (Armour control No. 4502) in potassium phosphate buffer *p*H 7.7, ionic strength 0.1, buffer capacity 0.01.

Lipoprotein-rich fractions were obtained by spinning unaltered human serum in the preparative ultracentrifuge at 30,000 r.p.m. for 18 hours. Certain of the low density lipoproteins pile up on the albumin boundary which was descending in the tube. This region was clearly seen by visual inspection of the tube with a flashlight and was pipetted off. Barbiturate buffer at *p*H 8.2, buffer capacity 0.04, and made up to 0.1 ionic strength with 0.06 *M* thiocyanate was used.

Compensated Boundary

The "boundary region" between two different ("end") solutions is defined as the region in which the composition is different from that of either original end solution. The "boundary position" is defined as the position of the maximum refractive index gradient of the boundary region. This is determined by using the schlieren optical system with a horizontal blade as a schlieren diaphragm and viewing the image of the cell on the ground glass of the camera (without the cylindrical lens).

When a boundary is "compensated," that is, moved from one position in the cell to another by hydrodynamic flow, the boundary region does not remain plane. The basic reason for this is that the solutions, like other viscous fluids, have zero velocity at the walls and maximum velocity in the center of the cell. A boundary between two solutions of different density has an inherent tendency to remain horizontally plane, since if part is displaced upwards or downwards, there will be a hydrostatic head tending to restore it. This elastic nature of a boundary is greater the steeper the density gradient, and keeps the boundary from being a profile of the velocity distribution in the solutions on either side of the boundary regions, yet is insufficient to keep the entire boundary region planar.

Figure 6 shows schematically the hydrodynamics of a compensating boundary. The curves a and e Fig. 6 represent velocity profiles on either side of the boundary region c. (A velocity profile at a certain time is the curve connecting all elements of fluid at that time which were originally along a straight horizontal line.) These two curves are identical if a given volume flow per unit time is maintained, as for example, with a motor driven syringe, because the law of conservation of mass requires the integrals under the two parabolas to be equal. This can only be so if the parabolas are identical. The boundary c, however, has the hydrostatic restoring force due to its density gradient and so has a different profile. The integral under its profile must again equal that under a or e, so that if the maximum gradient remains essentially straight, its velocity is the average velocity calculated from the geometry of the cell and the suction rate. The dotted lines show the average velocity. The curved arrow d shows the flow path relative to

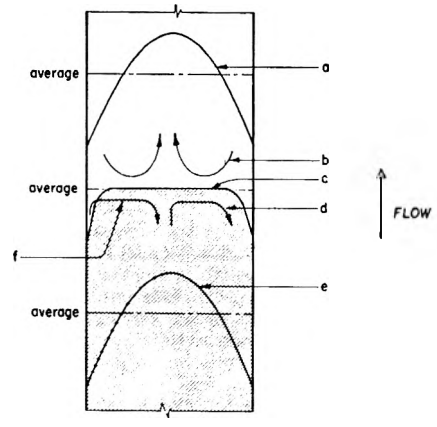

Fig. 6.—Hydrodynamics of a compensating boundary: a, e, velocity profile in solutions on either side of the boundary position, c; b, "turn around" flow lines on leading edge of boundary region; d, "turn around" flow lines on trailing edge of boundary region; f, convective flow due to less dense layer along wall.

the boundary due to fluid in the center of the cell having a velocity greater than that of the boundary (at the center) and that at the edges having a velocity less than that of the boundary (at the edges). Similarly, the flow pattern b on the advancing side of the boundary is sketched. Another effect of the difference in density between the two solutions on the boundary region is the following: The condition of zero velocity at the walls implies that there will be poor "rinsing" of the channel when one solution replaces another by hydrodynamic flow. The result is that there is a layer of material of different density along the walls so that the maximum refractive index gradient profile does not divide two homogeneous solutions, the trailing solution having a density distribution. This gives rise to convection in the trailing solution indicated by f. The arrows d and f are shown on opposite sides of the cell for simplicity, but both are present on each side and the net flow is the resultant of these two somewhat opposing flows.

The schlieren in the photographs showing these effects cannot be ascribed quantitatively to concentration gradients since the basic schlieren optical equation, with a constant of proportionality, has been derived on the assumption that the index of refraction is a function of the vertical coördinate only.[10] In these non-planar boundaries, it can be expected that solutions of the proper optical equations would give a different result. However, with no refractive index gradient, there will be no deflection so that, qualitatively, schlieren can be related to regions of inhomogeneity of concentration.

In Fig. 7 are photographs of a boundary being moved by hydrodynamic flow. All the photographs are not of the same boundary at the same time, but are so oriented that they can be considered

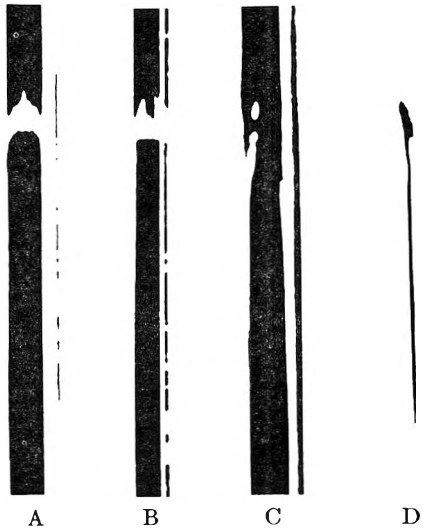

Fig. 7.—Photographs of a compensating boundary: The boundary region between a 1/2% sucrose solution and water is moving up, as seen, at a rate of 3 cm./min. in the micro cell. A, B, $\theta_s = 0$, horizontal blade for schlieren diaphragm; A, blade just below undeflected light source image; B, blade order of 1 cm. below undeflected light source image; C, D, $\theta_s = 90°$, vertical blade for schlieren diaphragm on one side of the undeflected light source image (C) or on the other (D).

(10) O. Lamm, *Z. physik. Chem.*, **A138**, 313 (1928).

four simultaneous views of the same boundary. A and B are taken with the slit and schlieren diaphragm in the horizontal position: A with the blade just below the undeflected light source image, and B with it approximately 1 cm. lower. A shows a "long finger" extending up in the center of the cell and B shows "horns" protruding into the leading solution from the position of maximum refractive index gradient. These characteristic patterns are related to the flow b of Fig. 6. C and D are taken with the slit and diaphragm in the vertical position: C with the blade on one side of the undeflected light source image and D with it on the other side. The long "tails" behind the position of the maximum gradient, indicated by a gap in the pattern C where light was completely thrown out of the optical system downwards and hence cannot give a record of its left or right deflection, are characteristic of the vertical patterns and are related to the no slip condition at the walls and the flows d and f of Fig. 6.

The effect of the flow f of Fig. 6 can be seen by itself after the suction is turned off which makes d vanish. The effect is especially vivid if instead of merely compensating a boundary to build up the wall layer, the compensation is preparatory to capillary sharpening described in the next section. In this case, at the end of the sharpening, the boundary develops horns into the trailing solution. Figure 8 shows the horns into the protein solution (A), and the corresponding asymmetric cylindrical lens pattern (B) when bovine albumin is compensated from the top of the photograph to the center. (The

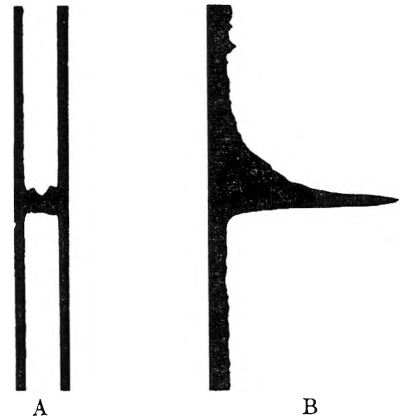

Fig. 8.—Convection in the protein solution as a result of compensation from below: The boundary between a 1/4% bovine albumin solution and phosphate buffer was compensated into buffer from the bottom piece (top of the photograph) to the center of the micro cell in 3 minutes and then sharpened for one-half minute by continuing suction on the capillary used for compensation. B was taken 5 1/2 minutes and A 9 minutes after suction was terminated. A, scanning camera, $\theta_s = 0$, fixed blade; B, cylindrical lens camera, $\theta_s = 0$, diagonal blade.

photographs are printed as they are seen on the ground glass; that is, the image of the cell is inverted.) Figure 9 shows the non-planar boundary resulting when the boundary is compensated into the protein solution leaving a wall layer of more dense protein solution above (below in Fig. 9) the boundary.

Whereas very high compensation rates (the or-

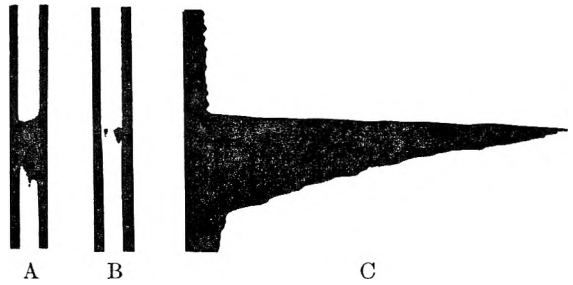

Fig. 9.—Convection in the buffer solution as a result of compensation from above: The boundary between a 1/4% bovine albumin solution and phosphate buffer was compensated into protein solution from the top piece (bottom of photograph) to the center of the micro cell in 3 minutes and then sharpened for one-half minute by continuing suction on the capillary used for compensation. A and B were taken approximately 4 minutes, and C 8 minutes after suction was terminated. A, scanning camera, $\theta_s = 0$, diaphragm high; B, scanning camera, $\theta_s = 0$, diaphragm lower; C, cylindrical lens camera, $\theta_s = 0$, diagonal blade.

der of 3 cm./min.) gave the pronounced horn pattern in Figs. 8 and 9, some effect is still observable with this same solution at 1 cm./hr. In addition to the compensation rate this convective disturbance depends upon the density difference between the solutions and on the diffusion constant. Sucrose, for example, shows only a small effect at very high suction rates. As the density becomes uniform in the trailing solution the convection ceases and the spreading of the boundary approaches that due to diffusion alone. The changes in the apparent diffusion constant with time and suction rate have been given empirically by Longsworth[11] and have led to the abandonment[11,12] of the Svedberg and Tiselius cells as such for diffusion. These considerations show that the substitution of the capillary sharpening technique does not completely solve the problem unless extremely low compensation rates are used preparatory to sharpening or if many volumes of solution are withdrawn through the capillary to effect rinsing. In the micro cell, 1/4 — 1/2 cm./hr. compensation rates preparatory to sharpening are recommended.

Capillary Sharpening Technique

Since 1945[7] many investigators have used a capillary with suction to form an initial boundary region between two solutions, the diffusion and/or electrophoretic properties of which are under investigation. The basic principle of the method is that the tip of the capillary will define some sort of boundary region, since under suction either one or both of the solutions are given an exit from the cell *via* the capillary. Because there is flow from the body of the solution into the capillary, it is possible to "compensate" a boundary up to the capillary tip as well as to sharpen it. The rough original boundary between the two solutions which is a prerequisite in order to have something to sharpen, will be termed the "preliminary boundary." This boundary is typically formed in the usual electrophoretic technique of sliding the parts of the cell together.

(11) L. G. Longsworth, *J. Am. Chem. Soc.*, **69**, 2514 (1947).
(12) E. M. Bevilacqua, M. M. Bender, and J. W. Williams, *Ann. N. Y. Acad. Sci.*, **46**, 320 (1945).

One way in which the cell may be used to study hydrodynamics is a "closed bottom" arrangement (see Fig. 10). The bottom piece is pushed to one side so that the channel used has a closed end; the center section is filled with the lower solution, and together with the bottom piece is slid to the side; the top piece is rinsed and filled with the upper solution. The preliminary boundary is formed by bringing the center and top sections into alignment. The capillary unit is lowered through this preliminary boundary until its tip is halfway down the center section. After the suction assembly is connected, suction is applied. Since fluid flows from the top down along the capillary, the boundary is compensated into view. It is noticed that the sharpened boundary takes a position about 1 mm. below the tip of the capillary with 3 cm./hr. suction rate in the micro cell (see Fig. 17) and that this displacement below the tip of the capillary is increased with greater rates of suction.

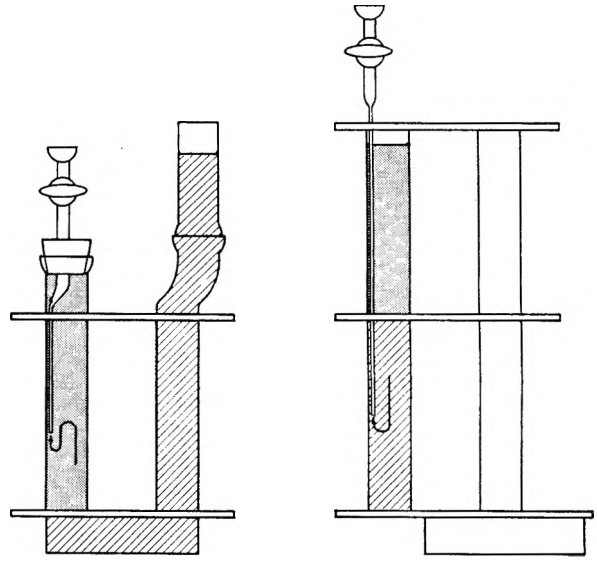

Fig. 10.—Single flow cells.

Another way of using a single flow arrangement is to put the closed end at the top of the top section (Fig. 10). In this case the preliminary boundary is formed at the junction of the center and bottom sections and the right limb of the cell is filled to an arbitrary height. When suction is applied in this system, the flow again compensates the boundary into view, and it is observed that the boundary takes a position 1 to 2 mm. above the tip of the capillary. Again the greater the suction rate, the greater this displacement. Since the boundary is above the tip of the capillary, removal of the capillary, no matter how slow, is bound to ruin the boundary by dragging material up into the upper solution, which should be completely free of any of the lower solution.

From these two types of arrangements, it can be suggested that the boundary takes a position of a horizontal tangent to the hydrodynamic flow pattern, for in the former case the flow lines must be U-shaped in order to come down the cell and get into the capillary, while in the latter case there ap-

parently is a path of flow which can double back up the cell a short distance past the tip of the capillary (Fig. 10).

In order to obtain flow of fluid in both solutions and to attempt to get the boundary to form at the tip, the Tiselius cell can be used in an open U arrangement (Fig. 11). Initially it is loaded similar to the way utilized in electrophoresis: the lower solution in the bottom section and right limb, and the upper solution in the left limb.

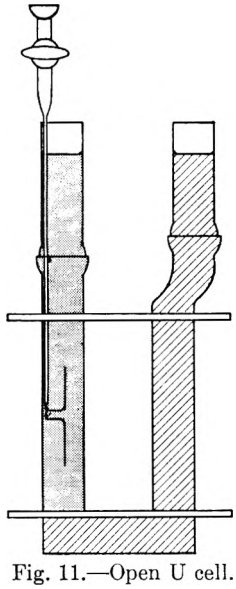

Fig. 11.—Open U cell.

The position of the maximum refractive index gradient, and in fact its nature, has been found to depend in this system on: (a) the location of the capillary in the cell; (b) the relative cross-sectional areas of the standpipes; (c) the rate of suction. By a proper choice of these three factors, it is possible to obtain what might be termed a hypersharp boundary in comparison to the sharp boundaries formed in the single flow cells.

Figure 12 shows what happens when the important factors above are varied. With the capillary in the center of the cell and equal cross-sectional areas of standpipes, there is a displacement between the tip of the capillary and the boundary, which may be split (A). The flow pattern at the tip of the capillary is extremely complicated, as implied by the split boundary region and as seen by watching dirt particles being drawn into the capillary. Since each fluid can of itself produce a sharpened boundary, the reason for the split is probably that the two possible positions do not coincide. The distance the upper fluid penetrates below the tip of the capillary in making a U-turn can sometimes be diminished by placing the capillary along the side of the cell. The conditions in Fig. 12B are the same as for A except that the capillary is along the side. There is no great change noted here, but it has been observed that the boundary is still split, and that the further boundary position is closer to the capillary tip. From this one can suppose that the lower of the two boundaries is caused by the U flow of the upper fluid, and that as a general rule, the closer the boundary positions are to the tip of the capillary, the narrower ("sharper") the boundary region will be.

To bring the boundary closer to the tip, consideration must be paid to the two remaining factors. If the cross sectional area of the left limb is decreased relative to the right limb, the upward flow will be relatively greater and can suppress somewhat the dominance of the U bend of the downward flowing fluid. Figure 12-C shows this situation.

If the resistance to flow is not the same in the upper solution as in the lower solution, then it is possible for the menisci in the standpipes to be at

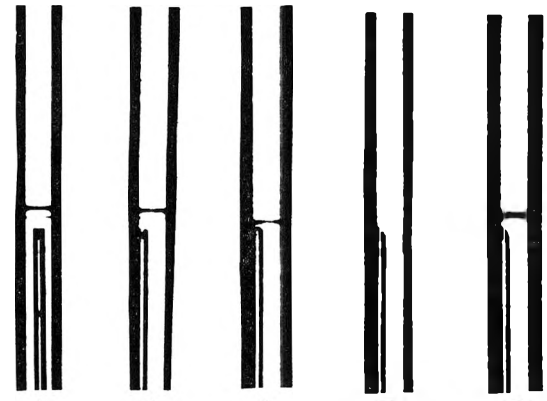

Fig. 12.—Capillary sharpening in the open U cell: Boundary is between $^1/_2$% sucrose solution and H_2O. Photograph is oriented as it would be seen on the ground glass; thus the capillary appears as coming out the bottom of the picture. A, equal areas of the standpipes, capillary in center of channel, 1.5 cc./min. suction; B, same as A except capillary along the side; C, right limb area 2.3 times left limb area, 1.5 cc./min. suction; D, right limb area 3.2 times left limb area, 4 cc./min. suction; E, boundary of D two minutes after suction was stopped.

different heights because the suction rate competes with the rate of hydrostatic leveling. The left limb seems to have greater resistance than the right limb, even though shorter, because of the presence of the capillary. As the suction rate is increased, the level in the right limb falls below that of the left limb, which means that there is greater differential flow than the relative cross-sectional areas alone would indicate. This changes the pattern of the opposing flows at the capillary and hence can change the boundary position with respect to the tip, even causing a split boundary above the tip (Fig. 12-D). After suction is discontinued the menisci will again become level and in so doing "compensate" the boundary. The boundary in Fig. 12-E is the boundary of D two minutes after suction was terminated.

Whereas standpipes of various size and plastic tabs for inserts to decrease the cross-sectional area were used to study the hydrodynamic factors involved, a practical arrangement of the open U cell for diffusion is that using an additional center section or two as the top piece (*cf.* closed bottom cell Fig. 10). The preliminary boundary is formed, by sliding, at the junction of the center and bottom sections. For the micro cell, a plastic tab 4 × 1.8 mm. in cross-section has been found useful in the capillary limb. When the boundary looks good on the ground glass with the schlieren diaphragm just below the undeflected light source image, quickly close off the capillary unit stopcock and slide the bottom piece to one side. Then turn off the suction device and slowly remove the capillary. No detectable disturbance at any camera angle has been noticed when a straight capillary was carefully withdrawn away from a boundary within about 0.5 mm. from its tip. Disturbance has been noticed when a right angle, or hook-shaped capillary was withdrawn. Note that vibrations of the capillary tip due to the vibration of the stirrer in the water-bath are absent when the capillary is along the wall of the channel, and hence the stir-

rer need not be turned off during the sharpening process.

In electrophoresis it is desirable for the most part to have both descending and ascending patterns start from sharp boundaries. The open U arrangement permits only one boundary to be sharpened with standard two channel cells, but the single flow principle offers the possibility of sharpening two boundaries at once by putting the protein in both channels of the center section and in the bottom piece as indicated in Fig. 13. The bottom piece is kept closed during the sharpening which uses the double capillary unit, one capillary in each channel. The boundaries obtainable with this single flow method are not as sharp as with the open U and definitely depend upon the density difference between the solutions. But even with the lipoproteins, boundaries satisfactory for electrophoresis have been obtained.

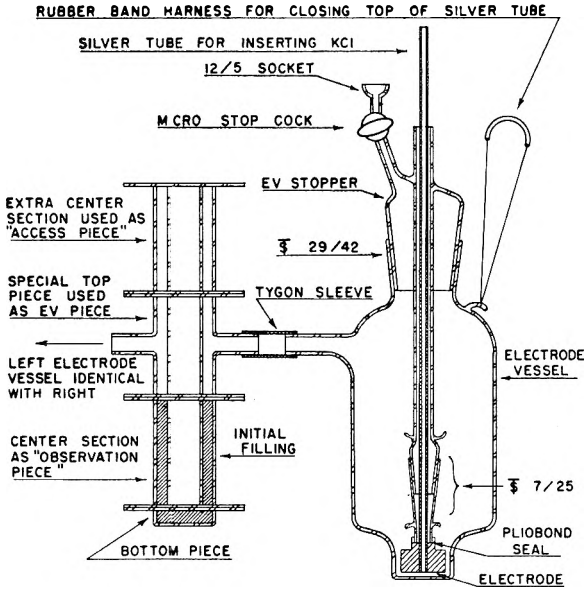

Fig. 13.—Apparatus for compensated electrophoresis with one side closed and starting from two capillary sharpened boundaries.

The capillary sharpening technique serves two purposes: (a) to compensate the Tiselius boundary slowly into view; (b) to clean up the non-planar nature of a compensated boundary first on the leading edge and then the trailing side. Used in this manner the capillary sharpening technique requires an additional amount of material over the usual Tiselius technique equal to the volume of one center section channel (total 3.5 cc. with the micro cell and 19 cc. with the standard cell). If only one pattern is desired, then the open U arrangement can be used with the cell loaded in an appropriate manner and just one boundary sharpened. The capillary sharpening technique is thus a very versatile, useful tool to enable compensation in open systems and/or sharpening.

Electro-osmosis in Electrophoresis

In Fig. 14 are two photographs of the boundaries obtained in the electrophoresis of bovine serum albumin in phosphate buffer 0.1 ionic strength at 20 v./cm. It is evident that these boundaries are not horizontally plane. The disturbance is not thermal convection since it is opposite in the two limbs. Study of this with the camera in both the horizontal and vertical positions indicates that this disturbance is strikingly similar to the compensator pattern. Compare, for example, Figs. 7 and 14.

Fig. 14.—Electro-osmotic disturbance in moving boundary electrophoresis: 1% bovine albumin in phosphate buffer *p*H 7.7, ionic strength 0.1, at 20 v./cm., thermostat at 0.0°; micro cell, as seen on ground glass; scanning camera, $\theta_s = 0$; A, 25 minutes, blade almost to undeflected light source image; B, 30 minutes, blade lower than in A.

Hence the disturbance is a hydrodynamic one, there being a velocity distribution across the cell which the boundary, by its density stability, tends to average. This type of disturbance has been reported for viruses[8] and has been called electro-osmotic streamings. Reference to the literature on the microscopic method of electrophoresis[13] shows that in a closed cell, a parabolic distribution of observed velocity of protein coated particles always occurs. This is attributed to a circulation of the water upon which a constant electrophoretic velocity is superimposed. Using hydrodynamic laws only, a parabolic distribution of water velocity can be derived on the assumption of water being driven at a velocity U at the walls of the closed cell.[14] This moving sheet of water at the walls, which has a return flow through the center of the cell, is considered to be dragged along by the movement under the impressed field of the excess cations in a layer near the wall neutralizing the negative protein ions adsorbed to the wall. These relations are shown in Fig. 15. The agreement of the parabolic nature of the distributions is taken as proof for the model. When the experimental curves extrapolate through zero velocity at the walls, it is claimed that the electro-osmotic velocity U is equal in magnitude but opposite in direction to the electrophoretic

(13) H. A. Abramson, L. S. Moyer and M. H. Gorin, "Electrophoresis of Proteins," Reinhold Publishing Corp., 1942.

(14) M. Smoluchowski, "Handbuch der Elektrizitat und des Magnetisms," Graetz, ed., Vol. 2, Leipzig, 1914, p. 366.

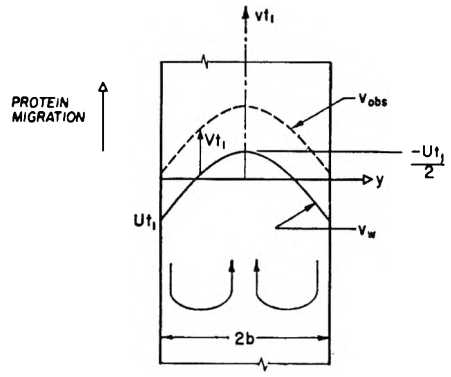

Fig. 15.—Electro-osmosis in closed microscopic method electrophoresis cell:

$v_{obs.} = v_w + V$

$\int_{-b}^{b} v_w \, dy = 0$ $\qquad \frac{1}{2b} \int_{-b}^{b} v_{obs.} \, dy = V$

Experimentally, $U = -V$ for many proteins; U, electro-osmotic velocity of water (at the wall); V, electrophoretic velocity of the protein with respect to the water; t_1, time after beginning at which profile is drawn; v_w, water velocity; $v_{obs.}$, observed protein velocity.

velocity V. From these considerations it is concluded then that the disturbance noted in the moving boundary electrophoresis of bovine albumin (Fig. 14) is due to electro-osmosis.

The apparent explanation for the neglect of electro-osmosis in moving boundary considerations of proteins, even though microscopic electrophoretic studies have led certain groups to believe that all proteins are adsorbed to glass surfaces, is probably threefold: (a) The density gradient across the boundary keeps it from being a profile of the flow in the body of the solution averaging out the electro-osmotic distribution. (b) Optical systems have been used which are not particularly sensitive to distortions across the cell, especially the cylindrical lens method. (c) Electro-osmotic disturbances have been confused with thermal convections which in the micro cell do not cause trouble until much higher field strengths than those which give a sufficient electro-osmotic flow to compete with the density gradient stabilization of a boundary region. With an a.c. power supply, it was found, for example, that field strength of 20 v./cm. in phosphate buffer of ionic strength 0.1 in the micro cell at a thermostat temperature of 0.0° did not cause noticeable distortion of the horizontal integrity of a 1% bovine albumin boundary in 30 minutes, whereas Fig. 14 shows electro-osmotic disturbance at this field strength. This disturbance can also be distinguished from thermal convections as noted above by comparison of the two patterns—ascending and descending. Thermal convections should be the same with respect to the channel on both sides, but the electro-osmotic disturbance in the center should be in the direction that the boundary is going regardless of whether that direction is up or down, and experimentally this is observed.

The velocity distribution of the protein ions across the cell can be made to disappear by balancing the distribution of the electro-osmotic flow with a superimposed compensator flow. This bucking principle is shown in Fig. 16. If U equals $-V$, the net protein velocity with respect to the cell will be

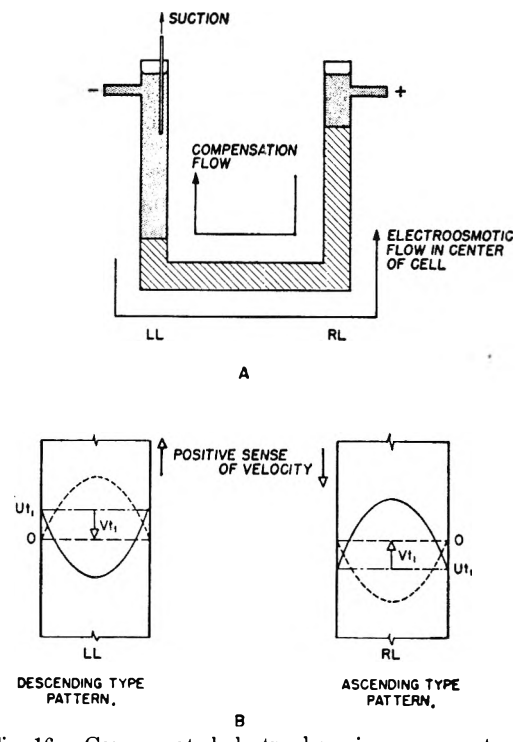

Fig. 16.—Compensated electrophoresis: ——, water profile due to electro-osmosis; - - - -, solution profile due to suction (compensation); — - —, net water profile; – – –, protein boundary profile.

zero, so that for these cases the old technique of holding a boundary stationary by a counter flow in order to keep it in the optical system and allow greater path for separation was a very good thing to do.

Figure 17 illustrates a single component system. Starting from the initial capillary sharpened boundary in the left limb (A, LL) a field of 8 v./cm. was applied such that the force on the albumin is down as seen in this figure. Simultaneously

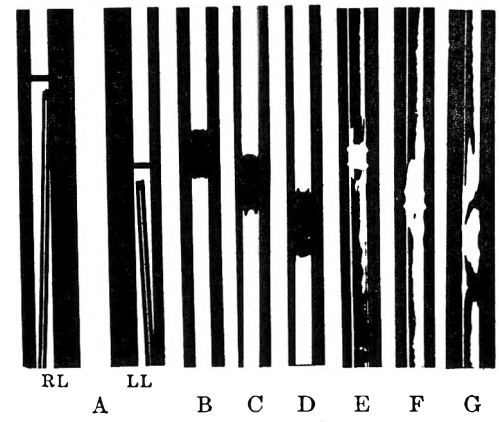

Fig. 17.—Compensated electrophoresis from capillary sharpened initial boundary: 1% bovine albumin in phosphate buffer pH 7.7, ionic strength 0.1, in micro cell, thermostat 1.5°, scanning camera photographs as seen on ground glass. A, left limb (LL) and right limb (RL) just after suction turned off; B, LL after 65 minutes at 8 v./cm. left electrode positive, and sufficient counter flow to keep albumin boundary stationary; C, LL 10 minutes after suction off, but field still on. D, LL 12 minutes after suction on alone. E, F, G, corresponding photographs at $\theta_s = 94.5°$ to B, C, D.

suction was applied to the right limb capillary (raised up out of view), giving compensation flow upward in the left limb as seen in the figure. With the scanning camera at 0°, B was taken 65 minutes later, and shows a rather nice boundary. The suction was turned off and the horns in C resulted in ten minutes. Then the field was turned off and the suction applied. D shows horns in the opposite sense 12 minutes later. At essentially the same times E, F and G were taken with the camera at 94.5°.

The boundary of 17-E is not perfect, *i.e.*, it is somewhat non-planar. This can be due to two causes: (a) The compensation rate was not quite correct. (b) Electro-osmosis is different in the two solutions so that there is no unique value of compensation to use. This is to be expected in boundary systems because the solutions between boundaries certainly contain different proteins at differing concentrations. This latter factor has been observed in electrophoresis of lipoprotein-rich fractions prepared as indicated in an earlier section (Fig. 18). Separate experiments indicate that the

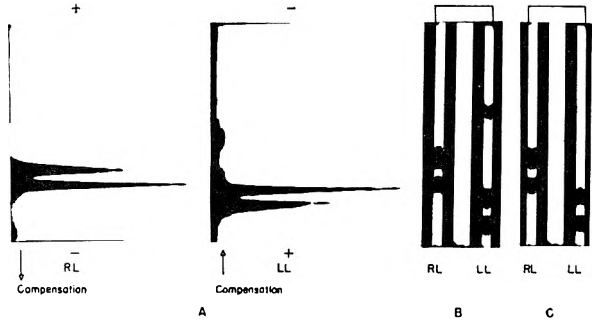

Fig. 18.—Compensated electrophoresis from capillary sharpened initial boundary—lipoprotein albumin fraction: 1% total protein in barbiturate buffer *p*H 8.2 buffering capacity 0.04 and made up to 0.1 ionic strength with SCN^-, in micro cell, thermostat 1.7°, photographs as seen on the ground glass: A, RL and LL cylindrical lens patterns 40° blade angle with respect to the horizontal after 40 minutes at 7 v./cm. LEV positive and suction on the REV of 0.1 microliter/sec. which kept the slower component stationary; B, $\theta_s = 0$, horizontal blade pattern after 3 minutes of field alone; C, same as B after 3 minutes of compensation alone.

albumin boundary is best when held stationary. When this is done in the fractions containing albumin and lipoprotein (lower mobility) the slower peak is completely wrecked. But when the lipoprotein peak is kept stationary it retains its horizontal integrity much better and allows a successful electrophoretic run to be made. In this case the albumin boundary is not perfect, there being too little compensation, and hence a resulting skewness on the leading edge similar to that of Figs. 7 or 8. Its greater density stability (some 15 times) over the lipoprotein boundary enables it to remain horizontal. In A of Fig. 18 are shown the cylindrical lens patterns when the main lipoprotein peak was held stationary for 40 minutes at 7 v./cm. and 0.1 microliter/sec. compensation in the micro cell. The scanning camera at 90° revealed that the lipoprotein boundaries were not quite perfect. To demonstrate as in Fig. 17, what would happen if compensated electrophoresis were not used, the compensation was turned off for three minutes. In B are the schlieren patterns of the cell which show the non-planar boundary regions "pointing" in the direction of the migration. In C is the same type of photograph three minutes after the compensator was turned on and the field off. Note that the boundaries "point" in the direction of the hydrodynamic flow of compensation.

The combination of compensation to bring a Tiselius boundary into view and electro-osmosis during the electrophoretic run lead to non-planar, broad boundary regions. Capillary sharpened, compensated electrophoresis is indicated if great resolution is desired of components of small difference in mobility, or small density difference solutions are to be studied. It should be noted that even with large density differences in the solutions and sharp boundary regions the turn around flow necessitated by a plane boundary wall to hydrodynamic flow on either side results in the boundary being chewed out and diffuse material being drawn away from the boundary position. Thus, in the classical technique, contamination of one component into the boundary regions of others is to be expected.

A practical arrangement of the cell assembly for compensated capillary sharpened electrophoresis is shown in Fig. 13. The extra center section on top of the electrode vessel connection piece (EV piece) affords a means of access to the channels for the capillaries and allows the system to be closed when the capillaries are withdrawn. The sharpening procedure was described in an earlier section. The compensation can be performed in either of two ways: (a) If an open system is desired, then merely raising the capillaries into the top section and applying suction to one of them will give a flow through the U-tube, the rate, however, depending on the relative cross-sectional areas of the free surfaces. (b) For compensated electrophoresis with one side closed, the access piece can be slid out of alignment after the capillaries are completely withdrawn. The same compensator which was used with the capillaries can be connected to the standard joint on the appropriate electrode vessel stopper.

VISCOSITY, DENSITY AND CRITICAL CONSTANTS OF OF_2

BY R. ANDERSON, J. G. SCHNIZLEIN, R. C. TOOLE AND T. D. O'BRIEN

Chemistry Department, University of Minnesota, Minneapolis, Minnesota

Received May 7, 1951

The viscosity of liquid OF_2 was determined over a small temperature range. The viscosity of liquid OF_2 at its boiling point (−145.3°) was 0.2826 centipoise. The density of liquid OF_2 is 1.521 at its boiling point. The critical temperature of OF_2 was experimentally found to be −58.0 ± 0.1°. The critical volume was calculated to be 97.6 cc./mole and the critical pressure 48.9 atmospheres.

Experimental

The preparation and purification of the OF_2 used in this work has been previously described.[1]

Viscosity.—The apparatus used for determining the viscosity of liquid OF_2 is shown in Fig. 1. The lower portion is an Ostwald viscometer of Pyrex glass, and the upper portion is designed to move the liquid OF_2 from bulb E upward against the force of gravity into bulb D. The two sections are connected with ground glass joints to facilitate the removal of the viscometer for cleaning.

In determining viscosity the following procedure is followed. The viscosity apparatus is connected through a vacuum system to the OF_2 sample tube. Constant temperature is maintained by immersing the viscometer in a large test-tube containing Freon-12 which is stirred by a vigorous stream of nitrogen. The Freon-12 bath is immersed in an unsilvered dewar flask containing liquid nitrogen. This outer dewar flask can be easily raised or lowered, so the temperature of the Freon-12 bath may be regulated by adjusting the amount of liquid nitrogen in contact with it. Temperatures were measured with a four-junction thermocouple. OF_2 was collected in the viscometer by condensation with liquid nitrogen, until the liquid height reached one of several fixed marks. The center stopcock was then closed while the upper and lower stopcocks remained open. The OF_2 sample tube was then allowed to warm up, resulting in an increase in pressure above bulb E, forcing the liquid OF_2 through the capillary and finally past the upper etched mark above bulb D. The upper stopcock was then closed and the middle stopcock opened, which equalized the pressure in both tubes of the viscometer and allowed the liquid OF_2 to fall through the capillary. The time for the fall of the liquid meniscus between the etched lines was measured with a stop watch.

The viscometer was calibrated with water at 20°. The viscosity of OF_2 was obtained from the relation $\eta_1 = (d_1 t_1 \eta_2)/d_2 t_2$ when η_1 is the viscosity of OF_2 and η_2 that of H_2O at 20° (η_2 = 1.005 centipoises), d_1 is the density of OF_2, and d_2 is the density of water at 20° (0.9982). t_1 and t_2 are the times of flow for OF_2 and water, respectively.

Since the time of flow was affected by the hydrostatic head of liquid, it was necessary to use the same volume of liquid in bulb E for all runs. Due to the method used in employing the vapor of OF_2 to force the liquid up through the capillary, this requirement was rather inconvenient. Therefore, measurements of the time of flow were made at a number of definite liquid volumes, for each of which a corresponding t_2 had been determined with water at 20°. Using these calibrations with water, the accepted viscosity values of ethyl ether from 20 to −90° have been obtained.

The effect of temperature on the accuracy of the viscometer is very small. The coefficient of thermal expansion of Pyrex glass is small, and much of the effect of thermal expansion is cancelled since both bulb D (which determines the amount of liquid whose flow time is measured) and the capillary (through which it flows) are similarly affected.

Density.—Measurements of the density of liquid OF_2 near its boiling point were made by the flotation–temperature method. This method consists essentially of observing the temperature at which a previously calibrated Pyrex glass float remains suspended in the liquid. At this temperature the liquid and the float have the same density.

This method is well suited to the determination of densities of small liquid samples and has been the basis of very precise measurements, *e.g.*, the determination of isotopic ratios.[2]

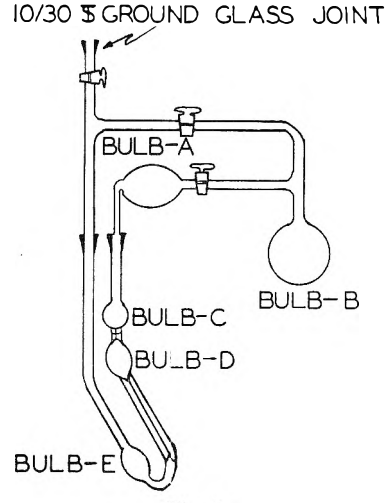

Fig. 1.

Densities of the floats were accurately determined by flotation in standard solutions of KI and in CCl_4. The float densities have been corrected to the operating temperature using the value of 9.6×10^{-6} for the cubical expansion coefficient of Pyrex glass.

Constant temperature of the liquid OF_2 was maintained as described under Viscosity.

Critical Constants.—The critical temperature was determined by the disappearance of the liquid meniscus in a sealed capillary. The capillary tubes of 1 mm. bore were one-third filled with liquid OF_2 and sealed rapidly with an oxygen flame. After testing the ability of the tubes to withstand the high pressures developed near the critical temperature, the sealed capillaries were immersed in a cryostat containing liquid Freon-12. Temperatures were measured with a five-junction–copper constantan thermocouple and a potentiometer accurate to 10 microvolts.

The critical state was approached from both higher and lower temperatures, *i.e.*, both the appearance and disappearance of the meniscus was noted. On all observations on each of four capillaries, the change of state occurred within a temperature range of 0.1°.

The critical temperature was found to be −58.0 ± 0.1°.

Results

The viscosities at various temperatures are shown in Table I.

When the log of the viscosity is plotted against the reciprocal of the absolute temperature ($\times 10^3$) a straight line is obtained. This relationship may be expressed by the equation $\log \eta = \frac{131.5}{T, \text{Å.}} - 1.5768$ which is shown graphically in Fig. 2. This expression is valid over the temperature range employed because the average deviation between experimental and calculated values represents a possible tem-

(1) J. G. Schnizlein, J. L. Sheard, R. C. Toole and T. D. O'Brien, *J. Phys. Colloid Chem.*, **56**, 233 (1952).

(2) Randall and Longtin, *Ind. Eng. Chem., Anal. Ed.*, **11**, 44 (1939).

TABLE I

Temperature, °C.	Density of OF_2	Flow time for OF_2 in sec.	Flow time for H_2O in sec.	Viscosity in centipoise units (Exptl.)	Viscosity (calcd.)	$\eta_{calcd.} - \eta_{exptl.} \times 10^3$
−145.8	1.523	67.6	363.4	0.2852	0.2852	0
−147.2	1.529	70.1	367.4	.2937	.2929	−0.8
−147.4	1.530	69.2	363.4	.2933	.2939	+0.6
−147.5	1.531	69.8	363.4	.2962	.2946	−1.6
−147.9	1.533	70.6	363.4	.2998	.2968	−3.0
−148.7	1.537	70.8	363.4	.3014	.3014	0
−148.8	1.537	71.8	367.4	.3024	.3022	−0.2
−150.6	1.546	73.3	363.4	.3140	.3131	−0.9
−150.8	1.547	73.8	367.4	.3129	.3143	+1.4
−151.0	1.548	75.4	375.0	.3134	.3157	+2.3
−151.1	1.549	74.0	363.4	.3176	.3162	−1.4
−151.3	1.550	76.2	375.0	.3171	.3175	+0.4
−151.5	1.551	75.8	371.3	.3188	.3188	0
−152.0	1.553	77.4	375.0	.3227	.3221	−0.6
−152.8	1.557	77.2	371.3	.3259	.3275	+1.6

perature variation of 0.2° which is within the limits of accuracy of these measurements.

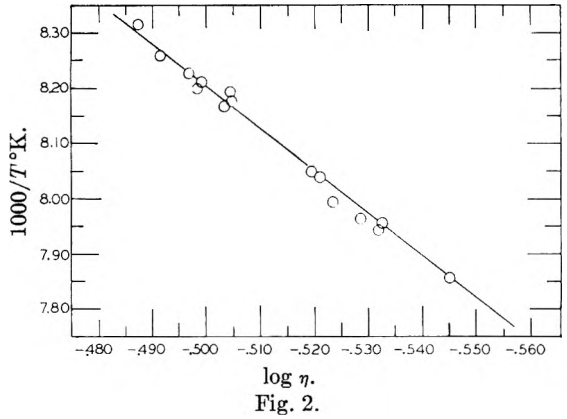

Fig. 2.

Extrapolation of the curve to −145.3 gives a viscosity of liquid OF_2 at its boiling point of 0.2826 centipoise.

The densities and the flotation temperatures are shown in the following table.

Density of float	Flotation temperature
1.528	−147.3
1.531	−147.7
1.538	−150.1
1.547	−150.5
1.569	−155.3
1.573	−155.9

These results are shown graphically in Fig. 3.

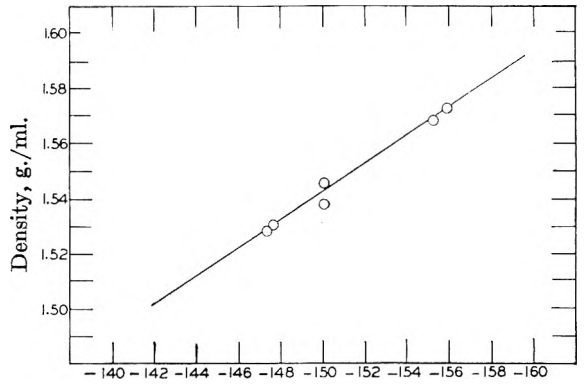

Fig. 3.

Extrapolation of the curve to the boiling point (−145.3) gives a density of 1.521.

The critical volume can be determined by applying the law of rectilinear diameters, using the previously determined values of the liquid densities, and assuming the orthobaric vapor densities to be ideal; *i.e.*, that they are given by the expression PM/RT, where M = molecular weight (54), R is the gas constant in cc.-mm./mole, and P is the vapor pressure of OF_2 obtained from the equation

$$\log P_{mm} = 7.2242 - \frac{555.42}{T°K.}$$

This assumption seems justified since the vapor densities contribute less than 1% to the mean densities over the temperature range in which the liquid densities have been determined. Plotting the mean densities against temperature gives a straight line represented by the equation $d_m = -2.40 \times 10^{-3}\ T,°K. + 1.069$. Extrapolation to the critical temperature gives a density of 0.553 g./cc. Thus the critical volume of OF_2 is 97.6 cc./mole.

The critical pressure can be evaluated by the Dieterici equation of state

$$P = \frac{RT}{V - b} e^{-a/VRT}, \quad T_c = \frac{a}{4Rb}, \quad V_c = 2b, \quad P_c = \frac{a}{4e^2b^2}$$

The constants a and b can be evaluated from the experimentally determined values of T_c and V_c.

$$b = \frac{V_c}{2} = 48.8 \text{ cc.}, \quad a = 4RT_cb = 3.45 \times 10^3 \text{ atm.-cc.}^2$$

$$\text{then } P_c = \frac{a}{4e^2b^2} = 48.9 \text{ atmospheres}$$

ON THE KINETICS OF EVAPORATION

By S. S. Penner

Guggenheim Jet Propulsion Center, California Institute of Technology, Pasadena, California

Received May 9, 1951

The kinetics of evaporation of liquids has been reconsidered from the point of view of classical reaction kinetics and also by application of the theory of absolute reaction rates. It is shown that evaporation treated as a unimolecular rate process, with a rate proportional to the surface concentration of energetic molecules, leads to the Knudsen equation for spherical molecules provided 6 square terms contribute to the energy of activation. As was pointed out in an earlier publication, the theory of absolute reaction rates, after correction for lack of equilibrium between normal molecules and the activated complex, leads to the Knudsen equation for spherically symmetric molecules if reasonable assumptions are made concerning the nature of the activated complex. Evidence is presented in support of the idea that the equilibrium theory of absolute reaction rates is not consistent with the model of the liquid used to determine evaporation rates. The theoretical treatment is next extended to polar liquids with restricted rotation and it is shown that the evaporation coefficient should be identified with the free-angle ratio, a conclusion which has been verified quantitatively by Wyllie.[1]

I. Introduction

The theory of absolute reaction rates[2] has been applied in previous publications to an analysis of the kinetics of evaporation of liquids,[3] which has also been examined by straightforward applications of kinetic theory[4] and elementary reaction kinetics.[5] The analysis using the theory of absolute reaction rates has been based on the free-volume model of the liquid rather than on the more adequate description of the liquid state developed by Kirkwood[6] and by Born and Green.[7] By introducing the hypothesis that the activated state formed during evaporation corresponds to a molecule moving freely in an area equal to the two-thirds power of the volume per molecule in the liquid, it was shown that a relation of the same form as the Knudsen equation is obtained for the specific evaporation rate. Here it was assumed that the rotational and vibrational partition functions of the liquid molecules and of the activated complex are the same.[3] Furthermore, the specific evaporation rate was shown to be practically identical with the Knudsen equation (with a transmission coefficient replacing the empirically observed evaporation coefficient[8]) after a suitable correction, suggested by the non-equilibrium theory of absolute reaction rates,[9] had been introduced. Thus it has been shown that absolute reaction rate theory, together with a simplified model of the liquid state, can be used to derive a relation for the evaporation rate which is known to have the correct functional form.

The treatment given previously applies only to liquids with spherically symmetric force fields which allow free rotation. For pure liquids of this type the evaporation coefficient is known to be close to unity,[10] whence it follows that the transmission coefficient must also be equal to unity in order to obtain agreement between experimental data and the result derived from the theory of absolute reaction rates.

Recently Wyllie[1] has called attention to an interesting quantitative correlation between the evaporation coefficient for polar liquids and the free-angle ratio introduced by Kincaid and Eyring[11] to allow for restricted rotation in the liquid. We shall show that this result is a direct consequence of our simplified rate theory when applied to polar liquids.

Before presenting the extension of the simplified theory for the kinetics of evaporation to polar liquids, we shall reconsider the problems of evaporation rates from the point of view of classical reaction kinetics in order to amplify some of the numerical calculations described previously.[5] In particular, it will be shown that evaporation treated as a unimolecular process, with the evaporation rate proportional to the concentration of energetic molecules at the surface, will lead to the Knudsen equation if it is assumed that 6 square terms contribute to the activation energy.[12] Finally, the problem of applicability of the non-equilibrium theory of absolute reaction rates is reconsidered. It is shown that the assumption of equilibrium between normal molecules and the activated complex leads to the requirement of an abnormally long energy barrier, thereby suggesting that equilibrium rate theory is not applicable to the problem at hand. Compelling reasons for using the particular non-equilibrium model considered by Hirschfelder[9] are, however, not apparent.

II. Evaporation Rates as a Problem in Classical Chemical Kinetics

A treatment of evaporation rates based on classical reaction kinetics requires the assumption of a specific mechanism for evaporation. Since vaporization is a surface phenomenon, it seems reasonable to suppose that the rate of loss of molecules $-dn_V/dt$ from a given volume V is proportional to the number of molecules n_s exposed at the surface, *i.e.*

(1) G. Wyllie, *Proc. Roy. Soc.* (*London*), **197A**, 383 (1949).

(2) S. Glasstone, K. J. Laidler, and H. Eyring, "The Theory of Rate Processes," McGraw-Hill Book Co., Inc., New York, N. Y., 1941.

(3) S. S. Penner, THIS JOURNAL, **52**, 950 (1948); *ibid.*, **52**, 1262 (1948).

(4) J. Frenkel, "Kinetic Theory of Liquids," Clarendon Press, Oxford, 1946, Chap. I; *Z Physik*, **26**, 117 (1924).

(5) S. S. Penner, THIS JOURNAL, **52**, 368 (1948).

(6) J. G. Kirkwood, *et al.*, *J. Chem. Phys.*, **18**, 1040 (1950), and earlier publications.

(7) M. Born and H. S. Green, "A General Kinetic Theory of Liquids," Cambridge University Press, Cambridge, 1949; also *Proc. Roy. Soc.* (*London*), Volumes **188A** to **194A**.

(8) The evaporation coefficient is defined as the ratio of the observed rate of evaporation to the evaporation rate calculated from the Knudsen equation.

(9) J. O. Hirschfelder, *J. Chem. Phys.*, **16**, 22 (1948)

(10) E. H. Kennard, "Kinetic Theory of Gases," McGraw-Hill Book Co., Inc., New York, N. Y., 1938, pp. 68–71.

(11) J. F. Kincaid and H. Eyring, *J. Chem. Phys.*, **6**, 620 (1938).

(12) L. Kassel, "Kinetics of Homogeneous Gas Reaction," Chemical Catalog Company, (Reinhold Publ. Corp.), New York, N. Y., 1932, Chapter V.

$$-\mathrm{d}n_V/\mathrm{d}t = j_e n_s \quad (1)$$

where j_e is a rate constant for evaporation. Since $n_V = nV$ and $n_s = n^{2/3}S$, where n is the number of molecules per unit volume and S is the surface area of the evaporating compound, it follows that

$$-\rho n\ \mathrm{d}V/\mathrm{d}t = \rho j_e n^{2/3} S$$

or

$$G = -\rho(1/S)\,(\mathrm{d}V/\mathrm{d}t) = j_e \rho/n^{1/3} \quad (2)$$

Here ρ is the density of the evaporating compound and G, the specific evaporation rate, represents the rate at which mass is lost by evaporation per unit time per unit surface area.

On the basis of elementary considerations in chemical reaction kinetics it seems intuitively obvious to equate j_e to the product of a frequency factor whose dimensions are sec.$^{-1}$ and an exponential factor involving an appropriate activation energy to single out the fraction of molecules with sufficient energy for evaporation. Therefore we may write

$$j_e = B \exp(-\Delta E_V/RT) \quad (3)$$

where ΔE_V is the molar activation energy for evaporation, R is the molar gas constant, T is the absolute temperature, and B is the as yet undetermined frequency factor. The term $\exp(-\Delta E_V/RT)$ in equation 3 arises because only the molecules with energy in excess of ΔE_V per mole can evaporate, and the fraction of molecules possessing the required energy at any given time is $\exp(-\Delta E_V/RT)$. The molar activation energy for evaporation is related to the heat of evaporation ΔH_V according to the well-known relation[2]

$$\Delta H_V = \Delta E_V + N p_s(v_g - v_f) \quad (4)$$

since the external work done during the expansion of one mole from the free volume per molecule v_f in the condensed state to the volume per molecule v_g in the gaseous state at the vapor pressure p_s is $Np_s(v_g - v_f)$ where N represents the Avogadro number. But v_f is negligibly small compared to v_g whence $Np_s(v_g - v_f) \simeq RT$ if the vapor behaves as a perfect gas. It therefore follows that, to a close approximation

$$j_e = eB \exp(-\Delta H_V/RT) \quad (5)$$

The evaluation of the frequency factor B corresponding to an upper limit for the rate of evaporation can be carried out intuitively by noting that B should represent some sort of an upper limit for the oscillation or collision frequency. An upper limit for the collision frequency of the evaporating molecules is given by the root mean square velocity of activated molecules divided by the mean free path. But the mean square velocity of activated molecules C^2 is simply the mean square velocity of molecules with energy in excess of ΔE_V per mole.[5] A simple calculation utilizing the Maxwell–Boltzmann law in two dimensions shows that C^2 is given by the relation

$$C^2 = \frac{1}{n_s e^{-\Delta E_V/RT}} \int_{\Delta E_V}^{\infty} \frac{n_s}{RT} e^{-E/RT} \times \frac{2E}{M}\,\mathrm{d}E$$

or

$$C^2 = (2/M)\,(\Delta E_V + RT) = (2\Delta H_V/M)$$

where M represents the molecular weight of the evaporating compound. Hence the frequency factor B is

$$B = \sqrt{C^2}/v_f^{1/3} = (2\Delta H_V/M)^{1/2}/v_f^{1/3}$$

and, therefore,

$$G = e\rho[(2\Delta H_V/M)^{1/2}/v_f^{1/3} n^{1/3}] \exp(-\Delta H_V/RT) \quad (6)$$

where the mean free path in the liquid has been set equal to the cube root of the free volume per molecule v_f in the condensed state. The free volume v_f for liquids can be calculated, for example, from the Kincaid–Eyring expression[11]

$$v_f = v\,(1/U)^3\,(RT\gamma/M)^{3/2} \quad (7)$$

where v is the volume per molecule in the liquid state, M is the molecular weight of the evaporating liquid, U is the sound velocity in the liquid, and γ is the ratio of the specific heat at constant pressure to the specific heat at constant volume. It has been shown that the use of equations 6 and 7 actually leads to results[5] which are in some cases in good agreement with numerical values calculated from the Knudsen equation, *i.e.*, with results calculated from the relation

$$G = \epsilon p_s (M/2\pi RT)^{1/2} \quad (8)$$

where the evaporation coefficient ϵ has been set equal to unity and p_s is the saturated vapor pressure of the evaporating compound. The numerical results calculated from equations 6 and 7 and from equation 8, respectively, are in fairly good agreement for compounds such as CCl_4, $CHCl_3$, C_6H_6, etc., for which the free volume model is a satisfactory description of the liquid state. For associated liquids such as water or alcohol v_f is not adequately represented by equation 7 and failure to obtain satisfactory agreement between the theoretical equations is therefore not surprising.

The equivalence of equations 6 and 8 can be demonstrated more explicitly by proceeding as follows. At room temperature $\Delta E_V >> RT$ for ordinary liquids. Therefore $(2\Delta H_V/M)^{1/2} \simeq (2\Delta E_V/M)^{1/2}$. Hence equation 6 can be written as

$$G \simeq (2\Delta E_V/M)^{1/2}(1/v_f)^{1/3}(\rho/n^{1/3})e \exp(-\Delta H_V/RT)$$

But it has been shown[2] that $(\Delta E_V/RT)^{1/2} \simeq (2)^{1/2}(v/v_f)^{1/6}$ and, therefore

$$G \simeq \left(\frac{2kT}{m}\right)^{1/2} \sqrt{2}(v/v_f)^{1/6} \frac{v_f^{2/3}}{v_f} \frac{\rho v^{1/3}}{n^{1/3} v^{1/3}}\, e \exp(-\Delta H_V/RT)$$

where k is the Boltzmann constant and m represents the mass per molecule. But $\rho v = m$, $n^{1/3}v^{1/3} = 1$ and

$$1/v_f = (p_s/kT)e^{\Delta H_V/RT} \quad (9)$$

whence

$$G \simeq p_s(m/2\pi kT)^{1/2}[2\sqrt{2\pi}\, e(v_f/v)^{1/2}] \quad (10)$$

In equation 9 p_s represents the saturated vapor pressure of the evaporating compound whose vapor is assumed to behave as a perfect gas. Equation 9 was obtained by Eyring and Hirschfelder[13] who noted that the Gibbs free energy of the evaporating substance and of the gas with which it is in equilibrium must be equal to each other.[14] Equation 10 is seen to be identical with the Knudsen equation 8

(13) H. Eyring and J. O. Hirschfelder, THIS JOURNAL, **41**, 249 (1937).

(14) It should be noted that equation 9 holds only for spherically symmetric liquid molecules.

with $\epsilon = 1$ except for the term in square brackets. Since $v_f/v \simeq 3 \times 10^{-3}$ at room temperature for many liquids, the term in square brackets is of the order of unity. This result accounts for the agreement observed at room temperature between the numerical values calculated from equations 6 and 8, respectively. However, since v_f/v varies with temperature, it is obvious that equations 8 and 10 do not have the same temperature dependence. This conclusion was reached previously as the result of empirical calculation.[5]

An equation equivalent to the Knudsen equation can be obtained by using some of the methods introduced into the classical theory of unimolecular decompositions[12,15-17] in a rather arbitrary manner. On the basis of a simple collision mechanism it might be expected that the frequency factor in the rate expression for evaporation is of the same order of magnitude as the mean collision frequency, *i.e.*

$$B = \bar{\dot{x}}/v_f^{1/3} = (kT/2\pi m)^{1/2}/v_f^{1/3} \qquad (11)$$

where $\bar{\dot{x}}$ is the mean translational velocity in a given direction of a molecule of mass m at the temperature T. On the basis of the preceding discussion it is, of course, obvious that the use of equation 11 with the exponential factor $\exp(-\Delta E_V/RT)$ will lead to low values for G. In order to obtain the Knudsen equation it is evidently necessary to increase the rate of production of energetic molecules. The desired result can be attained either by the arbitrary introduction of an entropy term or else by the equally arbitrary assumption that more than two square terms can contribute to the energy of activation, thus increasing the probability of the occurrence of energetic molecules.

It was pointed out a number of years ago that agreement with experimental results could be obtained for unimolecular decomposition if n square terms can contribute to the energy of activation where n appears to be related to the complexity of the decomposing molecule.[15,16] If a number of restrictive conditions are met, the effective frequency factor is found to be larger than the collision number by the factor

$$(\Delta E_V/RT)^{(1/2)n-1}/[(1/2)n - 1]! \qquad (12)$$

If the arbitrary assumption is made that 6 square terms can contribute to the energy of activation, then it can be seen that the effective frequency factor is

$$B = [2(kT/2\pi m)^{1/2}/v_f^{1/3}]\ (v/v_f)^{2/3} \qquad (13)$$

since

$$\Delta E_V/RT \simeq 2(v/v_f)^{1/3}$$

Equations 2, 3 and 13 lead to the relation

$$G = 2(1/v_f)\ (kT/2\pi m)^{1/2}(\rho v/n^{1/3}v^{1/3})\ \exp(-\Delta E_V/RT)$$

or

$$G = 2ep_s\ (m/2\pi kT)^{1/2} \qquad (14)$$

where use has been made of equation 9 as well as of the relations $\rho v = m$ and $n^{1/3}v^{1/3} = 1$. Equation 14 is the Knudsen equation with an evaporation coefficient of unity and multiplied by the factor $2e$.

(15) R. H. Fowler and E. K. Rideal, *Proc. Roy. Soc.* (*London*), **113A**, 570 (1927).

(16) C. N Hinshelwood, *ibid.*, **113A**, 230 (1927).

(17) O. K. Rice and H. C. Ramsperger, *J. Am. Chem. Soc.*, **49**, 617 (1927); **50**, 617 (1928).

On the basis of classical considerations it has thus proved to be possible to obtain a relation of the same form as the Knudsen equation by making use of an artifice which was introduced into the theoretical discussion of unimolecular decomposition prior to the advent of the theory of absolute reaction rates. The physical significance of the need for the assumption that 6 square terms can contribute to the energy of activation is obscure.

The classical considerations reviewed in the preceding discussion are not particularly convincing since they were designed to fit the desired results rather than the physical processes. A significant improvement over this type of argument can be registered through the application of the theory of absolute reaction rates as discussed in the following section.

III. Rates of Evaporation from the Point of View of the Theory of Absolute Reaction Rates

According to the statistical theory of reaction rates[2] the rate constant for evaporation j_e is given by the relation

$$j_e = K(kT/h)\ (Q^*/Q)\ \exp(-\Delta E_V/RT) \qquad (15)$$

where K is the transmission coefficient, h represents Planck's constant, Q^* is the partition function of the activated complex with the energy zero referred to the zero-point energy of the activated state and the translational partition function along the coordinate of decomposition removed and Q is the complete partition function of the normal molecules with energy zero referred to the zero-point energy of the normal molecules. The specific rate of evaporation is then given by introducing the value of j_e from equation 15 into equation 2. In order to obtain useful results from equation 15 it is necessary to write explicit relations for the partition functions, which can only be done after making definite assumptions concerning the structure of the normal molecules in the condensed state as well as of the structure of the activated molecules formed during evaporation

It will be assumed that the physical state is adequately described by the free volume model.[18,19] The partition function Q of the normal molecules is then given by the relation

$$Q = [(2\pi mkT)^{3/2}v_f/h^3]Qi \qquad (16)$$

where Qi includes the vibrational, rotational and internal electronic contributions to the partition function, which are assumed to remain unaltered during evaporation. If the partition function Q^* corresponding to the activated complex is similarly written as

$$Q^* = [(2\pi mkT)v_f^{2/3}/h^2]Qi \qquad (17)$$

then equation 15 becomes

$$j_e = K(kT/2\pi m)^{1/2}v_f^{-1/3}\ \exp(-\Delta E_V/RT) \qquad (18)$$

The values of j_e calculated from equation 18 with $K = 1$ are much smaller than the values predicted by the Knudsen equation.

Since the activated complex for evaporation occurs during the formation of freely moving mole-

(18) J. E. Mayer and M. G. Mayer, "Statistical Mechanics," John Wiley and Sons, Inc., New York, N. Y., 1940, pp. 319-326.

(19) E. A. Guggenheim, *Proc. Roy. Soc.* (*London*), **135A**, 181 (1932).

cules, it is not unreasonable to postulate that the activated complex consists of gas-like molecules which can move freely throughout a two-dimensional plane of area $v^{*2/3}$ where $v^* = v$ is the volume per molecule in the condensed state.[3] With this assumption equation 15 reduces to the relation

$$j_e = eK(kT/2\pi m)^{1/2}(v^{2/3}/v_f)\exp(-\Delta H_V/RT) \quad (19)$$

where $\exp(-\Delta E_V/RT)$ has been replaced by $e\exp(-\Delta H_V/RT)$.

Equation 19 with $eK = 1$ has been used[3] to calculate evaporation rates for a number of liquid compounds and metallic elements by determining the ratio $v^{2/3}/v_f$ from the Kincaid–Eyring expression[11] for the free volume of a liquid. The use of the Kincaid–Eyring free volume formula for metallic elements is justified by the fact that the Lennard-Jones free volume formula[20] for solids leads to results which are practically identical with numerical values calculated from the Kincaid–Eyring expression at room temperature.[21] It was found that equation 19 leads to results which are of the same order of magnitude as calculations based on the Knudsen equation. The agreement between the numerical values was observed to be best for the metallic elements and for non-associated spherical liquid molecules where the Kincaid–Eyring formula for the free volume is most likely to be valid. Equation 19 appeared to lead to evaporation rates with a temperature coefficient different from the temperature coefficient of the Knudsen equation.

The results obtained from the theory of absolute reaction rates, although they are perhaps as good as similar applications of this theory to rate processes other than evaporation rates, are not entirely satisfactory. It seems reasonable to suppose that correct application of the theory of absolute reaction rates should lead to an equation equivalent to the Knudsen equation. Failure to obtain this result may indicate an incomplete description of the initial state or of the activated complex as expressed by the respective partition functions. Thus, the description of the condensed state by the free volume model may be inadequate and may be the source of the discrepancies. A comparison of the results of the theory of absolute reaction rates with those obtained from the Knudsen equation, without explicit introduction of partition functions calculated on the basis of an approximate model for the liquid state appears highly desirable.

All references to the approximate description of the condensed state through partition functions can be eliminated from the theoretical relation for the rate of evaporation by proceeding as follows. The introduction of equation 19 into equation 2 leads to the relation

$$G = eK(kT/2\pi m)^{1/2}(\rho v/n^{1/3}v^{1/3})(1/v_f)\exp(-\Delta H_V/RT)$$

Replacing ρv by m in this expression for G and replacing $1/v_f$ by use of equation 9 it is found that

$$G = eKp_s(m/2\pi kT)^{1/2} \quad (20)$$

since the product $(nv)^{1/3} = 1$ as noted earlier in this discussion. Equation 20 is the Knudsen equation for the isothermal rate of evaporation with the evaporation coefficient ϵ replaced by the product of the base of the natural logarithm e and the transmission coefficient K.[3]

An alternate derivation of equation 20 can be given by noting[2] that

$$j_e = K(kT/2\pi m)^{1/2}(1/\delta)(Q^{*\prime}/Q) \quad (21)$$

where δ is the length of the energy barrier over which the activated complex passes during evaporation and $Q^{*\prime}$ is the complete partition function of the activated complex. The introduction of equation 21 into equation 2 leads to the result

$$G = K(kT/2\pi m)^{1/2}(\rho/n^{1/3}\delta)(Q^{*\prime}/Q)$$

or

$$G = K(mkT/2\pi)^{1/2}(1/vn^{1/3}\delta)(Q^{*\prime}/Q) \quad (22)$$

From equation 9 it can be seen that

$$p_s v^{2/3}\delta/kT = (\delta v^{2/3}/v_f)\exp(-\Delta H_V/RT)$$

But if the activated complex behaves as a gaseous molecule and the vibrational, rotational and internal contributions to the partition function remain unchanged during evaporation, then it is evident that

$$Q^{*\prime}/Q = e(\delta v^{2/3}/v_f)\exp(-\Delta H_V/RT) = ep_s\delta v^{2/3}/kT \quad (23)$$

Replacing $Q^{*\prime}/Q$ by $e\delta p_s v^{2/3}/kT$ in equation 22, it follows that

$$G = eKp_s(m/2\pi kT)^{1/2}$$

It is evident that results calculated from equation 20 with $eK = 1$ should be identical with results calculated from the Knudsen equation with the evaporation coefficient set equal to unity. It is therefore apparent that the discrepancies observed between the results calculated from equation 19 with $eK = 1$ and from equation 8 with $\epsilon = 1$ were introduced by an incomplete description of the physical state through partition functions calculated on the basis of the free volume model.[3]

IV. Application of the Non-Equilibrium Theory of Absolute Reaction Rates to Evaporation Kinetics

The derivation of equation 20

$$G = eKp_s(m/2\pi kT)^{1/2}$$

seems to be a straightforward result of the application of the usual theory of absolute reaction rates together with the assumptions that the activated molecules are gas-like molecules and that the vibrational, rotational and internal electronic contributions to the partition function remain unchanged during evaporation. Equation 20 cannot be a correct relation for the isothermal rate of evaporation since the maximum possible rate with $K = 1$ would be e times as large as the actual upper limit for the isothermal evaporation rate given through equation 8 with $\epsilon = 1$. Equations 20 and 8 do not lead to the same maximum values for the isothermal rates of evaporation unless K is restricted to values less than or equal to $1/e$. This limitation on the numerical values of K seems to be quite unreasonable and can probably not be justified by a more detailed analysis of the transmission coefficient for evaporation. Whatever the relation between K and ϵ may be, it is apparent that the theory of absolute reaction rates does not lead to the correct upper limit

(20) J. E. Lennard-Jones, *Proc. Roy. Soc.*, **52**, 729 (1940).
(21) S. S. Penner, *J. Chem. Phys.*, **16**, 745 (1948).

for the rate of evaporation unless the factor eK can be replaced by the factor K.

The derivation of equation 20, as well as most other applications of the theory of absolute reaction rates, involves the implicit assumption that equilibrium exists between normal and activated molecules. If this equilibrium does not exist, then the usual theory of absolute reaction rates will lead to evaporation rates which are too large.[9,22,23] The existence of non-equilibrium can be established for the case at hand by a *reductio ad absurdum* which leads to the conclusion that the energy barrier δ must be excessively long if equilibrium does exist between normal and activated molecules.

If equilibrium between normal and activated molecules did exist, then

$$-kT \ln (Q^{*\prime}/Q) = p_s(v^* - v_f)$$

Replacing $Q^{*\prime}$ and Q by their respective values leads to the relation

$$-kT[(-\Delta E_V/RT) + \ln(\delta v^{*2/3}/v_f)] = p_s (v^* - v_f)$$

Since $v^* << v_g$, it follows that

$$\Delta H_V - [\Delta E_V - Np_s (v^* - v_f)] \simeq RT$$

or

$$\Delta E_V - Np_s (v^* - v_f) \simeq \Delta E_V$$

where N is the Avogadro number. Therefore

$$e\delta v^{*2/3} = ev_f \exp(\Delta E_V/RT) = v_f \exp(\Delta H_V/RT)$$

But from equation 9

$$v_g = v_f \exp(\Delta H_V/RT)$$

The existence of equilibrium between normal and activated molecules therefore leads to the requirement

$$\delta/v^{*1/3} = (1/e)\,(v_g/v^*)$$

i.e., the length of the energy barrier must be equal to about 100 molecular diameters. This result is certainly incorrect and it therefore seems reasonable to conclude that equilibrium between normal and activated molecules cannot exist during evaporation if the gas-like model is a valid description of the activated state.

The mechanism assumed for evaporation seems to be in agreement with the supposition that the molecules move classically in the degree of freedom along which the molecules decompose with an average energy change of the order of kT between successive transfers of energy. Hirschfelder[9] has shown that in this case the equilibrium theory of reaction rates gives values which are too large by a factor of 1/0.387. The rate treatment for evaporation with Hirschfelder's correction factor therefore leads to the result

$$G = 0.387\, eKp_s\,(m/2\pi kT)^{1/2}$$

or

$$G \simeq Kp_s(m/2\pi kT)^{1/2} \qquad (24)$$

A comparison of equations 8 and 24 indicates that the non-equilibrium theory of absolute reaction rates leads to a result formally identical with the Knudsen equation except that the evaporation coefficient ϵ is replaced by the transmission coefficient K. Since ϵ is known to be very close to unity for pure liquids with spherically symmetric force fields (*e.g.*, Hg, CCl_4) it follows that $K = 1$ in order to obtain agreement between theory and experiment. There are no obvious reasons for not setting the transmission coefficient equal to unity.

(22) H. A. Kramers, *Physica*, **7**, 284 (1940).

(23) B. J. Zwolinski and H. Eyring, *J. Am. Chem. Soc.*, **69**, 270 (1947).

V. Evaporation of Associated Liquids with Hindered Rotation

The preceding discussion has been restricted to spherically symmetric molecules because equation 9 does not hold for liquids with hindered rotation. In fact, as was emphasized by Kincaid and Eyring,[11] for liquids with hindered rotation, equation 9 should be replaced by the relation

$$\frac{1}{v_f\varphi} = \frac{p_s}{kT} \exp(\Delta H_V/RT) \qquad (25)$$

where φ represents the free-angle ratio, *i.e.*, the ratio of the rotational partition function in the liquid to the rotational partition function of the gas. Without introducing any additional assumptions, we may replace the complete internal partition function by the relation

$$Qi = \varphi Q_{rot^\circ} Q_{vibr.} Q_{el}$$

where Q_{rot° represents the rotational partition function of the gas, and $Q_{vibr.}$ and Q_{el} are the vibrational and electronic partition functions, respectively, of the liquid molecules. After division by e to correct for the lack of equilibrium between normal and activated molecules, equation 19 now becomes

$$j_e = K(kT/2\pi m)^{1/2}\,(v^{2/3}\varphi/v_f\varphi) \exp(-\Delta H_V/RT) \qquad (26)$$

After combining equations 25 and 26 and introducing the resulting expression into equation 2 it is found that

$$G = K\varphi p_s(m/2\pi kT)^{1/2} \qquad (27)$$

where K would again be expected to be close to unity. Thus a comparison of equations 8 and 27 leads to the conclusion that the evaporation coefficient for polar liquids should be equal to the free-angle ratio φ, a result which has been amply confirmed by data published by Wyllie.[1]

In order to emphasize the correlation between ϵ and φ we reproduce Wyllie's compilation in Table I. References to the original literature on the experimental determination of the evaporation coefficient may be found in Wyllie's paper.[1] The theoretical treatment of evaporation rates given by Wyllie does not permit a clear-cut derivation of equation 27 for the specific evaporation rate of polar liquids.

TABLE I

COMPARISON BETWEEN MEASURED EVAPORATION COEFFICIENTS ϵ AND FREE-ANGLE RATIOS φ, AFTER WYLLIE[11]

Liquid	T, °K.	ϵ	φ
CCl_4	273	1	1
C_6H_6	279	0.90	0.85
$CHCl_3$	275	.16	.54
C_2H_5OH	273	.020	.018
CH_3OH	273	.045	.048
H_2O	283 to 303	0.036 to 0.040	.04

THE BOUNDARY TENSION AT WATER–ORGANIC LIQUID INTERFACES

BY D. JOSEPH DONAHUE AND F. E. BARTELL

University of Michigan, Ann Arbor, Michigan

Received May 7, 1951

The reciprocal solubilities of the water–organic liquid systems selected for this study were determined. The aqueous phase was analyzed by means of an interferometer and the organic phase by means of the Karl Fischer reagent. The pendent drop method was used for the determination of the equilibrium values of the surface tensions of organic liquids and of the saturated aqueous phases as also of the interfacial tensions for these systems. The interfacial tensions at water–organic liquid interfaces were found to be a linear function of the log of the "degree of miscibility" of the water with the organic liquids. A close parallelism between the behavior of the interfacial tension in the vicinity of the critical solution temperature and the behavior of the surface tension in the vicinity of the critical temperature was noted. Organic liquids were arbitrarily divided into three groups based upon the lens forming tendency of the liquids. Group I: Organic liquids which form lenses and for which the surface tension of the organic liquid, S_2, plus the interfacial tension S_{23}, is greater than the surface tension of water, S_3. Group II: Organic liquids which initially spread forming a film over water after which, at equilibrium, a lens having contact angles of appreciable size (for example, angles greater than 10°) is formed. Group III: Organic liquids which form no lenses or at most lenses which have very low angles of contact on water. Antonoff's rule was shown to be valid only when applied to the liquids of Group III.

Introduction

When two partially miscible liquids are brought into contact the interface thus formed possesses free surface energy, which is numerically equal to the interfacial tension. The interfacial tension is dependent not only upon the cohesional forces which exist between the molecules of each liquid, but also upon the adhesional forces of the molecules of one liquid for those of the other. Because of the complexity of the interfacial forces, but few fundamental studies have been made of the factors which contribute to the interfacial tension. It has long been known that at least a qualitative relationship exists between solubility and interfacial tension. It also has been shown that in some cases the value of the interfacial tension is closely related to the surface tensions of the two saturated liquid phases. The purpose of the present investigation was to make a further study of the relationship between the interfacial tension and the mutual solubility of the liquids as well as the relationship between the interfacial tension and the surface tensions of the two saturated liquid phases.

Experimental

The Pendent Drop.—The pendent drop method was selected as the most suitable for the determination of surface and of interfacial tensions. With this method measurements can be made, extending over periods of time, of the tensions of the pendent drops.

The surface tensions of the organic liquids were determined from pendent drops formed within closed cells. Equilibrium conditions were maintained by having the bottom of the cell covered with some of the liquid.

Interfacial tension measurements were made on systems which had been saturated by intermittent shaking in a water-bath held at 25.0 ± 0.1° for a period of at least three days. Subsequently the aqueous phase was transferred into the cell and the organic phase into the syringe of the drop forming mechanism. The density of the organic phase determined whether a "pendent up" drop or a "pendent down" drop would be used. Interfacial tension measurements with drops of different ages as well as with solutions of different ages showed that the interfacial tension values did not alter with time.

The surface tensions of the aqueous phases were determined from pendent-down drops of the liquid or from pendent-up bubbles formed within the aqueous phase. Measurement of tensions of drops of various ages showed that approximately two minutes were required after the formation of the drops for equilibrium conditions to be attained. The data reported were obtained with drops which had been formed five to fifteen minutes prior to photographing.

Liquids.—The liquids used were best reagent grades and were further purified by fractional distillation, by treatment with silica gel, and by other appropriate treatments.

Solubility.—Samples of purified water together with each of the organic liquids were placed in glass stoppered flasks and were shaken intermittently for at least three days in a water-bath held at 25 ± 0.1°. The organic phases were analyzed for water content by the Karl Fischer method and the aqueous phases were analyzed interferometrically.

Results and Conclusions

Interfacial Tension *versus* Solubility.—Table I contains the data determined by us in the study of the relationship between interfacial tensions and solubilities of the different liquids chosen for this investigation. The literature reveals that solubility and interfacial tension determinations have been made for many different water–organic liquid systems but there are comparatively few such systems for which both the reciprocal solubilities and the interfacial tension values are reported. Table II contains such data as were readily available. The compilation of Seidell[1] was the main source of the solubility data; included also are the solubility data for water in hydrocarbons reported at a later date by Black, Joris and Taylor.[2] The interfacial tension data were obtained from the International Critical Tables and from earlier work in this laboratory.

An empirical relationship was developed for the solubilities of the mutually saturated organic liquid and water phases and the interfacial tension which exists when these phases are brought into contact. The mole fraction of the water in the organic liquid phase, represented by N_1, plus the mole fraction of the organic liquid in the aqueous phase, represented by N_2, gives a measure of what we shall refer to as the "degree of miscibility" of the liquids. When the liquids are completely immiscible the sum of $N_1 + N_2$ is zero. As the miscibility increases, however, the numerical value of the sum increases and when the liquids are soluble in all proportions, the sum is equal to unity. A plot (Fig. 1) was made of the log of the sum of the solubilities (*i.e.*, the "degree of miscibility") against the interfacial tensions. All of the points determined in the

(1) A. Seidell, "Solubilities of Organic Compounds," 3rd Ed., Van Nostrand Co., Inc., New York, N. Y., 1941.

(2) C. Black, G. G. Joris and H. S. Taylor, *J. Chem. Phys.*, **16**, 537 (1948).

TABLE I

INTERFACIAL TENSION AND SOLUBILITY DATA

	Liquid	Density organic phase, g./ml.	Density aqueous phase, g./ml.	Interfacial tension (S_{21}), dynes/cm.	Mole fraction water (N_1)	Mole fraction organic (N_2)
1	*n*-Butyl alcohol	0.8432	0.9860	1.8	0.500	0.0188[a,b]
2	Isobutyl alcohol	.8328	.9849	2.0	.449	.0195
3	*n*-Amyl alcohol	.8325	.9935	4.4	.357	.00459[a,b]
4	*n*-Hexyl alcohol	.8284	.9962	6.8	.288	.00110[a]
5	*n*-Heptyl alcohol	.8268	.9967	7.7	.267	.000280[a]
6	*n*-Butyl acetate	.8710	.9967	14.5	.0745	.000995
7	Isopropyl ether	.7226	.9956	17.9	.0333	.00187
8	Nitrobenzene	1.1975	.9974	25.2	.0175	.000295
9	Ethyl bromide	1.4501	1.0007	31.3	.0048	.0015
10	Benzene	0.8730	0.9970	34.1	.0031	.00042
11	Bromobenzene	1.4886	.9972	38.1	.0029	.000053
12	Carbon tetrachloride	1.5851	.9973	43.7	.00083	.000097

[a] From the data of J. A. V. Butler, D. W. Thomson and W. H. Maclennan, *J. Chem. Soc.*, 674 (1933). [b] These values have also been checked by R. S. Hansen, Ying Fu and F. E. Bartell, THIS JOURNAL, **53**, 769 (1949).

TABLE II

INTERFACIAL TENSION AND SOLUBILITY DATA

	Liquid	Interfacial tension (S_{21}), dynes/cm.	Mole fraction water (N_1)	Mole fraction organic (N_2)
13	Cyclohexanol	3.9	0.406	0.008
14	Isoamyl Alcohol	4.8	.326	.0055
15	Aniline	5.8	.216	.0070
16	Methyl *n*-propyl ketone	6.3	.152	.0132
17	Ethyl acetate	6.8	.139	.0163
18	Nitromethane	9.5	.082	.025
19	Methyl butyl ketone	9.6	.176	.0050
20	Methyl amyl ketone	12.4	.123	.0031
21	Methylene chloride	28.0	.0113	.0042
22	Chloroform	31.6	.0050	.0012
23	Toluene	36.1	.0025	.00010
24	Xylene	37.2	.0023	.000024
25	Ethylbenzene	38.4	.0023	.000025
26	Carbon disulfide	48.1	.00070	.00028
27	Pentane	49.0	.00048	.00015
28	Hexane	49.7	.00060	.000029
29	Cyclohexane	50.0	.00055	.000022
30	Heptane	50.2	.00084	.000009
31	Octane	50.2	.00090	.000003

present investigation fall approximately on a straight line and it happens that, for each of the few points that deviate excessively from the line, only one reported value of the solubility of the water in the organic phase was available. Thus from these data it appears that the interfacial tension which exists between aqueous and organic liquid phases may be quite reliably considered as a linear function of the log of the "degree of miscibility" of the liquids.[3]

The cohesional and adhesional forces of the molecules of a liquid–liquid system are the factors which determine the magnitude of the interfacial tension; also, it is these factors which determine the extent to which a given solute is soluble in a given solvent. It is apparent therefore that the relationship between the interfacial tension and the "degree of miscibility" which was found in this study should not be unexpected.

Since the interfacial tension and the "degree of miscibility" of a system are directly related, the sign and magnitude of the temperature coefficient of miscibility should determine the sign and magnitude of the temperature coefficient of the interfacial tension. The temperature coefficient of miscibility is positive for most systems and accordingly the interfacial tension is normally found to decrease with temperature. An example of the reverse situation was, however, reported by Ssementschnko and Davidoffskaja,[4] who found that the interfacial tension of the water–nicotine system increased with an increase in temperature

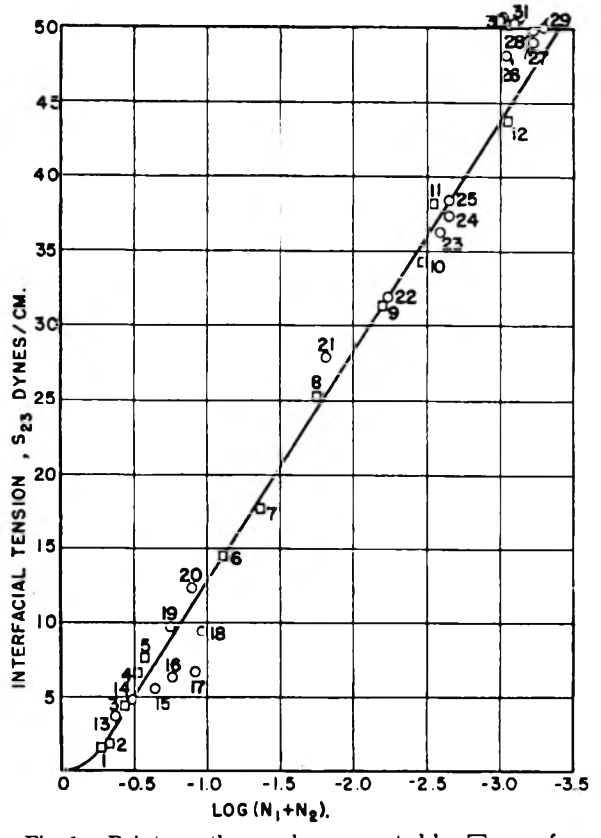

Fig. 1.—Points on the graph represented by □ were from data obtained in this investigation. Points represented by ○ were from data found in the literature.

(3) W. B. Hardy, *Proc. Roy. Soc.* (*London*), **88A**, 313 (1913).

(4) V. W. Ssementschenko and E. Davidoffskaja, *Kolloid. Z.*, **68**, 275 (1934).

in the region in which the temperature coefficient of miscibility is highly negative. As the temperature approaches the critical solution temperature, the interfacial tension decreases and of course becomes zero at the critical solution temperature. A similar phenomenon occurs at the boundary between a pure liquid and its vapor at the critical temperature.

The relationship between the interfacial tension and the log of the "degree of miscibility" deviates from linearity in the region of nearly complete miscibility. The line must curve as indicated in order that it may terminate at the point at which the components become completely miscible and the interfacial tension becomes zero. The tension at a liquid vapor boundary also becomes immeasurably small a few degrees below the critical temperature and the curvature of the line in Fig. 2 shows that the interfacial tension likewise becomes very small appreciably before the two phases become identical. Further evidence for the support of this conclusion was found by Silbereisen,[5] who reported that the interfacial tension between isobutyl alcohol and glycerol becomes very small 10° below the critical solution temperature. It has thus been shown that the behavior of the interfacial tension between two phases of partially miscible components closely parallels that of the surface tension at a liquid–vapor boundary.

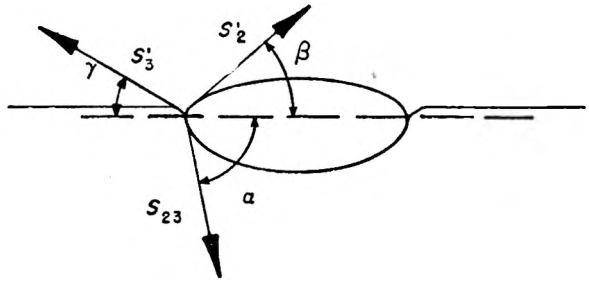

Fig. 2.

The data relating to the solubility of water in organic liquids are limited in amount; it follows then that a relationship which would permit the calculation of the approximate value of this quantity would be valuable. Since the solubility of water in organic liquids is usually 10 to 100 times as great as the reciprocal solubility of the organic liquid in water, the value for the solubility of the organic solute in water can be neglected, if it is not known, and an approximate value of the solubility of water in organic liquids can be obtained from interfacial tension values by using the relationship above presented.

Interfacial Tension *versus* Surface Tensions.—Relationships between the surface tension values of two saturated phases and the interfacial tension values of them can be studied by giving consideration to the forces which must act on a lens formed by one liquid upon the surface of the other liquid. In the case of an organic liquid lens on water, the force pulling the left edge of a lens in equilibrium to the left must be numerically equal to the force pulling it to the right (see Fig. 2). Such a balance of forces may be treated by the principles of Neuman's triangle and in the case in question may be expressed as

$$S_3' \cos \gamma = S_2' \cos \beta + S_{23} \cos \alpha \qquad (1)$$

where S_3' represents the surface tension of the water, saturated with organic liquid, phase; S_2' the surface tension of the organic liquid, saturated with water, phase; S_{23} the interfacial tension existing between the phases; and α, β, and γ the contact angles formed by the lens. Although the angles α, β and γ can be measured only with difficulty, this equation has been shown to be at least approximately valid by Coghill and Anderson[6] and by Miller.[7] The work of these investigators and that of Lyons[8] has shown that the angle γ is small for liquids having densities which do not differ excessively from that of water. Since the cosine of a small angle is approximately equal to one, equation (1) may be simplified when used for liquids of the type mentioned above, as

$$S_3' = S_2' \cos \beta + S_{23} \cos \alpha \qquad (2)$$

A further test of the validity of this simplified equation may be made by the use of the contact angle values of Fuchs[9] with the tension measurements made in this study. Table III contains the values for the three systems used in this investigation for which both α and β values are given by Fuchs. The agreement between the measured and the calculated values of the surface tensions of the water, saturated with organic liquid phases, S_3', further justifies the use of equation (2).

TABLE III

DATA FOR TEST OF NEUMAN'S TRIANGLE

Liquid	Measured S_2	Measured S_{23}	Measured α	Measured β	Measured S'	Calculated S_3'
	dynes/cm.		degrees		dynes/cm.	
Isobutyl alcohol	23.0	2.0	42.5	3.0	24.5	24.3
n-Butyl alcohol	24.2	1.8	65.9	3.4	24.9	25.3
n-Heptyl alcohol	26.8	7.7	66.9	16.0	28.8	28.4

This equation offers a fundamental basis for the study of an empirical rule stated in 1907 by Antonoff[10]: "the interfacial tension between two liquids, mutually saturated with each other, is equal or very approximately equal to the difference between the surface tension of the two phases." Expressed in equation form the rule is

$$S_3' - S_2' = S_{23}$$

although a large volume of literature concerning this rule has appeared, the validity or the extent of the validity of it is still a debatable issue. Much of the experimental data which have been used for testing this rule has been criticized by the author of the rule. He has expressed the belief that the data were not obtained with systems in true equilibrium. The surface and interfacial tension data obtained by us and presented in Table IV were obtained by means of the pendent drop method and with systems which had quite surely reached equi-

(5) K. Silbereisen, *Z. physik. Chem.*, **143A**, 157 (1929).

(6) W. H. Coghill and C. O. Anderson, U. S. Bur. Mines, Tech. Paper, 262 (1923).

(7) N. F. Miller, THIS JOURNAL, **45**, 1025 (1941).

(8) C. G. Lyons, *J. Chem. Soc.*, 623 (1930).

(9) V. N. Fuchs, *Kolloid Z.*, **52**, 262 (1930).

(10) G. N. Antonoff, *J. chim. phys.*, **5**, 372 (1907)

TABLE IV

DATA DETERMINED IN THIS INVESTIGATION: DENSITY, SURFACE TENSION, AND INTERFACIAL TENSION

Liquid	Density organic phase, g./ml.	Density aqueous phase, g./ml.	Measured S_3' dynes/cm.	Measured S_2 dynes/cm.	Measured S_{23} dynes/cm.	Calculated S_{23} dynes/cm.	Group
Bromobenzene	1.4886	0.9972	71.3	35.2	38.1	35.6	I[a]
Isobutyl alcohol	0.8328	.9848	24.3	23.0	2.0	1.3	II
n-Butyl alcohol	.8432	.9860	25.3	24.2	1.8	1.1	II
n-Amyl alcohol	.8325	.9935	26.7	25.0	4.4	1.7	II
n-Hexyl alcohol	.8284	.9962	28.4	25.8	6.8	2.6	II
n-Heptyl alcohol	.8268	.9967	28.9	26.8	7.7	2.1	II
Carbon tetrachloride	1.5850	.9974	69.4	26.1	43.7	43.3	III
Benzene	0.8730	.9970	62.3	28.2	34 1	34.1	III
Nitrobenzene	1.1975	.9974	67.8	43.0	25 2	24.8	III
Isopentane	0.6150	.9970	63.9	14.6	48.7	49.3	III
Ethyl *n*-butyrate	.8746	.9967	39.9	24.0	15.7	15.9	III
Ethyl ether	.7123	.9850	28.0	16.6	11.0	11.4	III
n-Butyl acetate	.8710	.9967	38.5	24.5	14.5	14.0	III
Isopropyl ether	.7226	.9956	35.3	17.1	17.9	18.2	III

[a] See also liquids in Table V, data for which were obtained from the literature.

librium conditions. Inasmuch as the surface tensions of dry organic liquids and of the same liquids saturated with water do not differ appreciably, the surface tensions of the dry organic liquids were measured and these data were used for the calculations.

An inspection of the data reveals that the rule is not of universal applicability as is claimed by its author but that some systems give values diverging greatly from the rule. According to equation (2) many deviations from the rule should be expected since many systems are known which form stable lenses with large angles and for such systems the rule could not apply.

Organic liquids for which data were available were arbitrarily divided into three groups based upon the lens-forming tendency of the liquids.

The liquids in the *first group* to be considered are insoluble oil-like compounds for which $S_3 < S_2 + S_{23}$. These liquids have long been known to form lenses upon the surface of water and from equation (2) one would predict non-conformity of these liquids to the rule. Table V contains a list of twenty such Group I compounds for which the surface tension and interfacial tension data are available in the literature. The numerical values of the surface tensions of organic liquids, S_2, and of interfacial tensions, S_{23}, are nearly unaffected by the process of saturation, while the surface tension of water, S_3, is lowered to an appreciable extent by most organic liquids during the saturation process. It is thus obvious that there is no conceivable means by which the tension of the aqueous phase, S_3', could ever become equal to the sum of the other two tensions, $S_2' + S_{23}$, for liquids of this type. This fact was first mentioned by Hardy[3,11] in 1912 and subsequently has been mentioned by nearly all other investigators who have had occasion to discuss the rule. Unfortunately, the author of the rule appears to have completely overlooked systems of this type both in his investigations and also in his discussions. A deviation of 2.5 dynes per centimeter was found for bromobenzene which was the only liquid of this group for which all tension values were actually determined in this investigation. Previous investigations by Harkins[12] and by Carter and Jones[13] have shown that carbon disulfide and methylene iodide deviate from the rule to a much greater extent than does bromobenzene. Reynolds[14] likewise found a large deviation for carbon disulfide but he attributed the deviation to chemical reaction of the components rather than to the limited validity of the rule.

TABLE V

LIQUIDS OF LOW SOLUBILITY IN WATER WHICH CANNOT CONFORM TO THE TENSION RULE[a]

(Group I Liquids)

Liquid	Temperature, °C.	S_2, dynes/cm.	S_{23}, dynes/cm.	$S_2 + S_{23}$, dynes/cm.
Decane	20	23.9	51.2	75.2
n-Tetradecane	25	25.6	52.2	77.8
Cyclohexane	25	23.8	50.2	74.0
Decalin	20	29.9	51.4	81.3
Ethylene tetrachloride	20	31.7	47.5	79.2
Carbon disulfide	20	31.4	48.4	79.8
Bromoform	20	41.5	40.9	82.3
Tetrabromoethane	20	49.7	38.8	88.5
Methylene iodide	20	50.8	48.5	99.3
Dibromoethane	20	38.7	36.5	75.2
Bromobenzene	25	35.2	38.1	73.3
Iodobenzene	20	39.7	41.8	81.5
Phenyl mustard oil	20	41.5	39.0	80.5
o-Bromotoluene	20	35.8	41.2	77.0
α-Bromonaphthalene	20	44.6	42.1	86.7
α-Chloronaphthalene	20	41.8	40.7	82.5
Tribromohydrin	25	44.8	38.0	82.8
Liquid petroleum	20	31.1	55.3	86.4
Stanolax	20	30.7	55.6	86.3
1,2,3-Tribromopropane	20	45.4	38.5	83.9

[a] Antonoff's rule is not applicable to these liquids.

The *second group* of liquids consists of compounds possessing polar groups, such as –OH and –COOH, which are capable of attaching themselves

(11) W. B. Hardy, *Proc. Roy. Soc.* (*London*), **86A**, 610 (1912).

(12) W. D. Harkins, Colloid Symposium Monograph VI, 17 (1928).

(13) E. G. Carter and D. C. Jones, *Trans. Faraday Soc.*, **30**, 1927 (1934).

(14) W. C. Reynolds, *J. Chem. Soc.*, **119**, 466 (1921).

to the surface of water and of forming an oriented monolayer over the water surface. Initially these liquids spread over a clean water surface but after saturation of the water phase and the formation of the monolayer upon the water surface the excess organic liquid forms a lens. The formation of a monolayer lowers the surface tension of the aqueous phase to a value which approaches that of the pure organic liquid. The low surface tension of the aqueous phase prevents the spreading of the excess organic liquid over the surface[7]. Contact angle measurement by Fuchs[9] and by others have shown that liquids of this type form lenses possessing angles of appreciable size. Thus the liquids of Group II should also be expected to deviate from the tension rule. Excessive deviations were found for all of the liquids of this type studied in the present investigation. Harkins[12] and Carter and Jones[13] have also reported large deviations for liquids of this type. Antonoff,[15] on the other hand, has investigated several such liquids but he apparently failed to find any deviations from this rule.

The third group of liquids consists of compounds which form no lenses or at most lenses which have very low angles of contact (approximately 10° or less) on water. Fuchs[9] and Fox[16] found the angles α and β to be very small or in some cases even zero for ethers, ketones, esters, chloroform, carbon tetrachloride, nitrobenzene, benzene and aliphatic hydrocarbons up to and including octane. Since the cosines of small angles are approximately unity, equation (2) indicates that for such liquids the tension rule should apply at least reasonably well. The tension data determined (Table IV) reveal that the liquids of this type, Group III, do conform closely to the rule. Similar agreement for liquids of this type has been found by Antonoff,[15] Reynolds,[14] Bartell, Case and Brown,[17] and Carter and Jones.[13] The only reported deviation in excess of about one dyne per centimeter for any of these liquids was found by Harkins[12] for benzene. It has since been shown, however, that the value used by him for the interfacial tension of benzene against water was approximately one dyne per centimeter too high. This error is sufficient to account for the apparent discrepancy.

The results of the present study indicate that as to lens forming tendencies all organic liquids can be classed into one of three groups. This study has shown further that Antonoff's rule is strictly valid only when applied to liquids in but one of the three groups mentioned. For this one group the rule should be valid and it can therefore be stated that the rule is of limited applicability.

(15) G. N. Antonoff, *Kolloid. Z.*, **59**, 7 (1932); M. Hecht and M. Chanin, THIS JOURNAL, **45**, 791 (1941); M. Chanin and M. Hecht, *ibid.*, **46**, 492 (1942); **46**, 497 (1942); **47**, 709 (1943).

(16) W. Fox, *J. Chem. Phys.*, **10**, 623 (1942)

(17) F. E. Bartell, L. O. Case and H. Brown, *J. Am. Chem. Soc.*, **55**, 2769 (1933).

ACTIVATED ALUMINA: HEAT OF WETTING BY WATER

BY VERNON M. STOWE

Aluminum Research Laboratories, East St. Louis, Illinois

Received May 7, 1951

A simple calorimeter was devised for measuring the heat of wetting, in which the quantity of heat evolved is measured by titration with cold liquid, such as ice-water. The integral heat of wetting of activated alumina by water is 18.0 cal. per gram of fresh adsorbent for Grade F-1, 24.4 cal. for Grade XH-51 and 14.1 cal. for Grade XF-21. The differential heat of wetting by water was determined by measuring the heat of wetting of the adsorbent which already contained various known quantities of uniformly adsorbed water. The heat of wetting by a monolayer of water derived from liquid water was calculated to be 170 ± 21 cal. per gram of water adsorbed for the forms of alumina so studied. Heat is evolved as adsorption proceeds into the multilayer region, probably until complete saturation is attained.

When a liquid is brought into contact with a solid, there is generally a thermal effect, known as the heat of wetting. If the solid is in a form which presents a large surface area, because of its extensive internal pore structure, as in commercial solid adsorbents, the thermal effect is readily perceptible. The heat of wetting has been discussed in some recent articles.[1-5] The purpose of the present paper is to report data which have been obtained for the heat of wetting of activated alumina by water.

Apparatus

For the work reported here a simple calorimeter of a new type was designed, consisting of a jacketed buret from which liquids at ice temperature, for example, can be measured into reactants in quantity just sufficient to offset the heat evolved in the reaction. When the calorimeter and the reactants are initially at room temperature the temperature can be returned promptly to the initial point as heat is evolved. The thermal leakage of the calorimeter is thus reduced without complication in the construction of the calorimeter, such as is encountered in most adiabatic calorimeters.

With this equipment it is unnecessary to provide any elaborate cover to retain heat, such as is described by White.[6] A simple barrier against evaporation is sufficient. A Beckmann thermometer may be used. It is unnecessary to know the heat capacity of the calorimeter, the thermometer system or even the reactants except for the liquid which is used to measure the heat. Stirring may be restricted enough to give negligible evolution of heat.

The design of the apparatus is given in Fig. 1. In this figure, C represents a wide-mouth dewar flask of 1-pint capacity which comprises the body of the calorimeter. This is covered with a piece of rubber dental dam, D, perforated to admit the Beckmann thermometer, T, and also

(1) R. A. Beebe and G. L. Kington, *J. Am. Chem. Soc.*, **72**, 40 (1950).

(2) D. T. Ewing and G. T. Bauer, *ibid.*, **59**, 1548 (1937).

(3) F. L. Howard and J. L. Culbertson, *ibid.*, **72**, 1185 (1950).

(4) J. C. Miller, H. Heinemann and W. S. McCarter, *Ind. Eng. Chem.*, **42**, 151 (1950)

(5) C. Pierce and R. N. Smith, THIS JOURNAL, **54**, 354 (1950); **54**, 795 (1950).

(6) W. P. White, "The Modern Calorimeter," Reinhold Publishing Corp., New York, N. Y., 1928.

the tip of the buret, F. The buret is of 50-ml. delivery capacity, and is offset so that the graduations lie near the side of the jacket, allowing easy reading, although the stopcock and tip are placed in the center of the boot. The stopcock is lubricated with silicone stopcock grease which functions well at ice temperature. The buret is surrounded by an evacuated, unsilvered glass jacket, J. This is closed at the bottom by a specially fabricated soft rubber boot, B, equipped with a drain tube, E. The soft rubber boot permits free manual control of the stopcock of the buret, and also allows the ice-water-bath to be stirred to prevent accumulation of water of increased density (around +4°) in the region marked "A" in the figure. Care is taken that the water level in the jacket, and the amount of crushed ice supplied to the jacket be adjusted so that some ice is present in the region marked "A" to ensure that all of the water in the buret will be at zero. The thermometer employed in the thermal measurements gave a reading of zero when ice was present in the liquid phase.

The method of operation may be illustrated as follows: The calorimeter, a stoppered bottle of the adsorbent and a stoppered flask of distilled water, as well as the miscellaneous equipment such as pipets, thermometers, iodine flasks and beakers are allowed to stand near each other overnight so that they will all be at room temperature.

The ice jacket is filled with water and ice, and the buret is filled with distilled water. It is convenient to have a supply of water prechilled so that it will reach the ice point rapidly. A suitable amount of the adsorbent is transferred from the storage bottle to an iodine flask and weighed. It is then poured into the dewar flask and the rubber dam with the Beckmann thermometer in place is inserted. The temperature of the adsorbent is determined on the Beckmann thermometer, from time to time until the reading is constant. During this time the adsorbent is stirred after each reading. The temperature of the water held in the stoppered storage flask is read on the Beckmann before each run. As a result of evaporation, it may show a tendency to cool below the ambient. This is taken into account in the calculation of the amount of heat absorbed. Fifty ml. of water from the stoppered storage flask is pipetted into the dewar flask. About 10 ml. of water is removed from the buret and discarded. The object of this is to remove any water of increased density, and hence at a temperature of about 4°, from the buret. Ice-water is then introduced into the dewar flask with the entire assembly placed as indicated in Fig. 1. The contents are stirred briefly after each addition of water. As the temperature returns to the vicinity of the initial point, sufficient time is allowed between each addition to reach a steady state. The temperature of the final mixture in the dewar flask is also determined with a laboratory thermometer graduated in degrees.

The heat evolved is the product of the number of milliliters of ice-water by the difference in temperature between the final temperature and the ice point, multiplied in turn by the heat capacity of the water over this range. To this is added a smaller amount of heat calculated as the difference between the final temperature and that of the stored water multiplied by 50 (the volume of stored water used, in ml.), multiplied by the heat capacity of water. (The final temperature was generally brought within ±0.05° of the temperature of the adsorbent at the start.)

Adsorbents Used and Methods of Preparation

Several commercial forms of activated alumina produced by the Aluminum Company of America were investigated. Data on the composition and some of the properties of these sorbents are presented in Table I.

The Grade F-1 mentioned in the table is made from alumina hydrate by processes which render it highly porous and adsorptive. The Grade XH-51 material is of the gel, or vitreous type, and has higher adsorptive capacity than the Grade F-1. The Grade XF-21 material is used as a fluid catalyst. It is similar to Grade F-1 in structure, but is produced in a particle size distribution such that it fluidizes effectively. The foregoing is a general description of the adsorbents used for determining the integral heat of wetting.

For study of the differential heat of wetting the sorbent was prepared along the following lines: Weighed portions of Grade F-1 and of Grade XH-51, 2 or 3 kilos each, were placed in 8-inch desiccators from which the trays had been removed. A dish containing the calculated weight of water was placed in each desiccator, resting on the bed of adsorbent. The cover was applied and the desiccator was evacuated until the water "flashed." The quantities of adsorbent and water were chosen to yield 5, 10, 15 and 20 parts water per hundred of Grade F-1, and 5, 10, 20 and 40 parts of water per hundred parts of Grade XH-51 (weight basis). The desiccators were allowed to stand until the water had been adsorbed, which took several months in some cases. The adsorbent was then removed to a closely stoppered bottle and mixed by turning the bottle over and over. The

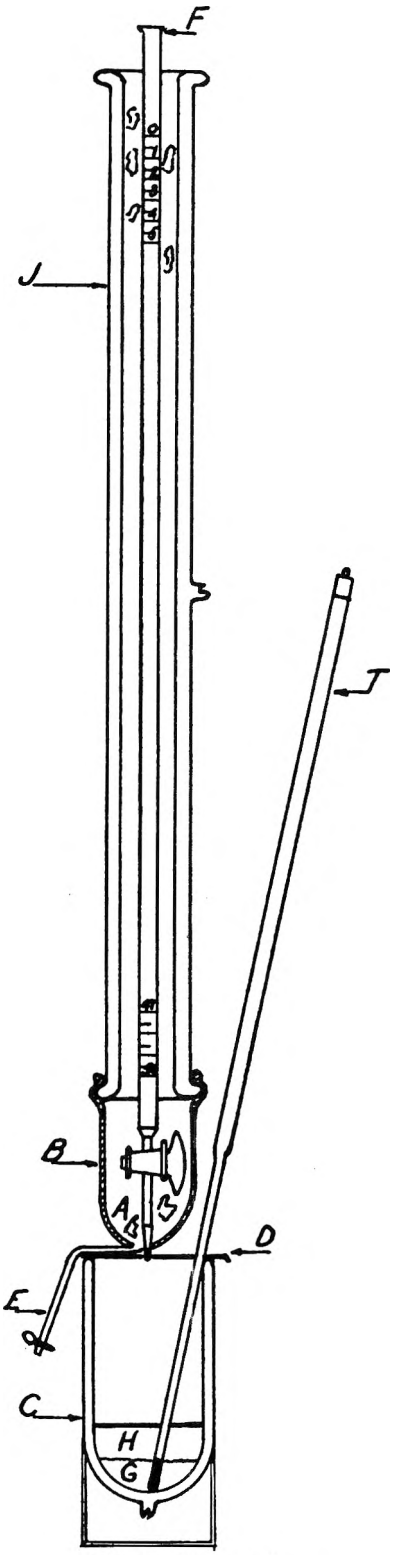

Fig. 1.—Calorimeter.

TABLE I

PROPERTIES OF THE ACTIVATED ALUMINAS

Grade	F-1	XH-51	XF-21
Mesh size (Tyler)	1/4 inch to 8 mesh	8-14 mesh	100-325 mesh
Chemical analysis:			
Loss at 1100°, %	9.20	5.20	8.70
SiO_2, %	0.09	6.18	0.02
Fe_2O_3, %	.13	0.09	.02
Na_2O, %	.50	1.36	.52
Surface area by N_2, sq. meters per gram by Brunauer, Emmett, Teller method	244	340	155
Adsorbed water required for a monolayer, g. per 100 g. adsorbent	7.30	10.20	4.65

bottles were allowed to stand for at least one month in order to allow the water to become evenly distributed, with further stirring in the bottle at frequent intervals. The products were analyzed for loss at 1100° and the actual weight of water per unit weight of activated alumina was calculated.

Experimental Results and Discussion

The differential heat of wetting can be determined as the difference between the heat of wetting of fresh adsorbent and that of adsorbent containing a given amount of previously adsorbed and uniformly distributed material.[7] Data for water, derived in this manner, are presented in Fig. 2.

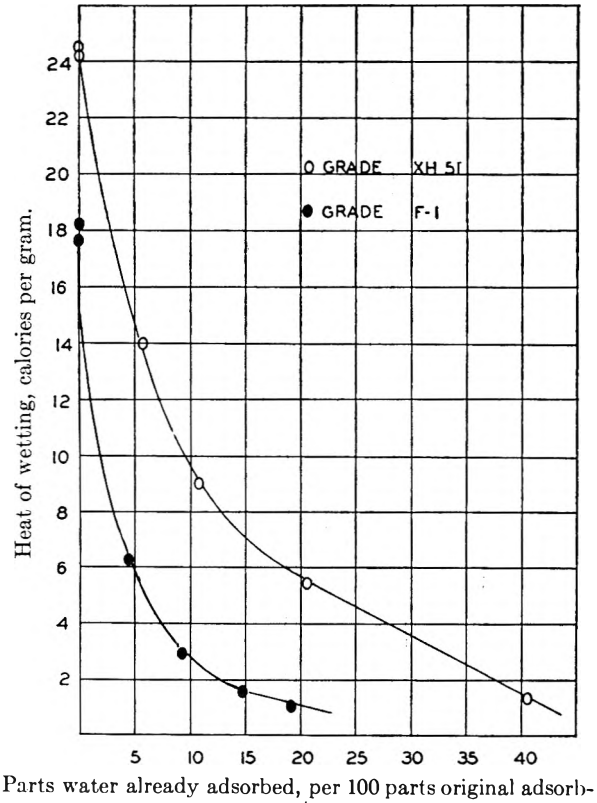

Fig. 2.—Heat of wetting activated alumina grades XH-51 and F-1 by water.

It may be noted for example that Grade F-1, in a freshly reactivated condition, showed an average heat of wetting by water of 18.05 cal. per gram of fresh adsorbent. When, however, 4.73 g. of water per 100 g. adsorbent had been previously adsorbed uniformly on the activated alumina the heat of wetting of this product with water amounted to only 6.3 cal. per gram of original adsorbent. The heat which had been given off when the 4.73 g. of water was uniformly adsorbed in the first place was therefore equal to 18.05 minus 6.3 or 11.75 cal. per gram of original adsorbent. This amounts then to about 250 cal. per gram of water adsorbed or about 4500 cal. per mole of water.

On the assumption that 1 g. of water adsorbed on 100 g. of activated alumina is capable of covering 33.4 square meters of surface in the monolayer, (*i.e.*, assuming that a molecule of water covers 10 Å.^{2}) the amount to be adsorbed to form a complete monolayer can be calculated, since the surface areas are known (Table I). These calculated figures are shown in Table I. The heat of wetting of activated alumina which already contained enough water to constitute a monolayer was read from the curves of Fig. 2, and the heat of adsorption of a monolayer of water from liquid water was calculated as shown in Table II.

TABLE II

HEAT OF WETTING BY WATER EQUIVALENT TO A MONOLAYER

Adsorbent	Grade F-1	Grade XH-51
Surface area, sq. m./g.	244	340
Water to cover surface area, g./100 g. adsorbent	7.30	10.20
Heat of wetting fresh adsorbent, cal./g.	18.05	24.45
Heat of wetting adsorbent to which has been added water equivalent to a monolayer, cal./g.	4.10	9.30
Difference, heat of wetting by adding a monolayer of water, cal./g.	13.95	15.15
Calories per gram of water in the monolayer	191	149
Calories per square meter of surface area	0.0572	0.0446

These data indicate that when a monolayer of water is added (starting with liquid water) the heat evolved is about twice the heat of fusion of ice, and does not vary greatly for the samples of alumina studied.

Figure 2 also shows that heat continues to be evolved, as water above that required for a monolayer is added. This agrees with the findings of Harkins and Jura[8] in their study of anatase.

Acknowledgment.—Thanks are expressed to Mr. C. Norman Cochran for the data relating to surface areas by nitrogen adsorption and to Dr. E. E. Marshall for the preparation of aluminas with varied amounts of adsorbed water by the desiccator method.

(7) A. N. Puri, "Soils: Their Physics and Chemistry," Reinhold Publishing Corp., New York, N. Y., 1949, p. 455.

(8) W. D. Harkins and G. Jura, *J. Am. Chem. Soc.*, **66**, 919 (1944).

ACTIVATED ALUMINA: HEAT OF WETTING BY HYDROCARBONS

BY VERNON M. STOWE

Aluminum Research Laboratories, East St. Louis, Illinois

Received May 7, 1951

The heat of wetting of activated alumina Grade XF-21 by four hydrocarbons containing 7 carbon atoms was investigated. The heat of wetting by *n*-heptane and triptane was about 2.7 cal. and by methylcyclohexane and toluene was 4.1 to 4.7 cal. per gram of alumina. When water in excess was added to alumina containing adsorbed aliphatic and cyclic hydrocarbons the heat relations indicated relatively complete displacement. However, when a cyclic hydrocarbon was added in excess to alumina containing an adsorbed aliphatic, there was no thermal evidence of a displacement. The data explain the performance of activated alumina in drying natural gas containing heavier hydrocarbons. The method offers a good approach to other problems of preferential adsorption.

Preferential adsorption is a fascinating field with many important commercial applications, including the drying of natural gas, drying of liquid hydrocarbons and refrigerants, chromatographic analysis, displacement of petroleum from oil-bearing sands by injection of water, and many others. In the work reported here, the heat of wetting of activated alumna by some hydrocarbons as well as by water was measured, to determine to what extent such data might form a basis for correlating the behavior of adsorbents in preferential adsorption.

Materials and Procedure

The apparatus and the adsorbent employed (activated alumina Grade XF-21 produced by the Aluminum Company of America) are described in another paper.[1] In the freshly reactivated form it contained 8.7% water of which most is combined water.

n-Heptane from Westvaco Chlorine Products Company was used. This was stated to have a boiling point of 98.44°, melting point minus 90.66°, density at 20° of 0.68382 g. per ml., and a refractive index of 1.38779. The triptane (trimethylbutane) was 99+% material donated by the Redford Laboratory of the General Motors Corp. The methylcyclohexane was obtained from Eastman Kodak Co., and was "practical grade." The toluene was obtained from Fisher Scientific Co., C.P. grade.

Heat capacities per milliliter were calculated from the data of M. P. Doss.[2]

TABLE I

VOLUMETRIC HEAT CAPACITY OF THE HYDROCARBONS

Hydrocarbon	Specific heat, cal./°C./g.	Specific gravity, g./ml.	Volumetric heat capacity, cal./°C./ml.
n-Heptane	0.525	0.684	0.359
Triptane	.497	.690	.343
Methylcyclohexane	.443	.769	.341
Toluene	.404	.867	.350

To prepare samples for study of the heat of wetting, 25 × 200-mm. test-tubes of Pyrex glass were constricted near the mouth, and weighed portions of adsorbent were introduced. The desired amount of adsorbate was introduced by means of a pipet. After withdrawing the pipet, the tube was turned so as to cover the wetted surface with fresh dry adsorbent, restricting losses by evaporation. The weight of adsorbate added was determined and the tube was sealed at the point of constriction. After cooling, the tube was turned about to ensure uniform mixture. In no case was enough liquid used to cause the particles to cling together after initial mixing had been effected. The contents of the tubes were stirred by turning about from time to time. At least one week was allowed for the material to come to a uniform adsorption throughout the tube. To make a determination, the contents of a tube were transferred to the dewar flask and an excess of the given hydrocarbon was added. The temperature was then reduced to the starting temperature by introducing more of the given hydrocarbon, precooled to 0° in the ice-jacketed buret.

Experimental Results and Discussion

The differential heat of wetting of activated alumina Grade XF-21 by the hydrocarbons studied, each containing 7 carbon atoms, is shown in Fig. 1. The data of Fig. 1 are represented by three smoothed curves. A point of inflection may exist between 2 and 4 g. of hydrocarbon per 100 g., of adsorbent, however.

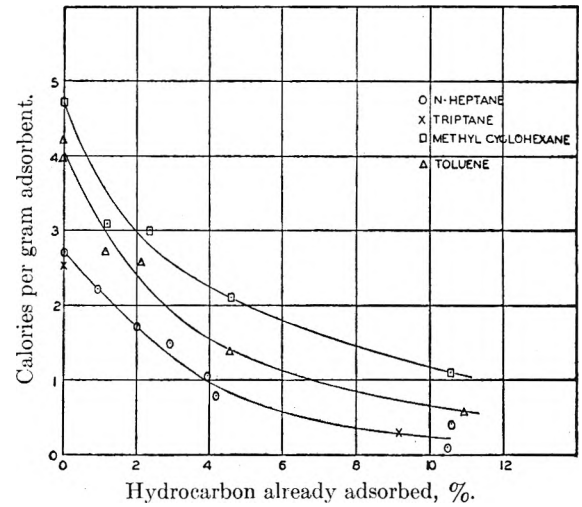

Fig. 1.—Heat of wetting activated alumina grade XF-21 by various hydrocarbons.

Wetting by the hydrocarbons investigated generates much less heat on activated alumina than does wetting by water. The maximum heat evolved with normal heptane was only 2.7 cal. per gram of freshly reactivated adsorbent. Triptane caused the evolution of 2.6 cal. per gram. Data for these compounds are represented by a single line in Fig. 1.

The ring compounds evolve nearly twice as much heat of wetting as do the aliphatic hydrocarbons tested, namely, 4.7 cal. per gram of adsorbent for methylcyclohexane and 4.1 cal. per gram of adsorbent for toluene.

Figure 1 shows that heat is being evolved even when 10 g. of the given hydrocarbon per 100 g. of adsorbent had already been adsorbed.

For a calculation of the heat of wetting by a monolayer of heptane derived from liquid heptane, the datum of Loeser and Harkins[3] for the cross sec-

(1) V. M. Stowe, THIS JOURNAL, **56**, 484 (1952).

(2) M. P. Doss, "Physical Constants of the Principal Hydrocarbons," The Texas Company, New York, N. Y., 1943.

(3) E. H. Loeser and Harkins, *J. Am. Chem. Soc.*, **72**, 3427 (1950).

tional area of the adsorbed heptane molecule was used, *i.e.*, 64 Å.[2] From this, the factor for conversion of weight of heptane, g. per 100 g. of adsorbent, to surface area, square meters per gram, is taken to be 38.5. Since the surface area of XF-21 is 155 sq. meters per gram, the weight of heptane required for a monolayer is 4.03 g. per 100 g. of the alumina. Bare alumina evolves 2.7 cal. per gram of adsorbent when wet by normal heptane, and from the curve of Fig. 1 it is estimated that 100 g. of alumina, on which 4.03 g. of heptane is already adsorbed, would evolve 1.0 cal. per g. on wetting with heptane. Hence, to cause a monolayer of heptane to be adsorbed on the activated alumina from liquid phase would result in the evolution of only 1.7 cal. per gram of adsorbent, or 42 cal. per gram of heptane. It is interesting to note that this quantity of heat exceeds the heat of fusion of heptane, *i.e.*, 33 cal. per g.[4] Cross sectional data were not at hand for similar calculations on triptane, methylcyclohexane and toluene.

A study was made of the behavior of aluminas thoroughly wet with heptane when water was stirred in with the mixture. The heavier water soon replaced the excess heptane which rose to the surface. The thermal effects shown in Table II also indicate that it displaced the adsorbed heptane.

TABLE II

HEAT EVOLVED WHEN ACTIVATED ALUMINA GRADE XF-21 ALREADY WET WITH *n*-HEPTANE IN EXCESS WAS TREATED WITH WATER IN EXCESS

Wt. of adsorbent (fresh), g.	34.7	29.9	32.3	32.2
Heat evolved, cal.	413	329	381	354
Cal. per gram adsorbent	11.9	11.3	11.8	11.0

From Table II, it appears that this operation released on the average 11.5 cal. of heat per gram of original sorbent. As reported in the previous paper, the heat evolved when fresh activated alumina is wet with water is 14.1 cal. per gram. The heat resulting from the prior wetting by heptane may be taken as the difference, 14.1 minus 11.5 or 2.6 cal.

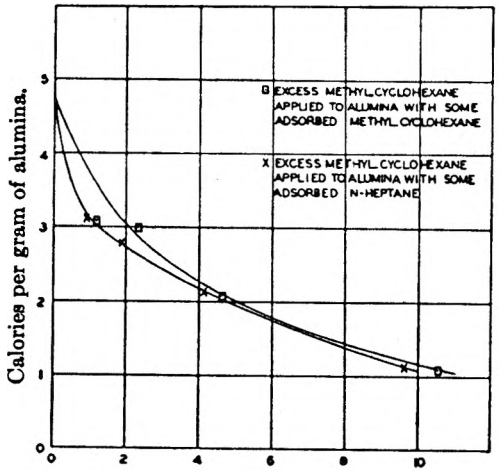

Parts of *n*-heptane or methylcyclohexane per 100 parts of alumina.

Fig. 2.—Heat of wetting activated alumina grade XF-21 by methylcyclohexane.

(4) K. S. Pitzer, *J. Am. Chem. Soc.*, **62**, 1224 (1940).

per gram of adsorbent. This is in good agreement with the measured heat of wetting by heptane, *i.e.*, 2.7 cal. per gram, and indicates that the water replaced essentially all of the adsorbed heptane. This behavior is in harmony with the performance shown by Ku, *et al.*,[5] who found that when natural gas containing water and also hexane, heptane or even butane was passed over activated alumina, substantially all the hydrocarbon and the water was adsorbed until about 12% of the combined materials had been taken up. Thereafter, for a time, substantially all the water continued to be adsorbed but no more hydrocarbon was adsorbed. Finally, as more water was taken up, the hydrocarbon content decreased until, when the alumina became saturated with water, practically no hydrocarbon remained on the alumina.

Another type of experiment was undertaken in which water was added in excess to alumina already containing various limited amounts of adsorbed hydrocarbon, *i.e.*, up to about 5% of methylcyclohexane. The data are shown in Table III.

TABLE III

HEAT OF WETTING BY WATER OF GRADE XF-21 CONTAINING ADSORBED METHYLCYCLOHEXANE

Parts adsorbed per 100 parts original adsorbent	0	1.62	2.29	4.67
Heat evolved, cal.	1345	466	436	393
Wt. of adsorbent used, g.	92.2	34.0	32.8	32.7
Cal. per g. adsorbent	14.1	13.7	13.3	12.0
Heat evolved by prior adsorption of methylcyclohexane, cal. per g. adsorbent (from Fig. 1)	..	1.5	1.9	2.6
Calculated heat of wetting by water, cal. per g. adsorbent	14.1	15.2	15.2	14.6

The calculations involved in Table III will be illustrated using the second column of data. The heat of wetting of bare alumina by methylcyclohexane is 4.7 cal. per gram of adsorbent (Fig. 1). From the curve plotted in Fig. 1 the heat of wetting by methylcyclohexane of alumina already containing 1.62 parts of adsorbed methylcyclohexane per hundred parts alumina is 3.2 cal. per gram. Hence the adsorption of 1.62 parts of methylcyclohexane from liquid phase caused the evolution of 4.7 minus 3.2 or 1.5 cal. per gram of alumina. The 1.5 cal. supplied for the desorption of the hydrocarbon is added to the observed value 13.7 giving 15.2 cal. per gram, the calculated heat of wetting of bare alumina by water. That the calculated heat of wetting lies somewhat above the actual measured heat of wetting by water (14.1 cal. per gram) may be due to experimental error. At any rate, complete replacement of the previously adsorbed methylcyclohexane is indicated.

In one other type of experiment, the heat of wetting by excess methylcyclohexane of alumina already containing various limited amounts of adsorbed heptane was tested. The results are shown in Table IV and in Fig. 2.

Since the heat of wetting of alumina by methylcyclohexane is about twice as great as by *n*-heptane,

(5) C. P. Ku, R. L. Huntington and L. S. Reid, *Am. Inst. Mining Met. Engrs.*, Tech. Publ. No. 1628 (1943).

TABLE IV

DIFFERENTIAL HEAT OF WETTING BY METHYLCYCLOHEXANE OF ACTIVATED ALUMINA GRADE XF-21 CONTAINING (ZERO TO ABOUT 10 G.) ADSORBED *n*-HEPTANE (PER 100 G. ADSORBENT)

Parts heptane adsorbed per 100 parts adsorbent	0	0.95	1.92	4.16	9.65
Heat evolved on adding methylcyclohexane, cal.	99	115	95	74	45
Wt. of adsorbent, g.	21.0	36.0	33.8	32.7	35.4
Cal. per g. adsorbent	4.7	3.2	2.8	2.3	1.3

treating these samples with methylcyclohexane should result in somewhat greater heat of wetting than for samples containing equal weights of methylcyclohexane, provided the excess methylcyclohexane is able to displace adsorbed *n*-heptane. However, it can be seen in Fig. 2 that the heat of wetting of activated alumina Grade XF-21, containing adsorbed *n*-heptane is about equal to that of alumina containing an equal weight of adsorbed methylcyclohexane (for which hydrocarbon the data are reproduced in Fig. 2 for convenient comparison). It is concluded that methylcyclohexane will not replace normal heptane from adsorption under these conditions. Probably more "drive" than 2 cal. per gram of adsorbent is required to effect displacement within the time involved in this type of experiment.

ON THE DEPENDENCE OF THE AVERAGE POLYMER MOLECULAR WEIGHT ON THE CHANGE IN THE PARTICLE DIAMETER OF A HOMOGENEOUS MONOMER EMULSION

BY G. NARSIMHAN

Department of Chemical Engineering, Laxminarayan Institute of Technology, Nagpur University, Nagpur, India

Received May 17, 1951

Two new equations are proposed for the determination of the average polymer molecular weight during the polymerization of a soap stabilized monomer emulsion. The derivation is based on the assumptions that the polymerization proceeds at the interface according to the limiting value of the Boltzmann distribution function and that the emulsion possesses a homogeneous radius distribution. The initiation and growth of the chain at the active centers is also assumed.

Emulsion polymerization has been assumed to proceed at the monomer interface by few workers. Even in the absence of micellar soap and catalyst, polymerization has been found to take place but slowly at the aqueous phase.[1] The initiation and progress of such a reaction is attributed to the diffusion of monomer molecules through the interfacial layer of soap into a few activated molecules present in the aqueous phase and the gradual growing of this complex as more molecules diffuse. On the other hand, Montroll[2] assumes polymerization to initiate and terminate at the emulsion interface for non-micellar soap and a water-soluble catalyst. The polymerization starts according to him, after the natural inhibitor concentration falls to an optimum value at the interface by the diffusion of the inhibitor molecules through the interface into the aqueous phase consequent on the disturbed equilibrium arising out of the reaction of the catalyst with the inhibitor present in the aqueous phase. For a homogeneous radius distribution, the reaction starts suddenly at the end of an initiation period and the extent of the reaction has been found to be a parabolic function of the polymerization time.

First Order Reaction.—Norrish[3] investigated the catalyzed polymerization of styrene and methacrylate and it was found that the active centers grow into long chains according to a zero order reaction and that the molecular weight of the polymer obtained was found to be proportional to the time of reaction and inversely so to the catalyst concentration. No general correlation has, till now, been possible between the average polymer molecular weight and the varying diameter for a given system and polymerization time, for interfacial polymerization. In the absence of any thermodynamic relation specifying the extent of reaction among the interfacial molecules in terms of physico-chemical constants, a general and rough relation has been derived for the dependence of the average polymer molecular weight on the change in the particle diameter of a soap stabilized monomer emulsion based on the following assumptions: (1) The reaction takes place at the boundary of the suspended spheres. (2) The reaction starts after the inhibitor concentration has fallen to an optimum value. (3) The interfacial molecules possess a few active centers (constant and proportional to catalyst concentration). (4) The reaction is initiated at these active centers and progresses according to Boltzmann's distribution law, the most frequent degree of polymerization being obtained based on the limiting value of the distribution function. (5) The interfacial polymerization stops after the reaction has progressed according to assumption 4. The reaction is again initiated only after the ejection of the polymer particle into the aqueous phase and the subsequent interfacial adsorption of non-micellar soap from the aqueous phase. This assumption is in agreement with the observed experimental fact that as polymerization proceeds, soap disappears from solution.[1]

Derivation

This is based on the assumption that interfacial polymerization is governed by the Boltzmann dis-

(1) W. D. Harkins, *J. Polymer Sci.*, **5**, 233 (1950).
(2) E. W. Montroll, *J. Chem. Phys.*, **13**, 337 (1945).
(3) R. G. W. Norrish and E. F. Brockman, *Proc. Roy. Soc.* (*London*), **A171**, 147 (1939).

tribution law. If r represents the length of the polymer chain obtained as a result of interfacial polymerization, to calculate the complexion as a function of r certain assumptions are essential regarding the chain and its mobility. If λ represents the chain length, n_0 the number of molecules present, θ the angle between two successive links and complete free rotation is assumed, then the probability that the ends of such a chain will be separated by the distance r, is given by

$$W(\eta_0,\lambda\theta,r)r^2\,dr\,3\left(\frac{6}{\pi n_0^{3/2}\lambda_\theta^2}\right)\exp\frac{-3r^2}{2\eta_0\lambda_\theta^2}r^2\,dr \quad (1)$$

where $\lambda_\theta^2 = \lambda^2((1+\cos\theta)/(1-\cos\theta))$; and r must naturally be less than r_{max}. It is evident from above that there is a most probable distance ϵ between the chain ends, *viz.*, that value of r at which the function given by eq. (1) has its maximum. This value as an easy calculation shows is

$$\epsilon = \lambda\left(\frac{2}{3}n_0\right)^{1/2} \quad (2)$$

If one gram of the monomer is dispersed as an emulsion with an initial particle diameter D the total number of reacting molecules are distributed in these particles. If interfacial polymerization is assumed according to the distribution function, then the relation $\epsilon = \lambda\left(\frac{2}{3}n_0\right)^{1/2}$ not only holds good for the entire number of molecules present in one gram of the monomer, giving the fraction polymerizing, but also holds for successive interfacial polymerization. This leads to the propagation of a finite number of polymer species as the diameter decreases, dependent upon the number of active centers present.

Consider one gram of the monomer, molecular wt. M_0, chain length λ cm., cross sectional area α sq. cm., density ρ g./ml., dispersed in a dilute soap solution, with a homogeneous radius distribution.

Let the diameter of the emulsion particle be D_1 initially and after a time lapse of t minutes, D_2 cm. The number of particles of diameter D will be $6/\pi D_1^3\rho$. The number of monomer molecules oriented at the interface of a single particle initially $= \pi D_1^2/\alpha$ and after the time of t minutes $\pi D_2^2/\alpha$. The amount of monomer left unreacted is $\frac{6}{\pi D_1^3\rho}\times\frac{\pi D_2^3\rho}{6} = \left(\frac{D_2^3}{D_1^3}\right)$ gram; the theoretical weight reacted $(1-(D_2^3/D_1^3)_{23}$ gram. Assuming Avogadro's number as $6.062\times10^{23} = N$, the number of monomer particles that have reacted theoretically $= N(D_1^3 - D_2^3)/M_0D_1^3 = S$. Since only a fraction of the total number undergo polymerization at the interface, the probable number reacting, according to eq. (2) in the time interval t minutes, giving rise to a cumulative molecular weight M_c

$$M_c = 3\left(\frac{6}{\pi S^{3/2}M_0^2}\right)^{1/2}\exp\frac{-3M_c^2}{2S\cdot M_0^2}$$

giving the limiting value to the expression when $M_c = M_0(2S/3)^{1/2}$. Hence the cumulative molecular weight of all the polymer molecules coming out of the monomer emulsion in the time interval t minutes is

$$M_c = [2N(D_1^3 - D_2^3)M_0/3D_1^3]^{1/2} \quad (3)$$

The probable number of interfacial molecules polymerizing in the beginning $(2\pi D_1^2/3\alpha)^{1/2}$ and after t minutes $(2\pi D_2^2/3\alpha)^{1/2}$ distributed amongst the active centers. Since the number of particles undergoing reduction in diameter during polymerization is $6/\pi D_1^3\rho$ (constant), the cumulative molecular weight of all the polymer particles of different molecular species coming out in the time interval is

$$\frac{6}{\pi D_1^3\rho}\sum_{D=D_1}^{D=D_2}M_0\left(\frac{2}{3}\frac{\pi D^2}{\alpha}\right)^{1/2}$$

Evaluation of

$$\sum_{D=D_1}^{D=D_2}M_0\left(\frac{2}{3}\frac{\pi D^2}{\alpha}\right)^{1/2} = M_0\times\left(\frac{2\pi}{3\alpha}\right)^{1/2}(D_1 + D' + D'' + \cdots + D_2) \quad (4)$$

Considering an initial particle of diameter D_1 cm., if the chain length of the molecules is λ cm., when all the interfacial molecules are removed the particle diameter will fall by 2λ cm. But since only a fraction of them react, the extent of reduction in the diameter is

$$\frac{2\lambda\left(\frac{2}{3}\frac{\pi D_1^2}{\alpha}\right)^{1/2}}{\pi D_1^2/\alpha} = \left(\frac{8\alpha\lambda^2}{3\pi}\right)^{1/2}/D_1 = c/D_1 \quad (5)$$

The second species will be initiated when the diameter is $D_1 - (C/D_1)$ cm. Hence the value of the term in brackets in Eq. (4) is

$$D_1 + \left(D_1 - \frac{C}{D_1}\right) + \left[\left(D_1 - \frac{c}{D_1}\right) - \frac{c}{\left(D_1 - \frac{c}{D_1}\right)}\right] + \left\{\left[\left(D_1 - \frac{c}{D_1}\right) - \frac{c}{\left(D_1 - \frac{c}{D_1}\right)}\right] - \frac{c}{\left[\left(D_1 - \frac{c}{D_1}\right) - \frac{c}{\left(D_1 - \frac{c}{D_1}\right)}\right]}\right\} + \cdots D_2 = \Sigma D \quad (6)$$

If the number of active centers present is n (constant) the probable number of molecular species that will be obtained during the polymerization time of t minutes $= n(D_1 - D_2)/(c/D_1) = nD_1\cdot(D_1 - D_2)/c$ (approximate value). The cumulative molecular weight of all the polymer particles numbering $6/\pi D_1^3\rho$ (constant) and of all the molecular species numbering $nD_1(D_1 - D_2)/c$ is

$$M_c = \frac{6}{\pi D_1^3\rho}\left[M_0\Sigma D\left(\frac{2\pi}{3\alpha}\right)^{1/2}\right]$$

The average molecular weight is the ratio of the cumulative molecular weight to the product of the number of polymer particles and the molecular species

$$M_{av} = \frac{M_0\Sigma D\left(\frac{2\pi}{3\alpha}\right)^{1/2}\times\left(\frac{8\alpha\lambda^2}{3\pi}\right)^{1/2}}{nD_1(D_1 - D_2)} = \frac{4\lambda M_0\Sigma D}{3nD_1(D_1 - D_2)} \quad (7)$$

Alternately

$M_{av} = M_c$ (eq. (3))/number $\times$ molecular species.

$$= \frac{M_c\pi D_1^3\rho}{6}\cdot\frac{c}{nD_1(D_1 - D_2)}$$

Substituting the values for M_c and c and simplifying

$$M_{av} = \frac{2\rho\lambda}{9n(D_1 - D_2)}[\alpha NM_0\pi D_1(D_1^3 - D_2^3)]^{1/2} \quad (8)$$

Conclusion

It is obvious from the above that eq. (8) is of better applicability than eq. (7) as it does not involve the term ΣD, the solution of which is difficult and has not been attempted. The entire derivation is based on the important assumption that interfacial polymerization is governed by the well-known distribution law. The only unknown in eq. (8) which makes a direct determination of the average polymer molecular weight difficult is the numerical value of n. n has been shown to be proportional to the catalyst concentration.[3] Hence for a monomer emulsion of constant catalyst concentration, undergoing polymerization at the interface for a definite time interval, the ratio of the average polymer molecular weight of the polymer coming out calculated from the equation proposed, assuming n equal to one, to that calculated from one of those already in vogue, will give the numerical value for n. If, for the same system, for a different time interval the calculated ratio is about the same, then the value of n can be assumed for subsequent determinations and the validity of the equation would be assured. Experimental work is in progress to test the applicability of the equation.

From the above analysis, it is considered probable that polymer formation in emulsion polymerization consists of discrete steps each of which represents: (a) interfacial adsorption of the emulsifying agent; (b) chain growth at the active centers; (c) termination of the chain and transfer of the active centers; (d) outward diffusion of the final polymer particle enveloped by a monomolecular layer of the emulsifying agent, into the aqueous phase.

THE SOLUBILITY OF SILVER PROPIONATE AND SILVER BUTYRATE IN AQUEOUS SODIUM NITRATE

BY SIGFRED PETERSON, JOHN L. JONES, JOSEPH M. SCHMITT AND LOUIS H. KNABESCHUH

College of Arts and Sciences, University of Louisville, Louisville, Kentucky

Received May 24, 1951

Solubilities of silver propionate and silver butyrate have been measured in aqueous silver nitrate solutions. The solubility increases with ionic strength as expected from normal activity coefficient behavior, but activity coefficients have not been calculated from the data in view of the uncertain degree of ionization of the salts. Techniques for the preparation of pure samples of these salts are described.

The effect of inert salts on the solubility of silver carboxylates can be interpreted[1] as due to a change in activity coefficients consistent with the theory of Debye and Hückel. However, electromotive force measurements have shown incomplete ionization in the case of the acetate,[2,3] chloroacetate,[4] and benzoate.[5,6] The quantitative interpretation of these measurements requires the estimate of the mean activity coefficient as a function of ionic strength based on solubility studies. With this in mind, measurements of the solubility of silver propionate and silver butyrate in sodium nitrate solutions were undertaken.

Materials and Experimental Method

Silver nitrate, sodium nitrate, sodium hydroxide and potassium thiocyanate were of reagent quality. The sodium nitrate was dried for two weeks at 175° and stored over magnesium perchlorate. Since the silver carboxylates are not available commercially and previous investigators[7-9] of these salts did not report adequate methods of preparation, the preparations will be given in some detail.

Silver Propionate.—Approximately 19 ml. of Eimer and Amend C.P. propionic acid was neutralized with 250 ml. of sodium hydroxide solution. 1 ml. of excess acid was added. To this was added slowly with vigorous stirring an equivalent amount of silver nitrate (44 g.) dissolved in 250 ml. of distilled water. The white precipitate was collected in a sintered Pyrex filter, washed twice with 100-ml. portions of water and twice with reagent grade methanol by removing the precipitate from the filter before each washing, and dried over magnesium perchlorate. All operations were carried out in dim illumination. Analysis of one preparation Ag, 59.65, 59.75, 59.47; second preparation 59.54, 59.74, 59.78; calcd. for $AgC_3H_5O_2$: Ag, 59.62.

Silver Butyrate.—Coleman and Bell C.P. butyric acid (23 ml.) was neutralized with 250 ml. of sodium hydroxide solution, then made slightly acid to litmus by addition of more acid. To this was added slowly in total darkness with vigorous stirring 44 g. of silver nitrate in 250 ml. of water. The precipitate was washed twice with 100-ml. portions of water and twice with 60-ml. portions of acetone and dried for two weeks over magnesium perchlorate. Samples prepared in this way were white and quite light stable, but precipitation with exposure to light, or washing with methanol, even in total darkness, gave dark products which dissolved with difficulty in dilute nitric acid and gave low silver analyses. Analysis of silver butyrate prepared as described showed Ag, 55.22, 55.52, 55.57 and 55.35; calcd. for $AgC_4H_7O_2$: Ag, 55.35.

Washing with water-miscible volatile solvents was used to effect reasonably rapid drying at room temperature, since silver salts of low molecular weight carboxylic acids sometimes decompose in the drying oven. Oven drying has been found satisfactory for the chloroacetate at 55°,[1] the benzoate at 120°,[5] the *t*-butylacetate at 110°[10] and the salts of several aromatic acids at 100–105°.[11]

Solubility Measurements.—A weighed portion of sodium nitrate and distilled water measured with a calibrated pipet were introduced into brown glass stoppered bottles along with an excess of the silver salt. The bottles were sealed

(1) F. H. MacDougall and J. Rehner, *J. Am. Chem. Soc.*, **56**, 368 (1934).

(2) I. Leder, *Svensk Kem. Tids.*, **58**, 129 (1946).

(3) F. H. MacDougall and S. Peterson, THIS JOURNAL, **51**, 1346 (1947).

(4) J. V. Parker, C. Hirayama and F. H. MacDougall, *ibid.*, **53**, 912 (1949).

(5) I. M. Kolthoff and W. Bosch, *ibid.*, **36**, 1702 (1932).

(6) I. Leden, *Acta Chem. Scand.*, **3**, 1318 (1949).

(7) S. Arrhenius, *Z. physik. Chem.*, **11**, 396 (1893).

(8) H. Goldschmidt, *ibid.*, **25**, 95 (1898).

(9) J. Knox and H. R. Will, *J. Chem. Soc.*, **115**, 853 (1919).

(10) W. T. Smith, Jr., and R. L. Hill, *J. Am. Chem. Soc.*, **72**, 3309 (1950).

(11) R. A. Barnes and R. J. Prochaska, *ibid.*, **72**, 3190 (1950).

TABLE I

MOLAL SOLUBILITIES OF SILVER PROPIONATE AND SILVER BUTYRATE IN AQUEOUS SODIUM NITRATE AND DENSITY OF THE SATURATED SOLUTIONS

m_{NaNO_3}	$m_{Ag\ P}$	d	m_{NaNO_3}	$m_{Ag\ P}$	d	m_{NaNO_3}	$m_{Ag\ B}$	d
0.0000	0.04934	1.002	0.2902	0.05849	1.019	0.0000	0.02403	1.000
.0000	.04932	1.003	.3008	.05899	1.019	.0000	.02441	1.000
.0000	.04897	1.001	.3605	.06098	1.023	.0160	.02495	1.000
.0253	.05088	1.004	.3653	.06061	1.021	.0280	.02569	1.001
.0322	.05134	1.004	.4366	.06126	1.027	.0663	.02670	1.003
.0720	.05310	1.007	.5070	.06219	1.030	.0822	.02721	1.005
.0756	.05333	1.007	.5481	.06236	1.034	.1298	.02844	1.008
.0991	.05408	1.008	.5912	.06361	1.035	.1580	.02883	1.010
.1204	.05466	1.009	.6783	.06415	1.040	.1937	.02914	1.011
.1302	.05516	1.010	.6783	.06378	1.040	.2164	.02951	1.012
.1750	.05648	1.012	.7477	.06438	1.045	.3361	.03061	1.020
.1973	.05670	1.014	.7608	.06522	1.044	.4132	.03131	1.023
.2165	.05731	1.015	.9065	.06582	1.052	.5313	.03180	1.029
.2326	.05778	1.015	.9503	.06645	1.052	.6459	.03268	1.035
.2516	.05808	1.017	.9965	.06681	1.055	.6989	.03245	1.040
.2740	.05880	1.018	1.051	.06720	1.056	.8229	.03291	1.040
						.8818	.03356	1.048
						1.0395	.03422	1.055
						1.1349	.03436	1.066

with paraffin, immersed in a thermostated water-bath for at least two weeks at 25.00 ± 0.05°, and shaken frequently during the equilibration. After equilibration samples of the solution were removed by pipetting through a cotton filter, weighed and analyzed for silver.

Silver analyses were by the Volhard method using potassium thiocyanate which had been standardized against fused silver nitrate.[12]

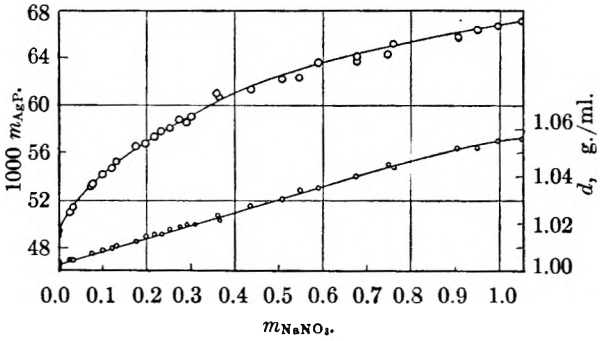

Fig. 1.—Solubility of silver propionate in aqueous sodium nitrate solutions and density of the saturated solutions.

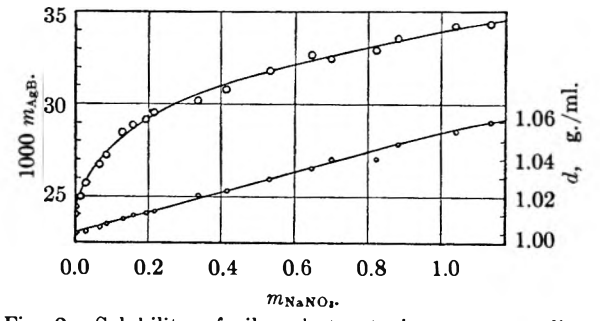

Fig. 2.—Solubility of silver butyrate in aqueous sodium nitrate solutions and density of the saturated solutions.

(12) I. M. Kolthoff and E. B. Sandell, "Textbook of Quantitative Inorganic Analysis," The Macmillan Co., New York, N. Y., 1937, Chap. XXXV.

Discussion and Results

The dependence of the molal solubility of silver propionate and silver butyrate on molality of sodium nitrate is shown in Table I and Figs. 1 and 2. Also included are the densities of the saturated solutions calculated from the weights of the samples analyzed and the volume of water delivered by the sampling pipet.

It can be seen that the solubility increases with ionic strength at about the rate expected from the usual decrease in activity coefficients of the ions. While this increase could probably be fitted with an activity coefficient equation in the same manner as the data for silver acetate and silver chloroacetate,[1] in view of the very high probability that the silver salts are not completely ionized it appears futile at this time to carry out this analysis. If the ionization constants of these salts are about the same as that of silver acetate,[3] the saturated silver propionate solution in pure water is about 80% ionized and the butyrate 90%.

Our values for the solubility of silver propionate in pure water are almost 2% lower than those of Goldschmidt[8] and Knox and Will.[9] Previous measurements with silver butyrate have not been made at this temperature, but our value appears somewhat lower than what would be found by interpolation in the data collected by Seidell.[13] Since the literature values are quite old, it is possible that the differences are due to lack of temperature control or contamination of the silver salts with silver nitrate in the work of the early investigators. While our solubilities in Table I are given to four figures on the basis of precision of the analyses, inspection of the graphs shows that consistency of the results limits the reliability to three figures.

(13) A. Seidell, "Solubilities of Inorganic and Metal Organic Compounds," Vol. I, 3rd Edition, D. Van Nostrand Co., New York, N. Y., 1940, p. 21.

ADSORPTION OF UX_1 AND RA E BY AN AQUADAG COATED DIPPING GEIGER–MUELLER TUBE[1]

BY I. ADLER AND J. STEIGMAN

Department of Chemistry of the Polytechnic Institute of Brooklyn, Brooklyn, New York

Received June 4, 1951

A method is proposed for the study of radio-colloids. A dipping Geiger–Müller counter is coated with an adsorbent, so that it serves simultaneously an accumulator and detector. The method was used to investigate UX_1 (thorium) in aqueous solutions. The increase in counting rate with time was not noticeably affected by temperature change or different thicknesses of adsorbent. Linear diffusion was shown to take place. The effect of different acids on UX_1 was examined by this technique. In acid solution there appeared to be an equilibrium between adsorbable and non-adsorbable species. Solutions of carrier-free radio-bismuth were studied. The formation of complex ions by chlorides, and the increased adsorption from more acid solution were demonstrated.

Radio-colloids are colloidal dispersions of substances at such low concentrations that radioactivity measurements constitute the only method of studying them which is known at the present time. They were first discovered by Paneth[2] almost forty years ago, as a result of investigations of radium E and radium F, two of the naturally-occurring radioactive isotopes of bismuth and polonium, respectively. He observed that when a solution containing very small quantities of radium D, radium E and radium F (lead, bismuth and polonium) was subjected to dialysis without adding macroscopic quantities of inactive isotopes of the same substances (*i.e.*, without adding carrier), the radiolead passed through the membrane, but the other two were retained. Further investigation using such techniques as electrophoresis and measurements of diffusion coefficients confirmed this result. The bismuth and polonium isotopes appeared to be colloidal in neutral, ammoniacal and weakly acid solutions. The lead isotope was ionically dissolved in weak acid, but appeared to be colloidal in ammonia solution.

A major dilemma arose in the application of the laws of chemical equilibrium to saturated salt solutions as a result of this discovery. It had been believed that the formation of a colloid required the same super-saturation which under other conditions produces a discrete solid phase. The solubility product constant of the insoluble compound must be exceeded to produce either colloid or precipitate. The difficulty which was presented by the new phenomenon was that colloids seemed to be formed at metal ion concentrations which were very much less than those required by the (previously established) solubility product constants—in many cases orders of magnitude less. Thus, for example, the solubility product constant of lead hydroxide is 1.2×10^{-10} at room temperature. In dilute ammonia (say, 10^{-1} M), with a hydroxyl-ion concentration of 10^{-3} M, the minimum concentration of Pb^{++} required to produce a precipitate is about 10^{-4} M. However, ThB (a radioactive lead isotope) behaves like a colloid at concentrations as low as 10^{-11} M in the same ammoniacal solution.

There has been much controversy about whether this unexpected behavior is due to the effect of traces of colloidal impurities,[3-5] or reflects the presence of true colloids.[2,6,7]

Haissinsky[8] has critically analyzed the work in this field, including the inevitable re-examination of the previously established solubility product constants. His view is that the radio-colloids are true colloids, although traces of colloidal impurities may contribute to the total phenomenon in a secondary manner. Among his conclusions there are several which we believe to be of first-rate importance for the application of equilibrium relationships to saturated solutions of insoluble compounds. His careful review of previous solubility determinations of insoluble hydroxides and sulfides[9] showed that different methods of solubility measurement gave quite different numerical results for the same compounds, sometimes orders of magnitude apart. In addition, the age of the precipitate was also an important factor in determining the numerical value of the solubility which was obtained in a particular experiment. When these considerations are applied to radio-colloid formation, it is difficult to escape his conclusion that for a number of these compounds[8] "one is · · · dealing with polydispersed systems containing ions both simple and complex, and colloidal micelles of various dimensions in a slow state of evolution. The ordinary principles of solubility and solubility product are not applicable."

One implication of this analysis is that for certain insoluble inorganic substances no true equilibrium exists between the solid state and the solution, but rather that an intermediate series of colloidal and sub-colloidal forms are in process of formation and break-down. This applies to a surprisingly wide variety of substances. Schubert[10] has demonstrated that many of the fission products of uranium show radio-colloidal behavior in the presence of appropriate reagents. This includes carrier-free barium ion in sulfuric acid solution. Thus the phenomenon is quite general, including the previously intensively investigated compound barium sulfate. What is clearly suggested is that saturated solutions of barium sulfate should be exam-

(1) This work is in partial fulfillment of requirements for the Ph.D. at the Polytechnic Institute of Brooklyn for Mr. Adler.

(2) F. Paneth, *Sitzungsber. d. Akad. d. Wiss. (Wien)*, **121**, 2193 (1912).

(3) O. Hahn and O. Werner, *Naturwissenschaften*, **17**, 961 (1929).

(4) O. Werner, *Z. physik. Chem.*, **A156**, 89 (1931).

(5) R. Zsigmondy, *Kolloid Z.*, **13**, 297 (1913).

(6) H. Benjamin, *Z. Elekt-ochem.*, **31**, 575 (1925).

(7) J. Starik, *Z. physik. Chem.*, **157**, 269 (1931); *Trav. Inst. Rad. Leningrad*, **1**, 29 (1930); **2**, 91 (1933).

(8) M. Haissinsky, "Les Radiocolloides," Hermann et Cie, Paris, 1934.

(9) M. Haissinsky, *J. chim. phys.*, **31**, 43 (1934).

(10) J. Schubert, A.E.C.D. 1910.

ined for the presence of colloidal particles. It would seem that behavior of this sort arises from a powerful interaction between barium and sulfate ions strong enough to overcome thermal forces even at vanishingly small concentrations. It is interesting that strontium sulfate does not form radio-colloids,[10] and that radium sulfate does.[11] At this stage it is not possible to do more than speculate about the nature of the interaction; but it is most certainly an important factor in determining solubility. In any event, the phenomena encompassed by the term radio-colloid would seem to be of some importance from the point of view of analytical and physico-chemical theory, and merit extended investigation.

A number of experimental criteria have been used to show the existence of radio-colloids. They include ultra-centrifugation, ultrafiltration, dialysis, adsorption on ion-exchange resins in the presence of concentrated electrolyte solutions (so-called anomalous behavior), low diffusion coefficients, and marked adsorption on glass and other surfaces.[10] We propose a simple and convenient method of studying radio-colloids and some of their properties, which is based upon the adsorption of colloids by various surfaces. In this method, whose principle was first established by Joliot[12] to examine the electrode potentials of very dilute solutions of radio-isotopes, the detecting instrument is simultaneously a collecting instrument for the species to be studied. We employ a dipping Geiger–Muller counter tube. This is a tube which is used for determining the radioactivity of a solution by direct immersion. The tube can be made to serve a dual function—as detector and collector—by coating the outside surface with an adsorbent like a carbon black. It is then immersed in the solution containing the radio-colloid. Particles in the immediate vicinity of the carbon black will be adsorbed. This will result in the impoverishment of radio-colloid in the liquid adjacent to the tube, and a concentration gradient of the adsorbed species will be established. Diffusion of this species into the effective detecting volume of the tube will then occur. The consequence of this experimental arrangement is that the measured counting rate of a given solution will increase in time, or (if the half-life is short) will decay more slowly than the true half-life. This experimental technique will be tentatively established if a number of radio-isotopes known to be ionically dispersed are not adsorbed, and if a number of previously established radio-colloids do adsorb. The objection may be raised that ions may be adsorbed in the carbon (by an exchange process). However, the addition of concentrated electrolyte solutions like sodium nitrate or sodium perchlorate should displace such ions, but on the contrary should have little or no effect on the adsorption of colloids. The effects of such added electrolytes have been described by Schubert[10] in connection with adsorption on ion-exchange resins.

The preliminary results which have been obtained by the use of this technique, together with some of its characteristics, are described in this first paper.

Apparatus.—The apparatus consisted of a dipping Geiger–Müller counter tube and a conventional scaling circuit and register. The dipping counter tubes were of the commercially available thin-walled glass β–γ detecting type (wall thickness about 30 mg./cm.^{2}). Thin-walled aluminum tubes were also satisfactory, but were protected against chemical attack by the examined solutions by insertion in thin plastic tubes. A light-tight box was used for those glass counters which were photosensitive. When stirring is indicated, a magnetic stirrer was used.

Preparation of Radioelements.—The majority of the radio-elements which were used in these experiments were naturally occurring isotopes. Uranyl nitrate solutions were used directly, without chemical separation, as sources of UX_1 and UX_2. Radio-bismuth (radium E) was prepared from old radon needles by the electrochemical displacement on nickel, acid solution, precipitation with $Al(OH)_3$ as carrier, and finally electroplating on platinum, according to the technique of Haissinsky.[13]

Preparation of Adsorbent.—The glass counter tubes were prepared for a run by coating them with colloidal graphite (or occasionally with a mixture of colloidal graphite and an activated carbon black). The colloidal graphite which is manufactured by the Acheson Colloid Company of Detroit, and sold under the trade name of Aquadag, was quite satisfactory. After a fivefold dilution with distilled water, it gave a satisfactory coating, which showed good adhesion to the glass. The dilution value is not critical. The diluted suspension is painted on the clean upright glass by means of a camel hair brush, and is dried under an infrared lamp. Water evaporation is rapid, and the tube remains comparatively cool. If more than one coat is required, the additional coats can be applied in the same manner, after the first coat has dried. The resulting coating has a black satin-smooth surface and is stable in neutral and moderately acid solutions. In 3 *N* sulfuric or nitric acid, slight blistering is sometimes observed; but this does not interfere with its use. In strong ammoniacal solution the coating peels off.

When a thin-wall aluminum Geiger–Muller tube is used, it is protected from chemical attack by a cellulose nitrate tube which encloses it. The Aquadag is then painted on the plastic shell; the adhesion of the coating to the plastic appears to be much better than that to glass. Two applications yield a coating whose thickness is approximately 1.5 mg./cm.^{2}.

The tubes were introduced to approximately the same level each time. Counts were taken at regular intervals (every half-hour to every hour). The statistical counting error was less than 2%. Many of the experiments reported here were performed without careful temperature control ($\pm 2°$). The experiments on reproducibility were performed in a constant-temperature bath ($\pm 0.3°$).

Adsorption on Aquadag.—Experiments were performed on uranyl nitrate solutions with coated and uncoated Geiger counter tubes. Uranyl nitrate is a convenient source of the two electron emitters, UX_1 (a thorium isotope) and UX_2 (a protactinium isotope).

In these series, the behavior of the thorium isotope (UX_1) is described by the results of the experiments which were performed. The wall of the Geiger tube is too thick to permit the passage of the α-particles of uranium. The UX_2 (protactinium) has a half-life of only one minute, compared to more than 24 days for the UX_1. This means that the system UX_1–UX_2 is in transient equilibrium under the experimental conditions. Actually, the electron emitted by the UX_1 is too soft to penetrate the counter wall. What is passed through is the much harder electron from the UX_2. Hence, in these experiments, the UX_2 is acting as an indicator for the UX_1.

(11) O. Erbacher and B. Nikitin, *Z. physik. Chem.*, **A158**, 216 (1932).

(12) F. Joliot, *J. chim. phys.*, **27**, 119 (1930).

(13) M. Haissinsky, "Electrochimie des Substances Radioactivités, etc.," Hermann et Cie, Paris, 1946.

The solution which was most extensively studied contained two grams of uranyl nitrate per liter. A dipping counter was coated with Aquadag, and inserted into the solution. The radioactivity was measured at regular intervals; results are shown in Fig. 1. The activity (counts per minute) or counting rate is observed to increase steadily with time. The sharp break in the curve occurs at the point when stirring was started; the rate of increase of activity is, of course, much greater (since the process is diffusion-controlled). In less than three hours, the activity rose from 3,000 counts per minute to 14,000 counts per minute. Most of the increase in activity is due to material adsorbed on the graphite coating. At the end of the run, the counter was removed from the solution and washed thoroughly with distilled water. The counting rate due to the adsorbed material was then determined in air. It was about 12,000 counts per minute.

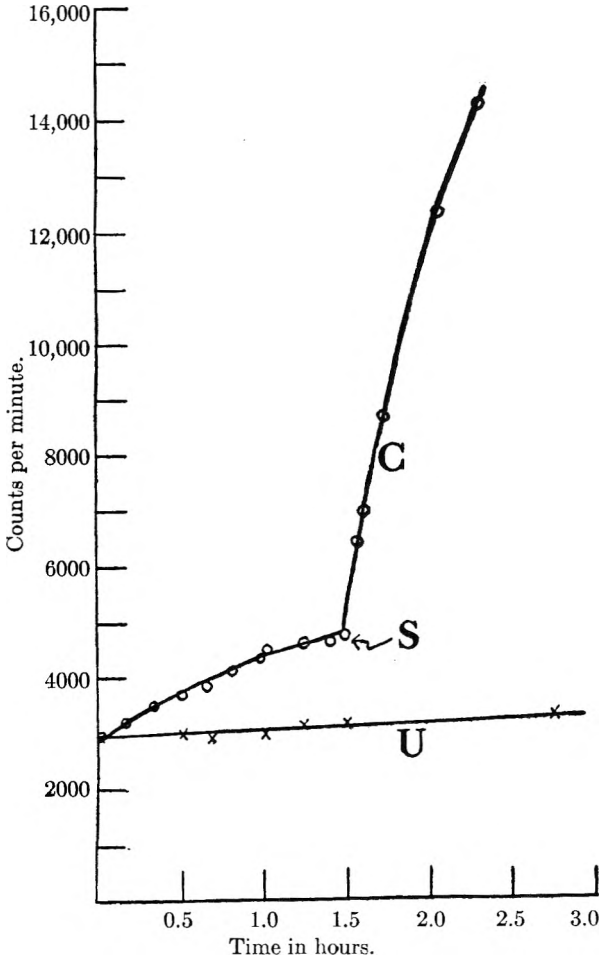

Fig. 1.—Adsorption of UX_1: C, coated with aquadag; U, uncoated; S, stirring begun.

The behavior of an uncoated Geiger tube in a similar solution is also shown in Fig. 1. It is clear that the adsorption is very much smaller than that occurring on the graphite coating.

Reproducibility of the Accumulation.—Some measure of the reproducibility of the accumulation rate is necessary for quantitative intercomparisons. The factors which at first glance might be expected to affect the accumulation rate of a colloid are: the nature and concentration of the dispersion, the history of the colloid, the viscosity and temperature of the medium and the nature, effective area and thickness of the absorbent. In the experiments which are described below, an attempt was made to limit the variables to three: the thickness of the coating, the temperature of the solution, and the available collecting area. This was done by diluting aliquot portions of the same stock saturated solution of uranyl nitrate immediately before the measurements were started, and by using Aquadag as the adsorbent coating each time. Two different Geiger counting tubes, with different surface areas, were used. Figure 2 shows the per cent. increase in counting rate for the two tubes, with different thicknesses of applied Aquadag. The studies were made at two different temperatures. For tube 1 these were 26.0 and 31.5° (±0.3°). For tube 2 the temperatures were 25.0 and 33.0° (±0.3°). It is clear that the number of applied coatings does not seriously affect the accumulation rates. In addition, the effect of temperature is quite small. It is probable that this is the case because most of the UX_1 is present as colloid, so that there are no complicating equilibria which would be temperature-sensitive. If a 0.2% uranyl nitrate solution with no added acid is shaken with an activated carbon, practically all of the UX_1 is removed. The insensitivity of the process to temperature (over a small temperature range) can then be attributed to the fact that only diffusion of colloidal micelles is involved. Diffusion phenomena have a relatively small temperature coefficient. One consequence of this situation is that where the material is almost all colloidal, rigorous temperature control is not required for this type of study.

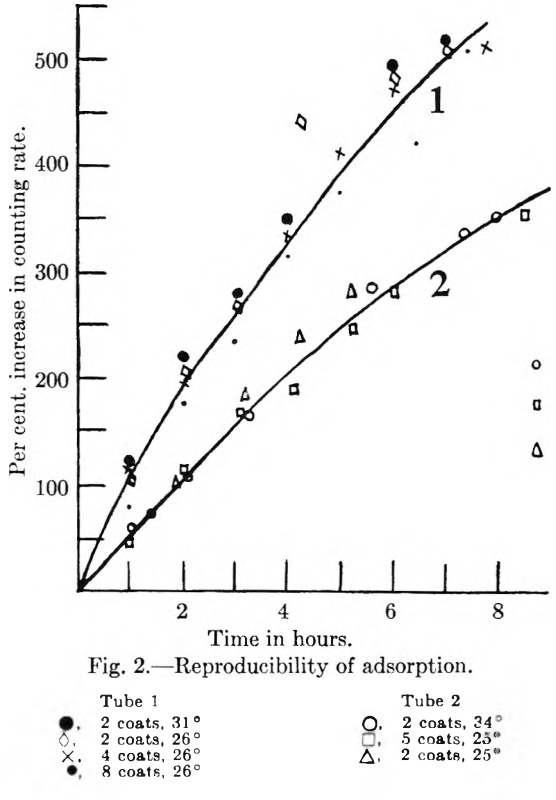

Fig. 2.—Reproducibility of adsorption.

In acid solution the reproducibility is very much poorer. This may be due to the much smaller percentage of adsorbable species (with the possibility of temperature-sensitive equilibria being involved). In addition, the history of the system may begin to play a more important role.

In general, different dipping counters can be expected to yield different quantitative results because of the difference in effective adsorbing area. However, since the studies which are described here are relative rather than absolute in character, no error is committed as long as the same tube is used for the given sequence of experiments.

Diffusion.—From the geometry of the system it would appear that linear diffusion is taking place, and that Fick's law would apply

$$\frac{\partial C}{\partial t} = D\frac{\partial^2 c}{\partial x^2}$$

The solution which is applicable under the boundary conditions that the concentration of diffusing species is uniform at $t = 0$, and that the concentration at the adsorbing surface is always zero, (*i.e.*, that no desorption occurs) is[14]

$$A = 2c_0\sqrt{Dt/\pi}$$

In this equation, A is the accumulation of diffusate in time t, c_0 is the initial concentration of the diffusing species, and D is the diffusion coefficient. At the start of a run it is assumed that the counting rate is proportional to c_0. The accumulation is calculated by subtracting the counting rate at zero time from the counting rate at time $= t$. The terms c_0 and D are not separately measured in these experiments. The accumulation should be proportional to the square root of the elapsed time. Figure 3 shows the relationship between these two factors, in a typical experiment in which UX_1 in a 0.2% uranyl nitrate solution was adsorbed on Aquadag.

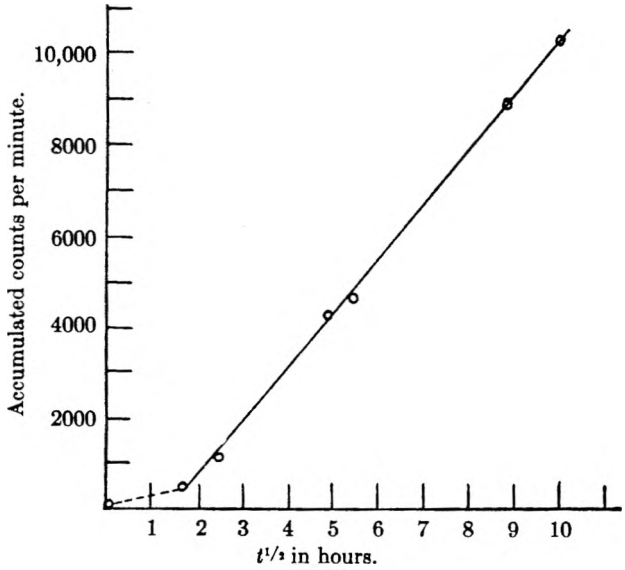

Fig. 3.—Accumulation *vs.* $\sqrt{\text{time}}$, 0.2% uranyl nitrate, *p*H 3, $A = 2C_c\sqrt{DT}/\pi$.

(14) H. S. Carslaw and J. C. Jaeger, "Conduction of Heat of Solids," Clarendon Press, Oxford, 1947.

The curve is linear, except for the first few hours, over a time period of one hundred hours.

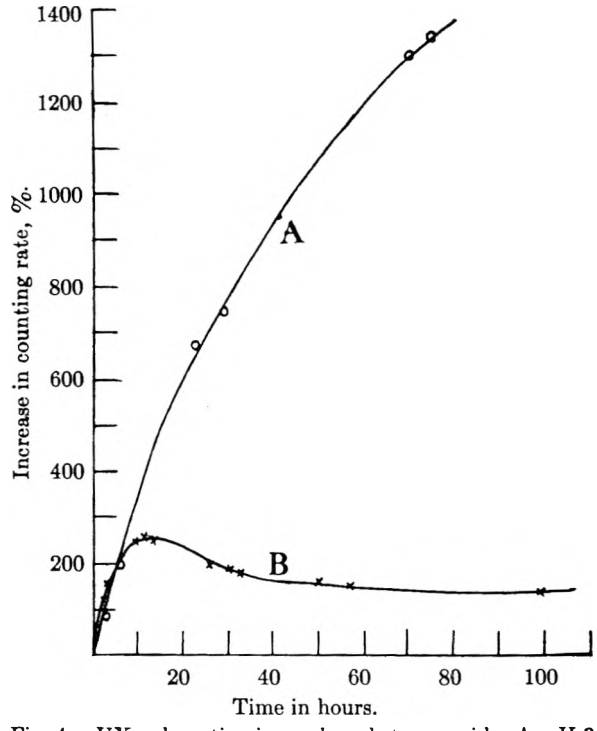

Fig. 4.—UX_1 adsorption in weak and strong acid: A, *p*H 3; B, 3 *N* HNO_3.

Behavior of UX_1 (Thorium) in Acid Solution.—One advantage of this technique is that changes in colloidal systems like UX_1 can be studied as a function of time. A solution containing two grams of uranyl nitrate per liter of 3 *N* nitric acid was prepared, and a coated counter was introduced into it. Figure 4 shows the increase in counting rate with time for this solution. The behavior of uranyl nitrate in distilled water is included for comparison. The experiments were performed at room temperature. It appears that the increase in counting rate is about the same for both systems in the early stages, but the increase becomes less marked for the nitric acid solution, a maximum in the counting rate is reached in approximately nine hours, and the activity then slowly decreases.

The occurrence of the maximum in the curve indicates the emergence of a competing process. One possible competing process is the slow chemical attack by the nitric acid on the UX_1 colloidal micelles, which would reduce their concentration, and hence reduce the rate at which diffusion is taking place. This hypothesis was tested experimentally by allowing a solution in 3 *N* nitric acid to age overnight, inserting a freshly coated counter, and measuring the change in counting-rate with time. If this hypothesis were correct, there should have been no increase (or very little increase) in activity with time, since the colloidal material would have been largely dissolved. This, however, is not the correct explanation, since repetition of the experiment a number of times on the same nitric acid solution gave approxi-

mately the same curve each time—and each time the same maximum was observed.

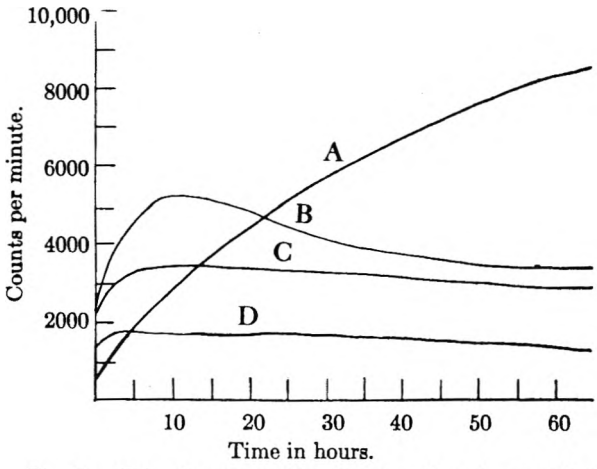

Fig. 5.—UX_1 adsorption in different acids: A, no added acid, *p*H 3; B, 3 *N* HNO_3; C, aged in concd. HNO_3—diluted to 3 *N*; D, aged in concd. H_2SO_4—diluted to 3 *N*.

A second possible explanation is the slow inactivation of the Aquadag by nitric acid, leading to a decrease in available adsorbing surface. This hypothesis was tested by soaking a freshly coated counter in a 3 *N* nitric acid solution for 24 hours, and then inserting it into the 3 *N* nitric acid solution of the UX_1. If the acid is inactivating the Aquadag, inactivation prior to the adsorption run should result in no adsorption, or markedly decreased adsorption. This experiment was performed a number of times, and each time the same rate of increase of activity with time and the same maximum was observed.

A third possible explanation is that some catalytic interaction involving the solution, the surface and the adsorbed gel is responsible for the phenomenon. If this were the case, agitation of a large quantity of active carbon with the nitric acid solution of UX_1 for several days should result in sorbing out the colloid, catalytically attacking it, and redissolving it. A coated counter introduced at this point should show no increase in activity. The solution was shaken with several grams of Darco activated carbon for five days. The carbon was allowed to settle, and a coated counter was introduced. An increase in activity with time was observed. The same result was obtained in another way. The acid solution was shaken with Darco and decanted. There was a measurable decrease in activity. The decanted solution was shaken with a fresh charge of Darco, and again decanted. There was again a definite decrease in activity, although the larger decrease occurred the first time. This strongly suggests that an equilibrium is fairly rapidly established between colloid and solution. The same type of phenomenon has been reported by Kurbatov and Kurbatov,[15] in connection with the retention of radio-yttrium by filter paper in acid solutions. In any event, a catalytic interaction involving solution, surface and gel is not a sufficient explanation for the behavior which is described in Fig. 4.

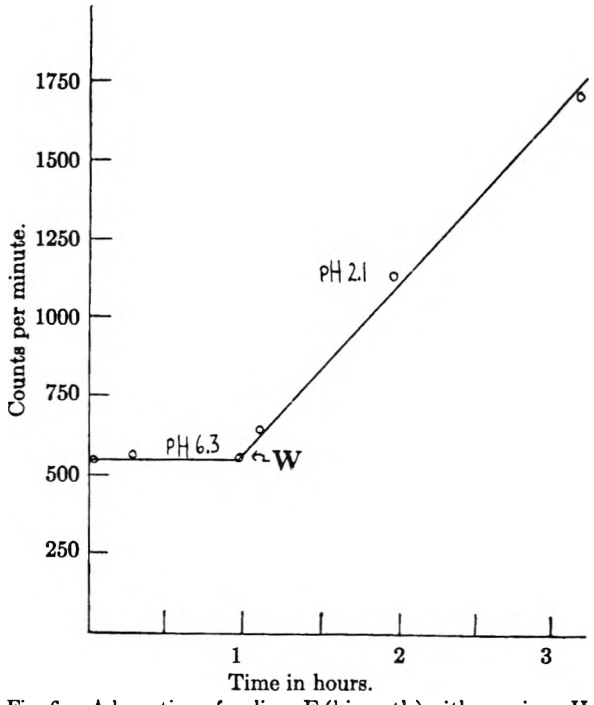

Fig. 6.—Adsorption of radium E (bismuth) with varying *p*H: W, *p*H adjusted at this point.

The interactions of colloids in these acid solutions are undoubtedly very complex. Figure 5 is presented only by way of illustrating some of the possible changes in time which can be investigated by the accumulator-detector technique. Different acids show quite different effects on the accumulation rate; so do different pretreatments with the same acid. It is interesting to note that UX_1 aged in strong nitric acid which is subsequently diluted to 3 *N* exhibits much less initial adsorption than the

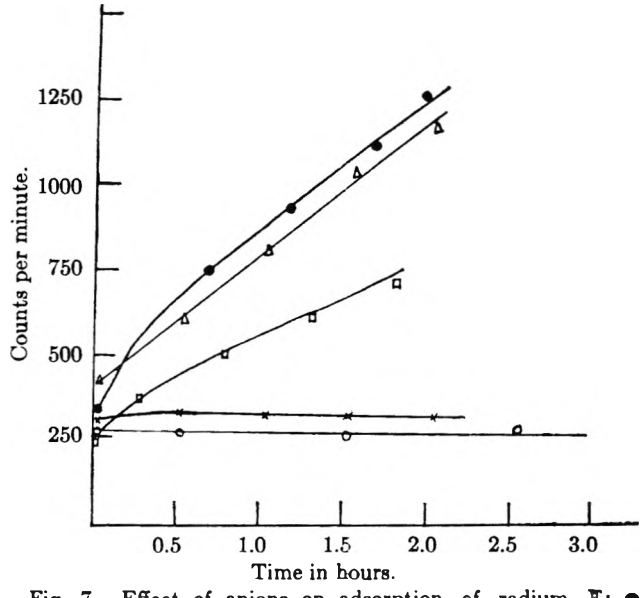

Fig. 7.—Effect of anions on adsorption of radium E: ●, 0.05 *M* NH_4Cl, *p*H 3.0; △, 2 *M* NH_4NO_3, *p*H 3.0; □, 2 *M* $NaNO_3$, *p*H 3.0; ×, 2 *M* NaCl, *p*H 2.9; ○, 2 *M* NH_4Cl, *p*H 2.9.

(15) J. D. Kurbatov and M. H. Kurbatov, THIS JOURNAL, **46**, 441 (1942).

3 *N* nitric acid solution previously reported, but tends in time to approach the same level of activity.

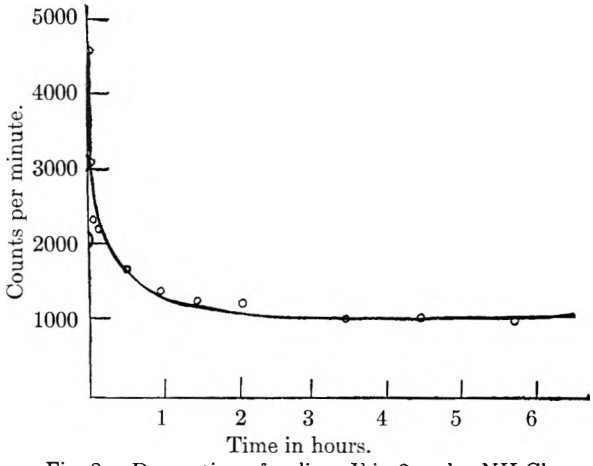

Fig. 8.—Desorption of radium E in 2 molar NH_4Cl.

Radio-bismuth (Radium E).—The colloidal behavior of bismuth salts in water (both in trace and macroscopic concentrations) has been investigated by Haissinsky.[8] The extent of colloidal aggregation, measured by centrifugation experiments, is markedly affected by the *p*H of the solution. For example, Haissinsky reported that much more colloid was formed at *p*H 2.5 than at *p*H 5. The results which were obtained with a coated dipping counter are at least qualitatively comparable. They are illustrated in Fig. 6. A nitric acid solution of radium E was adjusted to *p*H 6.3 by ammonia. There was virtually no increase in counting rate for an hour. At this point, the counter was removed, and nitric acid was added to *p*H 2.1. The same counter was re-introduced; the marked increase in counting rate is obvious.

Another aspect of the chemistry of bismuth is described below. It will precipitate from bismuth nitrate solutions upon the addition of small quantities of chloride ion. However, the resulting precipitate will redissolve in 4 *M* sodium chloride solution.[8] Figure 7 illustrates several experiments performed with radium E at *p*H 3 (where a considerable proportion of the bismuth is in the colloidal form). In the presence of 2 *M* sodium or ammonium nitrate there is a decided increase in counting rate with time. A low concentration of ammonium chloride (0.05 *M*) produces little change. However, in 2 *M* sodium chloride or 2 *M* ammonium chloride, at approximately the same *p*H, there is no increase in counting rate, and no adsorption.

Figure 8 shows the action of a concentrated ammonium chloride solution in complexing radio-bismuth. Radium E was cumulatively adsorbed from solution (having a *p*H of 3) on a coated counter for some hours. The tube was removed, and washed. The initial count in air was 4700 counts per minute. On immersion in a 2 *M* ammonium chloride solution (*p*H 3), the Radium E desorbed very rapidly to reach a constant count of about 1400 counts per minute.

Acknowledgment.—We wish to thank Professor F. C. Collins and Dr. Joseph Greenspan for many helpful discussions.

THE PHOTOLYSIS OF CADMIUM DIMETHYL[1]

BY R. DEAN ANDERSON AND H. AUSTIN TAYLOR

Department of Chemistry, New York University, University Heights, New York, N. Y.

Received June 25, 1951

The photolysis of cadmium dimethyl vapor both alone and in the presence of a four-fold excess of hydrogen has been studied in a temperature range up to 250°. In the presence of hydrogen, methane and ethane are the sole gaseous products. From the alkyl alone small amounts of ethylene, propane and butane in addition to ethane and methane are produced. An appraisal of the relative light intensity as a result of metal deposition during a run has been made by observing acetone photolysis in the air-poisoned vessel. The simplest mechanism consistent with the data leads, on the assumption of zero activation energy of the recombination of two methyl radicals, to a value of 13 ± 2 kcal. for the energy of activation of the reaction $CH_3 + H_2 \rightarrow CH_4 + H$ consistent with the strength of the C–H bond in methane and the energy of activation of the reverse reaction. The energy of activation of hydrogen abstraction by a methyl radical from cadmium dimethyl is found to be 14 ± 2 kcal.

The photolysis of mercury dimethyl has been studied by a number of workers[2] and each effort seems to have shown a greater complexity in the reaction than was suspected in earlier work. The interpretation of the effect of temperature on the reaction depends in large measure on the steps postulated in the mechanism. It is in this way that energies of activation of intermediate step, radical reactions are frequently arrived at.[3] By varying the source of the radicals some confirmation of the energy of activation may be possible.[4] The present paper is concerned with a study of the photolysis of cadmium dimethyl vapor both in the presence and absence of hydrogen in the expectation that from the similarities and dissimilarities of the mercury and cadmium compounds information significant to both mechanisms might be forthcoming.

Experimental

Apparatus.—Preliminary experiments carried out at temperatures below 50° showed ethane to be the sole gaseous product of the photolysis of cadmium dimethyl. The presence of ethane and absence of methane were demonstrated

(1) Abstract from a dissertation presented in partial fulfillment of the requirements for the degree of Doctor of Philosophy at New York University, February, 1951.

(2) R. D. Anderson and H. A. Taylor, THIS JOURNAL, **55**, 161 (1952).

(3) J. H. Cunningham and H. S. Taylor, *J. Chem. Phys.*, **6**, 359 (1938).

(4) H. S. Taylor and C. Rosenblum, *ibid.*, **6**, 119 (1938).

by infrared analysis.[5] The rate of production of ethane leveled off after about one minute due to the sharp decrease in light intensity penetrating the cadmium mirror deposited on the illuminated side of the reaction flask. Experiments made at 17, 32 and 47° showed no appreciable differences suggesting zero energy of activation of ethane production and recombination of methyl radicals as the source of ethane. It was from this experience that the apparatus used in the bulk of the experiments was developed.

The reaction vessel was a heavy-walled cylinder of transparent quartz about 6 cm. in length carrying two circular plane windows, 10 cm. in diameter, attached by a special sinter seal achieved at a temperature below that at which any significant strain could be introduced into the windows. A side-arm was joined to the curved part of the cell.

The furnace for the reaction cell was a narrow metal box thoroughly insulated and equipped with variable heating elements controlled in part by a bimetallic thermoregulator. Double quartz windows with an air space between them for insulation were fitted on both sides of the box and aligned with the windows of the reaction cell. Metal shutters sliding vertically served to screen these windows from the incident radiation. A fan circulated the air in the furnace preventing any temperature gradients. The temperature was measured by means of a chromel–alumel thermocouple. The variation in temperature during a run amounted to less than 0.1°.

The furnace for the reaction cell was installed inside a much larger oven designed to maintain two ultraviolet lamps, one for each window of the cell at a temperature of 45°. The lamps were flat spiral low-pressure mercury resonance lamps, Hanovia Type SC2537, operated on separate 120 milliamp. 5000 volt transformers which at 120 volts drew about 5.8 amp. The air in the oven was circulated rapidly over the lamp by two fans and heaters in series with a metallic thermoregulator maintained constant temperature. Separate thermometers recorded the temperature in the vicinity of the electrodes of each lamp.

The quartz reaction cell was connected by a quartz-to-Pyrex seal to a manifold through a Crist valve[6] which permits only platinum, silver and silver chloride to come in contact with a vapor stream passing through it. Provision was made for the handling of cadmium dimethyl vapor without contamination by mercury vapor, a second Crist valve confining the storage reservoir. When hydrogen was used it was passed through two traps in liquid nitrogen before entering a storage bulb, the pressure in which was registered on a mechanical vacuum gage sensitive to pressure changes of about 5 mm. and covering a range up to 760 mm. A helium storage bulb with vacuum gage was attached to the manifold as was also a storage flask for acetone. This manifold was never in direct contact with mercury and the reaction cell and its contents before and during a run were thus also free from mercury. A quartz spiral manometer was used as the pressure-measuring instrument. Readings were made through a forty magnification microscope with superimposed scale. In the range 0 to 35 mm. of mercury the manometer served as an absolute gage giving pressures reproducible to 0.1 mm. For pressures greater than 35 mm. the manometer was used as a null instrument.

A second manifold carried Toepler pumps, McLeod gage, mercury diffusion pump and Cenco Megavac oil pump. The two manifolds were connected through a two-way stopcock to the Crist valve attached to the reaction vessel, two liquid nitrogen traps in series standing between this stopcock and the portion of the second manifold exposed to mercury. The McLeod gage and the diffusion pump in addition were isolated through liquid nitrogen traps. All stopcocks with which cadmium dimethyl vapor or acetone came in contact were lubricated with a perfluorocarbon. Gas samples after photolysis were withdrawn by a Toepler pump through a trap in solid carbon dioxide and trichloroethylene and delivered to a sample flask with stopcock connected by a ball joint for easy detachment for analysis.

Materials.—Cadmium dimethyl was made by the reaction of anhydrous cadmium chloride with methylmagnesium iodide in ether solution. Details of the method and critical tests of purity showing that previously reported physical constants were in error have already been described.[2]

Acetone was prepared by distillation from the sodium iodide compound and stored at the temperature of solid carbon dioxide.

Tank helium described as 99.8% was found to contain traces of nitrogen and hydrogen. For rinsing purposes it was first passed over copper oxide at about 400° to remove hydrogen, through a drying tower containing potassium hydroxide pellets and through a trap in liquid nitrogen to its storage bulb on the main manifold.

Electrolytic tank hydrogen was passed over platinized asbestos at about 400°, dried over potassium hydroxide and through a trap in liquid nitrogen. Mass spectrometer analysis showed hydrogen, 99.7%, nitrogen 0.3%.

Procedure.—In all runs the initial pressure of cadmium dimethyl vapor in the reaction vessel was approximately 17.5 mm. at 27.0°. In the runs with hydrogen a fourfold dilution of cadmium dimethyl vapor with hydrogen was employed.

Preceding a run, the lamps were allowed to warm up to full intensity for half an hour. The cadmium dimethyl vapor was allowed to warm up for 15 minutes in the reaction cell before exposure. When hydrogen was present an additional 15 minutes was allowed. Special pyrolysis runs were made to correct the photolysis results for the decomposition of cadmium dimethyl during the warm-up periods.

Since even traces of oxygen react readily with cadmium dimethyl vapor the pumping procedure on all parts of the apparatus included a rinsing with helium prior to the final pumping. The control mechanism of the Crist valve permitted its use as a throttle to control the input of cadmium dimethyl vapor to the reaction cell. The pressure of the vapor was registered by the quartz spiral manometer. In taking the metal alkyl vapor from its reservoir in Dry Ice, the latter was partially removed and about one-third of the cadmium dimethyl melted. The Dry Ice was replaced freezing the liquid again and the system was pumped out to remove any ethane which might have formed. The alkyl was again melted and the vapor drawn into the reaction vessel. In runs using hydrogen a storage bulb was first filled to such a pressure of hydrogen that on opening it to the reaction cell with its desired quota of cadmium dimethyl and establishing pressure equilibrium the correct fourfold dilution was achieved almost instantaneously. This was accomplished by a volume calibration of the various parts of the whole apparatus. By such a procedure the Crist valve on the reaction cell was opened to a relatively high pressure of hydrogen which swept rapidly into the cell and minimized the possibility of a change in the amount of cadmium dimethyl in the cell. After the warm-up period for the hydrogen had elapsed, irradiation of the system was begun by raising the shutters. Since only a fraction of a second was required for this operation the timing of the run was quite accurate.

On completion of a run the reaction cell was opened so that residual cadmium dimethyl would move over into a trap in Dry Ice. Although experiment showed this would take less than one minute, 15 minutes were allowed for its completion. During this period the furnace around the reaction cell was adjusted to 100° which was the temperature used for all the acetone photolysis runs made for the purpose of measuring the density of the cadmium deposit. The remaining gases were transferred by a Toepler pump to the portion of the manifold in contact with the spiral manometer, their pressure was measured and by a second Toepler they were transferred to the sample tube for analysis by the mass spectrometer. The residual cadmium dimethyl was then vaporized and its pressure measured. Knowledge of the volumes of the different parts of the system permitted conversion of these pressures into quantities of material.

In runs at different temperatures in order to maintain constant concentration of the cadmium dimethyl and of the hydrogen for all runs the loading pressures had to be adjusted which for the former could not exceed the vapor pressure at room temperature. A pressure of 20 mm. was used for runs at 50° increasing to 30 mm. for runs at 250°. Similarly the hydrogen pressure was varied from about 80 to 120 mm.

Acetone Photolysis.—Light intensity within the reaction cell was appraised by means of a standardized acetone vapor photolysis carried out in the reaction cell after each cadmium dimethyl photolysis. Diminution of the light intensity

(5) These analyses were made on the Baird Model B Infrared Spectrometer by Dr. R. D. Schultz through the courtesy of the Brookhaven National Labs., Upton, N. Y.

(6) R. H. Crist and F. B. Brown, *Ind. Eng. Chem., Anal. Ed.*, **11**, 396 (1939).

within the cell was proportional to the density of the cadmium deposit.

When all measurements after a cadmium dimethyl run had been completed the evacuated reaction cell was opened to the air and the cadmium deposit left in contact with air for 15 minutes at 100°. This treatment did not alter the appearance or apparent transparency of the cadmium deposit. Glazebrook and Pearson[7] have shown, however, that a trace of oxygen will remove the capacity of a metallic deposit to react with free radicals. The reaction cell was evacuated, the lamps again warmed up and acetone, first pumped out while frozen in liquid nitrogen, was warmed up to 0° and a pressure of 69.8 mm. loaded into the cell. After a 15-minute warm-up period, irradiation for 15 minutes was made and subsequently the total pressure of products and residual acetone was measured. A number of runs similarly made but using a freshly-cleaned cell containing a strip of cadmium metal which was not in the light path gave an average pressure increase of 17.4 mm. Using the reaction cell with the cadmium deposit from a cadmium dimethyl run a smaller pressure increase would be observed. The ratio of this latter to 17.4 mm. gave a relative measure of light intensity within the cell at the end of the cadmium dimethyl run as compared with that at the beginning.

After the acetone run the reaction cell was filled with helium and cut from the system. Cold nitric acid removed all visible cadmium and the cell was rinsed with water, washed out with acetone and then heated to about 80° and rinsed three times with hot concentrated nitric acid. At least six washings with distilled water completed the cleaning. The outer surface was washed in dilute soap solution and rinsed thoroughly before the cell was re-sealed to the apparatus.

Analysis.—Analysis of the product gases from the photolysis and pyrolysis runs was carried out on Consolidated Engineering Corporation mass spectrometers.[8]

Results

Photolysis of Cadmium Dimethyl Vapor.—The cadmium deposits in the photolysis runs were not mirror-like in the range 150 to 275° as they were at lower temperatures. At first glance the cell windows appeared almost clean but slight magnification showed bright silvery particles of cadmium, uniform in size covering about one quarter of the irradiated area.

The analytical results of the photolysis and several pyrolyses are shown in Table I. All measurements are reported in mm. of mercury at 27°. The quantities of products refer to the amounts produced by the photolysis alone, that is, the total amounts observed corrected for the amounts produced by pyrolysis. The acetone run results are reported as the light flux as described above. Zero light then indicates pyrolysis.

In the runs in presence of hydrogen the cadmium deposits were mirror-like at 50° and somewhat less so at 100°. At the higher temperatures the deposits were much more transparent. The deposits covered the entire surface of the cell although most of it was confined to the windows. On magnification many very small black particles could be seen interspersed among the cadmium beads. The results of the product analyses are given in Table II. Two pyrolysis times were necessary for the runs with hydrogen due to the preliminary heat treatment of 15 minutes for the cadmium dimethyl alone and 15 minutes more after the addition of the hydrogen.

The variation of the light flux with time at each temperature was found to be exponential in form expressible by an equation of the form $I = ae^{-bt} + c$ where I is the fractional light intensity at time t in minutes. The values of a, b and c for each type of run are listed in Table III.

TABLE I

PHOTOLYSIS OF CADMIUM DIMETHYL VAPOR

Time, min.	$CdMe_2$ res.	CH_4	C_2H_6	C_2H_4	C_3H_8	C_4	Light flux
			Temperature 150°				
0	17.50	..	...	..	..	..	1.00
.5	15.33	0.02	2.30	..	..	..	0.88
1.5	11.03	.06	6.53	..	..	..	.83
3.0	4.54	.06	12.50	..	..	..	.83
15.5	17.12	.06	0.01	..	..	..	.00
			Temperature 200°				
0	17.18	..	...	..	..	..	1.00
.5	15.20	0.04	2.31	..	..	..	0.83
1.5	10.42	.10	6.60	0.06	..	..	.80
2.5	6.58	.06	10.62	.05	..	..	.80
3.0	4.26	.18	12.86	..	..	..	.82
16.0	17.17	.11	0.01	..	..	..	.00
			Temperature 225°				
0	17.16	..	...	..	..	..	1.00
.5	14.62	0.05	2.51	0.02	..	..	0.82
1.5	10.26	.16	6.75	.08	..	..	.78
2.5	6.09	.20	10.64	.11	..	..	.77
15.0	17.22	.12	0.01	..	..	..	.00
15.5	16.83	.11	.01	..	..	..	.00
			Temperature 250°				
0	17.16	..	...	..	..	..	1.00
.5	14.50	0.18	2.44	0.19	0.04	..	0.83
1.5	9.09	.28	7.31	.06	.06	0.02	.77
2.5	5.62	.43	10.88	.12	.11	.03	.79
15.0	17.22	.20	0.03	..	..	..	.00
			Temperature 275°				
0	17.26	..	...	..	..	..	1.00
.5	13.92	0.24	3.19	0.07	0.03	0.01	0.84
1.5	7.53	.67	8.85	.16	.12	.04	.83
2.5	4.35	.85	12.37	.07	.23	.06	.78
15.5	16.83	.10	0.01	..	..	..	.00

Discussion of Results

The equations from data in Table III indicate that the light variation with time was comparable for all runs carried out above 100°. It thus became possible to estimate rates of formation of the products at zero time with fair certainty. These were obtained from plots of the ethane and methane produced as a function of time. The ethane plots were practically straight lines indicating ethane production to be independent of cadmium dimethyl concentration. The methane plots showed more curvature especially at the highest temperatures. In order to ensure comparability large scale plots of methane production were made and the initial slope was taken to include that portion of the curve from zero time to one quarter of a minute. The curve was linear in this range. The rate data thus measured are listed in Table IV.

The photolysis of cadmium dimethyl vapor alone produced ethane with smaller amounts of methane, ethylene, propane and butane. The analysis was reliable above 150° for all products except ethylene. Thermochemical data indicate[9] that the energy of removal of both methyl radicals from the cadmium in the cadmium dimethyl molecule amounts to about 63 kcal. per mole. Since absorption of light of 2537 Å. wave length corresponds to an energy of 112 kcal. per mole, it is energetically possible for both methyl radicals to be freed by the initial absorption. The following mechanism is suggested

(7) H. H. Glazebrook and T. G. Pearson, *J. Chem. Soc.*, 567 (1937).

(8) Two-thirds of the analyses were obtained through the courtesy of the M. W. Kellogg Company of New Jersey; one-third through the Mass Spectrometer Analytical Service of the Consolidated Engineering Corporation, Pasadena, Calif.

(9) L. H. Long and R. W. G. Norrish, *Phil. Trans.*, **A241**, 587 (1948).

TABLE II

PHOTOLYSIS OF CADMIUM DIMETHYL AND HYDROGEN

Time, min.	$CdMe_2$ res.	H_2	CH_4	C_2H_6	Light flux
		Temperature 50°			
0	17.56	73.2	..	...	1.00
.5	16.06	69.2	0.15	1.56	0.78
1.5	14.06	72.6	.14	3.26	.51
3.0	11.17	73.0	.14	6.25	.31
6.0	8.10	73.2	.07	9.34	.20
15.0	.17	71.2	.14	17.10	.22
		Temperature 100°			
0	17.53	73.6	..	...	1.00
.5	15.71	73.8	0.07	1.80	0.76
1.5	12.52	73.7	.08	4.47	.66
3.0	9.26	74.2	.14	7.77	.53
6.0	2.56	71.0	.53	15.47	.47
		Temperature 150°			
0	17.50	74.1	..	...	1.00
.5	15.23	73.7	0.07	2.21	0.83
1.5	11.68	73.9	.14	5.09	.78
3.0	5.74	73.0	.39	11.50	.74
4.5	1.04	73.1	.64	16.78	.77
15–15	17.16	73.6	.16	...	.00
		Temperature 200°			
0	17.18	73.1	..	...	1.00
.5	14.90	72.3	.72	2.20	.83
1.5	10.43	71.5	1.28	6.44	.81
3.0	4.40	71.0	2.21	11.96	.75
4.0	.19	70.1	3.06	16.55	.80
15–15	16.47	73.5	.36	.03	.00
15–20	17.12	71.6	.51	.03	.00
		Temperature 225°			
0	17.16	73.3	..	...	1.00
.5	13.55	71.8	1.06	2.43	.87
1.5	9.10	71.5	1.93	6.39	.80
2.5	4.52	70.7	4.12	10.24	.80
22–15	16.66	73.5	1.00	.11	.00
		Temperature 250°			
0	17.16	73.3	..	...	1.00
.5	12.13	71.4	1.94	2.90	.88
1.0	8.64	69.5	4.69	4.92	.85
1.5	6.78	69.3	4.73	6.47	.83
2.5	1.61	66.2	8.98	10.59	.78
16.5–15.5	15.46	71.8	2.65	.42	.00
16.5–18	14.90	72.6	3.13	.45	.00

TABLE III

FRACTIONAL LIGHT INTENSITY $I = ae^{-bt} + c$

Temp., °C.	a	b	c
	Cadmium Dimethyl		
150	0.17	2.5	0.83
200	.20	2.8	.80
225	.23	2.9	.77
250	.22	3.0	.78
275	.22	2.6	.78
	Cadmium Dimethyl and Hydrogen		
50	0.80	0.66	0.20
100	.54	0.70	.46
150	.25	1.6	.75
200	.22	2.8	.78
225	.20	2.1	.80
250	.20	1.4	.80

TABLE IV[a]

RATE DATA AND ACTIVATION ENERGIES

Temp., °C.	$CdMe_2$ R_M	$CdMe_2$ R_E	$CdMe_2 + H_2$ R_M	$CdMe_2 + H_2$ R_E
50	..	..	..	3.2
100	..	..	..	3.8
150	..	4.8	.15	4.3
200	0.085	4.9	1.2	4.4
225	.14	5.7	1.8	5.0
250	.39	6.2	4.0	6.1
275	.76	7.8	..	..
	$E_M - 1/2E_E =$ 14 ± 2 kcal.		$E_M - 1/2E_E =$ 13 ± 2 kcal.	

[a] R_M and R_E represent rates of production of methane and ethane, respectively, in mm. (at 27°) per min. E_M and E_E represent similarly the activation energies.

as the simplest for the photolysis as here observed

$$Cd(CH_3)_2 + h\nu = 2CH_3 + Cd \quad (1)$$

$$2CH_3 = C_2H_6 \quad (2)$$

$$CH_3 + Cd(CH_3)_2 = CH_4 + CH_2 + Cd + CH_3 \quad (3)$$

The small amounts of ethylene, propane and butane may result from the methylene radicals by association with themselves or with methyl radicals to give ethyl radicals.

The Arrhenius plot of ethane production at temperatures above 150° from both cadmium dimethyl alone as also in presence of hydrogen is not linear, suggesting a constantly increasing energy of activation with increase in temperature. Since ethane production is relatively high at low temperatures and appears to be temperature independent the variation at higher temperatures must be due to variation in the concentration of methyl radicals, increasing with increase in temperature. Evidence has recently been presented[10] that reaction (2) has zero energy of activation. An alternative reaction producing ethane might be

$$CH_3 + Cd(CH_3)_2 = C_2H_6 + Cd + CH_3 \quad (4)$$

It was pointed out above, however, that ethane production is independent of the concentration of cadmium dimethyl and the contribution of reaction (4), if any, cannot be large.

This variation in methyl radical concentration with temperature must be taken into account in calculating the energy of activation of methane formation. Since the rate of ethane production is given by $R_E = k_2[CH_3]^2$ and of methane by $R_M = k_3[CH_3][Cd(CH_3)_2]$, eliminating the radical concentration gives $R_M/R_E^{1/2}$ proportional at a given cadmium dimethyl concentration to $k_3/k_2^{1/2}$ and the slope of an Arrhenius plot of $R_M/R_E^{1/2}$ should give the value of $E_3 - {}^1/_2 E_2$. As shown in Table IV the value found is 14 ± 2 kcal.

The fourfold dilution with hydrogen results in about a twelve-fold increase in the rate of methane production although the rate of ethane production remains virtually unchanged from that with the cadmium alkyl alone. The presence of hydrogen reduces the number of gaseous products to two, methane and ethane. The methane analysis was reliable for the runs above 150° where the dilution of the products by the hydrogen had less effect. The consumption of hydrogen necessarily lacks

(10) R. Gomer and G. B. Kistiakowsky, *J. Chem. Phys.*, **19**, 85 (1951).

precision, being the difference of two large quantities. At the highest temperature with the largest amounts of methane produced it would seem that the total methane produced is approximately twice the hydrogen consumed. This suggests the following additional reactions when hydrogen is present in excess, to those occurring in its absence

$$CH_3 + H_2 = CH_4 + H \qquad (5)$$
$$H + Cd(CH_3)_2 = CH_4 + Cd + CH_3 \qquad (6)$$

Application of the usual steady state consideration shows that at a given hydrogen concentration $R_M/R_E^{1/2}$ is proportional to $k_5/k_2^{1/2}$ and the slope of an Arrhenius plot should give the value of $E_5 - {}^1/_2 E_2$. The value found is 13 ± 2 kcal.

If the value of E_2 is taken as zero, the energy of activation of (5) is 13 ± 2 kcal. This agrees well with that calculated from the reverse reaction

$$H + CH_4 = CH_3 + H_2 \qquad E = 11 \pm 2^{11,12}$$

which reaction is 2 ± 1 kcal. exothermal since

$$CH_4 = CH_3 + H \qquad H = 101 \pm 1^{13}$$

and

$$H_2 = 2H \qquad H = 103.3^{14}$$

Therefore reaction (5) should be endothermal by 2 ± 1 and the energy of activation equal to 13 ± 3 kcal.

Since the energy of removal of two methyl radicals from cadmium dimethyl is about 63 kcal., whereas the comparable value for mercury dimethyl is 31 kcal.,[9] the "hot" radical effect should be less than that observed in mercury dimethyl.[15] The data of the latter research indicate no hot methyl effect above 150°. In the present research no such effect was observed above 100°.

A further significant difference exists between the photolyses of cadmium dimethyl and mercury dimethyl. In the former case the cadmium set free is deposited on the walls of the reaction vessel at all temperatures. Any back reaction with products must be of a heterogeneous nature. With mercury dimethyl at low temperatures most of the mercury from the decomposition is deposited on the walls but at higher temperatures the mercury exists almost exclusively as a vapor and any back reactions with products may proceed homogeneously. This may in part account for the lower activation energy value 9 ± 2 found from the photolysis of mercury dimethyl in presence of excess hydrogen (3) which has been assigned to reaction (5) and has caused conflict between the activation energies of (5) and its reverse and the strength of the C–H bond in methane. The above value of 13 ± 2 is consistent.

On the same assumption that E_2 is zero, the value of E_3 becomes 14 ± 2 kcal. Although the average deviation of ±2 appears to be the same from the treatment of the data as for E_5 it should be observed that the rates of methane production in the absence of hydrogen are much slower and the precision of the result cannot be as high. In comparison with hydrogen abstraction reactions, from paraffins,[16] the value seems high. However Cunningham and Taylor[3] found a value of 13 kcal. and Gomer and Noyes[17] a value of 11 kcal. for methane formation from mercury dimethyl. A somewhat higher value from cadmium dimethyl is not unreasonable.

(11) E. W. R. Steacie, B. de B. Darwent and W. R. Trost, *Discussion Faraday Soc.*, **2**, 80 (1947).

(12) M. G. Evans and M. Szwarc, *Trans. Faraday Soc.*, **45**, 940 (1949).

(13) M. Szwarc, *Chem. Revs.*, **47**, 75 (1950).

(14) A. G. Gaydon, *Proc. Phys. Soc.*, **58**, 525 (1946).

(15) M. K. Phibbs and B. de B. Darwent, *Trans. Faraday Soc.*, **45**, 541 (1949).

(16) A. F. Trotman-Dickenson, J. R. Birchard and E. W. R. Steacie, *J. Chem. Phys.*, **19**, 163 (1951).

(17) R. Gomer and W. A. Noyes, Jr., *J. Am. Chem. Soc.*, **71**, 3390 (1949).

THE HYDROGEN BOND IN ORGANIC CRYSTALS[1]

BY JERRY DONOHUE

Gates and Crellin Laboratories of Chemistry, California Institute of Technology, Pasadena, California[2]

Received June 25, 1951

The results of crystal structure investigations on organic crystals containing various types of hydrogen bonds have been collected together. These types are N–H· · ·N, N–H· · ·Cl, N–H· · ·O, O–H· · ·N, and O–H· · ·O. The lengths and strengths of these bonds are found to vary in a reasonable way with the departure of the angle C–XH· · ·X from the expected near-tetrahedral value, and with the situation of the donor and acceptor atoms. In general, strong hydrogen bonding occurs only when the hydrogen atom is collinear with the bonded atoms. Several proposed structures of the polypeptide chain in proteins, presumed to contain N–H· · ·O bonds, are examined on the basis of the characteristics found for this bond.

Introduction

The purpose of this review is to gather together the information which has thus far (*i.e.*, to about Feb., 1951) been obtained concerning hydrogen bonds in organic crystals. Inasmuch as deductions and generalizations about hydrogen bonds require that the crystallographic data be as accurate as possible, no attempt has been made to include the results on all crystals in which hydrogen bonds are presumed to be present; rather only the results of those X-ray investigations which in the opinion of the original authors, or others, yield interatomic distances accurate to 0.1 Å. or better. It is an unfortunate truth that many X-ray crystallographers have a tendency to overestimate the accuracy of their work, and it is still more unfortunate that there are in the literature a host of crystal structure investigations which are essentially incomplete because the authors neglected to refine the parameters defining the atomic positions to a degree warranted by their data. As will be seen, such inac-

(1) Presented as part of a symposium on "Hydrogen Bonds" at the Cleveland Meeting of the American Chemical Society, April 8–12, 1951.

(2) Contribution No. 1610.

curate or incomplete results are of little or no value in a discussion of the hydrogen bond. There are a large number of careful determinations which have been carried out, and it is on these that this paper is based. The results of structure determinations of a few inorganic substances have been included because of their obvious relation to the other results. The number of review articles on the hydrogen bond is now quite large. Since many of these concern themselves with aspects other than ours, no attempt has been made to include reference to them all in the present report.

As far as organic crystals are concerned there are five different kinds of hydrogen bonds which are important. These are: N–H· · ·N, N–H· · ·Cl, N–H· · ·O, O–H· · ·N, O–H· · ·O. We use here the conventional symbolism of the dash for a covalent bond, and the dots for the longer, electrostatic, contact with the acceptor atom. Information and discussion about these various kinds of bonds will be presented in the order in which they are listed above.

N–H· · ·N Bonds.—There are rather few crystals which have been investigated in which this kind of bond is present, it being of infrequent occurrence because of its relative weakness. Data on N–H· · · N bonds are collected in Table I.

Special mention should be made here of two cases which were formerly stated to be examples of N–H· · ·N bonding, but which, with our present knowledge, can be classified as simple van der Waals contacts. The first of these is a nitrogen–nitrogen contact of 3.15 Å. in dicyandiamide.[3] The following hydrogen bond scheme was assigned to this molecule

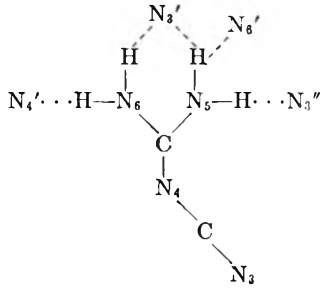

where the contacts $N_5 \cdots N_3'$ and $N_5 \cdots N_6'$ were considered to be an example of a bifurcated hydrogen bond. A quite serious objection to this interpretation is the fact that, while the atoms N_3', N_3'' and N_4' lie very nearly in the plane of the molecule, atom N_6' lies over 3 Å. below it. Since this molecule is a resonance hybrid, consisting mainly of the structures

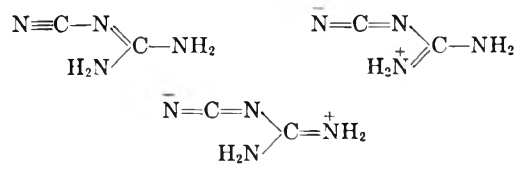

the entire molecule, including the hydrogen atoms, should be approximately planar. It is thus unlikely that the hydrogen atom on N_5 would be situated favorably for making contact with N_6'. A second objection is the principle that bifurcated hydrogen bonds occur rarely, if at all.[11,12] Elimination of this contact as a hydrogen bond leaves the very satisfactory picture of each $-NH_2$ group forming two, and only two, hydrogen bonds.

(3) E. W. Hughes, *J. Am. Chem. Soc.*, **62**, 1258 (1940).

TABLE I

DATA ON N–H· · ·N BONDS

Compound	N–H· · ·N, Å.	<X–N· · ·N	Reference
Adenine·HCl·$^1/_2H_2O$	2.99	134°	4
2-Amino-4,6-dichloro-	3.2	115	5
pyrimidine	3.37	127	
4-Amino-2,6-dichloro-	3.09	116	6
pyrimidine	3.28	107	
Ammonium azide	2.94		7
	2.99		
Dicyandiamide	2.94	120	3
	3.02	98	
	3.04	146	
	3.16	91	
Hexamethylene-			
diamine	3.21	107	8
Hydrazine	3.19	114	9
	3.30	132	
Melamine	3.00	136	10
	3.02	98	
	3.05	92	
	3.10	112	

A second example of a close N· · ·N contact formerly considered to be a hydrogen bond is an *intramolecular* one in phthalocyanine.[13]

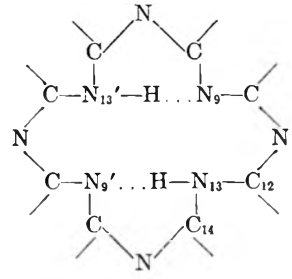

The contact $N_9' \cdots N_{13}$ of 2.65 Å. has frequently been cited as an example of an N–H· · ·N bond[14–16] but this is clearly impossible, for, if the hydrogen atom is assumed to lie on a line joining N_9' and N_{13}, the bond angles would then be $C_{14}–N_{13}–H = 82°$ and $C_{12}–N_{13}–H = 170°$, whereas these two angles would be expected to be equal or nearly so. Furthermore, this interpretation leaves the short $N_9' \cdots N_{13}$ distance of 2.76 Å. unexplained. Rather,

(4) J. M. Broomhead, *Acta Cryst.*, **1**, 324 (1948).
(5) C. J. B. Clews and W. Cochran, *ibid.*, **1**, 4 (1948).
(6) C. J. B. Clews and W. Cochran, *ibid.*, **2**, 46 (1949).
(7) L. K. Frevel, *Z. Krist.*, **94**, 197 (1936).
(8) W. P. Binnie and J. M. Robertson, *Acta Cryst.*, **3**, 424 (1950).
(9) R. L. Collin and W. N. Lipscomb, *ibid.*, **4**, 10 (1951).
(10) E. W. Hughes, *J. Am. Chem. Soc.*, **63**, 1737 (1941).
(11) L. Pauling, "The Nature of the Chemical Bond," 2nd. Ed., Cornell University Press, Ithaca, N. Y., 1940, p. 286.
(12) A. F. Wells, *Acta Cryst.*, **2**, 128 (1949).
(13) J. M. Robertson, *J. Chem. Soc.*, 1195 (1936).
(14) M. Huggins, THIS JOURNAL, **40**, 723 (1936); *J. Org. Chem.*, **1**, 407 (1937).
(15) L. Hunter, *Annual Reports of the Progress of Chem.*, 141 (1946).
(16) Y. K. Syrkin and M. E. Dyatkina, "Structure of Molecules and the Chemical Bond," Interscience Publishers, Inc., New York, N. Y., 1950, p. 273.

there is plenty of room in the center of the molecule to place the two hydrogen atoms with only slight deformations of the normal bond angles. Moreover, although these distances are considerably shorter than normal van der Waals contacts, the usual radii do not, of course, apply with rigor to intramolecular distances in a closed system such as this. For example, the diagonal C· · ·C distance in cyclobutane is about 2.2 Å., far less than a "normal" van der Waals contact.

An example of the type of information which may be obtained by a consideration of the hydrogen bonding scheme in a crystal is found in melamine, for which Hughes[10] demonstrated that the molecule has the structure A rather than B.

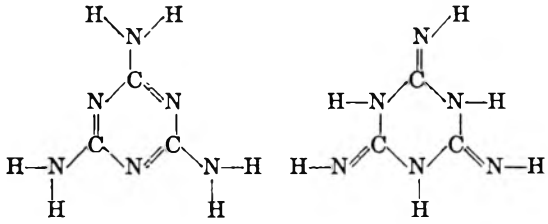

A B

It is interesting to note that in this crystal only four of the six hydrogen atoms are used in hydrogen bond formation. A somewhat similar situation occurs in hexamethylenediamine, where only two of the four hydrogen atoms are used. This situation is probably due to the relatively low energy of the N–H· · ·N bond.

In the case of adenine hydrochloride hemihydrate, Broomhead states[4]: "Unfortunately the results reported above are not sufficiently accurate for reliable conclusions to be drawn about the hydrogen positions." With reference to the X-ray data and electron density plots this is certainly true. There are, on the other hand, several interesting conclusions which may be reached by a simple consideration of the intermolecular hydrogen bonding scheme in the crystal. The chemical formula of adenine is usually written in one of two ways

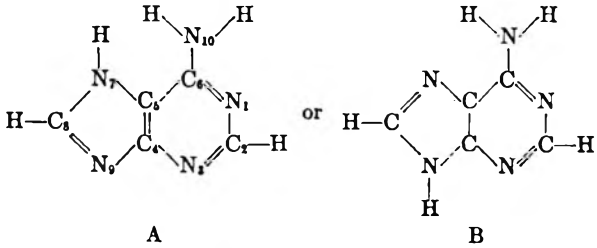

A B

where the usual benzene type resonance in the pyrimidine ring gives each of these tautomers two resonance structures. (There are two other tautomeric forms in which a hydrogen atom is bonded to N_1 and N_3, respectively, there being none on N_7 or N_9; these forms do not have two resonance structures as do A and B, and appear usually to be ignored. Structures in which N_{10} is part of an imino rather than an amino group are likewise ignored.) In crystals containing adenine molecules we should expect to find either form A or form B, whichever is the more stable. In addition, when adenine combines with hydrochloric acid, it must be assumed that another hydrogen atom is added to one of the four nitrogen atoms, and there is no *a priori* way of predicting to which one it goes.

Examination of the results of the crystal structure investigation show that one molecule makes the following short intermolecular contacts with its neighbors

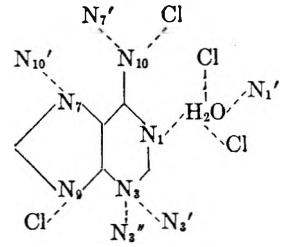

It is obvious at the outset that not all of these short distances indicate hydrogen bonds, since there are ten such distances and we have, in the group of atoms shown, only eight hydrogen atoms available for hydrogen bond formation. However, we may eliminate the possibility of hydrogen bond formation between N_3 and $N_{3''}$ for the following reason: a hydrogen bond formed by N_3 would be expected to be coplanar with the adenine molecule, whereas atom $N_{3''}$ lies almost 2 Å. above this plane; similarly, the possibility of hydrogen bond formation between N_3 and $N_{3'}$ may be eliminated because, although $N_{3'}$ lies very nearly in the plane of the molecule, the angles C_4–N_3· · ·$N_{3'}$ and C_2–N_3· · ·$N_{3'}$ are 161 and 85°, respectively, and hence quite unfavorable for satisfactory hydrogen bond formation. Moreover, the distances N_3· · ·$N_{3'}$ and N_3· · ·$N_{3''}$, *viz.*, 3.17 and 3.23 Å. are the longest of the short N· · ·N contacts, and are quite comparable to normal van der Waals contacts of 3.20 Å. and longer which have been observed in melamine.[10]

In order to assign positions to the hydrogen atoms, we need make only the very reasonable assumption that none of the hydrogen atoms is covalently bonded to chlorine. Immediately this places hydrogen atoms on N_9 and N_{10}. Since both hydrogen atoms of the water molecule must be used in forming O–H · · · Cl bonds, there must be a hydrogen atom bonded to N_1. The placement of a hydrogen atom on N_9 requires the molecule to have structure B, hence in the contact N_7 · · · N_{10}, the hydrogen atom must be bonded to N_{10}. Strong confirmation of the assignment of structure B is afforded by a comparison of the bond distances C_8–N_7 and C_8–N_9, which are 1.28 and 1.37 Å., respectively, indicating a quite large degree of double bond character in the C_8–N_7 bond. The adenine ion may thus be considered to be a resonance hybrid of the forms

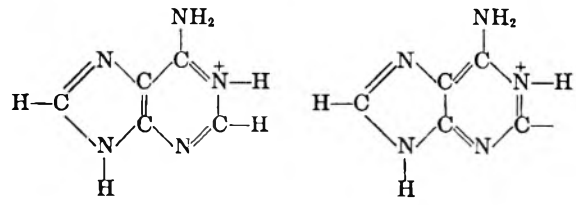

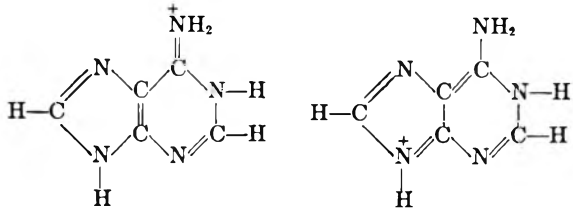

Unfortunately it is not possible to make a quantitative treatment of the contributions of each of these forms, for example, as was done for isatin by Goldschmidt and Llewellyn,[17] or to determine whether any of various other forms is significant because of the relatively large experimental errors in the interatomic distances, this structure having been determined by projection methods alone.[18]

N–H···Cl Bonds.—The N–H···Cl hydrogen bond occurs in the chloride salts of organic bases. Data for it are collected in Table II.

A rather common phenomenon in crystals which contain $-NH_3^+$ groups and Cl^- ions is, in addition to three short N···Cl distances, which may be ascribed to hydrogen bond formation,[19] a short contact with a fourth chloride ion which is generally situated on the extension of the X–N covalent bond, so that the angle X–N···Cl_4 is near 180°. Examples of this are found in hexamethylenetetramine·2HCl, with N···Cl_4 = 3.37 Å., ∠C–N···Cl_4 = 164°, hydrazine·2HCl, with N···Cl_4 = 3.10

TABLE II

DATA ON N–H···Cl BONDS

Compound	N–H···Cl	X–N···Cl	Reference
Adenine·HCl·$^1/_2H_2O$	3.11	116°, 135°	4
	3.21	139	
Hexamethylenediamine·2HCl	3.15[a]	104	21
	3.25[a]	104	
	3.25	98	
	3.01[a]	128	
	3.07[a]	115	
	3.33[a]	88	
Hydrazine·2HCl	3.10	100	22
Hydroxylamine·HCl[a]	3.16	99	23
	3.23	90	
	3.26	95	
Geranylamine·HCl	3.17	101	24
	3.22	102	
	3.22	102	
m-Tolidine·2HCl	3.10	108	25
	3.22	105	
	3.26	101	

[a] These values differ significantly from those published. The values quoted in the Table were recalculated using the published parameters and cell constants. The value N–O = 1.47 Å. in hydroxylamine·HCl is obtained (instead of 1.45 Å.) if one uses the parameters and cell constants given by Jerslev (taking the value *y* for nitrogen = 0.664, as on p. 24, rather than the value of 0.644 on p. 25). The N–O distance in the hydroxylammonium ion is thus equal, within the limits of error, to the N–N and O–O distances in hydrazine and hydrogen peroxide, respectively (unless both values of *y* are topographical errors).

TABLE III

DATA ON N–H···O BONDS

Compound	N–H···O, Å.	<X–N···O	Reference
Acetamide	2.83	127°	26
	2.99	128	
Acetylglycine	3.03	132	27
Adenine·HCl·$^1/_2H_2O$	2.87		4
DL-Alanine	2.80	105	28,
	2.84	103	29
	2.88	116	
Cytidine	2.93	142	30
	3.00	137	
Diketopiperazine	2.85		31
Glycylglycine	2.68	100	32
	2.80	115	
	2.81	99	
	3.07	131	
Hydroxy-L-proline	2.69	102, 113	33
	3.17	81, 133	
Isatin	2.93		17
p-Nitroaniline	3.07	144	34
	3.11	119	
DL-Serine	2.79	99	35
	2.81	98	
	2.87	121	
L-Threonine	2.80	98	36
	2.90	116	
	3.10	132	
Urea	2.99	98	37
	3.04	129	
Urea·H_2O_2	2.94	132	38
	3.04	112	
Urea oxalate	2.89	118	39
	2.97	117	
	3.00	108	
	3.14	130	

(17) G. H. Goldschmidt and F. J. Llewellyn, *Acta Cryst.*, **3**, 294 (1950).

(18) (Added July 20, 1951). In a very careful reinvestigation of adenine hydrochloride hemihydrate, W. Cochran (*Acta Cryst.*, **4**, 81 (1951)) has recently found good evidence for the hydrogen atoms in the electron density plots. The positions he found are identical with those deduced here.

(19) There is a rather remarkable statement by Wells[20] that Cl^- is incapable of entering into hydrogen bond formation. This is certainly not in accord with the structural features of the crystals referred to in this section.

(20) A. F. Wells, "Structural Inorganic Chemistry," 2nd Ed., Oxford University Press, Oxford, 1950, p. 247.

(21) W. P. Binnie and J. M. Robertson, *Acta Cryst.*, **2**, 180 (1949).

(22) J. Donohue and W. N. Lipscomb, *J. Chem. Phys.*, **15**, 115 (1947).

(23) B. Jerslev, *Acta Cryst.*, **1**, 21 (1948).

(24) G. A. Jeffrey, *Proc. Roy. Soc. (London)*, **A183**, 388 (1945).

(25) F. Fowweather and A. Hargreaves, *Acta Cryst.*, **3**, 81 (1950).

(26) F. Senti and D. Harker, *J. Am. Chem. Soc.*, **62**, 2008 (1940).

(27) G. B. Carpenter and J. Donohue, *ibid.*, **72**, 2315 (1950).

(28) H. A. Levy and R. B. Corey, *ibid.*, **63**, 2095 (1941).

(29) J. Donohue, *ibid.*, **72**, 949 (1950).

(30) S. Furberg, *Acta Cryst.*, **3**, 325 (1950).

(31) R. B. Corey, *J. Am. Chem. Soc.*, **60**, 1598 (1938).

(32) E. W. Hughes and W. J. Moore, *ibid.*, **71**, 2618 (1949).

(33) J. Donohue and K. N. Trueblood, to be published.

(34) S. C. Abrahams and J. M. Robertson, *Acta Cryst.*, **1**, 252 (1948).

(35) R. B. Barieau, D. P. Shoemaker, J. Donohue and C. S. Lu, to be published.

(36) D. P. Shoemaker, J. Donohue, V. Schomaker and R. B. Corey, *J. Am. Chem. Soc.*, **72**, 2328 (1950).

(37) R. W. G. Wyckoff and R. B. Corey, *Z. Krist.*, **89**, 462 (1934); P. A. Vaughan and J. Donohue, to be published.

(38) C. S. Lu, E. W. Hughes and P. A. Giguère, *J. Am. Chem. Soc.*, **63**, 1507 (1941).

(39) A. F. Schuch, L. Merritt and J. H. Sturdivant, to be published.

Å., ∠N–N···Cl_4 = 180°, hydroxylamine·HCl, with N···Cl_4 = 3.21 Å., ∠O–N···Cl_4 = 167°, geranylamine, with N···Cl_4 = 3.24 Å., ∠C–N···Cl_4 = 170°, and *m*-tolidine·2HCl with N···Cl_4 = 3.26 Å., ∠C–N···Cl_4 = 148°. This feature of these structures is probably due in large part to the large size of the chloride ions, the packing of which dominates the structures.

N–H···O Bonds.—The N–H···O bond is of rather frequent occurrence. Data concerning it are collected in Table III.

As might be expected there appears to be a definite correlation between the length of the bond and the angle X–N···O. This correlation is illustrated in Fig. 1, where the data for the compounds which contain $-NH_3^+$ groups are plotted. The amides do not appear to fit into this scheme, probably because other effects, such as the situation of the atom accepting the bond, have been neglected.

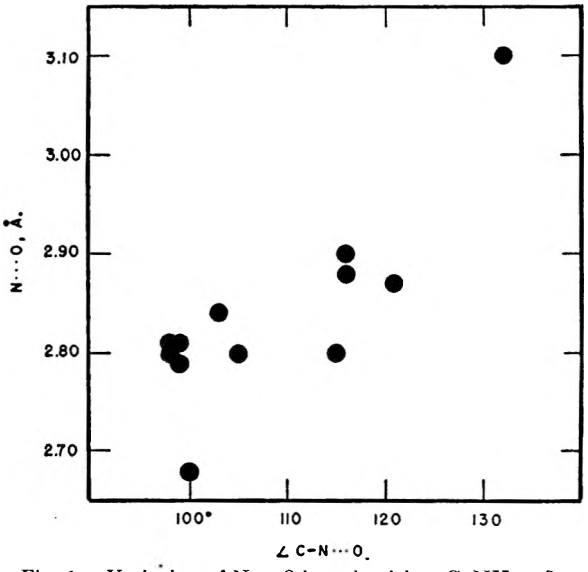

Fig. 1.—Variation of N···O length with <C-NH···O.

A second, and very important, observation to be made, is with reference to the structures of the amides and imides, to wit, glycylglycine, acetylglycine, urea, urea oxalate, acetamide, urea·H_2O_2 and isatin. These compounds have the common structural feature

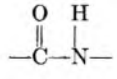

and in all of them we find that: (1) the C–N distance is in the range 1.29–1.38 Å. considerably shorter than the single bond distance of 1.47 Å. found in amines, and (2) the three bonds around the nitrogen atom are coplanar. Thus, for example, in the peptides the grouping

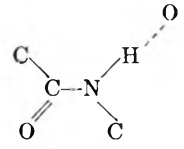

lies in one plane, and in urea and its complexes, the entire grouping

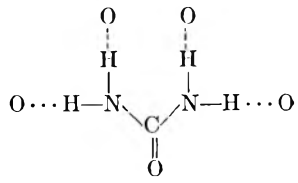

is coplanar. This observation is scarcely surprising, and the observed structural features are due to the contribution of the structure

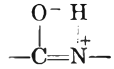

This fact has been known for some time, but, it is worth emphasizing it because of the restrictions it places on the position of the acceptor atom of the hydrogen bond from the nitrogen atom.

O–H···N Bonds.—There are but two known examples of bonds of the type O–H···N. It is necessarily of infrequent occurrence, because O–H···O bonds are preferentially formed when possible. Data are presented in Table IV.

There is apparently no significant difference between the lengths of O–H···N and N–H···O bonds.

O–H···N Bonds.—The first question to be discussed in connection with a hydrogen bond between two oxygen atoms is whether this bond ever assumes the symmetrical configuration, *i.e.*, O–H–O with both O–H bonds of equal strength and the hydrogen atom equidistant from the two oxygen atoms. An energy curve of the modified Morse type given by Huggins[14] would seem to indicate that for oxygen–oxygen distances of less than about 2.65 Å. there is no double minimum, and the bond is symmetrical. Evidence against this conclusion is reviewed by Davies,[40] the most convincing of which is the excess entropy, impossible for a symmetrical bond, of various inorganic salts which contain hydrogen bonds, *e.g.*, KH_2PO_4, in which O···O = 2.54 Å. Since the symmetrical bond is expected to occur for distances *shorter* than an as yet unknown value, it is safe to conclude that all O–H···O bonds with O···O > 2.54 Å. are unsymmetrical. Additional evidence of a more indirect nature is found in the work of Westrum and Pitzer,[41] who showed that in KHF_2, the hydrogen atom in the HF_2^- ion was symmetrically located. Now, the observed F···F distance in this ion is 2.26 Å.[42]; the single bond covalent distance observed in gaseous HF

TABLE IV

DATA ON O–H···N BONDS

Compound	O–H···N, Å.	<X–O···N	Reference
Cytidine	2.87	111°	30
4,6-Dimethyl-2-hydroxypyrimidine	2.78 2.89		43

is 0.92 Å. The fluorine–fluorine distance in HF_2^- is therefore expected to be twice 0.92, −4 (0.300 log $^1/_2$) = 2.20 Å., on the basis of Pauling's relation[44]

(40) M. Davies, *Annual Reports of the Progress of Chem.*, 5 (1946).
(41) E. Westrum and K. Pitzer, *J. Am. Chem. Soc.*, **71**, 1940 (1949).
(42) L. Helmholz and M. Rogers, *ibid.*, **61**, 2590 (1939).
(43) G. J. Pitt, *Acta Cryst.*, **1**, 168 (1948).
(44) L. Pauling, *J. Am. Chem. Soc.*, **69**, 542 (1947).

TABLE V

DATA ON O–H · · · O BONDS FROM CARBOXYL GROUPS

Compound	O_1–H · · · O, Å.	Acceptor oxygen in	Dimensions of donor carboxyl group[a]		Reference
Acetylene dicarboxylic acid·$2H_2O$	2.56	Water	1.26 (117°)	1.26 (120°)	46
Acetylglycine	2.56	Carbonyl	1.31 (112)	1.19 (124)	27
Adipic acid	2.68	Carboxyl	1.29 (114)	1.23 (120)	47a
Diacetylene dicarboxylic acid·$2H_2O$	2.55	Water	1.25 (120)	1.25 (117)	47
Glutaric acid	2.69	Carboxyl	1.30 (115)	1.23 (123)	48
Oxalic acid·$2H_2O$	2.50	Water	1.24 (119)	1.25 (116)	45
Sebacic acid	2.68	Carboxyl	1.27 (116)	1.24 (120)	49
Succinic acid	2.64	Carboxyl	1.30 (114)	1.25 (124)	50
Urea oxalate	2.50	Carbonyl	1.29 (113)	1.22 (122)	39

[a] The dimensions are given as follows: C–O_1 (<C_α–C–O_1), C–O_2 (<C_α–C–O_2).

between bond radius and bond character, assuming, that in F–H–F the hydrogen atom is forming two half-bonds. The agreement between the observed and calculated values suggests that the relation should likewise hold for the symmetrical O–H–O case: the predicted oxygen–oxygen distance is then 2.30 Å. (twice 0.97 Å., the O–H distance in water, +0.36 Å. half-bond correction). No O–H–O bond as short as this has yet been observed. The shortest, with O · · · O = 2.50 Å., is found in urea oxalate, and there is good reason to believe that this is also an unsymmetrical bond, as discussed below. It is therefore assumed in the following discussion, that all of the O–H · · · O bonds as yet found are unsymmetrical. This is in agreement with recent work.[40,41]

In examining structures in which O–H · · · O bonds occur, it is convenient to divide these into several classes. The first such class includes hydrogen bonds from essentially un-ionized carboxyl groups. These are collected in Table V.

The inequality of the C–O distances and Cα–C–O angles in each carboxyl group immediately suggest that we have a predominance of the structure

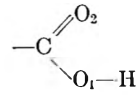

in each of these situations, as might be expected. The relative lengths of the various hydrogen bonds lead to the reasonable conclusion that the oxygen atom in either a water molecule or a carbonyl group is somewhat more electronegative than an oxygen-2 atom in a carboxyl group.

There is a possibility that in the dicarboxylic acid dihydrates the crystals consist, partly or wholly, of $R(COO^-)_2$ ions and H_3O^+ ions.[45] This type of structure is suggested by the rather more symmetrical carboxyl groups in these compounds. On the other hand, the observed results are also consistent with a greater contribution (relative to the other acids in Table V) of the structure

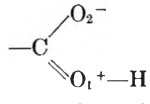

This structure is stabilized by the acceptance by O_2 of *two* hydrogen bonds.

The case of urea oxalate deserves special attention because this is the shortest O–H · · · O bond yet observed, and therefore the most likely one to be symmetrical. In this crystal, the short bond is between the carboxyl group and the oxygen of a urea molecule; now if the situation was symmetrical, then the structures usually written as contributing partially to the normal state of urea,[51] *viz.*

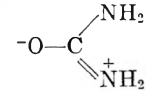

would be stabilized by the formation of the half-bond to the oxygen atom, and we would expect to find that in urea oxalate, the C–O distance would be significantly longer and the C–N distances shorter than the corresponding distances in urea itself. This, however, is not the case, the distances being

TABLE VI

DATA ON O–H · · · O BONDS FROM HYDROXYL GROUPS

Compound	O–H · · · O, Å.	Acceptor oxygen in	<X–O · · · O	Reference
Cytidine	2.74	Carboxyl	117°	30
	2.83	Hydroxyl	135	
4,6-Dimethyl-2-hydroxypyrimidine	2.75 or 2.93	Water	124 or 112	43
Hydrogen peroxide	2.78	Hydroxyl	97	52
	2.78	Hydroxyl	112	
Hydroxy-L-proline	2.80	Carboxyl	99	33
KH-bis-*p*-hydroxybenzoate	2.69	Hydroxyl		53
Pentaerythritol	2.69	Hydroxyl	90	54
Quinol·SO_2	2.75	Hydroxyl	107 or 115	55
	2.76	Hydroxyl	115 or 107	
α-Resorcinol	2.66	Hydroxyl	118 or 116	56
	2.75	Hydroxyl	117 or 131	
β-Resorcinol	2.70	Hydroxyl	118 or 118	57
	2.75	Hydroxyl	114 or 121	
DL-Serine	2.67	Carboxyl	107	35
L-Threonine	2.66	Carboxyl	120	36
Urea·H_2O_2	2.63	Hydroxyl	102	38

(45) J. D. Dunitz and J. M. Robertson, *J. Chem. Soc.*, 142 (1947).

(46) J. D. Dunitz and J. M. Robertson, *ibid.*, 148 (1947).

(47) J. D. Dunitz and J. M. Robertson, *ibid.*, 1145 (1947).

(47a) J. D. Morrison and J. M Robertson, *ibid.*, 987 (1949).

(48) J. D. Morrison and J. M. Robertson, *ibid.*, 1001 (1949).

(49) J. D. Morrison and J. M. Robertson, *ibid.*, 993 (1949).

(50) J. D. Morrison and J. M. Robertson, *ibid.*, 980 (1949)

(51) L. Pauling, "The Nature of the Chemical Bond," 2nd Ed., Cornell University Press, Ithaca, N. Y., 1950, p. 212.

(52) S. C. Abrahams, R. L. Collin and W. N. Lipscomb, *Acta Cryst.*, **4**, 15 (1951).

(53) J. Skinner and J. C. Speakman, *J. Chem. Soc.*, 185 (1951).

(54) F. J. Llewellyn, E. G. Cox and T. H. Goodwin, *ibid.*, 882 (1937).

(55) D. E. Palin and H. M. Powell, *ibid.*, 208 (1947).

(56) J. M. Robertson, *Proc. Roy. Soc.* (*London*), **A157**, 79 (1936).

(57) J. M. Robertson and A. R. Ubbelohde, *ibid.*, **A167**, 122 (1938).

C–O = 1.26 Å. in both crystals, and C–N = 1.34 and 1.35 A. in urea oxalate and 1.33 Å. in urea.

There are numerous examples of hydrogen bonds from hydroxyl groups. These are collected in Table VI.

There is here a rather wide variation in the lengths of these bonds, and there does not appear to be any obvious correlation of these lengths with other properties.

The third class of O–H···O bonds are those formed by water molecules. These are collected in Table VII.

TABLE VII

DATA ON O–H···O BONDS FROM WATER MOLECULES

Compound	O–H···O, Å.	∠O···O···O	Reference
Acetylene dicarboxylic acid·$2H_2O$	2.82 2.89	89°	46
Diacetylene dicarboxylic acid·$2H_2O$	2.83 2.90	87	47
4,6-Dimethyl-2-hydroxypyrimidine	2.73 2.75 or 2.93	117, 123 or 109, 120	43
Ice	2.76	109	
Oxalic acid·$2H_2O$	2.86 2.89	85	45
Sodium sesquicarbonate·$2H_2O$	2.72 2.77	120	58

These bonds are apparently longer than those of either of the other classes.

There remain a number of O–H···O bonds for which it is not possible to state or to deduce into which class they fall. These are collected in Table VIII.

TABLE VIII

MISCELLANEOUS O–H···O BONDS

Compound	O–H···O, Å.	Type	Reference
4,6-Dimethyl-2-hydroxypyrimidine	2.75	Water...hydroxyl	36
	2.93	Water...hydroxyl	
KH Bis-*p*-hydroxybenzoate	2.58	Water...hydroxyl	53
Tartaric acid[a]	2.74	Hydroxyl...carboxyl	59
	2.78	Hydroxyl...carboxyl	
	2.87	Hydroxyl...carboxyl	
	2.87	Carboxyl...carboxyl	

[a] The case of tartaric acid is discussed below.

There are three compounds in which a symmetrical hydrogen bond appears to be required by the symmetry of the crystal, *i.e.*, the two oxygen atoms involved are related by a center of symmetry. These are: sodium sesquicarbonate·$2H_2O$,[58] potassium hydrogen bis-phenylacetate,[60] and potassium hydrogen bis-*p*-hydroxybenzoate.[53] The O···O distances are 2.53, 2.55 and 2.61 Å., respectively. These are not short enough to correspond to the symmetrical case (see above), and, since hydrogen atoms are not located in the X-ray experiment, it is not valid to state that the bond is required to be symmetrical on crystallographic grounds. It is likely that these crystals have random structures—this conclusion could be checked by entropy measurements.[60a]

(58) C. J. Brown, H. S. Peiser and A. Turner-Jones, *Acta Cryst.*, **2**, 167 (1949).

(59) F. Stern and C. A. Beevers, *ibid.*, **3**, 341 (1950).

(60) J. C. Speakman, *J. Chem. Soc.*, 3357 (1949).

(60a) ADDED IN PROOF, Feb. 27, 1952.—In a recent paper M. Davies and W. J. O. Thomas (*J. Chem. Soc.*, 2858 (1951)) have shown that the infrared absorption spectrum of potassium hydrogen bis-phenylacetate does not support the suggestion that the hydrogen atom is located symmetrically, a conclusion in agreement with that given here.

Consideration of the structure of tartaric acid provides yet another example of the deductions which may be made on the basis of the known properties of hydrogen bonds. The close oxygen–oxygen contacts for one molecule of tartaric acid in the crystal were found to be

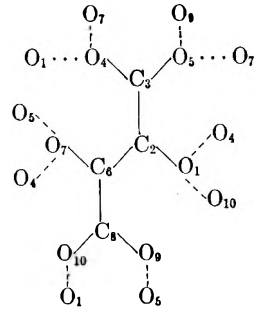

There are ten such contacts per molecule, but only eight hydrogen atoms are available for bond formation. Beevers and Stern mentioned that "the $O_1\cdots O_4$ bond is the most doubtful one because of its greater length," notwithstanding the fact that its length is equal, within the stated limits of error,[61] to those of the bonds $O_1\cdots O_{10}$ and $O_5\cdots O_9$. There is, however, a very good way of showing that the contact $O_1\cdots O_4$ is not a hydrogen bond, but a van der Waals contact (the $O_1\cdots O_4$ distance is 2.92 Å., slightly more than twice the usual van der Waals radius for oxygen). For, if this contact involves a hydrogen atom, then either the angle $O_4\cdots O_1$–C_2 or the angle C_3–$O_4\cdots O_1$ would be expected to be near the tetrahedral value, depending on to which oxygen atom the hydrogen atom is covalently bonded; the published parameters yield for these angles the values 175 and 172°, respectively, both far too large. It is now possible to assign positions for the hydrogen atoms, assuming that the remaining eight contacts are indeed hydrogen bonds (the eight angles lie, acceptably, between 107 and 136°). We start by assigning a hydrogen atom to O_{10} of the lower carboxyl group; this places a hydrogen atom on O_5, since the carboxyl group includes but one hydrogen atom. In the other carboxyl group then, there is no hydrogen atom on O_4, but one on O_7. But for the $O_5\cdots O_7$ bond, there must be a second one placed on O_7, of course an impossible situation. We therefore conclude that the original assumption is invalid. By going through analogous procedures, it is easily shown that there are only two possible arrangements for the hydrogen atoms.

It is interesting that no structure in which O_{10} covalently bonds a hydrogen atom is possible. The observed angles C_6–C_8–O_{10} = 128° and C_6–C_8–O_9 = 108° are in agreement with this conclusion; the distances (which may be in error by more than 0.05 Å.) are C_8–O_{10} = 1.17 Å. and C_8–O_9 = 1.20 Å. The angles in the carboxyl group at the other end of the molecule, C_2–C_3–O_5 = 125° and C_2–C_3–O_4 = 112° suggest that structure A is perhaps more important than structure B. The distances here are C_3–O_4 = 1.21 Å. and C_3–O_5 = 1.24 Å. Further refinement of the parameters is obviously needed in or-

(61) The limits of error stated by Stern and Beevers are ±0.05 Å. in a parameter and ±0.05 Å. for interatomic distance.

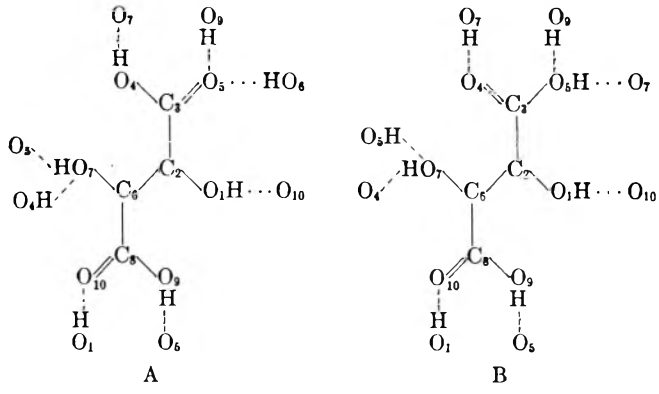

A B

der to make a thorough discussion of the structure possible.

Discussion

We are now in a position to make some general remarks concerning hydrogen bonding in organic crystals. With the exception of the weak N–H···N bond, examination of the structures of the crystals cited in the foregoing tables reveals the rather remarkable fact that only in very exceptional cases does a hydrogen atom bonded to nitrogen or oxygen occupy a position such that hydrogen bond formation is impossible. Thus in the case of the hydrochlorides of Table II, all three hydrogen atoms of the $-NH_3^+$ groups form N–H···Cl bonds. Some of these, naturally enough, are weaker than others, since in general it is sterically impossible to satisfy all requirements simultaneously. The same situation is true for the amino compounds of Table III. For example, in the case of the four amino acids which contain $-NH_3^+$ group, namely, alanine, glycylglycine, serine and threonine, all three hydrogen atoms are involved in N–H···O bonds. The longer, hence weaker, bonds are those for which the angles C–N···O deviate from the tetrahedral value, due to other requirements of the structure. Similarly, in urea, urea oxalate and urea·H_2O_2, all four hydrogen atoms of the urea molecules are involved in hydrogen bonds. For the crystals with O–H···O bonds we find that, even though the structures are considerably more complicated, especially in the case of the polyhydroxy compounds, it is exceedingly rare to find an "unused" hydrogen atom. One occurs, for example, in potassium hydrogen bis-*p*-hydroxybenzoate, but in not one of the other compounds of Tables V to VIII. A very striking example of the greater stability of a structure in which all possible hydrogen bonds are formed is found in the structure of glucose,[62] in which all five hydroxyl groups are involved in hydrogen bonds. It will be interesting, after this structure has been refined, to see whether any correlation exists between bond angles and bond strength, since in this molecule marked variation between the electronegativities of the oxygen atoms is not expected, and it is certainly variations in this property which obscure the first effect.

Proposed Structures of the Polypeptide Chain

The problem of the way in which amino acid residues combine to form the polypeptide chain of protein molecules has been the subject of a considerable amount of speculation. A large number of previously proposed structures have recently been collected and examined by Bragg, Kendrew and Perutz.[63] In addition, their paper includes descriptions of a number of models not previously proposed. Another recent paper, by Pauling, Corey and Branson,[64] proposes two models not discussed by Bragg, *et al.* We shall limit our discussion to the models described in these two papers.

The problem at hand is to construct models of

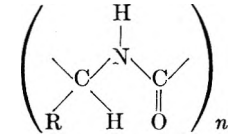

It is generally assumed that the chains have a screw axis of symmetry, as emphasized by Huggins.[65] In this way N–H groups in one residue may be brought into position to bond >C=O groups in another residue further along the chain. Bragg,[66] *et al.*, point out that the screw axis need not be of a crystallographically permissible type, *e.g.*, it may be a fivefold axis, but they make the tacit assumption that it must be integral. Several of the structures which they propose, and in particular those designated $2_{13}\cdot{}^1/_3$ and $2_{14}\cdot{}^1/_3$ (the former one originally suggested by Astbury and Bell[67]) may be looked upon with doubt because only one-third of the hydrogen atoms are involved in hydrogen bond formation, and thus violate the principle of maximum hydrogen bonding discussed above. It is not valid to argue, in this connection, that perhaps the unused hydrogen atoms are bonding solvent molecules, for it has been demonstrated by Pauling[68] that the initial water absorption by some proteins, at least, is correlated with the number of polar side chains from which fact it might be inferred that the >C=O and >N–H groups in the chain already are bonded to each other and thus are not available for solvent bonding. It is possible, on the other hand, that steric factors, such as the presence of prolyl residues, will prevent maximum hydrogen bonding in a chain.

Since this paper of Bragg, *et al.*, is the very first one in which numerical coördinates have been assigned to the atoms in the chain, it is possible for the first time to examine the various structures in a rather detailed manner in order to determine whether they conform to the important criteria for good hydrogen bond formation. Inspection of their figures shows that in the chains 2_{7a} (proposed

(62) T. McDonald and C. A. Beevers, *Acta Cryst.*, **3**, 394 (1950).

(63) W. L. Bragg, J. Kendrew and M. F. Perutz, *Proc. Roy. Soc. (London)*, **A203**, 321 (1950).

(64) L. Pauling, R. B. Corey and H. R. Branson, *Proc. Natl. Acad. Sci.*, **37**, 205 (1951).

(65) M. Huggins, *Chem. Revs.*, **32**, 195 (1943).

(66) We retain the notation of this paper. Each chain has a designation $S_R\cdot 1/q$, where S denotes the screw symmetry, R the number of members in the hydrogen bonded ring, and $1/q$ the fraction of NH (or CO) groups forming hydrogen bonds.

(67) W. Astbury and F. Bell, *Nature*, **147**, 696 (1941).

(68) L. Pauling, *J. Am. Chem. Soc.*, **67**, 555 (1945).

by Huggins),[65] 2_{7b} (proposed by Zahn,[69] and Ambrose and Hanby[70]), 2_8 (proposed by Huggins[65]: the non-linearity of C=O···H–N was pointed out by Bragg, *et al.*), 3_{10} (proposed by Taylor[71]; see also Huggins[65]), $2_{13}\cdot{}^1/_2$, $2_7\cdot{}^1/_2$ and $2_8\cdot{}^1/_2$, the hydrogen atom in the bond N–H···O lies much too far from the line joining the nitrogen and oxygen atoms. Another structural feature which should be emphasized is that the group

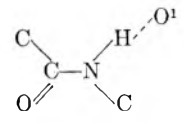

should be planar. As we have already pointed out, this group is planar in all crystals which contain it, although this condition does not apply quite so rigorously to the hydrogen-bonded oxygen atom, O′. The chains $2_{13}\cdot{}^1/_3$, $2_{14}\cdot{}^1/_3$, 3_8 and 4_{13}, as drawn, appear to violate the planarity requirement.

The paper by Pauling, Corey and Branson proposes two possible structures for a coiled polypeptide chain. Although they do not quote coördinates for the individual atoms, it is clear from their discussion and from inspection of their diagrams that all of the stereochemical requirements have been satisfactorily complied with. This is necessarily true because they include among their basic postulates the three conditions which we have applied above. One interesting feature of their structures is the presence of a non-integral screw axis as an element of symmetry. Whether or not the structures proposed by them are of significance in the protein problem is beyond the scope of this paper.

(69) H. Zahn, *Z. Naturforschung*, **26**, 104 (1947).
(70) E. J. Ambrose and W. E. Hanby, *Nature*, **163**, 483 (1949).
(71) H. S. Taylor, *Proc. Am. Phil. Soc.*, **85**, 1 (1941).

STRUCTURAL COLORS IN EMULSIONS[1]

BY ALFRED W. FRANCIS

Socony-Vacuum Laboratories, A Division of Socony-Vacuum Oil Co., Inc., Research and Development Department, Paulsboro, N. J.

Received June 25, 1951

Emulsions of colorless liquid phases of equal refractive indices but different dispersions show brilliant colors by transmitted light with a light barrier. The color appears at the barrier and is a function of the temperature and composition of the emulsion. The series of colors is complementary to the rainbow colors and includes pink and purple but not green. The opal behaves in the same manner. The phenomenon is explained, and some practical applications of it are presented.

Certain systems of two colorless liquid layers show at any one time one of several brilliant opalescent colors when shaken and viewed by transmitted light, preferably daylight from a window with partitions between the panes. The color appears at the partitions, and is especially effective when viewed through a horizontal tube held close to the eyes. If the emulsion is fairly permanent, a good method is to hang a tube close in front of a window screen, giving a magnified colored grain effect. With artificial light an effective method is to view the surface of the emulsion from below by total reflection.

The opalescent color shown by any system can be changed throughout the entire spectrum (unless the phases mix or one of them freezes) by changes in temperature or adjustment of composition. The opalescent spectrum consists of the colors yellow, amber (brownish-orange), brick red, magenta, lilac, purple, indigo, light blue. This is usually the order with descending temperature, but it may be reversed. The range for the spectrum is usually about 20 to 40° in temperature, or one to 30% in composition. The magenta, lilac, purple and indigo colors seem clear and uniform. With the other colors the system is slightly turbid, and looks like an emulsion.

The requirements for color in the emulsion beside the light barrier mentioned, are that the two liquid phases have the same refractive index for some wave length in the visible spectrum (that they be isoöptic), and that their dispersions (differences between the indices for the Hβ and Hα lines) differ by at least 0.0003.

Some binary systems have been found to meet these requirements, as follows (the colors are those shown at room temperature): nitromethane or methyl sulfate with *n*-heptane or other paraffins of similar refractive index (yellow); formamide–chloroform (magenta); ethanolamine–carbon tetrachloride (light blue); hydroxyethylethylene diamine–benzene (light blue). Acetic anhydride fails to give any color with paraffin hydrocarbon mixtures of equal refractive index because the dispersions also are nearly equal; other two liquid isoöptic systems fail for the same reason.[2a] The system, water–*n*-butane,[2b] shows hardly perceptible colors in spite of equality of refractive index at 15 to 19°.

However, many ternary systems can be adjusted in composition to give the colors. Thus, the refractive index of glycerol, 1.473, can be matched by that of a mixture of hydrocarbons such as benzene and *n*-heptane. Similarly, the index of a hydrocarbon can be matched by that of a mixture of non-hydrocarbons immiscible with it.

Holmes and Cameron[3] described these systems,

(1) Presented before the Division of Physical and Inorganic Chemistry at the 121st Meeting of the American Chemical Society, Buffalo, N. Y., March 24, 1952.

(2) (a) The disappearance of the interface due to equal refractive indices and dispersions may be the cause of some reported observations of critical solution temperature which are apparently far too low, *e.g.*, formic acid–*n*-pentane, reported 28°, estimated 175° (*cf.* ref. 10). (b) A. W. Francis, *Ind. Eng. Chem.*, **33**, 554 (1941); *Ind. Eng. Chem., Anal. Ed.*, **15**, 447 (1943).

(3) H. N. Holmes and D. H. Cameron, *J. Am. Chem. Soc.*, **44**, 71 (1922).

first observed for two liquid phases by Bodroux,[4] as "chromatic emulsions." They stated correctly the requirements that the two phases must have equal refractive indices but different dispersions. They did not mention the requirement of a light barrier. Their explanation of the color phenomenon, ascribing it to "prisms" (really droplets) of one liquid in the midst of the other seems inadequate. If it were analogous to the rainbow, which is due to such a mechanism, or if it resulted from any actual refraction, there should be a simultaneous appearance of all rainbow colors, or else the color seen should vary over the rainbow spectrum with the position of the eye. Actually at any one temperature for a system only one color is conspicuous, and this color is almost independent of position. Moreover, some of the colors observed do not match any portion of the rainbow, and one rainbow color, green, is not seen. Wood's explanation[5] is similar to that of Holmes and Cameron.

The order of colors, which is obviously different from that of the usual spectrum, makes it clear that the colors are complementary colors of the latter. The phenomenon can be explained as follows: Light of one wave length passes straight through the emulsion without reflection because of the equality of the refractive indices. For that wave length the emulsion is optically homogeneous. A ray of any other colored light also passes through in an effectively straight line (contrary to Wood's explanation[5]) subject only to very slight deviations due to refraction or reflection, so that without a light barrier (as with a background of sky or white paper) the emulsion is uncolored and transparent. At a point where direct light is blocked by a light barrier, however, the only light reaching the eye is that reflected at slight angles from the surfaces of droplets. This light has lost one color or wave length band, which cannot be reflected, and so appears as the complementary color. And since this light results from reflection and not refraction, the color is independent of the angle of observation, and depends only upon the color eliminated. At constant composition the color is usually a function of the temperature because one phase has a higher temperature coefficient of refractive index than the other.

Green is never observed as the opalescent color in a system of colorless liquids with daylight because "there are no complementaries to the colors in the range 498 mμ to 559 mμ."[6] "Complementaries" is here used in the narrow sense of a pair of complementary monochromatic lights. Daylight from which this range is removed is a magenta-pink; but no single wave length band could be removed from daylight to leave green. If one liquid is yellow, however, the indigo opalescence appears as a brilliant green, and a bluish-green color may result from the use of artificial light containing an excess of yellow rays. Moreover, when colorless liquids show a bright magenta band due to an obstruction, the light transmitted adjacent to the band has a pale green color. When the two phases have largely separated, the interface shows a narrow fringe of other colors. This is probably due to refraction since it varies with the angle of observation, and may be any spectrum color, including green.

In order to make the emulsion more lasting, so as to diminish the frequency of shaking required, the densities of the two layers also can be matched (they can be made isopycnic) by using four components. Thus, with glycerol, the non-glycerol layer may consist largely of carbon tetrachloride, with enough benzene to raise the refractive index and enough lighter hydrocarbon to lower the density to equal the respective properties of glycerol. High viscosity in the continuous phase is desirable for permanence of the emulsion. A sample of the system just mentioned, with glycerol in large excess, showed brilliant colors after standing six weeks without agitation. Holmes and Cameron[3] accomplished the same purpose with an emulsifying agent.

An opal may be a solid emulsion of this type. This is suggested by the description of its origin and behavior,[7] "the transmitted light is complementary to the reflected." However, the explanation of the colors is inadequate. "The resulting heterogeneity of the opal gives it a varying refractive index, which affects the light in the same way as a soap bubble."

A viscous opalescent emulsion is disappointing when first made up in comparison with an older one, partly because air bubbles caused by the necessary vigorous shaking dim the color considerably. Moreover the fine droplets necessary for a brilliant color are slow to form. Temperature fluctuations or occasional shaking followed by standing to eliminate air bubbles seem necessary to develop the full brilliance of the color.

A Pyrex glass cell with two plane parallel surfaces, 30 mm. thick and 64 mm. in diameter with a stem in the edge has been constructed and filled with a glycerol opalescent liquid. When held before the lens of a lantern projector, no color appears on the screen without a slide. But with a slide all of its lines are changed from black to a color depending on the temperature of the cell. When the cell is used to observe objects in a room, they appear clearly in natural colors except that any white or bright object is surrounded by a halo of the color which depends on the temperature of the cell. The effect is striking with street lights, headlights, or the moon.

A solid may be substituted for one of the liquids[5,8,9] provided it is isotropic. A sample of arrowroot starch was found to have an index of 1.53, using a mixture of benzene and carbon disulfide. Ammonium chloride crystals in cold carbon disulfide gave colors, but many crystalline materials have failed to show a color under similar conditions probably because they are anisotropic. Ground Pyrex glass gave opalescent colors in mixtures of benzene with non-aromatic hydrocarbons when the index was about 1.484. Therefore the shape of particles of the dispersed phase is not necessarily spherical.

Unless special precautions are taken,[5,9] the colors with powdered glass are pale and muddy because of contaminants and bubbles. However, colors nearly as brilliant as those with emulsions have been obtained by packing tightly in parallel position a multiplicity of uniform capillary tubes 75 mm. long and 1.36 mm. o.d. and 0.8 mm. i.d. open at both ends, such as are sold for melting point observations. The liquid was benzene containing 8% by volume of cyclohexane. The system gives blue at room temperature and purple, magenta and yellow, etc., with rising temperature. It

(4) F. Bodroux, *Compt. rend.*, **156**, 772 (1913).

(5) R. W. Wood, "Physical Optics," 3rd ed., The Macmillan Co., New York, N. Y., 1934, pp. 115–117.

(6) "International Critical Tables," McGraw-Hill Book Co., Inc., Vol. I, New York, N. Y., 1926, p. 93.

(7) Encyclopedia Britannica, **16**, 801 (1941).

(8) C. Christiansen, *Wied. Ann.*, **23**, 298 (1884).

(9) J. W. S. Rayleigh, *Phil. Mag.*, **xx**, 358 (1885).

looks different from the emulsions because the system as a whole is anisotropic. It shows longitudinal striations due probably to imperfect uniformity of the refractive index of the glass. It is, of course, quite permanent since it cannot settle out.

One practical use for the phenomenon is the observation of refractive indices of substances as liquids above their normal boiling points. This is accomplished by sealing the sample with a less volatile liquid immiscible with it, such as water, an aqueous solution, or a fluorocarbon, selected to match the sample in refractive index at some observable and desired temperature. The temperature read is that giving a dark bluish purple color, since this is definite in appearance, and the color is nearly complementary to that of the sodium D line. The precision is higher than that obtainable by observation of the disappearance of the interface using monochromatic light.[2] The color often lasts only a fraction of a second after shaking, but the observation can be repeated indefinitely.

The method is not accurate if the mutual solubility of the components is appreciable, nor if a complex is formed between the components, *e.g.*, water with sulfur dioxide, even though it remains in solution. The method has been found applicable to C_4 hydrocarbons, hydrogen sulfide, chlorine, ethyl chloride, Freons and approximately so to ammonia, methyl chloride, sulfur dioxide, propane and propylene. It is apparently inapplicable to ethane, ethylene, carbon dioxide, nitrous oxide, methyl ether and other liquids of refractive index below 1.25, because no less volatile liquid of comparable low index is available.

Another use for the phenomenon is in the locating of tie lines for the binodal curves of certain ternary systems. Known compositions are made up in the two-phase area giving colored opalescence near each side of the binodal curve. Such compositions giving matching colors at the same temperature are evidently on the same tie line. Diagrams have been drawn with tie lines colored to match the colors exhibited. One of these is shown in Fig. 1.

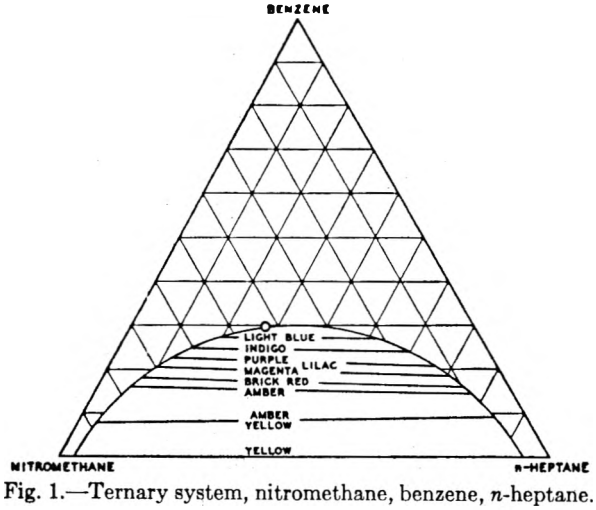

Fig. 1.—Ternary system, nitromethane, benzene, *n*-heptane.

Unlike most ternary systems this one shows opalescent colors over the entire two-phase area. The color is relatively insensitive to composition, especially up to 15% benzene, because benzene divides almost evenly between the nitromethane and heptane layers, and so raises the refractive index of each to about the same extent. As temperature is increased, the curve shrinks, reaching the base line at the binary critical solution temperature, 115°.[10] The colors also shift downward at nearly the same rate, so that the base line (binary system) "becomes" indigo at 95° and colorless at 115°. In other systems the colored band is much narrower, sloping and tapering, like other groups of tie lines; and the colors often shift upward on the diagram with rising temperature.

Another possible use for the phenomenon is in the analysis of glycerol and other compounds. Glycerol containing less than 6% water gives no color with carbon tetrachloride, but with 7 to 8% water the color passes through the whole opalescent spectrum. A sample of concentrated glycerol in contact with carbon tetrachloride can be titrated with water to a standard color.

The table of refractive indices and dispersions in "International Critical Tables"[11] is convenient for selecting components in these systems. For most liquids the two properties are related approximately by the equation, dispersion = $0.0060 + (1/3)(n^{20}_D - 1.34)^2$ (Fig. 2). Many liquids close to the line in the index range, 1.34 to 1.40, are omitted from Fig. 2 to avoid congestion. Several others up to carbon disulfide (1.631 and 0.0345) are beyond the range of the graph but close to the curve. Since all of the latter are mutually miscible, they can be used to raise the index of the less polar phase, as is benzene in some of the described experiments.

Liquids such as glycerol, ethylene glycol, ethanolamine and decalin with dispersions appreciably below the curve of the equation, and those with high dispersions, nitromethane, formamide, olefins, and aromatic hydrocarbons, are favorites as one component; but almost any transparent liquid can be used as a major component in a suitable combination to give colors. Even water containing 15 to 20% formamide gives pale colors with ether or pentane; and a water–ethanolamine mixture can be used with nitromethane. Incomplete miscibility of the phases is a prime requirement. The table recently published[10] may be helpful in this respect if a hydrocarbon is a component.

(10) A. W. Francis, "Physical Chemistry of the Hydrocarbons," Edited by A. Farkas, Academic Press, Inc., New York, N. Y., 1950, pp. 273–300.

(11) Ref. 6, pp. 276–279. It would be still more convenient if the names of the compounds were given there. The following substantial corrections to dispersion values listed were noted from incongruities in the present research resulting from use of the I.C.T. values:

No.	Compound	Dispersion $10^4(H\beta - H\alpha)$ or $(nF - nC)$ Listed	Revised	References
10	*n*-Pentane	40	61.3	(12, 13c)
55	*n*-Heptane	91	67.2	(12, 13c)
87	2,5-Dimethylhexane	80	69.1	(12)
275	Ethyl bromide	93	77.0	(13b)
446	Ethanolamine	35	85	(14)
580	Mesitylene	113	153.3	(13a)

(12) A. V. Grosse and R. C. Wackher, *Ind. Eng. Chem., Anal. Ed.*, **11**, 614 (1939).

(13) Landolt-Börnstein-Roth-Scheel, "Tabellen," Julius Springer, Berlin: (a) Hauptwerke, 980 (1923); (b) Erg. II, 820 (1931); (c) Erg. III, 1685–1686 (1935).

(14) L. Knorr, *Ber.*, **30**, 1492 (1897) (Hβ interpolated).

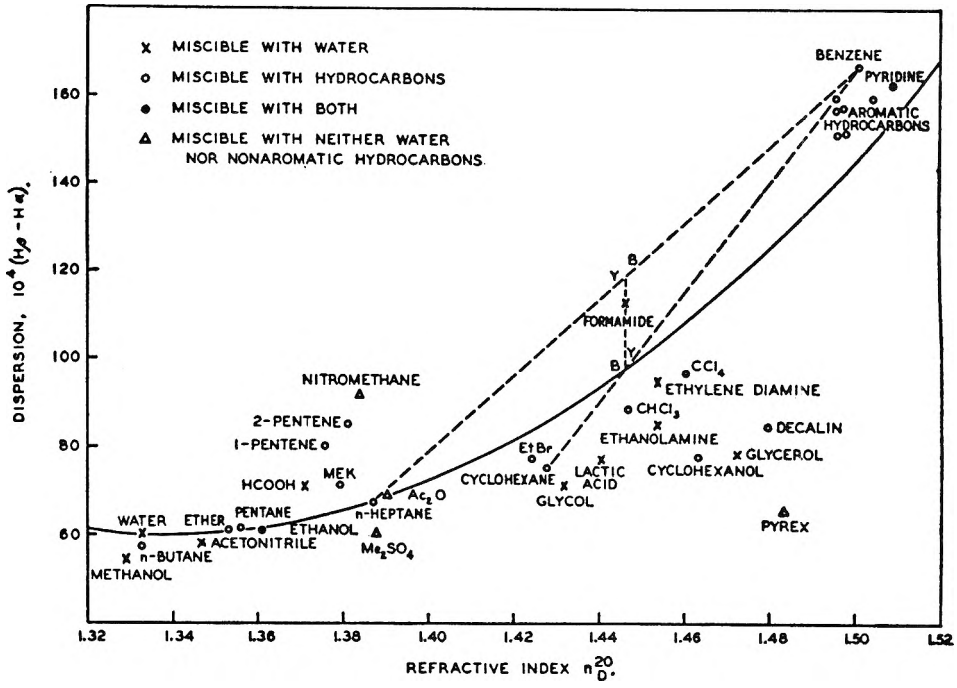

Fig. 2.—Relation between dispersion and refractive index.

The differentiation in types of points in Fig. 2 was intended to facilitate selection of reagents.

A system shows "warm" colors, yellow, amber, or red, if the phase of higher dispersion has a slightly lower value of n^{20}_D; and it shows a "cool" color, purple or blue, if n^{20}_D for that phase is equal to or higher than that of the other phase.

The direction of the shift of color with temperature depends on whether the less polar phase (heptane in the system of Fig. 1) has a higher or lower dispersion (in that case lower) than has the other phase, since the less polar compounds have higher temperature coefficients of refractive index.

The direction of the shift with respect to composition may depend upon the same relations, as illustrated by experiments with formamide, which is practically immiscible with hydrocarbons. If its index, 1.447, is matched by adding benzene to *n*-heptane, the color sequence is from yellow to blue. If its index is matched by adding benzene to cyclohexane, the color sequence is from blue to yellow. The reason for the opposite order appears from Fig. 2. The dotted line connecting the points for *n*-heptane and benzene passes above the point for formamide, while that connecting the points for cyclohexane and benzene passes below the point for formamide.

The direction of the shift also depends upon the distribution of the added substance. Thus the color of the nitromethane–*n*-heptane system shifts from yellow to blue with chloroform addition (which goes mostly to the nitromethane layer); and the yellow color returns with addition of cyclohexane (which goes mostly to the heptane layer). The methyl sulfate–*n*-heptane system gives the reverse effects with the same two addenda because in this case the heptane layer has the higher dispersion.

The minimum difference in dispersion necessary to give colors was determined by titrating the same two binary systems with acetic anhydride (which goes mostly to the non-heptane layer) until the colors were imperceptible. All four reagents have nearly the same refractive indices, 1.384 to 1.391, but the dispersions ($\times 10^4$) vary, nitromethane 92, acetic anhydride 69, *n*-heptane 67.2, methyl sulfate 60. During the titration, in order to keep the system in the color band, the index of heptane had to be adjusted gradually, almost to that of acetic anhydride by addition of about 10% of cyclohexane. This raised its dispersion to 67.9. Color could be detected until the dispersion of the non-heptane layer was below 71 in the case of nitromethane, or above 65 in the case of methyl sulfate, each as interpolated from its composition on a volume basis. The threshold difference in dispersion is therefore about 3×10^{-4} in each case. A similar value was obtained by titrating a mixture of cyclohexanol and glycerol with decalin (which extracts cyclohexanol from the mixture) until a faint purple color was discernible. A greater difference in dispersion, about 10^{-3}, is required for bright colors, but beyond this there is no evidence to support the claim of Holmes and Cameron[3] that "The greater this difference the more intense the resulting color."

A CONTRIBUTION TO THE KNOWLEDGE OF SOME PHYSICO-CHEMICAL PROPERTIES OF POLYSTYRENE

BY NILS GRALÉN AND GÖSTA LAGERMALM

Swedish Institute for Textile Research, Gothenburg, Sweden

Received May 29, 1951

Determinations have been made of different physico-chemical constants for a fractionated and several unfractionated samples of polystyrene. A method for "graphical fractionation" is described, and the result, in the case of the fractionated sample, compared with the result from a summation method based on investigation of the individual fractions. A polymolecularity curve is given for the fractionated sample and from the data obtained conclusions are drawn concerning the degree of branching of the different fractions. In general, the fractions with highest molecular weights contain more linear molecules than the other fractions. The investigation of the other samples shows that the weights and shapes of the molecules are extremely sensitive to alterations in the polymerization conditions, and also that elevated temperature or the presence of catalyst favor the formation of several maxima in the sedimentation diagram. The molecular weights from the sedimentation and diffusion measurements are compared with those calculated from the viscosity data.

Introduction

The first part of this investigation, which includes fractionation experiments and the theoretical basis of constructing the frequency curve for the sedimentation constants of the sample, has partly been published earlier.[1,2] As the original paper is only the first part of a more extensive work, and as the results obtained must be judged as a whole in order to give the best possibilities of drawing conclusions from the experiments, it has been regarded necessary to give a short review here.

Materials.—The following materials were investigated:

Code	Description
L 0—L VII	Polymerized from monomer styrene Dow N 100 Caustic, which had been washed with $N/10$ NaOH, water, dried over $CaSO_4$ and redistilled at 10 mm. pressure. The temperature of polymerization was 60° and the polymerization was performed in Pyrex glass tubes of 37 mm. outer diameter in a nitrogen atmosphere without any catalyst. The time of polymerization was 34 days. The polymerizate contained 4.36% volatile material. This sample was subjected to fractionation and the code L 0 refers to the unfractionated material, the codes L I to L VII refer to the fractions in the proper sequence.
A	Polymerized (from same material as L 0) at 180°. The polymerization was performed in Pyrex tubes of 8 mm. outside diameter in a nitrogen atmosphere without any catalyst. The time of polymerization was 5 hours. The polymerizate contained 2.97% volatile material.
B	The monomer was produced in this Laboratory by distillation of cinnamic acid. The polymerization was performed at room temperature and under the influence of air and of daylight during a period of about 10 months.
E	Polymerized at 30° with 0.02% benzoyl peroxide added.
P	Polymerized at 80° without any catalyst. The polymerization process was not carried beyond 10%. The polymer was precipitated with methanol to free it from monomer.
H M	Fraction 11/1/48, distributed by Prof. H. Mark for investigation at different laboratories in order to compare the results obtained. The sample was bulk polymerized at 93° without any catalyst. After 12 hours it was cooled to 20° and hydroquinone added. HM is one of the 40 fractions obtained from the original material by precipitation with methanol.

The samples L, A, E and P were kindly supplied by Dr. R. Boyer of the Dow Chemical Company.

Investigation of Sample L

Of the samples mentioned above the one given the code L was found suitable for a more thorough investigation.

Fractionation.—Sample L was dissolved to a concentration of 0.4% in methyl ethyl ketone and fractionated by precipitation with *n*-butanol. The alcohol was first added to a concentration slightly below the beginning of precipitation, and its concentration was increased by successive evaporation of the solvent–precipitant mixture at a pressure of about 10 mm. The process was carried out in a thermostat at 40°. At this temperature the vapor pressure of methyl ethyl ketone is about 190 mm. and that of the alcohol only about 25 mm. Thus the evaporation means an increase in the concentration of butanol. In order to avoid concentration gradients during precipitation the process was performed under intensive stirring. When a precipitate was formed, it was allowed to settle and formed a gel on the bottom of the flask which could be easily pipetted off. The precipitates were redissolved and reprecipitated. Each fraction was washed with *n*-butanol and dried at low pressure (35–36 mm.) for one day. The fractionation scheme is given in Fig. 1, where the areas of the squares are proportional to the size of the fractions. The weights of the final fractions are given in Table I.

TABLE I

FRACTIONATION OF POLYSTYRENE

Fraction	Weight, g.	%
L I	0.375	7.6
L II	.738	15.0
L III	.690	14.0
L IV	.342	7.0
L V	.556	11.3
L VI	.940	19.1
L VII	1.012	20.6
Sum	4.653	94.6

Sedimentation Experiments.—The fractions and the original sample were subjected to sedimentation experiments in the ultracentrifuge. The measurements were made at 800 r.p.s. corresponding to a centrifugal force of about 165,000 times gravity. The sedimentation constants are given in Svedberg units ($1\ S = 10^{-13}$ cm./sec. dyne) reduced to 20° and the solvent methyl ethyl ketone and also corrected for the influence of the hydrostatic pressure on the density and the viscosity of the solvent.[3] The sedimentation constants are given in Table II. Figure 2 is an idealized sedimentation picture.

For such molecules, which show a very low diffusion, *e.g.*, linear molecules, the widening value, dB/dx, of the

(1) N. Gralén and G. Lagermalm, *Festskrift J. Arvid Hedvall, Göteborg*, 215 (1948).

(2) P. O. Kinell and B. G. Rånby, *Advances in Colloid Sci.*, **3**, 212 (1950).

(3) H. Mosimann and R. Signer, *Helv. Chim. Acta*, **27**, 1123 (1944).

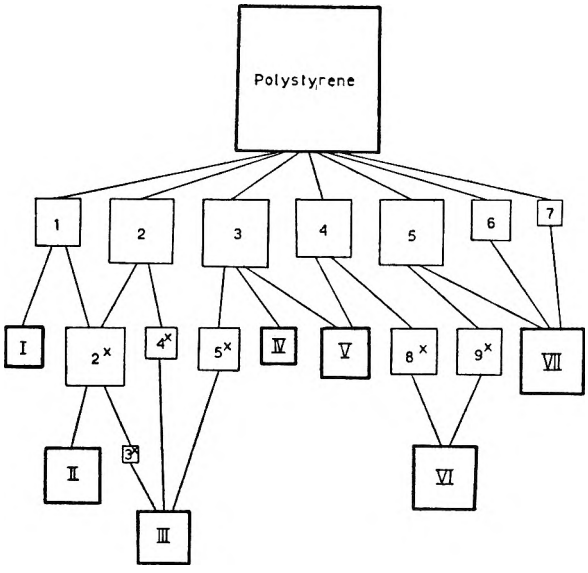

Fig. 1.—Fractionation scheme of polystyrene. The areas of the squares are proportional to the size of the fractions.

sedimentation curves is a measure of the polydispersity;[4] here B is the quotient between area (A) and the maximum height (H) of the curve

$$B = A/H$$

x is the distance in the cell. $(dB/dx)_0$ is the widening of the curve extrapolated to zero concentration. The following formula can be derived

$$\left(\frac{dB}{dx}\right)_0 = \left(\frac{dB}{dx}\right) + Kcs$$

K is a constant, c is the concentration. Thus, it can be assumed that dB/dx is approximately a linear function of the product sc.[4]

TABLE II

SEDIMENTATION MEASUREMENTS

	% of original sample	s_0	$(dB/dx)_0$
L 0	100	35	1.04
L I	8	45	.55
L II	15	48	.20
L III	14	30	.32
L IV	7	45	.27
L V	11	37	.33
L VI	19	31	.34
L VII	21	21	.58

It can be seen from Table II that the polydispersity of the fractions is considerably smaller than that of the original sample but even the fractions are rather polydisperse. This is true especially for the first and last fractions.

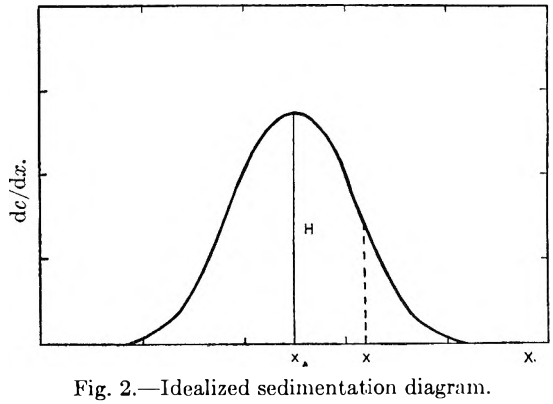

Fig. 2.—Idealized sedimentation diagram.

Frequency Curves.—Figure 3 gives a summation of the frequency curves of the sedimentation constants of the fractions, in order to give a view of the frequency curve for the whole sample of polystyrene. The frequency of each fraction is approximated to an isosceles triangle with the area proportional to the weight of the fraction. The apex of the triangle is located at the s_0-value for the fraction, and the width at half the height of the triangle is equal to $(dB/dx)_0 s_0$. This approximation was first assumed by Rånby.[5] The method gives its best results when the number of fractions is rather high and when the fractions have rather low $(dB/dx)_0$ values.

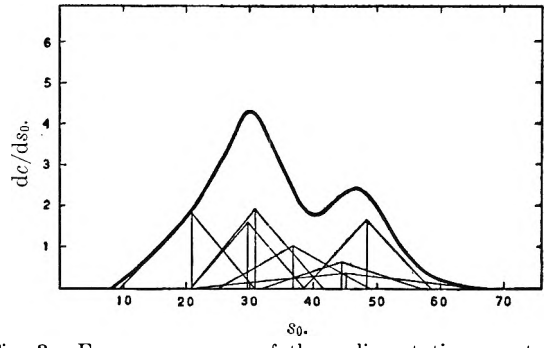

Fig. 3.—Frequency curve of the sedimentation constants, obtained by summation of the fractions.

The frequency function can also be obtained by an extrapolation from the sedimentation curves of the original samples. Using the formula

$$s = ds_A \frac{\ln x/x_0}{\ln x_A/x_0}$$

the x-scale of the sedimentation curves is transformed to an s-scale. In this formula (see Fig. 2), s_A is the sedimentation constant for the apex (abscissa x_A), s_1 is the sedimentation constant for the point x_1, x_0 is the position of the meniscus, and d is the ratio between the pressure correction factors for the points x and x_A. One sedimentation curve for every concentration should be transformed in this way. In order to get the best possible results the curve should be in a state where its broadening has reached such an amount that all possible details are recognized at their best. That means that the curve should not represent the state immediately after the start of the sedimentation and, at the same time, no component should yet have reached the bottom of the cell.

The curves in Fig. 4 give the relation between dc/ds and s for the sample L0. These curves are integrated and then give the distribution curves of Fig. 5. In these curves, the concentration is given as the percentage of the total concentration in the experiment. By horizontal equidistant lines, the integral curves are divided into a number of parts (*e.g.*, 10). In this way, a theoretical fractionation is obtained, and the s-values of each "fraction" are read from the intersections between the horizontal lines and the distribution curves. These s-values are extrapolated in the usual way for every

(4) N. Gralén, Dissertation, Uppsala, 1944.

(5) B. G. Rånby, *Norsk Skogsindustri*, **12**, Dec. (1947).

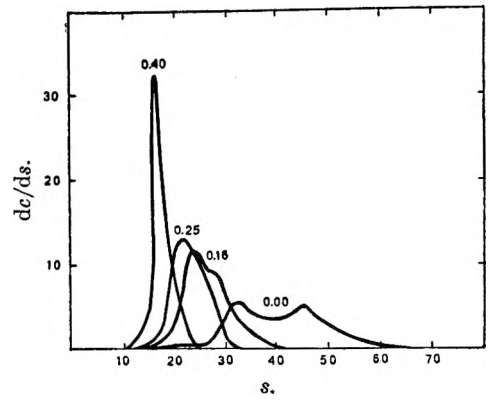

Fig. 4.—Frequency curves of the sedimentation constants at different concentrations (given in g./100 cc.). The curve at zero concentration is obtained by extrapolation.

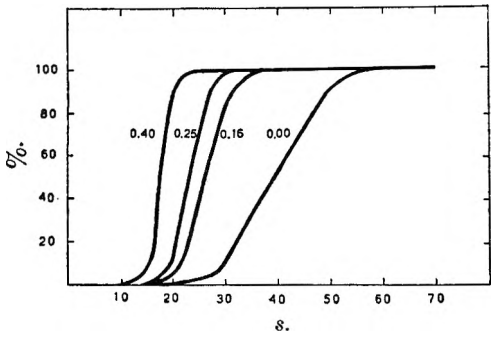

Fig. 5.—Distribution curves at different concentrations (given in g./100 cc.). The curve at zero concentration is obtained by extrapolation.

fraction and thus the distribution curve at infinite dilution (see Fig. 5) is obtained. This curve is graphically differentiated, and in that way the extrapolated frequency curve ($c = 0$ in Fig. 4) is obtained.

This method of obtaining the sedimentation distribution by extrapolation from the experimental sedimentation curves does not take into account the spreading introduced by the diffusion. In the actual cases, however, with elongated molecules, the diffusion is always very small and can be neglected during the time of a sedimentation experiment. Another assumption necessary for the use of this method, is that a change in concentration does not change the order of the "fractions" in the sedimentation. Very probably this assumption is well justified.

Figure 6 gives a comparison between the results from the fractionation and the extrapolation. Considering the graphical methods involved, the agreement is rather good. The extrapolation method is, of course, much simpler in use than the fractionation method. It needs, however, rather exact measurements, and it is reliable only when low concentrations can be used. For a general estimation of the distribution curve, it should be of some value.

Diffusion Experiments.—It is seen from the sedimentation-frequency curve that the sample investigated has two different peaks. To get a more thorough knowledge of it it was necessary to carry out diffusion measurements thereby gaining more information regarding the molecular weight and

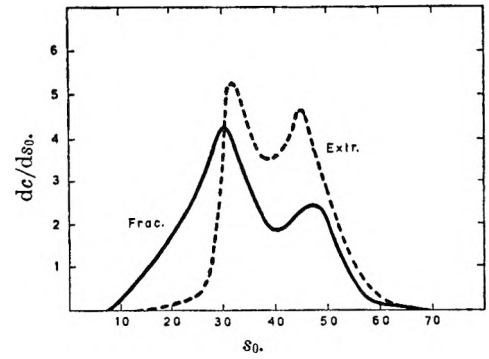

Fig. 6.—Frequency curves obtained by fractionation and by extrapolation.

shape of the unfractionated sample and its fractions. These experiments were carried out according to the method of Lamm[6] where a uniform scale is photographed through the diffusion cell. The curves are obtained by plotting the scale line displacement against the scale line position, x.

Glass cells of the Svedberg type were used, the temperature of the thermostat was 20.0 ± 0.05°. The solvent was here methyl ethyl ketone, the same as was used in the sedimentation and viscosity experiments.

The calculations of the diffusion constants were made according to the detailed description given by Gralén.[4] The formulas used are

$$D_A = A^2/4\pi t H^2$$

and

$$D_m = m_2/2tA$$

where the symbols denote

D_A = the diffusion constant calculated from the area and the height of the diffusion curve
A = the area between the diffusion curve and the x-axis
H = the height (maximum ordinate) of the diffusion curve
t = the time in sec. after the start of the diffusion (corrected for the influence of disturbing factors)
D_m = the diffusion constant calculated from m_2
m_2 = the second moment of the curve about a vertical axis through the x-position of the original boundary

Several exposures from every experiment were measured and the values of $(A/H)^2$ and m_2/A (also called σ^2) were plotted in a diagram like the one shown in Fig. 7. The intersection between

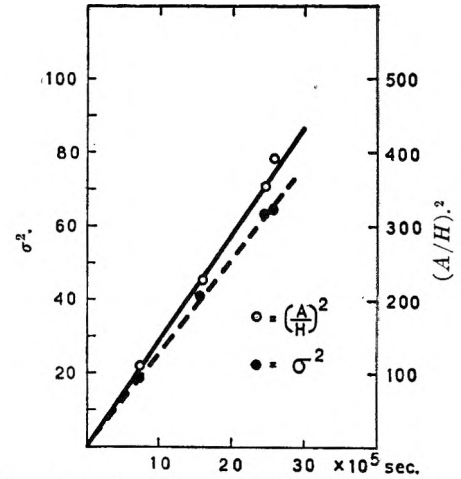

Fig. 7.—σ^2 and $(A/H)^2$ as functions of the time for L I.

(6) O. Lamm, Dissertation, Uppsala, 1937.

the straight lines and the time axis is taken as zero-point in the determinations of the time for the experiments, and the slopes of the lines are used for the calculations of the D_A and the D_m values. The lines do not always pass through the origin, in some cases they intersect the time axis at positive value, which may indicate a retardation of the diffusion process in the beginning (Gralén[4]). In other cases, however, the curves intersect the axis at a negative value. This may be due to a slight blurring of the boundary in the moment of starting. These runs made in methyl ethyl ketone were much more sensitive to disturbances than are most water solutions.

The D values obtained are given in Table III. As will be seen D_A and D_m do not have the same value. Theoretically the height of the diffusion curve for a polydisperse substance is always greater than could be assumed for a homogeneous substance.[6] As stated by Gralén[4] the ratio D_m/D_A should thus give a measure of the polydispersity. As seen from Table III, where the $(dB/dx)_0$ values are given for comparison, no such relationship can be concluded from the data obtained in this case. Gralén[4] found the same for cellulose solutions.

TABLE III

	c_i g./100 cc.	D_A[a]	D_m	D_n/D_A	$(dB/dx)_0$	D_0 (Boltzmann)
L 0	0.40	2.11	2.19	1.04	1.04	1.82
L I	.34	1.42	1.60	1.13	0.55	1.48
L II	.32	1.20	1.15	0.96	.20	0.81
L III	.32	1.40	1.27	0.91	.32	.83
L IV	.28	1.11	1.12	1.01	.27	.84
L V	.33	1.33	1.50	1.13	.33	.98
L VI	.46	2.10	2.19	1.04	.34	1.70
L VII	.34	2.94	2.81	0.96	.58	2.60

[a] The diffusion constants are given in units of 10^{-47} cm.^{2}/sec.

The diffusion curves obtained are often skew, the part facing the solvent being steeper than the part facing the solution. The curves can be transformed into normal coördinates, x_n and y_n by the equations

$$x_n = x/\sigma \quad \text{and} \quad y_n = y(\sigma/A)$$

where σ is the standard deviation, $\sigma = \sqrt{m_2/A}$. This transformation eliminates the individual differences in the diffusion curves caused by the time factor. Their individual irregularities can be eliminated by drawing a curve in normal coordinates representing the mean values. If curves which for instance represent an earlier stage than the point where a normal diffusion has started (compare the intersection of the time axis at a positive value), it will easily be recognized that this curve does not fit into the curve in normal coordinates, originating from the other individual curves. Figure 8 gives the diffusion curve of L 0 in normal coördinates. Figures 8, 9, 10 and 11 are examples of the curves obtained with the different fractions. In these figures the dotted lines indicate the gaussian normal frequency curve.

The skew diffusion curve is found to be a result of concentration dependence of the rate of diffusion.[4,7,8] In cases of concentration dependence the diffusion

(7) A. Polson, *Kolloid-Z.*, **83**, 172 (1938).

(8) A. F. Schick and S. J. Singer, THIS JOURNAL, **54**, 1028 (1950).

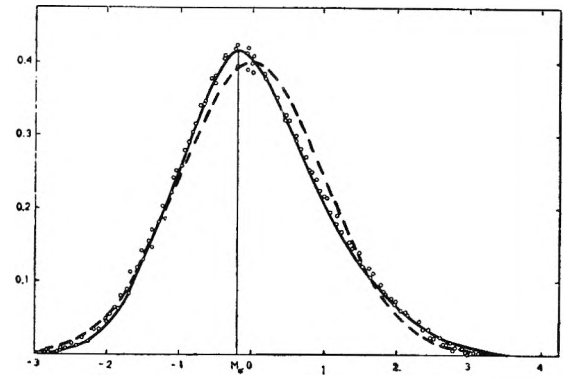

Fig. 8.—Diffusion curve of L 0 in normal coördinates. M_0 is the maximum point (the mode). In Figs. 8–11 the dotted line indicates the normal frequency curve.

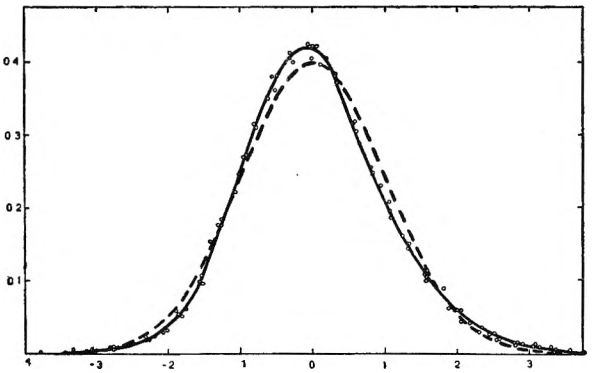

Fig. 9.—Moderately skew diffusion curve from L I in normal coördinates. The curve is higher than the corresponding normal frequency curve.

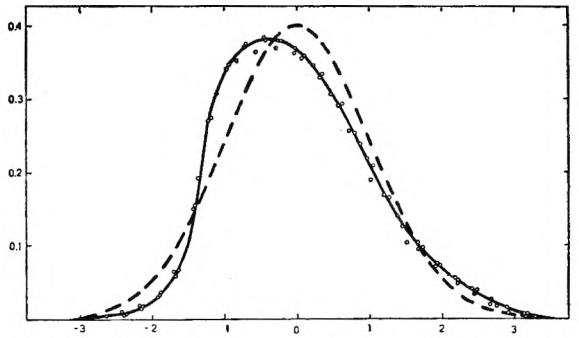

Fig. 10.—Skew diffusion curve from L III in normal coordinates. The steep side of the curve faces the solvent and the curve is lower than the normal frequency curve.

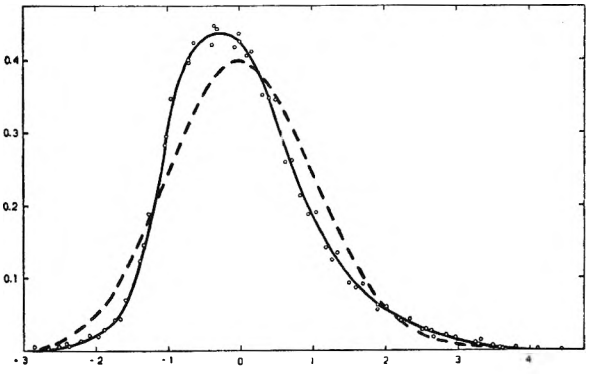

Fig. 11.—Skew diffusion curve from L V in normal coordinates. The curve has a pronounced steepness and is higher than the normal frequency curve.

constant can be calculated from the Boltzmann equation

$$D = \frac{1}{2ty}\int_x^\infty xy\,dx$$

which is valid independently of the form of the concentration function. The diffusion constant is calculated and given as a function of the concentration along the diffusion curve (Fig. 12). From this curve the diffusion constant is found by extrapolating to zero concentration. This constant, D_0, can also be calculated according to the formula of Gralén[4]

$$D_0 = D_m + (AM_0/4Ht)$$

where M_0 is the coördinate of the maximum point (the mode) of the curve (see Fig. 8). As M_0 generally is negative $D_0 < D_m$. For details in the calculations of diffusion constants the reader is referred to the work of Gralén. Calculations of D_0 have been performed both according to the equation of Boltzmann and according to the formula of Gralén. It was, however, found that the formula of Gralén in several cases gave a too low value for D_0. This was especially the case when the shape of the curves deviated appreciably from the shape of the normal frequency curve, either by being lower or having a more flat peak or by a high degree of skewness. Such a discrepancy between the two formulas is quite natural, because in the derivation of Gralén's formula from Boltzmann's only the central part of the curve is used.

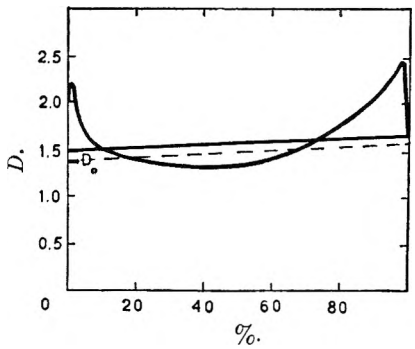

Fig. 12.—Diagram illustrating the calculation of D_0 according to the Boltzmann equation.

When the curves were moderately skew and did not deviate too much from the normal shape the agreement between $D_{0\text{Boltzmann}}$ and $D_{0\text{Gralén}}$ was satisfactory. A remarkable feature was that the most skew diffusion curves were obtained with the fractions having the lowest $(dB/dx)_0$ values, *i.e.*, the lowest polydispersity.

Determination of the Molecular Weight.—The molecular weight, M, which is given in Table IV, is calculated according to Svedberg's formula

$$M = RTs/D(1 - V\rho)$$

where

R is the gas constant (8.313×10^7)
T the temperature in Kelvin degrees
V the partial specific volume of the solute
ρ the density of the solution

As the s and D values obtained by the sedimentation and diffusion measurements are weight averages or very near to them, the molecular weight will be a weight-weight average. This average lies between the number average and the weight average.[9]

TABLE IV

	s_0	D_0	$M \times 10^{-3}$
L 0	35	1.82	1.800
L I	45	1.48	2.800
L II	48	0.81	5.500
L III	30	.83	3.400
L IV	45	.84	5.000
L V	37	.98	3.500
L VI	31	1.70	1.700
L VII	21	2.60	750

The partial specific volume was determined by an Ostwald–Sprengler pycnometer. The result was 0.91 which is in agreement with the value given by Signer.[10]

The Shape of the Molecules.—The data obtained by the sedimentation and the diffusion measurements give possibilities of calculating the shape of the molecules. The frictional coefficient for the filamentous molecules is greater than that for a spherical molecule. The ratio between the frictional coefficients can be calculated from the formulas[11]

$$f = RT/D = M(1 - V\rho)/s$$
$$f_0 = 6\pi\eta N\,(3MV/4\pi N)^{1/3}$$

or

$$f/f_0 = \frac{1}{\eta}\left(\frac{R^2T^2(1 - V\rho)}{162\pi^2N^2D^2Vs}\right)^{1/3}$$

where

f = frictional coefficient of the molecule in question
f_0 = frictional coefficient of a spherical molecule
N = the Avogadro number (6.06×10^{23})
η = viscosity of the solvent
the other symbols have the previously assigned significance

For unhydrated molecules having the shape of oblong ellipsoids with the axial ratio l/d (l = length, d = diameter) Herzog, Illig and Kudar[12] have derived an equation giving the relation between f/f_0 and l/d. Numerical values for the f/f_0 and l/d ratios are given by Svedberg and Pedersen[11] and Gralén.[4] When the ratio l/d has been determined the values of l and d can be calculated from the formula

$$\pi ld^2/6 = MV/N$$

The results are given in Table V.

TABLE V

	f/f_0	l/d	l, Å.	d, A.
L 0	3.40	68	2900	42.5
L I	3.59	77	3700	47.4
L II	5.25	170	7800	45.6
L III	6.05	225	8000	35.3
L IV	5.24	169	7500	44.2
L V	5.05	156	6300	40.2
L VI	3.71	82	3200	39.2
L VII	3.18	59	2000	33.4

(9) I. Jullander, The Svedberg, Uppsala, 166 (1944).

(10) R. Signer in T. Svedberg and K. O. Pedersen, "The Ultracentrifuge," Oxford, 1940; "Die Ultrazentrifuge," Dresden and Leipzig, 1940.

(11) T. Svedberg and K. O. Pedersen, *ibid.* (1940).

(12) R. O. Herzog, R. Illig and H. Kudar, *Z. physik. Chem.*, **A167**, 329 (1933).

TABLE VI

		s[b]	% of total concn.	D_m[a]	D_A	D_m/D_A	D_0	c in g./100 cc. (diffusion expr.)	$M_{w,w} \times 10^{-3}$	f/f_0	l/d	l, Å.	d, Å.
A	w	12		9.60	8.3	1.15	12.0	0.40	90	1.38	7.1	240	33.6
	1	17	40										
	2	11	30										
	3	8	20										
	4	5	10										
B	1	17	40	5.80	6.7	0.87	6.4	.21	180	2.05	21.0	620	29.2
	2	13	30										
	3		20										
	4		10										
P	w	21		2.40	2.20	1.09	2.04	.40	960	3.75	84.0	2700	32.2
	1	22	85										
	2	19	10										
	3	17	5										
HM		24		3.83	3.19	1.20	3.24	.51	700	2.62	38.4	1450	37.6

[a] The diffusion constants are given in units of 10^{-7}. [b] The sedimentation constants are given in Svedberg units. s_w = the weight average sedimentation constant; s_1 = the sedimentation constant for peak no. 1; s_2 = the sedimentation constant for peak no. 2; s_3 = the sedimentation constant for peak no. 3; s_4 = the sedimentation constant for peak no. 4.

It would also be possible to treat the molecules as random coils and obtain the distance between ends of the polymer chain from the theory of Kirkwood and Riseman.[13] For the later discussion this would probably be as helpful and give about the same qualitative results.

Viscosity Measurements.—The viscosity was measured in an Ostwald viscometer at 20.0°. The intrinsic viscosity $[\eta]$ was calculated from the formula

$$[\eta] = \lim \frac{t_c/t_0 - 1}{c}$$

where

t_c = the efflux time for the solution of concentration c
t_0 = the efflux time for pure solvent
c = the concentration in g./100 cc.

The values obtained are given in Table VII. (It should be observed that the viscosity values given by Gralén and Lagermalm[1] for the same sample and fractions refer, as do all other measurements in that paper, to concentrations in g./100 g.)

TABLE VII

	$[\eta]$	$M \times 10^{-3}$ from viscosity measurements	$M \times 10^{-3}$ from viscosity measurements, with the constants of Goldberg, Hohenstein and Mark[14]	$M \times 10^{-3}$ from sedimentation and diffusion measurements
L 0	2.0	2.700	3.200	1.800
L I	2.9	5.300	6.400	2.800
L II	2.6	4.300	5.400	5.500
L III	1.7	2.000	2.400	3.400
L IV	2.6	4.300	5.400	5.000
L V	2.0	2.700	3.200	3.500
L VI	1.5	1.600	1.700	1.700
L VII	1.0	800	870	750
A	0.30	90	90	90
B	.40	160	160	180
E	.60	310	350	
P	.80	540	600	960
HM	.95	700	800	700

(13) J. G. Kirkwood and J. Riseman, *J. Chem. Phys.*, **16**, 565 (1948).

(14) A. I. Goldberg, W. P. Hohenstein and H. Mark, *J. Polymer Sci.*, **2**, 503 (1947).

Comparison Between the Sedimentation Frequency Curve and the Molecular Weight Frequency Curve.—If the polymerization process was governed by a single mechanism we would obtain a sedimentation frequency diagram with a single peak.[15, 16] In this case we might assume a simple relationship[4]

$$s = KM^{\alpha}$$

where K and α are constants. It would thus be possible to transform a sedimentation frequency diagram into a molecular weight frequency diagram.

The sedimentation frequency diagram, however, has two peaks which means that the polymerization process has proceeded simultaneously according to at least two different mechanisms. Thus it does not seem improbable that we have to do with both branched and unbranched molecules, or molecules with different degrees of branching. It can not be assumed that the D values for these different molecule types will fit into one single relationship between s and D values. It is also evident that the method with addition of triangles representing the different fractions would not give a correct molecular weight diagram. The $(dB/dx)_0$ value, which is the basis of the method, is determined from sedimentation measurements and it might well be possible that a fraction is composed of two different molecule types with the same sedimentation constant but different molecular weight. Thus, the $(dB/dx)_0$ value adds to the accuracy of the sedimentation frequency diagram but may confuse the molecular weight frequency diagram.

To give a picture of the molecular weight frequency function the method of Schulz and Husemann[17] has been adopted. In this method the cumulative per cent. (the sum of all fractions with a lower molecular weight plus half of the actual

(15) G. V. Schulz, *Z. physik. Chem.*, **B30**, 379 (1935); **B43**, 25 (1939); **B44**, 277 (1939).

(16) P. J. Flory, *J. Am. Chem. Soc.*, **58**, 1877 (1936); **59**, 1, 241 (1937); **62**, 1561 (1940); **63**, 3083, 3091, 3096 (1941).

(17) G. V. Schulz and E. Huseman, *Z. physik. Chem.*, **B34**, 187 (1936).

fraction) is plotted against the molecular weight. The sequence of the fractions when plotted in the diagram is determined by their molecular weight and not by their fraction number. In this way the distribution curve (the dotted line) in Fig. 13 is obtained. By plotting the slope (dc/dM) of this curve against the molecular weight the frequency curve in Fig. 13 is obtained. It must, however, be kept in mind that this method does not at all take into account the polymolecularity of the individual fractions. To give an impression of the

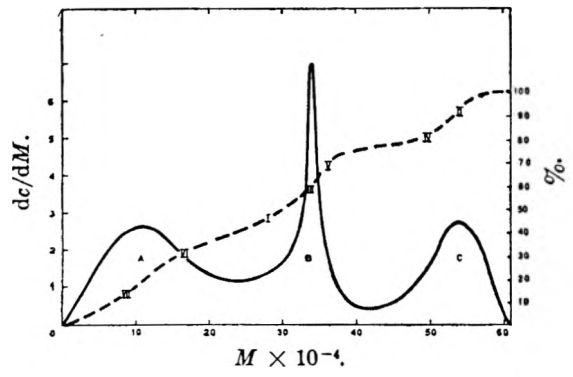

Fig. 13.—Distribution curve (the dotted line) and molecular weight frequency curve of L. The roman numbers indicate the positions of the individual fractions.

selectivity of the method, the sedimentation frequency curve, according to the same method, is compared in Fig. 14 with the corresponding curve obtained by addition of the triangles. It is seen that the peaks, although being much steeper, are situated at almost the same s_0 values as in the "triangle-diagram." It can correspondingly be assumed that even if the shapes of the peaks are not correct their number and also their positions are in accordance with the realities. Thus we have three maxima: one at a molecular weight of about 1,000,000, one at a molecular weight of about 3,500,000 and one at a molecular weight of about 5,500,000.

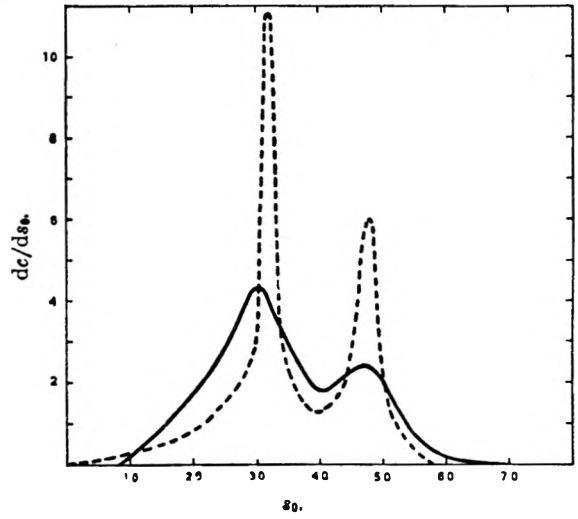

Fig. 14.—Comparison between sedimentation frequency diagrams obtained by the triangle methods and the cumulative per cent. method.

Conclusions

The sedimentation frequency diagram shows two peaks: the molecular weight frequency diagram shows three peaks. This difference must depend upon the above-mentioned fact that we have to do with different molecular shapes. If the three peaks are called A, B and C, in the order of increasing molecular weights, it can be noted that A is mainly composed by L VII and L VI, B is mainly composed by L I, L III and L V, C is mainly composed by L IV and L II.

L VI and L III have very nearly the same s_0 value, but different D_0 values. L VI, in spite of its lower molecular weight, has the same sedimentation constant as L III. The reason must be that L VI has a less extended molecular shape. This means that, if we presume L III to be unbranched, L VI must be branched, or if L III is branched L VI must be branched to a still higher degree. As at present there is no evidence that L III is branched, we will assume it to be unbranched. In the same way it can be concluded that L I contains branched molecules and L IV mainly unbranched. The data for L II are similar to those of L IV, there is an increase in the s_0 value and a corresponding decrease in the D_0 value, thus also L II ought to be composed mainly of unbranched molecules. If L V is compared with L III and L IV it is seen that $s_{0(III)} < s_{0(V)} < s_{0(IV)}$ (the indices denote the number of the fractions) but $D_{0(IV)} < D_{0(V)}$ and also $D_{0(III)} < D_{0(V)}$. This means that L V probably has a branched molecular shape. A comparison with L I or L VI, however, shows that it cannot possibly be branched to the same degree as they are as $D_{0(V)} < D_{0(I)}$ and $D_{0(V)} < D_{0(VI)}$. As to L VII no such conclusions can be drawn by analogy, but as its polydispersity is rather high it may be composed of a mixture of all types of molecules.

The conclusions ought to be that the three peaks represent: A, branched molecules and perhaps also unbranched molecules of low molecular weight; B, mainly unbranched molecules of rather high molecular weight, but also molecules branched to a lower degree than in A; C, unbranched molecules of high molecular weight.

The equation $M = \text{const.}/D^3$ is valid not only for spherical particles but also for the more general case that f/f_0 is a constant.[4] It is, however, seen from Table V that this assumption is not valid in the actual case.

If we assume the molecules to be linear, quite extended chain molecules the equation $M = \text{const.}/D$ should be valid.[4] If we compare this with Svedberg's formula which could be written $M = \text{const.} \times s/D$ it is seen that for this extreme case which represents the free draining type, s should be independent of the molecular weight. Gralén suggests the more general equations $M = \text{const.}/D^a$ and $M = \text{const.} \times s^b$ where a and b are constants, a with a value between 1 and 3. The constants then must satisfy the condition $(a - 1)(b - 1) = 1$.

If $\log s$ and $\log D$ are plotted in a diagram against $\log M$ as has been done in Fig. 15, straight lines through points representing the same molecule type should be obtained. As to the points repre-

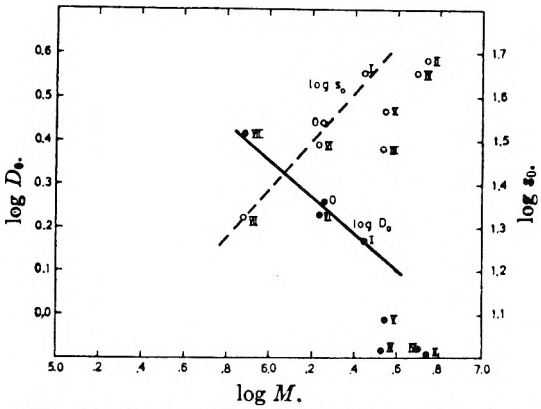

Fig. 15.—log s_0 and log D_0 as functions of log M.

senting the sedimentation data there is evidence that the points split up into two groups. The one group consists of L VII, L VI and L I, *i.e.*, the fractions which could be assumed to be branched (see earlier discussion). The points belonging to the other group seem to be more scattered. They represent both the unbranched fractions L III, L IV and L II and the partly branched fraction L V. Of course it is not advisable to draw a line through only 3 points, but as it seems to be in accordance with results obtained in other ways it may be justifiable to indicate a line through VII, VI and I. For the other group, however, it is more doubtful if any line may be indicated. This partly because L V is branched to a low degree, but also because L III, which will be discussed later, seems to be composed of molecules of a more extended type than L II and L IV.

As to the points representing the diffusion data the spread in the second group is still more pronounced, the points VII, VI, I, however, do still fit into a straight line. The slope of the indicated lines give the values $b = 1.74$ and $a = 2.35$, which is in agreement with the condition $(a - 1)(b - 1) = 1$. For the branched molecule type represented by the fractions L I, L VI and L VII we should then get the formulas

$$M = \frac{\text{const.}}{D^{2.35}} \text{ and } M = \text{const. } s^{1.74}$$

If we consider the shape of the molecules, similar conclusions as above can be drawn. A comparison of the l/d values shows that L 0, L I, L VI and L VII all give values considerably lower than those of the unbranched or lesser branched fractions. If d is plotted against l, as in Fig. 16, or against M, as in Fig. 17, this will show up as the existence of two groups, corresponding to those of the log D, log s, log M chart. As before VII, VI and I fit into a straight line. In the d–M diagram it might be possible to draw a straight line through either V, IV and II or III, IV and II. The V, IV, II line may also be drawn in the d–l diagram, but the point III there deviates from the general picture. L III has a remarkably low d value in relation to its rather high molecular weight, and at the same time a diffusion constant very near that of L IV and L II which represent still higher molecular weights than L III. From this it can be concluded that L III represents a more extended molecule type

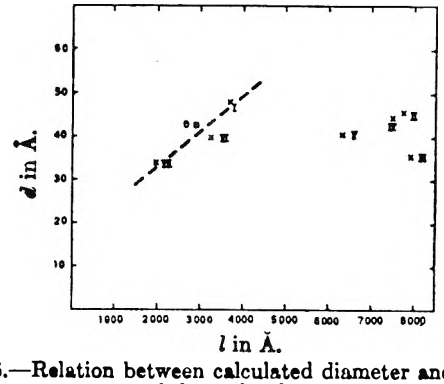

Fig. 16.—Relation between calculated diameter and length of the molecules.

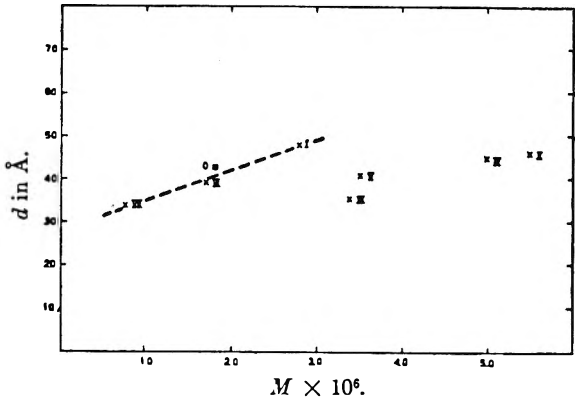

Fig. 17.—Relation between calculated diameter and weight of the molecules.

than any of the other fractions. It may be said that L III and L V belong to the same group as L II and L IV, but their individual deviations are so important that it cannot be justifiable to include them in a linear relationship if a relative amount of accuracy is needed.

If the $[\eta]$ values are plotted against M as in Fig. 18, a similar splitting up into two main groups is indicated.—The question of calculating the molecular weight from the viscosity data will be dealt with under "Investigation of Other Samples."

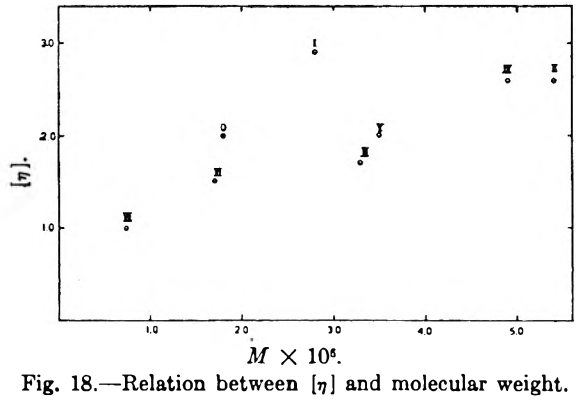

Fig. 18.—Relation between $[\eta]$ and molecular weight.

The conclusions concerning the individual fractions can be summed up as follows: L I, branched, constituent of the middle peak of the molecular weight frequency diagram (MFD); L II, unbranched, constituent of the peak with the highest molecular weight in the MFD; L III, unbranched, the most elongated shape of all fractions, con-

stituent of the middle peak in the MFD; L IV, unbranched, constituent of the peak with the highest molecular weight in the MFD; L V, branched to a low degree, constituent of the middle peak of the MFD; L VI, branched, constituent of the peak with the lowest molecular weight in the MFD; L VII, contains low molecular compounds mainly of branched configuration, constituent of the peak with the lowest molecular weight in the MFD.

Investigation of Other Samples

In addition to the detailed investigation of the fractionated sample produced in the absence of catalyst and oxygen at 60°, some other samples of different origin were also investigated. Information about the manner in which they were produced is given at the beginning of this paper.

Sedimentation Experiments.—The samples A, B, E and P all showed several peaks. At higher concentrations usually one single peak occurred, but at increasing dilution the number of peaks increased and at the lowest concentrations the smaller peaks disappeared and only the main peak or peaks were left. This made the analysis of the sedimentation diagram more complicated and also had the consequence of diminishing the accuracy in the measurements. Examples of the diagrams obtained are given in Figs. 19 and 20. Usually it was not possible to measure all the peaks in a sample from a single exposure, this because a schlieren effect was often obtained for one or several of the peaks when another of them was photographed at its optimal resolution.

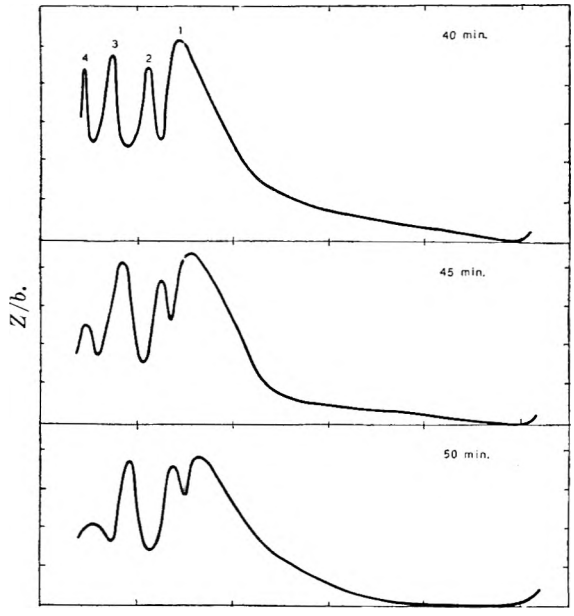

Fig. 19.—Sedimentation diagrams of polystyrene sample A.

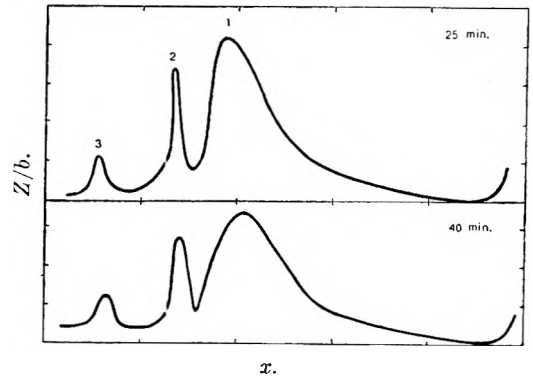

Fig. 20.—Sedimentation diagrams of polystyrene sample P.

Thus it was several times necessary to make exposures at different scale distances in order to study the diagrams of the individual peaks. To determine their correct positions it was also necessary to try to split up the complex diagram into its different components. To identify the peaks at different times during the same run $\log x$ was plotted against t, which gives straight lines for corresponding peaks. In the cases where it was not possible to get sufficient experimental data to determine the sedimentation constant for a peak this was determined from the value for another peak according to the formula

$$s_1 = s_2 \frac{\log x_1 - \log x_0}{\log x_2 - \log x_0}$$

where

x_0 denotes the position of the meniscus
x_1 denotes the position of peak no. 1
x_2 denotes the position of peak no. 2
s_1 denotes the sedimentation constant for peak no. 1
s_2 denotes the sedimentation constant for peak no. 2

For details of these different analysis of the curves the reader is referred to the monograph of Svedberg and Pedersen.[3] For some of the samples an estimation of the quantities of the different components has been made. This had to be made as an average from different concentrations and exposures. It is known that the slower moving component influences the velocity of the faster ones. This interference makes an evaluation less accurate and it is more pronounced the more concentrated the solutions are. These effects have been discussed by Signer and Gross[18] and Eneksson.[19]

Sample A (Fig. 19) which was run at 800 r.p.s., showed four distinct peaks, one of them (1) apparently rather polydisperse and probably composed of several smaller peaks. The more concentrated solutions showed a single peak, the most diluted ones just gave the peaks A1 and A2. The calculated sedimentation constants are given in Table VI together with an estimation of the amounts constituting the different peaks. As these sedimentation constants are weight averages the weight average sedimentation constant for the whole sample, s_w, can be calculated when the composition of the sample is known.

Sample B, which was run at 800 r.p.s., showed four peaks. The development of the sedimentation diagram was similar to that of A with different numbers of peaks depending upon the concentration of the solution. The sedimentation constants could only be calculated for the two peaks with the highest constants. Thus no s_w can be calculated and the $M_{w,w}$ is an approximative one.

Sample E gave several peaks of which at least four main peaks could be distinguished. The diagrams, however, were very complex and no sedimentation constants were calculated.

Sample P (Fig. 20), which was run at 600 r.p.s., showed a development similar to that of samples A and B. The most concentrated solution gave a single peak. The more diluted ones gave three peaks. At increased dilution and at the highest dilution the sedimentation diagram was one with a single peak (1) of rather high polydispersity and with the tendency of forming a small peak on the part facing still higher sedimentation constants.

Sample HM was run at 600 r.p.s. The sedimentation diagram showed only a single peak with a rather high polydispersity. The effect mentioned by Gralén[4] of the steeper side facing the higher sedimentation constants was pronounced.

Diffusion Experiments.—The results are given in Table VI. All the curves, in normal coördinates except that of sample B, are higher than the corresponding normal curve. They are also somewhat skew, in the case of samples A and B the steeper side is that facing the solution, which is contrary to the general case.

Molecular Weights.—These are given in Table VI. In the case where several peaks could be recognized in the sample only one molecular weight, corresponding to s_w has been calculated. Even if it is possible to calculate the sedimentation constants for the different peaks, it is not possible to

(18) R. Signer and H. Gross, *Helv. Chim. Acta*, **17**, 726 (1934).
(19) B. Eneksson, *Nature*, **161**, 934 (1948).

calculate the corresponding diffusion constants. D_0 is a weight average value which combined with the s_w value gives a weight–weight average, $M_{w,w}$ ($M_{w,w}$ denotes that the value is referred to s_w and D_w), which is the usual molecular weight calculated from sedimentation and diffusion experiments.[9]

The Shape of the Molecules.—The values for f/f_0, l/d, l and d are given in Table VI. It should be observed that in the cases where the sample gives a sedimentation diagram with several peaks, these values are based upon s_w, D_0 and $M_{w,w}$ and thus only indications of the molecular shape of an "average" molecule.

The Viscosity.—The viscosities (the concentrations in g./100 cc.) are given in Table VII.

If the conventional modification of the Staudinger equation

$$[\eta] = KM^{\alpha}$$

is applied we should get values for the molecular weight. Goldberg, Hohenstein and Mark[16] have given

$$[\eta] = 7.0 \times 10^{-4} \times M^{0.53}$$

valid for methyl ethyl ketone and for measurements made at 40°. As the experiments referred to in this paper have been carried out at 20° efforts have been made to determine the constants at this temperature. The log $[\eta]$ values were plotted against the log M values obtained from the sedimentation and diffusion experiments. A straight line was drawn through the points and the constants were determined graphically. As the collection of samples is somewhat heterogeneous it is not surprising that some of the points do not fit into the straight line. The formula obtained is

$$[\eta] = 5 \times 10^{-1} \times M^{0.56}$$

Table VII also gives the molecular weights calculated with the constants of Goldberg, Hohenstein and Mark. The difference is rather small between the molecular weights calculated with the constants valid for 20 and 40°. The constants of Goldberg, Hohenstein and Mark refer to osmotic measurements which give the number average, M_n, while the sedimentation and diffusion measurements give a weight–weight average, $M_{w,w}$. As pointed out by Jullander[10] $M_{w,w}$ is not identical with the weight average molecular weight and generally $M_n < M_{w,w} < M_w$.

Discussion

If the s, D and M values obtained for A, B, P and HM are plotted in the graph given in Fig. 15 it will be seen that the points do not fit into either of the two groups of data from the fractions of sample L. In the cases of A, B and P this can be explained by the heterogeneity of the samples. As they are mixtures of molecules of different shapes it is not to be expected that the constants a and b should be identical with those of more well defined fractions. This is also confirmed if the d and l values are plotted in the diagram given in Fig. 16. Neither A, B and P nor HM fit into the two groups of the graph. For A, B and P the explanation has already been given, for sample HM the explanation probably is that the degree of branching may be other than in the fractions of sample L, the rather high polydispersity of HM may also be a contributing factor.

General Conclusions

Some general conclusions can be drawn from the investigation of both the fractions and the unfractionated samples. The well known fact that low temperature and absence of catalysts favor the formation of molecules of higher molecular weight is confirmed. Moreover it is indicated that in the case of several peaks in the molecular weight–frequency curve the peaks representing the highest molecular weights also represent the most linear molecular shapes. A polymerization process performed at a moderate temperature and in the absence of oxygen or catalysts seems to give a more homogeneous sample than processes performed under other conditions. Even if the process is well defined it is obviously very difficult, if at all possible, to get molecules of a uniform shape, because different polymerization mechanisms will occur simultaneously. Branching can occur in different ways due to different polymerization conditions, and therefore give rise to different physico-chemical behavior. In order to get a detailed picture of the polymolecularity it is necessary to carry out both sedimentation and diffusion measurements, as different molecular species may have the same sedimentation constant but different diffusion constants or *vice versa*. From this it can also be understood that molecular weight determinations based upon viscosity measurement will also be influenced by the different behavior of the different molecular species. If the same constants are used in the modified Staudinger formula, this phenomenon will contribute to the inaccuracy of the molecular weight determination.

Acknowledgment.—We want to express our sincere thanks to Dr. R. Boyer of the Dow Chemical Company for kindly supplying us with several samples, to Mr. B. Olofsson for valuable discussions and to Mr. I. Walldén for skillful assistance in the calculations.

DUAL ADSORPTION OF POLAR ORGANIC COMPOUNDS ON STEEL[1]

BY NORMAN HACKERMAN AND E. L. COOK[2]

Department of Chemistry, University of Texas, Austin, Texas

Received June 7, 1951

A portion of the surface of steel powder is specific to the irreversible adsorption of alkyl carboxy acids, amines, alcohols and esters. Certain areas apparently will irreversibly adsorb either acid or amine, whereas other areas are specific to the acid or to the amine. Alcohols and esters are not irreversibly adsorbed to the extent the acids are on fresh steel powder but appear to be irreversibly adsorbed on certain of the same sites which adsorb acids. Alcohols and esters are not irreversibly adsorbed by steel powder on which an acid has already been irreversibly adsorbed. The extent of total adsorption (reversible plus irreversible) of the second solute, for systems investigated in this study, is only slightly reduced by the pretreatment of the steel powder with another solute. The maximum amount of irreversible adsorption observed with the organic solutes is not sufficient to form a closed packed monolayer over the surface of the steel powder available for krypton adsorption.

Previous studies on the adsorption of polar organic compounds from benzene solution on steel powder showed that all of the adsorbed component could not be desorbed by repeated washings with benzene.[3] The amount of irreversible adsorption was shown to differ for the alkyl carboxy acids, amines, alcohols and certain esters, but was essentially constant within each homologous series. This behavior suggested that the irreversible adsorption process occurred on areas of the metal surface which were to some degree specific toward certain functional groups. The present investigation was undertaken to obtain further information on the degree of specificity of the surface of the steel powder toward the various functional groups.

Experimental

The steel powder, polar organic compounds and benzene solvent used were taken from the same lots as in earlier work.[3] The equipment and technique for measuring the amount of adsorption have also been described in detail earlier. The procedure for this study was developed to permit a second adsorption process to be carried out on steel powder samples upon which a polar material had already been adsorbed. The procedure was as follows: Freshly washed and cleaned samples of steel (SAE 1020) powder were repeatedly contacted with benzene solution of a given polar organic compound until adsorption was complete as indicated by no further increase in weight of the steel powder samples after removal of excess solution from the powder and drying. After the adsorption had reached equilibrium, the steel powder samples were subjected to a desorption process which consisted of thoroughly washing the steel powder with benzene solvent until the dried samples showed no further weight loss. It was observed that not all of the adsorbed component could be desorbed with repeated washings, the amount remaining irreversibly adsorbed being characteristic of the functional group of the polar organic compound and to a large extent independent of the molecular weight of the alkyl chain.

Steel powder samples pretreated in this manner were then contacted with benzene solution containing polar compounds with a different functional group but having a hydrocarbon chain containing the same number of carbon atoms. The contacting was continued over a period of several days until no further adsorption was indicated by increases in weight of the dried steel powder samples. It was observed that the pretreated steel samples showed weight increases due to adsorption of solute from the second set of solutions. The steel powder samples were then subjected to the desorption process and the washings were continued until no further weight loss was obtained.

Results

In Fig. 1 are shown results of the dual adsorption of stearic acid and octadecylamine. The stearic acid first adsorbed was only partially desorbed by the washing procedure as formerly described.[3] Subsequent contacting of the pretreated powder with octadecylamine solutions gave a weight increase due to adsorbed octadecylamine. The weight increase of the dried powder over the weight with the undesorbable stearic acid is shown as adsorbed octadecylamine. The amount of adsorbed amine is slightly less than the amount adsorbed on fresh steel powder which had not previously been contacted with stearic acid solutions.

Desorption of amine by repeated washings until there was no further weight loss showed an incomplete desorption of the amine. Assuming no desorption or displacement of the firmly adsorbed stearic acid occurred during the subsequent contacts with amine solution and washings, the total amount of undesorbable material would account for the original undesorbable stearic acid and an additional amount of undesorbable octadecylamine being present on the surface at the same time. The amount of undesorbable amine present, however, was less than in the case where the amine had been the first component adsorbed.

In Fig. 2 are shown results of adsorption of stearic acid on steel powder samples which had been pretreated with octadecylamine. The adsorption of stearic acid on the pretreated samples was slightly less than on fresh steel samples. Again assuming no desorption or displacement of the first adsorbed amine, the amount of undesorbable stearic acid was considerably less than that observed when fresh steel samples were used. A similar set of data were developed using lauric acid and dodecylamine as the adsorbed components. The results obtained with the C_{12}-compounds corresponded closely to the data obtained with the C_{18}-compounds.

In Fig. 3 are shown the results of the adsorption of octadecyl alcohol from benzene solution on steel powder samples which had been pretreated with stearic acid in the same manner as described above. The adsorption of octadecyl alcohol was slightly less than that observed when fresh steel samples were used. Upon being subjected to repeated washings with benzene, however, the weight losses observed indicated that all of the adsorbed alcohol was desorbed, if no desorption of the stearic acid occurred.

Figure 4 shows the results obtained when stearic acid was adsorbed from benzene solution by steel powder which had been pretreated with octadecyl

(1) Presented before the Division of Colloid Chemistry at the 115th National Meeting of the American Chemical Society, which was held in San Francisco, California, March, 1949.

(2) Magnolia Petroleum Co., Dallas, Texas.

(3) E. L. Cook and N. Hackerman, THIS JOURNAL, **55**, 549 (1951).

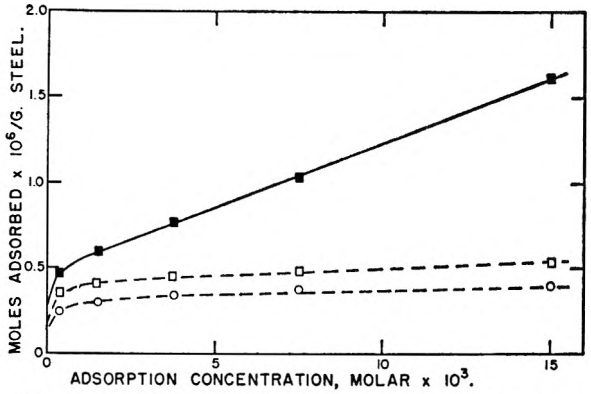

Fig. 1.—Dual adsorption of stearic acid and octadecylamine: total adsorption (——); irreversible adsorption (– – –); O, acid; □, amine.

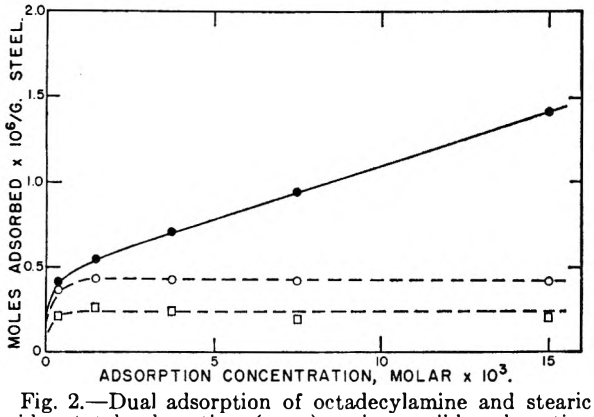

Fig. 2.—Dual adsorption of octadecylamine and stearic acid: total adsorption (——); irreversible adsorption (– – –); O, acid; □, amine.

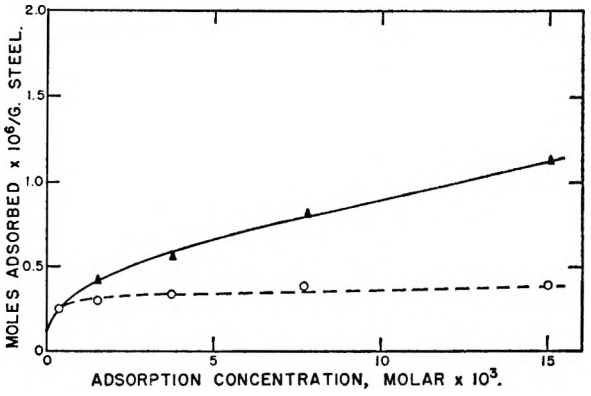

Fig. 3.—Dual adsorption of stearic acid and octadecyl alcohol: total adsorption (——); irreversible adsorption (– – –); O, acid; Δ, alcohol.

alcohol. The adsorption of stearic acid was slightly less than that observed on fresh steel powder samples. Upon desorption by benzene washings, weight losses indicated that a portion of the stearic acid was not desorbed and remained on the powder along with the undesorbed alcohol remaining from the pretreatment. The total amount of undesorbed alcohol and acid was very nearly equivalent to the amount of stearic acid which could not be desorbed from fresh steel powder samples. Due to experimental mishap, results from the full range of solute concentrations covered by other experiments in this study were not obtained. The results

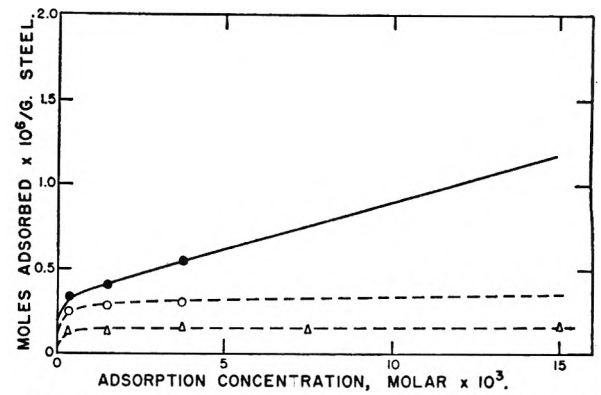

Fig. 4.—Dual adsorption of octadecyl alcohol and stearic acid: total adsorption (——); irreversible adsorption (– – –); O, acid; Δ, alcohol.

were extrapolated into the higher concentration range according to trends observed in systems with other solutes.

A study of the dual sclute system of stearic acid and methyl stearate ester (Figs. 5 and 6) indicated a behavior similar to that observed with the stearic acid–octadecyl alcohol system.

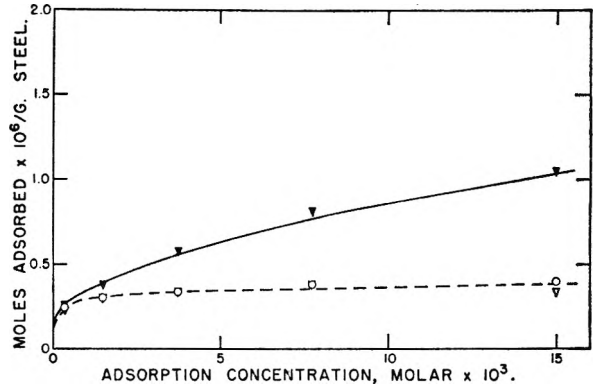

Fig. 5.—Dual adsorption of stearic acid and methyl stearate: total adsorption (——); irreversible adsorption (– – –); O, acid; ▽, ester.

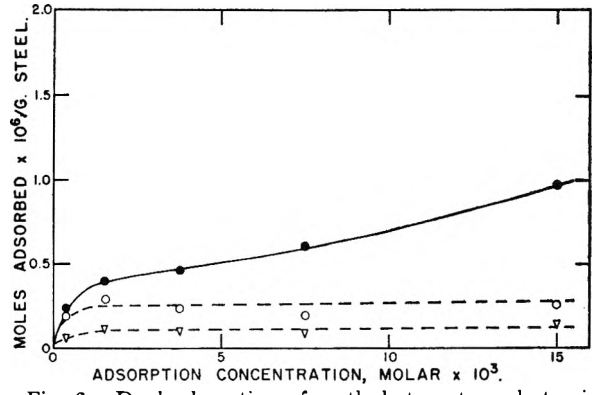

Fig. 6.—Dual adsorption of methyl stearate and stearic acid: total adsorption (——); irreversible adsorption (– – –); O, acid; ▽, ester.

Discussion

The results obtained with the acid–amine system (Figs. 1 and 2) suggest that the portion of the adsorbed components which could not be desorbed were, to some extent, situated on specific adsorption

sites. It appears that certain areas adsorbed only acid or amine, whereas other areas could adsorb either acid or amine. The amount of the second component which was readily removable by solvent treatment was not altered greatly by the presence of the first adsorbed component.

In either of the dual solute systems, acid–alcohol or acid–ester, if the acid were the first solute to be adsorbed on the fresh steel powder, no appreciable amount of the second solute, alcohol or ester, was irreversibly adsorbed. Since alcohols and esters have been previously shown to be capable of being irreversibly adsorbed on fresh steel powder, this is interpreted as an indication that both alcohols and esters are adsorbed on some of the same adsorption sites as the acid. The acid, being the first adsorbed prevents any further irreversible adsorption of alcohol or ester. The assumption that displacement was not a major factor is supported by the fact that with the reverse system the total irreversibly held components is greater than for either one alone. The pretreatment of the powder with alcohol or ester, neither of which is irreversibly adsorbed on fresh steel powder to the extent observed with the acid, apparently does not interfere with further irreversible adsorption of the acid which is irreversibly adsorbed to a greater extent than alcohol or ester on fresh steel surfaces. The acid is adsorbed to the extent that the amount of the first irreversibly adsorbed component, either alcohol or ester, plus the then irreversibly adsorbed acid is approximately equivalent to the amount of acid which is irreversibly adsorbed on fresh steel powder.

Based on the surface area of the steel powder which was determined to be 0.10 $m.^2/g.$ by low temperature adsorption of krypton, and assuming a cross sectional area of 21 $Å.^2$ for the adsorbed organic molecule, the maximum amount of irreversible adsorption observed in the dual systems did not exceed 70% of that required for a close packed monolayer.

Acknowledgment.—The authors wish to thank the Office of Naval Research for their financial support of this work, under contract N5 ori-136, T. O. II.

STATISTICAL THERMODYNAMICS OF THE TRANSITION REGION BETWEEN TWO PHASES. I. THERMODYNAMICS AND QUASI-THERMODYNAMICS[1,2]

BY TERRELL L. HILL

Naval Medical Research Institute, Bethesda, Md.

Received June 25, 1951

The thermodynamics and quasi-thermodynamics of plane and spherical surfaces are discussed, including an alternative formulation of Gibbs' surface thermodynamics and an improvement on the Tolman quasi-thermodynamic theory. The results of this paper will be applied later to approximate statistical mechanical calculations now in progress.

I. Introduction

In these papers we shall investigate the statistical thermodynamics of interfacial regions using approximate methods which are more refined than those employed by Tolman.[3] Kirkwood and Buff[4] have given a rigorous statistical discussion of the plane surface case, but their *general* equations are apparently too complicated for numerical applications. However, they have made calculations in the approximation that the gas and liquid densities are both assumed constant right up to a mathematical surface of density discontinuity. The present theory introduces an approximation in the statistical model at the outset but leads to equations which can be solved numerically and predicts a continuous transition in density in the interfacial region, as must be the case physically and as would be found from the general equations of Kirkwood and Buff if they could be applied. Tolman introduced the van der Waals equation as a statistical model, but in such a way that there is still some discontinuity in density at a mathematical surface.

In earlier notes[5] we outlined the general approach, which is applicable to plane or curved interfaces with one or more components, spherical drops and bubbles, plane interfaces with one phase under an extra hydrostatic pressure, and physical adsorption. Numerical calculations on these topics are in progress, based on van der Waals and improved approximate theories of the liquid state. These results will be published later.[5a] However, we may mention here that preliminary calculations, based on (a) a van der Waals model[5,6] and (b) a hard sphere model[6,7] with a superimposed van der Waals type smoothed potential, give results in semi-quantitative agreement with those of Tolman and Kirkwood and Buff for the magnitude of the surface tension and the location of the surface of tension (and hence for the superficial density of matter at the surface of tension and for the dependence of

(1) The opinions contained herein are those of the writer and do not necessarily reflect the views of the Navy Department.

(2) Presented at an American Chemical Society meeting, Boston, April, 1951.

(3) R. C. Tolman, *J. Chem. Phys.*, **16**, 758 (1948); **17**, 118, 333 (1949); see also F. O. Koenig, *ibid.*, **18**, 449 (1950).

(4) J. G. Kirkwood and F. P. Buff, *ibid.*, **17**, 338 (1949).

(5) T. L. Hill, *ibid.*, **19**, 261 (1951); **19**, 1203 (1951).

(5a) The results for a plane surface with one component have been published: T. L. Hill, *ibid.*, **20**, 141 (1952).

(6) T. L. Hill, paper presented at an American Chemical Society Meeting, Boston, Mass., April, 1951.

(7) L. Tonks, *Phys. Rev.*, **50**, 955 (1936).

surface tension on pressure and curvature) in a one-component system. Model (b) gives a value of the surface tension for argon in much better agreement with experiment than model (a), as expected.

The present paper is concerned with the necessary thermodynamic and quasi-thermodynamic (definition below) background for the statistical mechanical calculations.

II. Plane Surface, $p_\alpha = p_\beta$

Consider a two phase (α and β) system with a plane interface of area $\mathcal{A}$ in *complete* equilibrium.

Following Verschaffelt,[8] Bakker (and van der Waals, Jr.),[9] and especially Guggenheim,[10] the Helmholtz free energy A of the *entire*[11] system is determined by T, V, $\mathcal{A}$ and the numbers of molecules (or moles) of the various components, N_1, $N_2, \cdots$. In particular

$$dA = -SdT - pdV + \gamma d\mathcal{A} + \Sigma\mu_i dN_i \qquad (1)$$

$$\gamma \equiv (\partial A/\partial \mathcal{A})_{T,V,N_i}$$

where $p = p_\alpha = p_\beta$ and the μ_i are the equilibrium pressure and chemical potentials. Integrating Eq. 1 keeping temperature and composition constant

$$\gamma = [pV - (\Sigma\mu_i N_i - A)]/\mathcal{A} \qquad (2)$$

This is the only result we will need. For further details see Guggenheim.[10]

It will be noted that in this analysis there is no *necessity* for introducing non-macroscopic concepts such as "dividing surface," "surface excess," etc.

Quasi-Thermodynamic Treatment

We now derive an expression for γ, based on quasi-thermodynamic concepts (that is, thermodynamic concepts on a molecular level), which will be needed in our approximate statistical approach to this problem. Let the z axis be normal to the plane interface and let the bottom and top of the container of volume V be at $z = 0$ in phase α and at $z = h$ in phase β, respectively. Let $\rho_i(z)$ be the mean molecular density of the i-th component at z and let $\mathrm{A}_i(z)$ be the mean contribution of a molecule of type i at z to A. The functions $\rho_i(z)$ and $\mathrm{A}_i(z)$ must of course be provided by a molecular theory. Then

$$V = \int_0^h \mathcal{A}dz \qquad (3)$$

$$N_i = \int_0^h \mathcal{A}\rho_i(z)dz \qquad (4)$$

$$A = \Sigma \int_0^h \mathcal{A}\rho_i(z)\mathrm{A}_i(z)dz \qquad (5)$$

Substituting Eqs. (3)–(5) into Eq. (2)

$$\gamma = \int_0^h [p - p'(z)]dz \qquad (6)$$

$$p'(z) = \Sigma\rho_i(z)[\mu_i - \mathrm{A}_i(z)] \qquad (7)$$

In either bulk phase $p' = p(\mathrm{A}_i^\alpha \rightarrow \mathrm{A}_i^\alpha$ or $\overline{\mathrm{A}}_i^\beta$, partial molal quantities). Choosing a new origin ($z' = 0$) in the neighborhood of the interface at, say, $z = d$

$$\gamma = \int_{-\infty}^{+\infty} [p - p'(z')]dz' \qquad (8)$$

where of course $p'(z')$ in Eq. (8) is understood to mean $p'(d + z')$ in the notation of Eq. (7), and the value of γ is clearly independent of the arbitrary choice of d. In a one-component system, aside from the location of the origin, the curves $\rho(z')$, $\mathrm{A}(z')$ and $p'(z')$ are completely determined by the temperature only, and p, μ and γ are functions of temperature only.

Equation 8 is the formal and rigorous quasi-thermodynamic equivalent of the more detailed statistical mechanical equation of Kirkwood and Buff. Equation 8, it should be noted, avoids the incorrect interpretation of p' by Tolman.[3,4]

Although we can avoid use of a Gibbs dividing surface here, for future reference we give a mechanical definition of the surface of tension. From Eq. 8, we may regard $(p - p')dz'$ as a force (per unit length) acting parallel to the physical surface and there is such a force for each dz'. From elementary mechanics, these separate forces can be replaced by a single resultant force γ with a plane of action located at

$$\bar{z}' = (1/\gamma) \int_{-\infty}^{+\infty} [p - p'(z')]z'dz' \qquad (9)$$

and called the surface of tension. Choosing another new origin ($z'' = 0$) at the surface of tension, Eq. 9 becomes

$$\int_{-\infty}^{+\infty} [p - p'(z'')]z''dz'' = 0 \qquad (10)$$

III. Curved Surfaces

We confine ourselves to the case of spherical surfaces. In the absence of external fields this is the case of interest, while if external fields are present they should be included explicitly in the thermodynamics. In this section the curvature is taken sufficiently large so that (1) edge effects (see Fig. 1) may be neglected and (2) the bulk properties of the respective phases are reached on either side of the interface. Very small drops and bubbles will be discussed in Section IV.

Guggenheim[10] has remarked that Gibbs' discussion[12] of curved surfaces is "difficult" and "obscure." The alternative formulation given below begins by extending Guggenheim's own treatment of plane surfaces to spherical surfaces, and this, the writer believes, makes possible a rather more transparent formulation.

It has been noted that the thermodynamic treatment of plane surfaces above (Eq. 1 and 2) is entirely in terms of macroscopic thermodynamic properties of the system. We begin in an analogous fashion here. Consider a spherical cone of solid angle ω and let r be a distance from the center of the cone (Fig. 1). The numbers of molecules N_1, $N_2, \cdots$ are introduced into a container consisting of that part of the cone between $r = R_\alpha$ (phase α) and $r = R_\beta$ (phase β), $R_\beta > R_\alpha$, at temperature T, with

(8) J. E. Verschaffelt, *Acad. roy. Belg., Bull. Classe sci.*, **22**, 373, 390, 402 (1936).

(9) G. Bakker, "Handbuch der Experimentalphysik," Vol. VI, 1926.

(10) E. A. Guggenheim, *Trans. Faraday Soc.*, **36**, 397 (1940); also "Thermodynamics," North Holland Publishing Co., Amsterdam, 1949.

(11) Guggenheim considers a thin sheet parallel to and including the transition zone, but points out that the restriction "thin" is not essential. We find it convenient to omit this restriction and discuss the entire bulk two phase system including the interface between phases.

(12) The collected works of J. Willard Gibbs, Vol. I, Yale University Press, New Haven, 1948.

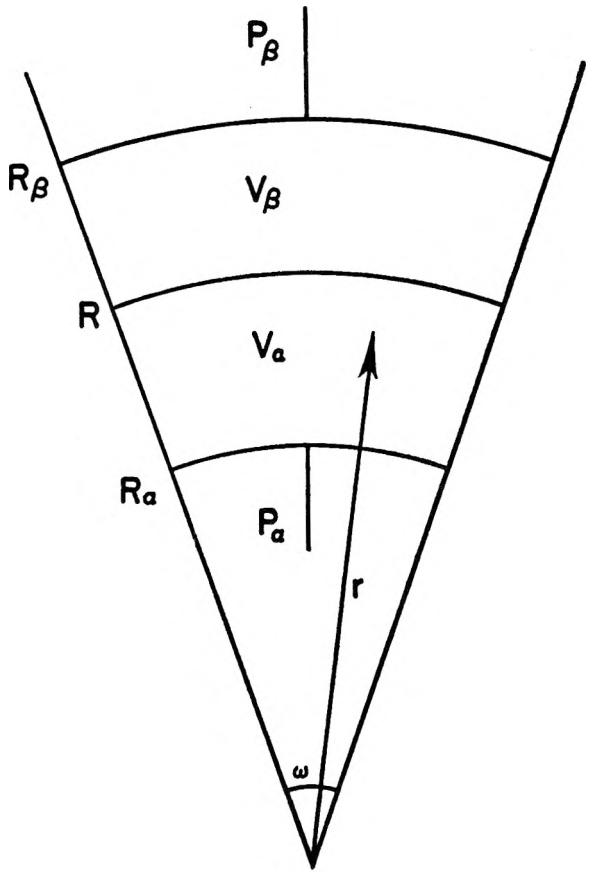

Fig. 1.

the constraint that contours of equal density, etc., lie on spherical surfaces with center at $r = 0$. The system is assumed to be in a state of complete equilibrium, and all the thermodynamic properties of the system are completely determined by the macroscopic quantites T, R_α, R_β, ω, N_1, $N_2, \cdots$. We are interested only in such values of these quantities as lead to a two phase (α and β) system. The equilibrium pressures in the bulk phases, far from the interface, are p_α and p_β.

With constant geometry we have the general requirement

$$dA = -SdT + \Sigma\mu_i dN_i \quad (R_\alpha, R_\beta, \omega \text{ constant}) \qquad (11)$$

Also, there is no uncertainty about the external work terms associated with dR_α, dR_β and $d\omega$. The complete expression for dA is

$$dA = -SdT - p_\beta \omega R_\beta^2 dR_\beta + p_\alpha \omega R_\alpha^2 dR_\alpha + \sigma d\omega + \Sigma\mu_i dN_i \qquad (12)$$

where

$$\sigma \equiv (\partial A/\partial\omega)_{T,R_\alpha,R_\beta,N_i}$$

Integrating this equation at constant T, R_α, R_β and composition

$$\sigma\omega = A - \Sigma\mu_i N_i \qquad (13)$$

which is the analog of Eq. 2.

Up to this point we have introduced macroscopic properties only. To proceed further we must now turn to concepts such as "dividing surface," "surface excess," etc. This is not necessary in dealing with plane surfaces (with $p_\alpha = p_\beta$) partly because the definition of $\mathcal{A}$ in this case is unambiguous; but with curved surfaces the "area" $\mathcal{A}$ depends on the precise location of the "surface."

To define the area $\mathcal{A} = \omega R^2$, the value of R locating the dividing surface must be specified. The various bulk intensive properties of the system have constant values in the separate phases but depend on r in the interfacial region (the μ_i are constant everywhere). In general the dividing surface may be located by means of some arbitrarily chosen condition or recipe based on the variation in one or more of the bulk or surface intensive (or extensive, in some cases) properties of the system in the interfacial region. There are an infinite number of possibilities, but, for example, we might choose R so that for the k-th component $\rho_k(R) = (\rho_k^\alpha + \rho_k^\beta)/2$; or R might be chosen so that the so-called surface excess of the k-th component is zero; etc. In any case, once the *condition* is specified, R is determined by T, R_α, R_β, ω, N_1, $N_2, \cdots$, since *all* properties of the system, including the r dependence of intensive and extensive properties, are determined by these variables.

Having found R from the chosen dividing surface condition and the values of T, R_α, R_β, ω, N_1, $N_2, \cdots$, we have immediately the volumes V_α and V_β and the area $\mathcal{A}$

$$V_\alpha = (\omega/3)(R^3 - R_\alpha^3) \qquad (14)$$

$$V_\beta = (\omega/3)(R_\beta^3 - R^3) \qquad (15)$$

$$\mathcal{A} = \omega R^2 \qquad (16)$$

Also

$$dV_\alpha = (d\omega/3)(R^3 - R_\alpha^3) + \omega(R^2 dR - R_\alpha^2 dR_\alpha) \qquad (17)$$

$$dV_\beta = (d\omega/3)(R_\beta^3 - R^3) + \omega(R_\beta^2 dR_\beta - R^2 dR) \qquad (18)$$

$$d\mathcal{A} = R^2 d\omega + 2\omega R dR \qquad (19)$$

where it is understood that in general dR may represent a change in the value of R as a result of changing T, R_α, R_β, ω, N_1, $N_2, \cdots$, to a neighboring equilibrium state, the dividing surface *condition* being fixed, of course. Further, it is easy to verify—as one would expect merely from the number of independent variables involved—that R may instead be considered a function of T, V_α, V_β, $\mathcal{A}$, N_1, $N_2, \cdots$, for a given dividing surface condition.

Solving Eq. 17–19 for dR_α, dR_β, and $d\omega$ in terms of dV_α, dV_β, $d\mathcal{A}$ and dR, and substituting these expressions into Eq. 12, we find, using Eq. 13 to eliminate σ

$$dA = -SdT - p_\alpha dV_\alpha - p_\beta dV_\beta + \gamma d\mathcal{A} + CdR + \Sigma\mu_i dN_i \qquad (20)$$

where the symbols γ and C are used to represent the expressions

$$\gamma = [p_\alpha V_\alpha + p_\beta V_\beta - (\Sigma\mu_i N_i - A)]/\mathcal{A} \qquad (21)$$

$$C = \omega R^2(p_\alpha - p_\beta) - 2\omega\gamma R \qquad (22)$$

It should be emphasized that Eq. 20 applies to the system in a state of complete equilibrium. Thus there is, for example, no *additional* condition of mechanical equilibrium to be imposed, this condition being already automatically taken care of (Eq. 22). Equation 21, it may be noticed, is consistent, as it must be, with the result of integrating Eq. 20 at constant T, R and composition.

R is not an additional independent variable in

Eq. 20, as already mentioned. Hence we can eliminate dR with the result

$$dA = -(S - C(\partial R/\partial T))dT - (p_\alpha - C(\partial R/\partial V_\alpha))dV_\alpha - (p_\beta - C(\partial R/\partial V_\beta))dV_\beta + (\gamma + C(\partial R/\partial \mathcal{A}))d\mathcal{A} + \Sigma(\mu_i + C(\partial R/\partial N_i))dN_i \quad (23)$$

Equation 23 is valid for *any* choice of dividing surface condition. However, because of the relative complexity of the coefficients in Eq. 23 for an arbitrary dividing surface, this approach does not appear to be especially convenient.

Instead of eliminating the term $C\,dR$ in Eq. (20), as above, without restricting the dividing surface condition, we can as an alternative dispose of this term by using $C = 0$ *as the dividing surface condition.* The result is

$$dA = -S dT - p_\alpha dV_\alpha - p_\beta dV_\beta + \gamma d\mathcal{A} + \Sigma\mu_i dN_i \; (C = 0) \quad (24)$$

where, unlike Eq. 23, Eq. 24 is valid *only* for this particular condition ($C = 0$) specifying the location of the dividing surface. Gibbs calls the dividing surface so obtained the "surface of tension" (because of the mechanical significance of Eq. 25 below).

From Eq. 21 it is clear that the value of γ depends on the location of the dividing surface through $\mathcal{A}$, V_α and V_β. From Eq. 22, the condition for the surface of tension is

$$2\gamma/R = p_\alpha - p_\beta \qquad (C = 0) \quad (25)$$

That is, for given values of T, R_α, R_β, ω, N_1, $N_2, \cdots$, the right-hand side of Eq. 25 is independent of the location of the dividing surface while both γ and R depend on its location. The surface of tension is therefore found by choosing that particular dividing surface which gives the quantity $2\gamma/R$ the same value as the invariant quantity $p_\alpha - p_\beta$.

Returning to Eq. 20, the concept of surface excesses in thermodynamic functions, with respect to the dividing surface, may now be introduced as done by Gibbs. One easily obtained result we shall need is

$$\mathcal{A}d\gamma = -S^s dT - \Sigma N_i^s d\mu_i + C dR \quad (26)$$

$$= -\Sigma N_i^s d\mu_i \qquad (T \text{ constant}, C = 0) \quad (27)$$

where S^s and N_i^s represent surface excesses, Eq. 27 applying to the surface of tension only. C in Eq. 26 is of course given by Eq. 22.

In conclusion, we consider that the present treatment using only *complete* equilibrium states and starting with Eq. 12 has several advantages. Explicit expressions appear quite naturally for the differential coefficients of Eq. 20. There is no chance of confusion about the number of independent variables, and physically impossible (for a system maintained in complete equilibrium) virtual variations are not employed (*e.g.*, see Guggenheim's[10] remark "...it is therefore impossible to conceive of a variation of an interface apart from a variation in at least one of the bulk phases..."). Also, any possible uncertainty about the actual correctness of the coefficients of dT, dV_α, dV_β and dN_i in Eq. 20 is eliminated by beginning with Eq. 12 which avoids introduction at the outset of the concept of a dividing surface. Equation 12 is based on macroscopic thermodynamics only, and therefore furnishes a completely reliable starting point. Finally, Eqs. 25 and 21 provide an explicit and general criterion for locating the surface of tension (as does also Eq. 27, in different form).

Surface Tension and Curvature

We have modified the derivation but not any of the results of Gibbs' thermodynamics of surfaces. Also, the rigorous *thermodynamic* analyses of the dependence of surface tension on curvature by Tolman[3] and by Koenig[3] are of course unaffected. This should be made clear since Tolman's quasi-thermodynamics and molecular theory are open to some criticism.

Quasi-Thermodynamic Treatment

We have (see Eq. 3–5)

$$A = \Sigma \int_{R_\alpha}^{R_\beta} \omega r^2 \rho_i(r) A_i(r) dr, \text{ etc.} \quad (28)$$

Then (Eq. (21))

$$\gamma\mathcal{A} = \int_{R_\alpha}^{R} \omega r^2 [p_\alpha - p'(r)]dr + \int_{R}^{R_\beta} \omega r^2 [p_\beta - p'(r)]dr \quad (29)$$

$$p'(r) = \Sigma\rho_i(r)[\mu_i - A_i(r)] \quad (30)$$

or, writing $x = r - R$ and $c = 1/R$

$$\gamma = \int_{-a}^{0} (1 + cx)^2 [p_\alpha - p'(x)]dx + \int_{0}^{+b} (1 + cx)^2 [p_\beta - p'(x)]dx \quad (31)$$

where the origin is at the (arbitrary) dividing surface, and it is understood that $p'(x)$ in Eq. 31 means $p'(R + x)$ in the notation of Eq. 30. The constants a and b are sufficiently large so that $x = -a$ is in bulk α and $x = b$ is in bulk β; otherwise they are arbitrary and for convenience can be set equal to infinity.

Substitution of Eq. 31 into Eq. 25 gives the exact quasi-thermodynamic condition for the position of the surface of tension; that is, the value of R, locating the origin in Eq. 31, is adjusted until $2\gamma/R$ has the value $p_\alpha - p_\beta$.

In the one-component case, for a *given dividing surface condition,* taking the origin at the dividing surface, the curves $\rho(x)$, $A(x)$ and $p'(x)$ are completely determined by the temperature and curvature ($c = 1/R$) of the dividing surface; and p_α, p_β, μ and γ are functions of T and c only. In this connection we shall make use below of derivatives such as $(\partial\rho(x)/\partial c)_T$, $(\partial\mu/\partial c)_T$, etc., the dividing surface *condition* being arbitrary but constant.

Tolman has derived an approximate expression for the surface of tension condition, in the one-component case, essentially as follows. For T, V_α, V_β and $\mathcal{A}$ constant, Eq. 20 becomes

$$dA = C'dc + \mu dN \quad (32)$$

$$C' = -CR^2$$

We now regard c as an independent variable so N becomes a function of T, V_α, V_β, $\mathcal{A}$ and c. Hence

$$C' = (\partial A/\partial c)_{T,V_\alpha,V_\beta,\mathcal{A}} - \mu(\partial N/\partial c)_{T,V_\alpha,V_\beta,\mathcal{A}} \quad (33)$$

The condition for the surface of tension can then be written

$$(\partial A/\partial c)_{T,V_\alpha V_\beta,\mathcal{A}} = \mu(\partial N/\partial c)_{T,V_\alpha,V_\beta,\mathcal{A}} \; (C = 0) \quad (34)$$

Using Eq. 28 and the analogous equation for N, but neglecting the dependence of p_α, p_β and $p'(x)$ on curvature, Eq. 34 reduces to Tolman's *approximate* condition for the surface of tension

$$\int_{-a}^{0}(1+cx)x(p_\alpha - p')\mathrm{d}x + \int_{0}^{b}(1+cx)x\,(p_\beta - p')\mathrm{d}x = 0 \quad (35)$$

However, if no approximations are made, Eq. 34 becomes instead

$$2\int_{-a}^{0}(1+cx)x(p_\alpha - p')\mathrm{d}x + 2\int_{0}^{b}(1+cx)x(p_\beta - p')\mathrm{d}x + \int_{-a}^{0}(1+cx)^2\left[\left(\frac{\rho}{\rho_\alpha}-1\right)\frac{\partial p_\alpha}{\partial c}+\frac{\partial}{\partial c}(p_\alpha - p')\right]\mathrm{d}x + \int_{0}^{b}(1+cx)^2\left[\left(\frac{\rho}{\rho_\beta}-1\right)\frac{\partial p_\beta}{\partial c}+\frac{\partial}{\partial c}(p_\beta - p')\right]\mathrm{d}x = 0 \quad (C=0) \quad (36)$$

Using Eq. 31, this simplifies to

$$\mathfrak{A}(\partial\gamma/\partial c) + N^s(\partial\mu/\partial c) = 0 \quad (C=0) \quad (37)$$

as the condition for the surface of tension, which is essentially just Eq. 27.

Equation 25 ("mechanical") and 27 ("differential") provide alternative but equivalent conditions for the surface of tension. The differential condition is, however, not very convenient in applications. We might note that the mechanical condition (Eq 25 and 31) can be written as

$$\int_{-a}^{0}(1+cx)x(p_\alpha - p')\mathrm{d}x + \int_{0}^{b}(1+cx)x(p_\beta - p')\mathrm{d}x + (1/c)\int_{-a}^{0}(1+cx)(p_\alpha - p')\mathrm{d}x + (1/c)\int_{0}^{b}(1+cx)(p_\beta - p')\mathrm{d}x - (p_\alpha - p_\beta)/2c^2 = 0 \quad (C=0) \quad (38)$$

As $c \to 0$, the last three terms cancel and there remains the (mechanical) condition for a plane surface

$$\int_{-\infty}^{+\infty} x(p - p')\mathrm{d}x = 0 \quad (C=0,\ c=0) \quad (39)$$

identical with Eq. 10 and employed by Kirkwood and Buff.[4] In summary, the exact Eq. 25 and 31 should be used for a curved surface in place of Eq. 35 (Tolman); Eq. 39 is exact for the plane surface.

IV. Small Spherical Drops and Bubbles

We cannot use the geometry of Fig. 1 for very small drops and bubbles because of edge effects and the fact that the interior phase α may not have "bulk" properties even at $r = 0$. So we must take $R_\alpha = 0$ and $\omega = 4\pi$. It must also be kept in mind that thermodynamics may not apply to drops and bubbles which are too small.

We introduce $N_1, N_2, \cdots$ molecules into a spherical container of radius R_β and at temperature T. These quantities determine all the equilibrium properties of the system. We have the macroscopic equation[13]

$$\mathrm{d}A = -S\mathrm{d}T - p_\beta 4\pi R_\beta^2 \mathrm{d}R_\beta + \Sigma\mu_i \mathrm{d}N_i \quad (40)$$

(13) We note that we cannot integrate Eq. 40 as we did Eq. 12.

An arbitrary dividing surface condition and R_β, T, N_1, N_2, ..., determine the location R of the dividing surface. Then

$$V_\alpha = 4\pi R^3/3,\ V_\beta = 4\pi(R_\beta^3 - R^3)/3,\ \mathfrak{A} = 4\pi R^2 \quad (41)$$

The procedure from this point is somewhat arbitrary but we adopt the suggestion of Gibbs[14] and introduce a reference bulk phase α^0 in order to obtain final equations formally identical with those of Section III. T, p_β and the composition of bulk β determine all the intensive properties of a bulk phase α^0 with the same temperature and chemical potentials as β. Let $p_\alpha^0(\neq p_\beta)$ be the pressure on α^0. We now *define* γ by

$$\gamma = [p_\alpha^0 V_\alpha + p_\beta V_\beta - (\Sigma\mu_i N_i - A)]/\mathfrak{A} \quad (42)$$

If we solve Eq. 42 for A, take differentials of both sides of the resulting equation, eliminate $\mathrm{d}A$ using Eq. 40, and then eliminate $\mathrm{d}V_\alpha$, $\mathrm{d}V_\beta$ and $\mathrm{d}\mathfrak{A}$ using Eq. 41, the result is

$$\mathfrak{A}\mathrm{d}\gamma = -S\mathrm{d}T + V_\alpha \mathrm{d}p_\alpha^0 + V_\beta \mathrm{d}p_\beta + C\mathrm{d}R - \Sigma N_i \mathrm{d}\mu_i \quad (43)$$

where

$$C = 4\pi R^2(p_\alpha^0 - p_\beta) - 8\pi\gamma R \quad (44)$$

We define the surface of tension by the condition $C = 0$, or

$$2\gamma/R = p_\alpha^0 - p_\beta \quad (C=0) \quad (45)$$

We introduce surface excesses S^s, N_i^s, etc., using bulk β in $R \leqslant r \leqslant R_\beta$ and *bulk* α^0 in $0 \leqslant r \leqslant R$. Equation 43 then becomes formally identical with Eq. 26 and 27. These results are sufficient to show that the thermodynamics of large drops and bubbles can be extended to small drops and bubbles, with the appropriate introduction of the reference phase α^0 as indicated.

The quasi-thermodynamic expression for γ (see Eq. 31) becomes

$$\gamma = \int_{-R}^{0}(1+cx)^2[p_\alpha^0 - p'(x)]\mathrm{d}x + \int_{0}^{b}(1+cx)^2[p_\beta - p'(x)]\mathrm{d}x \quad (46)$$

V. Plane Surface, $p_\alpha \neq p_\beta$

A system of two phases, with a plane interface, in "equilibrium" at different pressures is of some theoretical interest. If T, p_β and x_β (representing the composition of β) are specified, these determine the μ_i^β, and hence the μ_i^α, and hence $p_\alpha(\neq p_\beta)$ and x_α. The nature of the interface in this case is therefore a well-defined problem in statistical mechanics. The usual device, which we shall not use, of introducing an "inert" supplementary gas to provide the pressure difference is convenient thermodynamically but is an undesired and unnecessary complication for a statistical investigation. However, presumably because of this absence here of hydrostatic equilibrium, the following *thermodynamic* discussion is somewhat intuitive.

The present problem clearly has important features in common with both Sections II and III, and unfortunately proves to be rather difficult unless these analogies are made use of. A dividing sur-

(14) Reference 12, pp. 252-253.

face must be introduced as in Section III to split the total volume V into V_α and V_β (associated with p_α and p_β). By analogy with Eq. 23 and 24, we may conclude that an arbitrary choice of dividing surface will in general (see Eq. 52) lead to complicated coefficients of dT, dV_α, dV_β and dN_i in the expression for dA, but that a particular surface, the surface of tension, will give the desired simple expression

$$dA = -SdT - p_\alpha dV_\alpha - p_\beta dV_\beta + \gamma d\mathfrak{A} + \Sigma\mu_i dN_i \quad \text{(S.T.)} \quad (47)$$

where

$$\gamma \equiv (\partial A/\partial \mathfrak{A})_{T,V_\alpha,V_\beta,N_i}$$

S is the *total* entropy of the entire system of volume V, etc., as in Section II, and "$S.T.$" means "surface of tension." That is, we may take Eq. 47 itself as a (differential) *surface of tension condition*. Integrating Eq. 47 in the usual way

$$\Sigma\mu_i N_i = A + p_\alpha V_\alpha + p_\beta V_\beta - \gamma\mathfrak{A} \quad \text{(S.T.)} \quad (48)$$

Now let some arbitrary dividing surface condition be used, leading to a dividing surface a distance ϵ from the surface of tension in the direction of phase β. The new volumes are

$$V_\alpha' = V_\alpha + \epsilon\mathfrak{A}$$
$$V_\beta' = V_\beta - \epsilon\mathfrak{A} \quad (49)$$

We define γ' by

$$\Sigma\mu_i N_i = A + p_\alpha V_\alpha' + p_\beta V_\beta' - \gamma'\mathfrak{A} \quad (50)$$

and note that the value of γ' depends on the dividing surface condition

$$\gamma' = \gamma + (p_\alpha - p_\beta)\epsilon \quad (51)$$

Substituting Eq. 49 into Eq. 47 gives

$$dA = -SdT - p_\alpha dV_\alpha' - p_\beta dV_\beta' + \gamma' d\mathfrak{A} + \Sigma\mu_i dN_i + (p_\alpha - p_\beta)\mathfrak{A}d\epsilon \quad (52)$$

Now ϵ can be regarded (dividing surface *condition* fixed) as a function of, say, p_α, T, x_α, or of T, V_α', V_β', $\mathfrak{A}$, N_i. With the latter choice the term in $d\epsilon$ in Eq. 52 may be eliminated leading to a complicated equation analogous to Eq. 23 and valid for *arbitrary* dividing surface condition.

Returning to Eq. 47 and introducing surface excesses with respect to the surface of tension, we find (compare Eq. 26 and 27)

$$\mathfrak{A}d\gamma = -S^s dT - \Sigma N_i^s d\mu_i \quad \text{(S.T.)} \quad (53)$$

If the $d\mu_i$ are eliminated using, say

$$d\mu_i = -\bar{s}_i^\alpha dT + \bar{v}_i^\alpha dp_\alpha \quad (x_\alpha \text{ constant}) \quad (54)$$

then

$$(\partial\gamma/\partial T)_{p_\alpha,x_\alpha} = -[(S^s/\mathfrak{A}) - \Sigma\Gamma_i\bar{S}_i^\alpha] \quad \text{(S.T.)} \quad (55)$$

$$(\partial\gamma/\partial p_\alpha)_{T,x_\alpha} = -\Sigma\Gamma_i\bar{v}_i^\alpha \quad \text{(S.T.)} \quad (56)$$

where $\Gamma_i = N_i^s/\mathfrak{A}$, in formal agreement with the curved surface equations (see Koenig[3]) as may have been anticipated on comparing Eq. 24 and 47. Equation 56 may be regarded as a differential surface of tension condition, more convenient than Eq. 47 (but still not very practical in applications). That is, Eq. 56 is not satisfied for an arbitrary dividing surface (γ' and Γ_i').

Let us introduce an auxiliary dividing surface located by the condition (Koenig[3,15])

$$\Sigma\Gamma_i^0\bar{v}_i^\alpha = 0 \quad (57)$$
$$\Gamma_i^0 = N_i^0/\mathfrak{A}$$

where N^0 is the surface excess in N_i at the auxiliary dividing surface. Let δ be the distance of the auxiliary surface from the surface of tension in the direction of phase β, and let V_α^0 and V_β^0 be the volumes on either side of the auxiliary surface. Then from Eq. 56

$$(\partial\gamma/\partial p_\alpha)_{T,x\alpha} = -(1/\mathfrak{A})\Sigma[N_i - \rho_i^\alpha(V_\alpha^0 - \delta\mathfrak{A}) - \rho^\beta(V_\beta^0 + \delta\mathfrak{A})]\bar{v}_i^\alpha = -\delta(1 - \Sigma\rho_i^\alpha\bar{v}_i^\alpha) \quad (58)$$

in agreement with the curved surface result (Koenig[3]) in the limit of zero curvature. In the special case of a one-component liquid (α) in equilibrium with vapor (β), Eq. 57 becomes $\Gamma^0 = 0$ and

$$(\partial\gamma/\partial p_\alpha)_T = -\delta[1 - (\rho^\beta/\rho^\alpha)] \cong -\delta \quad (59)$$

The calculations (in the case $p_\alpha = p_\beta$) of Tolman,[2] Kirkwood and Buff[4] and Hill[6] all indicate that $\delta > 0$ (compare Rice[16]).

Let γ^0 be the value of γ' at the auxiliary dividing surface (Eq. 50), $\epsilon = \delta$. Then differentiating Eq. 51, using Eq. 58 and

$$(\partial p_\beta/\partial p_\alpha)_{T,x\alpha} = \Sigma\rho_i\beta\bar{v}_i\alpha \quad (60)$$

we find

$$(\partial\gamma^0/\partial p_\alpha)_{T,x\alpha} = (p_\alpha - p_\beta)(\partial\delta/\partial p_\alpha)_{T,x\alpha} \cong 0 \quad (61)$$

Quasi-thermodynamic Treatment

With an arbitrary dividing surface as origin, Eq. 50 becomes

$$\gamma' = \int_{-\infty}^{0}[p_\alpha - p'(z)]dz + \int_0^{\infty}[p_\beta - p'(z)]dz \quad (62)$$

$$p'(z) = \Sigma\rho_i(z)[\mu_i - A_i(z)] \quad (63)$$

We may regard (Eq. 9 and 10) γ' as a resultant force (per unit length) with a plane of action at

$$\bar{z} = (1/\gamma')\left[\int_{-\infty}^{0}(p_\alpha - p')zdz + \int_0^{+\infty}(p_\beta - p')zdz\right] \quad (64)$$

In general the arbitrary dividing surface and its associated plane of action will *not* coincide ($\bar{z} \neq 0$).

With a plane interface and $p_\alpha = p_\beta$, the plane of action of γ has the same location for *any* arbitrary dividing surface and is called the surface of tension. With a curved interface, there is a unique dividing surface, called the surface of tension, giving mechanical equilibrium of the form of Eq. 25. If an arbitrary dividing surface does not coincide with the mechanical surface of tension, the thermodynamic consequence is the complicated Eq. 23. By analogy with this situation, we conclude, for a plane interface with $p_\alpha \neq p_\beta$ that Eq. 47 will be consistent with the following mechanical condition for the surface of tension: the dividing surface must be so chosen that it *coincides* with its associated plane of action. That is

$$\int_{-\infty}^{0}(p_\alpha - p')zdz + \int_0^{+\infty}(p_\beta - p')zdz = 0 \quad \text{(S.T.)} \quad (65)$$

a result which might have been anticipated from Eq. 38.

(15) See E. A. Guggenheim and N. K. Adam, *Proc. Roy. Soc.* (*London*), **A139**, 218 (1933).

(16) O. K. Rice, *J. Chem. Phys.*, **15**, 333 (1947).

THE EFFECT OF ATMOSPHERIC GASES ON THE INTERFACIAL TENSION BETWEEN MERCURY AND SEVERAL DIFFERENT LIQUIDS[1]

BY F. E. BARTELL AND RICHARD J. BARD[2]

Department of Chemistry, University of Michigan, Ann Arbor, Michigan

Received July 2, 1951

The pendent drop method of measuring fluid–fluid boundary tensions was adapted to the measurement of mercury–liquid interfacial tensions under specially controlled conditions. Time studies of interfacial tension were employed throughout. A readily reproducible value for the initial interfacial tension between mercury and deoxygenated water was observed. This value was identified as corresponding to mercury at its potential of instantaneous immersion in water and at the potential of the electrocapillary maximum of the mercury–water system. Oxygen was found to have a pronounced effect in systems containing liquids which support ionization. It was shown that in the absence of an applied potential and in the initial absence of potential determining ions such systems nevertheless assume the properties of electrocapillary systems as a result of chemical interaction between mercury and dissolved oxygen. Some of the results obtained for mercury in contact with oxygen-saturated or aerated water were shown to be predictable from existing electrode potential and electrocapillary data. Oxygen was shown to have no effect on the interfacial tension between mercury and non-polar liquids. The data on the combined effects of oxygen and carbon dioxide in mercury–water systems enabled a quantitative explanation of the low values previously reported for the interfacial tension between mercury and water. It is concluded that the corrosion of mercury in contact with aerated liquids which support ionization and the resulting electrocapillary effects must be considered in the measurement of interfacial tension in unpolarized systems and that the definite, single values of interfacial tension reported in the literature for such systems provide an insufficient description of the systems upon which the measurements were made. It is also concluded that equilibrium values of interfacial tension in such systems can be obtained only after the electrochemical requirements for equilibrium have been satisfied.

Mercury–liquid interfacial tensions are measured in two distinctly different types of experiments. In one type a charge is imparted to the mercury by means of an applied potential and the interfacial tension at that potential is measured. Gouy's experiments[3] on electrocapillarity may be classified as of this type. In the other type no potential is applied to the mercury, and any charge which develops on the mercury arises from an interaction between the mercury and the contiguous liquid. Systems employed in the second type of experiment are said to be "unpolarized." Interfacial tension studies of unpolarized mercury–liquid systems may be grouped as follows: (a) the investigation of electrocapillary behavior resulting from the presence of potential determining ions,[4] (b) the study of mercury–solution interfacial tension as a function of solution concentration for aqueous salt solutions[5–9] and for binary mixtures of organic liquids[10] and (c) the study of interfacial tensions between mercury and "pure" liquids.[10–14]

In the past it has been the practice to report definite, single values for the interfacial tensions between mercury and "pure" liquids in unpolarized systems. It appears to have been assumed that these values were equilibrium values of interfacial tension. Since the workers cited above in connection with the studies of interfacial tensions between mercury and "pure" liquids in unpolarized systems did not report any attempts to remove dissolved air from the experimental systems, it must be assumed that the definite, single values of mercury–liquid interfacial tension reported by them were measured on systems containing dissolved air. Recently in this Laboratory Bartell and Bjorklund[15] demonstrated that the interfacial tensions between mercury and each of two liquids, water and benzene, are dependent upon the time of contact of mercury with the contiguous liquid whenever dissolved air is present.

The present investigation of interfacial tensions in unpolarized mercury–liquid systems was undertaken to determine (a) the effect of atmospheric gases, (b) the significance of the definite, single values reported in the literature and (c) the conditions under which equilibrium values of interfacial tension can be observed. Time studies of interfacial tension were used throughout to provide the necessary experimental data.

Experimental

Materials.—Reagent grade mercury, dispersed into fine droplets, was caused to fall through a column filled with a 20% solution of mercurous nitrate in 18% nitric acid. This wet oxidation procedure was repeated four times. The mercury was then washed five times with distilled water and was dried under vacuum. Vapor phase oxidation was accomplished by distilling the mercury in a stream of purified air three times, an appreciable residue being discarded after each distillation.

Water was purified by redistilling laboratory distilled water from dilute alkaline permanganate solution in a double-baffled, all Pyrex still. Water prepared in this manner had a specific conductance of 1×10^{-6} ohm^{-1} cm.$^{-1}$ after exposure to the atmosphere.

Reagent grade benzene was shaken with successive portions of concentrated sulfuric acid, was washed with 20% sodium hydroxide solution and with distilled water, was dried over calcium oxide and was then fractionally distilled. The middle fraction, which boiled at a temperature constant to within 0.1°, was refluxed over clean mercury for 48 hours.

(1) The data in this paper were taken from a portion of a thesis of Richard J. Bard, submitted to the School of Graduate Studies of the University of Michigan in partial fulfillment of the requirements for the Ph.D. degree, June, 1951.

(2) Allied Chemical and Dye Corporation Fellow, 1950–1951.

(3) M. Gouy, *Ann. Chim. Phys.*, **29**, 145 (1903); **8**, 291 (1906); **9**, 75 (1906).

(4) S. R. Craxford, *Phil. Mag.*, **16**, 66 (1933).

(5) K. E. Glidden, *J. Am. Chem. Soc.*, **57**, 236 (1935).

(6) W. C. McC. Lewis, *Z. physik. Chem.*, **73**, 129 (1910).

(7) W. A. Patrick, *ibid.*, **86**, 545 (1914).

(8) M. Potau, *Anales real. soc. espan. fis. y. quim.*, **44A**, 445 (1948).

(9) R. K. Schofield, *Phil. Mag.*, **1**, 641 (1926).

(10) H. Dunken, *Z. physik. Chem.*, **B47**, 195 (1940).

(11) (a) F. E. Bartell, L. O. Case and H. Brown, *J. Am. Chem. Soc.*, **55**, 2419 (1933); (b) H. Brown, *ibid.*, **56**, 2564 (1934).

(12) G. F. Dasher, Thesis, Univ. of Michigan, 1949.

(13) (a) W. D. Harkins and W. W. Ewing, *J. Am. Chem. Soc.*, **42**, 2539 (1920); (b) W. D. Harkins and E. H. Grafton, *ibid.*, **42**, 2534 (1920).

(14) M. G. Quincke, *Phil. Mag.*, **41**, 251 (1871).

(15) F. E. Bartell and C. W. Bjorklund, THIS JOURNAL, **56**, 453 (1952).

No scumming of the mercury was observed. The benzene was then shaken with freshly activated silica gel for two periods of 24 hours each and was stored over the second charge of silica gel. Immediately prior to use the benzene was decanted from the silica gel and distilled again to remove any fine particles of silica gel in suspension. Reagent grade *n*-heptane was subjected to a similar purification.

Absolute ethyl alcohol was refluxed for 24 hours over magnesium and iodine according to the dehydration method of Lund and Bjerrum.[16] During refluxing the still was swept with purified nitrogen. A middle fraction was then distilled directly into the pendent drop cell and tip assembly after the unit had been thoroughly swept with purified nitrogen. The cell and tip assembly unit was sealed without exposure of the ethyl alcohol to the atmosphere.

Nitrogen was purified according to the method of Meyer and Ronge.[17] Air, oxygen and hydrogen were purified by passage through dehydrite, ascarite and low temperature traps. The oxygen–carbon dioxide mixtures were prepared by passing purified oxygen through a mixture of potassium carbonate and potassium bicarbonate at several different temperatures.

All glassware was cleaned in a hot mixture of sulfuric and nitric acids. After a prolonged rinse with distilled water, the glassware was steamed and dried.

All apparatus used in the purification of materials and in the preparation of systems was completely grease free.

Measurement of Tensions.—The pendent drop method of measuring fluid–fluid boundary tensions[18] was used since this method is precise, accurate and ideally suited to the measurement of the variation of interfacial tension with time. Values of the pendent drop function, $1/H$, corresponding to given ratios of selected plane diameter to maximum diameter of the pendent drop were obtained from the theoretical tables which have been reported independently by Niederhauser[19] and by Fordham.[20]

The apparatus for photographing pendent drops utilized a Western Union Company 300-watt concentrated arc lamp and a collimating lens as a source of parallel light and was equipped with a Bausch and Lomb Type H camera with a special lens. All components of the apparatus were mounted on an optical bench. The entire apparatus was shock insulated to prevent the transmission of building vibrations to the pendent drops. Sealed systems in which pendent drops were formed were mounted in the optical beam in an air thermostat which was controlled to within several tenths of a degree of 25°. Preliminary experiments proved that the apparatus used in this research was capable of an absolute accuracy of 0.2%.

Tension–time curves, determined by measuring each value of interfacial tension on an independently formed drop, were readily reproducible for a given sealed system. Reproducibility of tension–time curves measured on independently prepared systems was obtained only when extreme care was used in the preparation of the systems.

Preparation of Systems.—Immediately prior to a run, a portion of purified mercury was distilled at a pressure of 1–2 mm. of mercury. The pendent drop tip was inserted below the surface of the freshly distilled mercury and the syringe, used to form the pendent drops of mercury, was filled. The tip was then inserted into an optical cell containing the liquid whose interfacial tension against mercury was to be studied.

Systems which were subsequently treated by prolonged bubbling of the liquid in the cell with a purified gas were sealed except to the purified gas stream. After bubbling was completed, the gas stream was diverted and the systems were completely sealed by allowing mercury to flow from the bottom of cup joints into capillary bends.

Systems for the measurement of the interfacial tensions between mercury and degassed water were prepared under vacuum. Water was alternately frozen and thawed until no gas bubbles could be detected in the ice and was then transferred to the pendent drop cell. The cell and tip assembly unit was sealed without exposure to the atmosphere.

(16) H. Lund and J. Bjerrum, *Ber.*, **64B**, 210 (1931).

(17) F. R. Meyer and G. Ronge, *Angew. Chem.*, **52**, 637 (1939).

(18) J. M. Andreas, E. A. Hauser and W. B. Tucker, THIS JOURNAL, **42**, 1001 (1938).

(19) D. O. Niederhauser, Thesis, Univ. of Michigan, 1947.

(20) S. Fordham, *Proc. Roy. Soc.* (*London*), **A194**, 1 (1948).

Mercury–Water Interfacial Tensions

In Laboratory Air.—An average of the results obtained from measurements on mercury–water systems which had been exposed to laboratory air and had not been further treated following exposure yielded the curve in Fig. 1. The dependence of interfacial tension on time is very similar to that reported by Bartell and Bjorklund.[15]

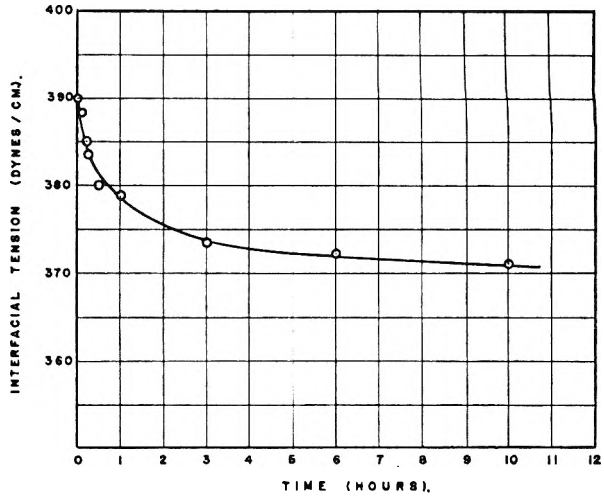

Fig. 1.—Interfacial tension between mercury and water containing dissolved laboratory air as a function of time; temperature, 25°.

For experimental purposes the possible components of laboratory air were grouped as follows: (a) inactive gases (nitrogen, hydrogen and inert gases); (b) oxygen; (c) carbon dioxide; (d) water vapor; (e) organic vapors; (f) miscellaneous gases reactive toward water (HCl, SO_3, NO_2, H_2S, SO_2, NH_3).

Nitrogen, hydrogen and inert gases are classified as inactive with respect to effect on the interfacial tension between mercury and water because from an energy consideration these gases would not be expected to be adsorbed at a mercury–water interface and because Henry and Jackson[21] found no appreciable difference among the definite, single values of interfacial tension measured in atmospheres of nitrogen and of hydrogen and in systems containing only mercury and water.

It was assumed that oxygen, carbon dioxide, organic vapors and gases which react with water to form weakly dissociated acids or bases could be removed by prolonged bubbling with an inactive gas. The results obtained with oxygen-saturated water established the validity of this assumption. Non-removable contamination of the water by trace amounts of HCl, SO_3 and NO_2 in the laboratory air was not detectable. No difference in behavior was observed between systems which were prepared by distilling water directly into the cell under an atmosphere of purified nitrogen and systems in which water was bubbled with purified nitrogen after the cell had been filled in laboratory air. In addition, the non-removable contamination detected in certain oxygen-saturated systems was found to be characteristic of given batches of water rather than

(21) D. C. Henry and J. Jackson, *Nature*, **142**, 616 (1938).

of preliminary exposure of the water to laboratory air.

In the "Absence" of Dissolved Gases.—The variation with time of the interfacial tension between mercury and water from which dissolved gases were removed by alternate freezing and thawing is illustrated by Fig. 2. A great deal of effort was expended to ensure freedom from contamination in the apparatus used to prepare systems containing degassed water. In view of the large dependence of interfacial tension on time, however, the possibility of contamination must be considered and the effectiveness of the degassing method must be questioned. The only reproducible value of interfacial tension observed in systems containing degassed water was the initial value, which was measured after the pendent drop of mercury had been exposed to the water for 30 seconds. As will be shown in the following section, this value is characteristic of mercury which has been in contact with deoxygenated water for only a short time.

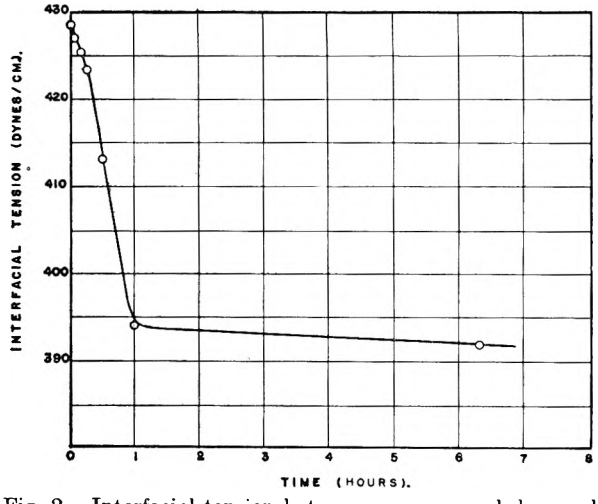

Fig. 2.—Interfacial tension between mercury and degassed water as a function of time; temperature, 25°.

In Inactive Gases.—The curves of Fig. 3 summarize the extensive efforts made to determine the time dependence of the interfacial tension between mercury and water in the presence of inactive gases. Each curve corresponds to the system which displayed the smallest time dependence of interfacial tension for the designated treatment. The tension–time curves for any given bubbling treatment were not sufficiently reproducible to warrant averaging.

The initial value of interfacial tension observed in these systems agreed with that observed with degassed water and was readily reproducible. An average value of approximately 428 dynes/cm. was obtained for a total of ten systems in which oxygen was removed from the water by bubbling with nitrogen, by bubbling with hydrogen, by bubbling with helium and by degassing under vacuum. This

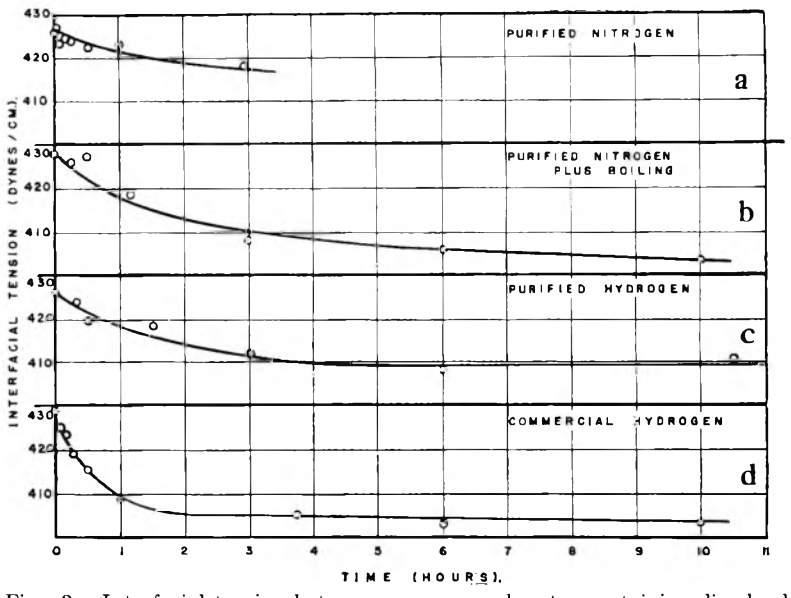

Fig. 3.—Interfacial tension between mercury and water containing dissolved inactive gas as a function of time; temperature, 25°.

average initial value agrees very closely with the value of 426–427 dynes/cm. obtained by Henry and Jackson[21] for the interfacial tension between unpolarized mercury and deoxygenated water. Gouy[22] measured the interfacial tensions between mercury and a number of dilute capillary inactive salt solution at the potentials of the electrocapillary maxima by means of the sessile drop method and found that the maximum interfacial tensions agreed very closely for these solutions. He identified the average value of 426.7 dynes/cm. at 18° as the interfacial tension between mercury and pure water at the potential of the electrocapillary maximum for that system.

The close agreement between the value obtained by Gouy for polarized systems and the average initial value obtained in the present investigation of unpolarized interfaces in systems in which dissolved oxygen was removed indicates that the charge must have been the same in both cases. Since the mercury possesses zero charge at the potential of the electrocapillary maximum, the initial charge on the mercury in contact with deoxygenated water in the present investigation must also have been zero. Philpot[23] showed that the potential of instantaneous immersion of a mercury electrode in a solution is the same as the potential of the electrocapillary maximum for mercury in the same solution. Thus the initial interfacial tension value of approximately 428 dynes/cm. must correspond to a mercury potential very close to the potential of instantaneous immersion of mercury in water.

The time dependence of the curves in Figs. 2 and 3 may have resulted from adsorption of contaminants which were not removable by degassing or by gas bubbling, from the development of charge on the mercury with consequent electrocapillary effects or from a combination of both factors. The system used to determine the curve in Fig. 3(b) was subsequently treated with purified oxygen.

(22) M. Gouy, *Ann. Phys.*, **6**, 5 (1916).
(23) J. St. L. Philpot, *Phil. Mag.*, **13**, 775 (1932).

The features of the curve for the oxygen-saturated system indicated the absence of contaminants. For this reason electrocapillary effects must be considered in connection with the lowering of interfacial tension with time shown in Figs. 2 and 3.

Since the systems initially contained no mercury ions, charge could have developed on the mercury only as the result of chemical reactions taking place at the interface. Reactions involving hydrogen and hydrogen ions are extremely slow at an unpolarized mercury–water interface.[24] Thus it seems highly probable that any charge effect corresponding to the lowering of interfacial tension with time in Figs. 2 and 3 involved traces of oxygen remaining in the systems after deoxygenation.

The Effect of Oxygen.—Figure 4 contains data on oxygen-saturated systems. The upper curve in Fig. 4 corresponds to the oxygen-saturated system which showed the least dependence of interfacial tension upon time. The lower curve in Fig. 4 is an interfacial tension–time curve for a system treated in an identical manner but showing contamination.

All oxygen-saturated systems were prepared and treated in exactly the same manner. A relatively small fraction of the independently prepared samples of water yielded curves similar to the upper curve in Fig. 4. All remaining samples of water led to curves which did not show rapid attainment of a relatively constant mercury–water interfacial tension but showed a large and continuous fall in tension out to the longest time used in the present research.

Data obtained for mercury in contact with water saturated with purified and CO_2-free air were very similar to those obtained with oxygen-saturated water. Again great difficulty was encountered in obtaining uncontaminated samples of water.

For the oxygen-saturated systems an average of all points between 10 minutes and 3 hours for the three best curves gives a value of 388.7 ± 0.2 dynes/cm. A similar average for systems saturated with purified and CO_2-free air gives a value of 390.9 ± 0.4 dynes/cm. However, the difference between these averages is so close to the experimental error of the method of measurement that the difference can be assigned no definite significance. It must therefore be stated that no appreciable difference in behavior of mercury in contact with oxygen-saturated water and in contact with water saturated with purified and CO_2-free air was observed in the present investigation.

In the corrosion of mercury in water containing dissolved oxygen the reduction of oxygen takes place according to the over-all reaction, $4Hg + O_2 + 2H_2O \rightarrow 2Hg_2^{++} + 4OH^-$. Positive charge due to the excess of mercury ions in the metal builds up on the mercury and the tendency for mercury ions to go into solution greatly increases. Since mercury has little tendency to develop a protective oxide film in the presence of dissolved oxygen,[25] mercury ions escape into solution and the

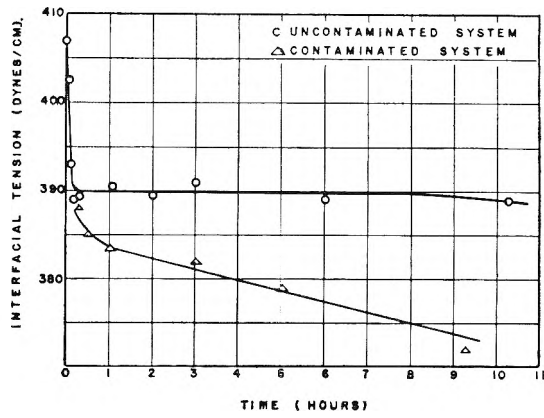

Fig. 4.—Interfacial tension between mercury and oxygen-saturated water as a function of time; temperature, 25°.

potential of the mercury is determined by the equilibrium between mercury ions in the metal and in the solution.

Since the relationship between interfacial tension, potential, charge and surface area is independent of the way in which the potential on the mercury is developed,[2] an unpolarized mercury–water system must behave as an electrocapillary system whenever oxygen is present.

The potential of a $Hg/HgO/OH^-$ electrode at a *p*H of 7 is 0.51 volt positive to a standard hydrogen electrode. According to Craxford[2] the mercury–water interfacial tension corresponding to this value of potential is approximately 35 dynes/cm. below the value at the potential of the electrocapillary maximum. If Gouy's value of 426.7 dynes/cm. is taken as the value of the interfacial tension between mercury and water at the electrocapillary maximum, an interfacial tension value of approximately 392 dynes/cm. corresponds to a potential of +0.51 volt on the standard hydrogen scale. It is interesting to note that the relatively constant value of interfacial tension which was rapidly reached in oxygen-saturated and in air-saturated systems in the present investigation agrees very closely with the above value even though the systems were far from electrochemical equilibrium when the measurements of tension were made.

The relatively constant values of interfacial tension which persisted for several hours in systems containing high concentrations of oxygen could not have been true equilibrium values because the potentials corresponding to these values of tension could not have been static. In such systems the static potential is reached only after the concentration of mercury ions in solution is fixed by the precipitation of mercuric oxide. According to Gatty and Spooner,[26] this process takes hundreds of hours even when the system is agitated.

The Effect of Carbon Dioxide.—Figure 5 contains data showing the effect of dissolved carbon dioxide on the interfacial tension between mercury and oxygen-saturated water. Oxygen-saturated water was used as a reference system since it yielded the most reproducible time variation curves and was the least difficult to prepare. Due to the close agreement between the results for oxygen-saturated

(24) O. Gatty and E. C. R. Spooner, "The Electrode Potential Behaviour of Corroding Metals in Aqueous Solutions," Oxford Univ. Press, London, 1938, p. 43.

(25) G. W. Akimov and G. B. Clark, *Trans. Faraday Soc.*, **43**, 679 (1497).

(26) O. Gatty and E. C. R. Spooner, ref. 24, p. 135.

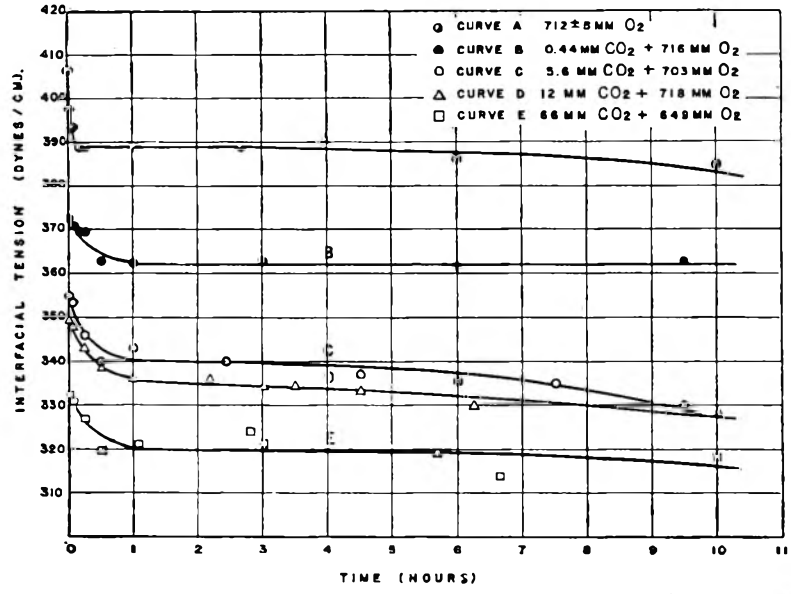

Fig. 5—Interfacial tension between mercury and oxygen-saturated water containing carbon dioxide as a function of time; temperature, 25°.

water and for water saturated with purified air, it was considered that any effect observed in oxygen-saturated water also held true for water containing dissolved purified air. No attempt was made to determine the effect of dissolved carbon dioxide on deoxygenated water systems since electrocapillary data[1] indicate that carbonate, bicarbonate and hydronium ions cause no appreciable depression of the electrocapillary maximum. In addition, the time dependence of interfacial tension in deoxygenated water systems was not sufficiently reproducible to provide a reference curve with which to compare the interfacial tension–time curves for water containing carbon dioxide.

The lower curve of Fig. 6 was obtained by plotting the relatively constant values of interfacial tension shown in Fig. 5. The upper curves of Fig. 6 were obtained by plotting the interfacial tension values at 30 seconds and at 5 minutes. If laboratory air has a carbon dioxide concentration of approximately 350 parts per million,[27] water saturated with laboratory air should yield a value of interfacial tension against mercury no greater than 375–378 dynes/cm. when the measurements are made at times between 30 seconds and 5 minutes. In the determination of mercury–liquid interfacial tension by the drop weight method the rate of drop formation falls within this time range. Most of the drop weight values reported in the literature for the interfacial tension between mercury and water lie between 374 dynes/cm., and 377 dynes/cm. Thus the combined effects of oxygen and carbon dioxide account for the magnitude of previously reported definite, single values of mercury–water interfacial tension.

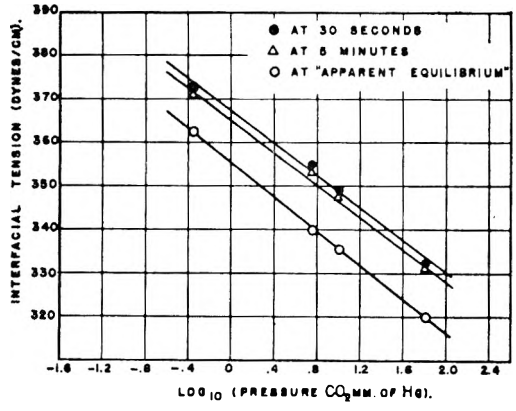

Fig. 6.—Interfacial tension between mercury and oxygen-saturated water containing carbon dioxide as a function of carbon dioxide pressure; temperature, 25°. Interfacial tension *vs.* logarithm of carbon dioxide pressure.

(27) E. L. Quinn and C. L. Jones, "Carbon Dioxide," Reinhold Publishing Corp., New York, N. Y., 1936, p. 120.

Mercury–Organic Liquid Interfacial Tensions

n-Heptane.—Figure 7 summarizes the data on mercury–heptane interfacial tensions as a function of time. Figures 7(b), 7(c) and 7(d) show clearly that neither oxygen nor carbon dioxide individually has any effect on the interfacial tension between mercury and heptane. The lack of oxygen effect in this case proves that an

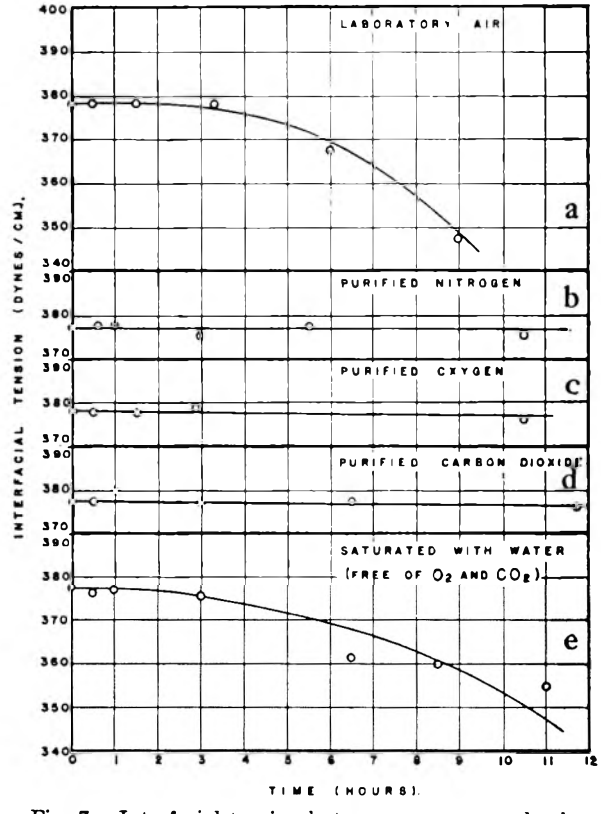

Fig. 7.—Interfacial tension between mercury and *n*-heptane as a function of time; temperature, 25°: 7(a), heptane exposed to laboratory air; 7(b), heptane bubbled with purified nitrogen; 7(c), heptane bubbled with purified oxygen; 7(d), heptane bubbled with purified carbon dioxide; 7(e), heptane saturated with water—entire system; oxygen-free and carbon dioxide-free.

ionic mechanism is necessary for rapid chemical interaction between mercury and oxygen dissolved in a contiguous liquid. In the absence of an oxygen effect carbon dioxide would be expected to have no effect on the interfacial tension between mercury and heptane since the conditions necessary for double layer formation, *i.e.*, charge on the mercury and ions in the contiguous liquid, are absent.

The behavior shown in Fig. 7(a) indicates the presence of contamination. The heptane used for this determination was carefully purified and dried. It was exposed to laboratory air for less than one minute during the assembly of the apparatus. The contamination must have been very slight since its presence did not become apparent until after the mercury had been in contact with heptane for several hours. Figure 7(e) shows the variation of interfacial tension with time for mercury in contact with heptane saturated with water. The water and heptane were very carefully treated to remove dissolved carbon dioxide and dissolved oxygen by prolonged boiling and by sweeping with purified nitrogen. Therefore it is possible to identify the effect shown in Fig. 7(a) as partially due to dissolved moisture.

The unusual feature of the tension time curves of Figs. 7(a) and 7(e), corresponding to contaminated mercury–heptane systems, should be noted. These curves show an increase with time in the rate of decrease of interfacial tension. In all other systems investigated in the present research a decrease with time in the rate of decrease of interfacial tension was observed, regardless of whether chemical reaction or physical adsorption was involved.

The systems used to determine the curves in Figs. 7(a) through 7(d) were all prepared in the same manner up to the point of sweeping with a purified gas. The effectiveness of gas bubbling for removing dissolved moisture from hydrocarbons is clearly indicated by the features of the curves.

An average of all values out to four hours yields an interfacial tension value of 377.7 ± 0.2 dynes/cm. between mercury and *n*-heptane. This value agrees closely with the values reported by several previous investigators.[10,11]

Benzene.—Figure 8 summarizes the data on mercury–benzene interfacial tensions as a function of time. Most of the results are similar to those observed with *n*-heptane. The curves in Figs. 8(b) and 8(c) confirm the observation made in the case of heptane that, within the limits of time used in the present investigation, oxygen has no detectable effect on the interfacial tension between mercury and a solvent which does not support ionization.

The curve of Fig. 8(a) indicates contamination as a result of brief exposure of carefully purified and dried benzene to laboratory air. The behavior shown in Fig. 8(a) is very similar to that reported by Bartell and Bjorklund.[15] Mercury in contact with benzene saturated with water in the absence of oxygen and carbon dioxide yielded the tension–time curve shown in Fig. 8(d). Since a larger decrease in interfacial tension was observed with the system corresponding to Fig. 8(a) than with the system corresponding to Fig. 8(d), it must be concluded that contamination in addition to that by moisture resulted from the brief exposure of the benzene to laboratory air.

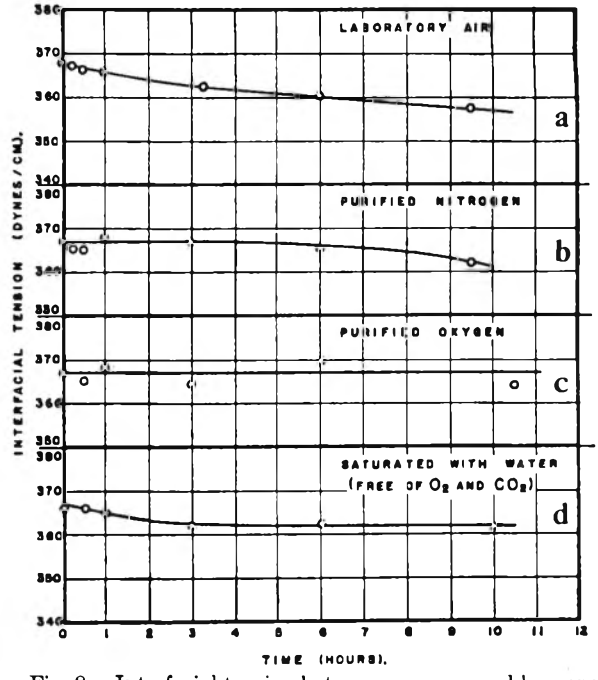

Fig. 8.—Interfacial tension between mercury and benzene as a function of time; temperature, 25°: 8(a), benzene exposed to laboratory air; 8(b), benzene bubbled with purified nitrogen; 8(c), benzene bubbled with purified oxygen; 8(d), benzene saturated with water—entire system; oxygen-free and carbon dioxide-free.

Bartell and Bjorklund[15] observed that the interfacial tension between mercury and benzene saturated with water decreased from an initial value of 365 dynes/cm. to a value of 336 dynes/cm. after 13 hours when dissolved laboratory air was present in the system. A comparison of their data with the curve of Fig. 8(d) shows that dissolved moisture alone affects mercury–benzene interfacial tension to a much smaller degree than does a combination of dissolved moisture and dissolved laboratory air.

The average initial value of approximately 368 dynes/cm. for the interfacial tension between mercury and benzene observed in the present in-

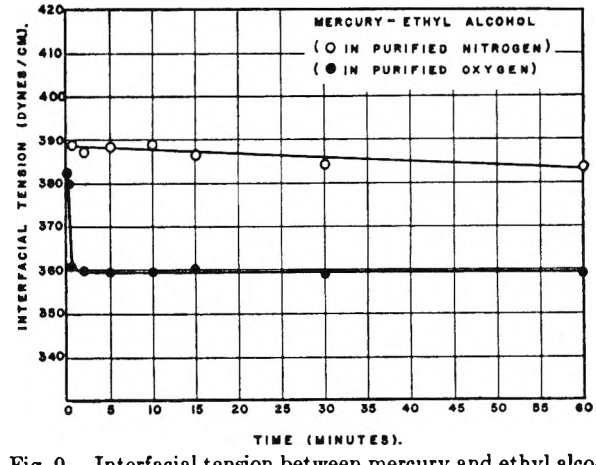

Fig. 9.—Interfacial tension between mercury and ethyl alcohol as a function of time; temperature, 25°.

vestigation is several dynes/cm. higher than any of the previously reported values at 25°.[10,15]

Ethyl Alcohol.—Figure 9 shows the variation of mercury–ethyl alcohol interfacial tensions with time. The system corresponding to the upper curve was prepared with ethyl alcohol which had been dehydrated, distilled and transferred in an atmosphere of purified nitrogen. The lower curve was obtained after the same system had been bubbled with purified oxygen for one hour.

The pronounced effect of dissolved oxygen on the interfacial tension between mercury and ethyl alcohol is further evidence that rapid chemical attack of a mercury surface by oxygen takes place in the presence of a solvent which supports ionization and that under such conditions electrocapillary effects must be considered. By analogy to the mercury–water system, it seems probable that carbon dioxide would have an effect on the interfacial tension between mercury and ethyl alcohol containing dissolved oxygen.

The first two points on the lower curve of Fig. 9 correspond to measurements made at 5 and 15 seconds. The value of interfacial tension measured at 30 seconds was close to the minimum value. The initial rate of decrease of interfacial tension with time was much greater in the mercury–alcohol system than in any of the mercury–water systems.

Previously reported values for the interfacial tension between mercury and ethyl alcohol range from 364 dynes/cm. (at 20°)[13a] to 381.6 dynes/cm. (at 18°).[10] No values were reported for the concentration of dissolved oxygen in the ethyl alcohol used to obtain these values of interfacial tension.

OXYGEN DEFICIENT SILICA PHOSPHORS

BY G. H. WAGNER AND D. G. DOBAY

Laboratory of Linde Air Products Company, Tonawanda, N. Y.

Received July 2, 1951

By the hydrolysis of $SiCl_4$ containing small amounts of $SiHCl_3$, silicas were obtained which contained SiH bonds. Heating these hydrolysates to 500–600° eliminated the hydrogen, and left an oxygen deficient silica which was luminescent under ultraviolet light. The intensity of the luminescence in the best preparations was about one-tenth that of a high efficiency phosphor. Oxygen deficient silicas with the properties of phosphors were also prepared from the cohydrolyzates of Si_2Cl_6–$SiCl_4$ and $C_6H_5SiCl_3$–$SiCl_4$.

Introduction

It is well known that the hydrolysis of $SiCl_4$ leads to silica or silica gel. It is also known[1] that the hydrolysis of $SiHCl_3$ gives a white amorphous powder of the composition $SiHO_{3/2}$, which on heating to 350° and above loses hydrogen to give Si_2O_3. We have investigated the cohydrolysis of $SiCl_4$ and $SiHCl_3$ mixtures and in this way prepared silicas in which the regular silicon–oxygen network was interrupted occasionally by SiH bonds. On heating to 500° and above these materials lost hydrogen and became phosphors. They were white under normal daylight, luminescent under both 2537 and 3650 Å. ultraviolet, and gave a phosphorescent afterglow.

The preparation of a silica phosphor by these means may be represented schematically by the chemical changes

$$x\mathrm{SiCl_4} + \mathrm{SiHCl_3} - (\text{excess})\mathrm{H_2O} \xrightarrow[\text{temperature}]{\text{room}}$$

$$(4x+3)\mathrm{HCl} + -\mathrm{O}\left[\begin{array}{c}\mathrm{O}\\ \mathrm{SiO}\\ \mathrm{O}\\ |\end{array}\right]\begin{array}{c}\mathrm{O}\ \mathrm{O}\ \mathrm{O}\\ \mathrm{SiOSiOSi}\\ \mathrm{H}\ \mathrm{O}\ \mathrm{O}\\ \quad\ |\ \ |\end{array}_{(x-2)} \quad (1)$$

$$-\mathrm{O}\left[\begin{array}{c}\mathrm{O}\\ \mathrm{SiO}\\ \mathrm{O}\\ |\end{array}\right]\begin{array}{c}\mathrm{O}\ \mathrm{O}\ \mathrm{O}\\ \mathrm{SiOSiOSiO}-\\ \mathrm{H}\ \mathrm{O}\ \mathrm{O}\\ \quad\ |\ \ |\end{array}_{(x-2)} \xrightarrow[\text{or greater}]{500^\circ}$$

$$-\mathrm{O}\left[\begin{array}{c}\mathrm{O}\\ \mathrm{SiO}\\ \mathrm{O}\\ |\end{array}\right]\begin{array}{c}\mathrm{O}\ \mathrm{O}\ \mathrm{O}\\ \mathrm{SiOSiOSiO}-\\ \cdot\ \ \mathrm{O}\ \mathrm{O}\\ \quad\ |\ \ |\end{array}_{(x-2)} + 1/2\ \mathrm{H_2} \quad (2)$$

where $0.78 < x/(x+1) < 0.997$

The best phosphors were prepared from $SiCl_4$ solutions containing only 1 to 2% $SiHCl_3$ whereas the above limits of $x/(x+1)$ merely define the limits where luminescence was definitely observed. Reaction (2) represents the activation treatment necessary to convert these materials into phosphors. The SiH bond is probably broken homolytically in reaction (2) giving an atomic hydrogen and an electronically deficient silicon atom, *i.e.*, $\mathrm{Si{:}H} \rightarrow \mathrm{Si\cdot} + \mathrm{H\cdot}$. The atomic hydrogen is free to diffuse and combine to form molecular hydrogen whereas the electronically deficient silicon is fixed somewhat in the rigid silica network. With extended heating, the color of the products (in ordinary light) was changed from white to light tan; the luminescence deepened correspondingly from white through to red. This is believed to be due to the diffusion and self-neutralization by reaction (3) of the electronically deficient silicon atoms.[2]

$$\mathrm{Si\cdot} + \mathrm{Si\cdot} \longrightarrow \mathrm{Si{:}Si} \quad (3)$$

In the dilute range of concentrations (1 to 2% $SiHCl_3$) where we find the greatest luminescence, reaction (3) would be approaching its minimum.

In a recent paper[3] Ewles has described a lumines-

(1) Mellor, "A Comprehensive Treatise on Inorganic and Theoretical Chemistry," Vol. VI, Longmans, Green Co., New York, 1, N. Y., p. 228.

(2) Si_2O_3 formed by heating pure $SiHO_{3/2}$ is dark tan and has no phosphor properties.

(3) Ewles, *Nature*, **165**, 812 (1950).

cent silica. His method of preparation and interpretation of the mechanism differ somewhat from ours. His luminescent silica was prepared by heating silica with hydrogen at 300° or above. He attributed the luminescence to the formation of SiO by the reaction $SiO_2 + H_2 \rightarrow SiO + H_2O$. Judged from the brief description of his products, ours are believed to be more luminescent.

Experimental

(1) **Analyses.**—Heating the silicas containing SiH in 20% aqueous KOH liberates hydrogen.[4] The reaction is

$$SiH + H_2O \xrightarrow{OH^-} SiOH + H_2 \qquad (4)$$

which corresponds to 1 mole of hydrogen per equivalent of SiH. For precise measurements of small amounts of SiH a microgas buret with a small attachment for heating the silica in caustic was used. The buret was thermostated at all times. The heating chamber was thermostated for a zero reading previous to heating the sample and after the completion of the hydrogen evolution. The $SiHO_{3/2}$ content of the sample was calculated from the amount of hydrogen liberated.

It should be pointed out that SiSi bonds also liberate one mole of hydrogen per equivalent.[4] This is of interest in our case since the formation of SiSi bonds during the activation treatment of the phosphor was postulated in the previous section.

(2) **Hydrolysis.**—A typical preparation of silica containing SiH may be described by the following procedure. A six-liter round-bottom flask was filled with 3000 ml. of distilled water at room temperature. The flask was provided with a condenser, mercury seal stirrer and addition tube. A mixture of 195 ml. of $SiCl_4$ and 5.0 ml. of $SiHCl_3$ was added dropwise to the stirred water. The addition required about one hour. The precipitate which formed was collected on a buchner funnel and washed six times with distilled water and finally heated to 200° for 16 hours to dry. The product weighed 6.9 g. (5.5% yield) and contained 0.71% $SiHO_{3/2}$.

The yields obtained by the direct addition of the chlorosilane to water were low (see curve A, Fig. 1). Better yields were obtained by the addition of water to a benzene solution of the chlorosilane. A typical experiment follows. A 3-liter round-bottom flask, provided with condenser, mercury seal stirrer, and addition tube, was filled with 530 ml. of reagent grade benzene, 90 ml. of $SiCl_4$ and 10 ml. of $SiHCl_3$. Distilled water was added dropwise to the vigorously stirred solution. After the addition of about 55 ml. of water, copious gas evolution from the surface of the precipitate was noted. A total of 100 ml. of water was added. The solution was stirred for one-half hour after the addition of water was completed. The precipitate was filtered, washed five times with distilled water, and heated in an oven at 225° for 60 hours. The product weighed 43.1 g. (80.8% yield) and contained 3.47% $SiHO_{3/2}$. Figure 1 compares the yields obtained by the two methods.

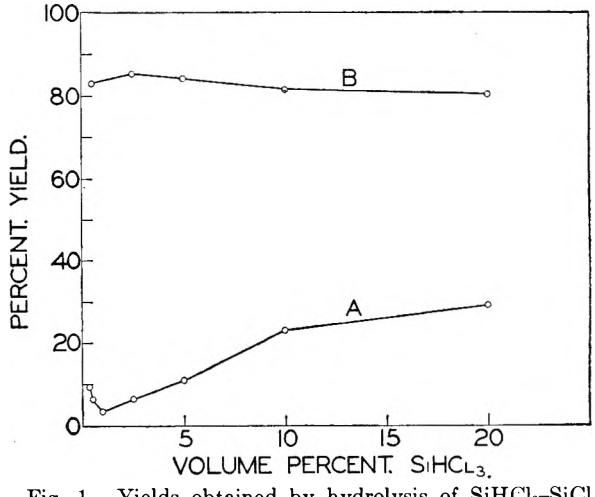

Fig. 1.—Yields obtained by hydrolysis of $SiHCl_3$–$SiCl_4$ mixtures: curve A, direct addition of chlorosilanes to water; curve B, addition of water to benzene solution of chlorosilanes.

The precipitates which first formed by these hydrolysis methods, and which were the only precipitates considered in calculating the yields, were the solids which were converted to phosphors. The aqueous filtrates from the above methods yielded gels on standing overnight. These gels were essentially pure silica gels containing no SiH and were not suited for phosphor preparation. The formation of these pure gels may be attributed to two effects: the first effect would be concentration of the SiH in the initial precipitate due to more rapid hydrolysis of $SiHCl_3$ than of $SiCl_4$; the second effect would be hydrolysis of SiH under acid conditions.[5] Whereas the first effect would increase the SiH content of the first precipitates the second effect, the hydrolysis of SiH, would cause a loss. That the second effect is mostly responsible is shown by Fig. 2 where the SiH content of the precipitates is shown to be always lower than the theoretical value.

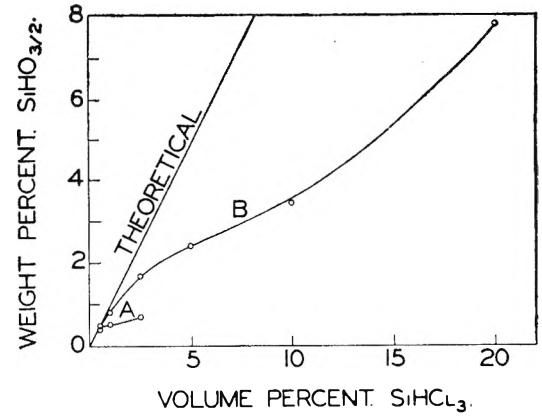

Fig. 2.—$SiHO_{3/2}$ content of hydrolysates as first precipitated: curve A, hydrolysates obtained from direct addition of $SiHCl_3$–$SiCl_4$ mixture to water; curve B, hydrolysates obtained from addition of water to benzene solutions of $SiHCl_3$–$SiCl_4$ mixtures.

(3) **Activation.**—The cohydrolysis products as prepared had no luminescence. A heat treatment was necessary to convert suitable compositions to phosphors. Various experimental arrangements were used to effect the heat treatment. In early work at temperatures up to 500°, the heating was conducted in Pyrex tubes heated in electrical furnaces. Heating to 900° was done in Vycor, heating at 1000 to 1100° in quartz. In order to improve the distribution of heat, a stainless steel tube was slipped between the heating elements of the furnace and the tube containing the sample.

For most of the work reported here at temperatures at 700° and under, a salt-bath was used as the heating medium. Pyrex or Vycor tubes containing the samples could be dipped into the molten bath[6] and brought quickly to temperature. When heating periods of only 10 min. or so were required for optimum activation, this gave a more precise measure of the time at temperature.

The heat treatments were conducted in controlled atmospheres. Nitrogen was used where the temperatures were 500° or less. Argon of 99.99% purity was used at higher temperatures. The impurities in the argon were chiefly nitrogen and less than 15 p.p.m. oxygen.

(4) **Luminescence.**—The samples were examined visually in a dark room under excitation from 2537 and 3650 Å. Some of the best samples were compared with a visual photometer in intensity to a high efficiency phosphor. The latter was a potassium uranyl sulfate with a quantum efficiency of approximately 30% at both the 2537 and 3650 Å.

(4) Rochow, "Chemistry of the Silicones," John Wiley and Sons, Inc., New York, N. Y., 1946, p. 6.

(5) Burkhard and Norton, *Anal. Chem.*, **21**, 304 (1949).

(6) 50–50 mixture of KNO_3 and $NaNO_2$.

excitation wave lengths. Also the potassium uranyl sulfate emitted a banded structure centering in the visible green which made it particularly suited for visual observation. The composition, activation treatment, and the relative brightness of some silica phosphors are shown in Table I.

TABLE I

COMPOSITION AND RELATIVE BRIGHTNESS OF SOME SILICA PHOSPHORS

Phosphors	$SiHO_{3/2}$ content, % Initial hydrolyzate	$SiHO_{3/2}$ content, % After activation	Activation Temp., °C.	Activation Time, min.	Relative brightness at excitation wave lengths 2537 Å.	Relative brightness at excitation wave lengths 3650 Å.
Potassium uranyl sulfate	..	..	...	..	1	1
Silica phosphor 83–14	..	..	603–614	15	0.038	0.007
Silica phosphor 76–8	0.36	0.10	606–616	30	.041	.008
Silica phosphor 79–6	1.67	..	599–603	70	.066	.036
Silica phosphor 74–4	1.67	.14	600–602	37	.080	.036
Silica phosphor 76–6	1.67	.14	588–600	40	.099	.035

Discussion

The optimum condition for the heat treatment was at temperatures of 600° for 30–40 min. At 400° no phosphors could be prepared; at 500° it was possible to obtain phosphors but the heating times were long (several hours) and the products had less luminescence than products prepared at higher temperatures. For example, 16 hr. at 525° resulted in only moderate luminescence as did shorter heating (1 hr.) at 575°. At 600° the luminescence increased up to heating times of 30–40 min. and then decreased. At longer times at 600° and at higher temperatures, the intensity of the luminescence decreased and the color of the fluorescence shifted from white to orange. At temperatures of 700–800°, luminescent products could still be prepared but the appearance of the samples became charred in visible light and heterogeneous under ultraviolet.

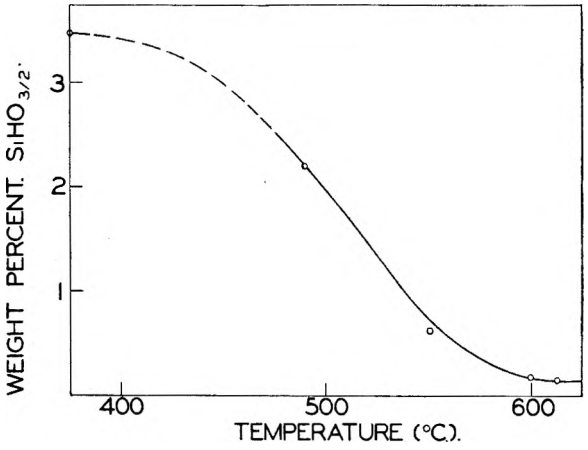

Fig. 3.—Effect of temperature on $SiHO_{3/2}$ content of a typical hydrolysate, one-half hour heating time.

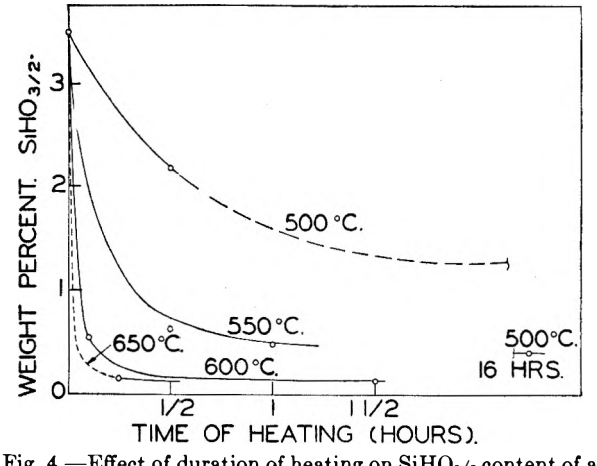

Fig. 4.—Effect of duration of heating on $SiHO_{3/2}$ content of a typical hydrolysate.

Figures 3 and 4 show the effect of these activation treatments on the $SiHO_{3/2}$ content of the silicas. Although these curves are for a single original material which contained 3.5% $SiHO_{3/2}$ they depict the general behavior of samples with higher or lower $SiHO_{3/2}$ contents. In a general way it is possible to correlate the loss of $SiHO_{3/2}$ content with the development of phosphor properties. Luminescent properties became faintly evident as soon as the $SiHO_{3/2}$ content reached about 0.5% and improved steadily as the $SiHO_{3/2}$ content dropped to about 0.15%. However, at this point longer heating adversely affected the phosphor properties without any significant change in the $SiHO_{3/2}$ content as mentioned above. The loss of phosphor properties on extended heating we ascribe to reaction (3).

In theory the curves in Figs. 3 and 4 should approach 1.75% (one-half of the original $SiHO_{3/2}$ content) with increasing time or temperature. This is based on the fact that the analytical procedure used cannot differentiate between SiH and SiSi which is formed from SiH by the reaction

$$2SiHO_{3/2} \longrightarrow Si_2O_3 + H_2 \qquad (5)$$

Experience in our laboratory has shown that the above reaction occurs with pure $SiHO_{3/2}$ above 350° but only in the temperature range 700 to 900° is the rate fairly rapid. The product, Si_2O_3, yields only one-half mole of hydrogen per silicon when treated with aqueous alkali in the analytical procedure

$$SiSi + H_2O \xrightarrow{OH^-} SiOSi + H_2 \qquad (6)$$

One possible reason for our failure to obtain this amount of hydrogen in our present work may be due to the reaction

$$SiH + HOSi \longrightarrow SiOSi + H_2 \qquad (7)$$

In other words, SiH may be lost during the activation by reaction with silanol groups which have avoided condensation, or possibly with adsorbed water. A small amount of side reaction of this type, reaction (7), might not be noted when working with 100% $SiHO_{3/2}$ but might be appreciable in this work where very small amounts of $SiHO_{3/2}$ are under consideration.

Other Systems.—Materials with luminescent properties under ultraviolet light were also prepared from the cohydrolyzates of Si_2Cl_6–$SiCl_4$. Mixtures of Si_2Cl_6 and $SiCl_4$ were hydrolyzed and heat treated similar to the $SiHCl_3$–$SiCl_4$ hydrolysates. The optimum range of temperature for 30-min. heat treatments of these hydrolyzates for maximum luminescence is given in Table II. The sample containing 10.3% Si_2O_3 was highly sensitive to temperature and exhibited a sharp maximum at 600 ± 5°.

The formation of phosphors from Si_2Cl_6–$SiCl_4$ hydrolysates is quite comparable to their formation from $SiHCl_3$–$SiCl_4$ hydrolysates. This arises from the fact that Si_2Cl_6 may hydrolyze to a HOSiSiOH

TABLE II

OPTIMUM HEATING RANGE FOR Si_2Cl_6–$SiCl_4$ HYDROLYSATE (30-MIN. HEATING PERIOD)

Si_2O_3,[a] %	Optimum range, °C.
6.7	500–675
10.3	595–605
27.4	680–780

[a] Calculated from hydrogen liberated by aqueous caustic. These agreed well with the theory for the composition hydrolyzed, indicating no loss of SiSi on hydrolysis.

grouping, which rearranges[7] to SiH on heating, *i.e.*

$$\begin{matrix}\text{SiSi} \\ \text{OO} \\ \text{HH}\end{matrix} \longrightarrow \begin{matrix}\text{SiOSi} \\ \text{O H} \\ \text{H}\end{matrix} \qquad (8)$$

This reaction is very exothermic[8] with the pure hydrolysate of Si_2Cl_6 but proved to be of no trouble in the case of the cohydrolysates with $SiCl_4$. Reaction (8) indicates that the chemistry of the Si_2Cl_6–$SiCl_4$ hydrolysates is too complicated for drawing any direct conclusions as to the activation mechanism to the $SiHCl_3$–$SiCl_4$ hydrolyzates. However, the fact that the Si_2Cl_6–$SiCl_4$ hydrolysates were not phosphors in the unheated state indicates that the phosphors of the $SiHCl_3$–$SiCl_4$ hydrolysates were not dependent on the formation of Si–Si bonds.

In some preliminary experiments, the hydolysates of phenyltrichlorosilane–$SiCl_4$ were found to develop phosphor properties when heated to 700° and above. The mechanism in this case is not known but it is probably due to the actual cleavage of the phenyl–silicon bond, *i.e.*, $C_6H_5Si \rightarrow \cdot Si + C_6H_5\cdot$.

Acknowledgment.—Professor Brian O'Brien of the University of Rochester has kindly made the relative brightness measurements reported here on our phosphors.

(7) Martin, *Ber.*, **45**, 2097 (1912).

(8) Comparable in energy to the decomposition of ammonium nitrate or black powder (private communication of A. D. Kiffer of this Laboratory).

VARIABLES IN THE SELF-ABSORPTION OF LOW-ENERGY BETA PARTICLES

BY GEORGE K. SCHWEITZER AND JAMES W. NEHLS

Department of Chemistry,[1] *University of Tennessee, Knoxville, Tennessee*

Received July 16, 1951

The effects of a number of factors in the self-absorption of the low-energy β-particles of sulfur-35 and calcium-45 have been investigated. Variations in the atomic number of the sample material, the atomic number of the backing, the sample-to-counting tube window distance, and the counting tube window thickness all have an appreciable effect upon the shape of the per cent. specific activity *versus* surface density curve. The atomic number of the siding material surrounding the sample does not appear to influence the shape of the per cent. specific activity plot. Some data have been accumulated on samples containing both sulfur-35 and calcium-45. The results are in accord with what one would expect from the energies of the β-particles being emitted by the two nuclides.

Introduction

In the last few years, a number of investigations have been carried out dealing with the difficulties and corrections involved in counting low-energy β-emitters in the form of solid samples.[2] The use of nuclides having maximum energies below 0.35 mev. presents problems usually not encountered when hard β-emitters are involved. Self-absorption, self-scattering, back-scattering, side scattering and absorption and scattering in the air path and counting tube window could be responsible for variations in counting rates.

This investigation has been devoted to an elucidation of these conditions in order to determine for which factors corrections must be made and which will not really affect the accuracy of counting measurements. Among the factors to be discussed are the average atomic number of the nuclide-containing sample material, which will influence self-scattering, the atomic number of the material used as a mount for the sample, which will determine back-scattering, the atomic number of the siding or shielding which causes side scattering, the distance from the surface of the sample to the counting tube window, the thickness of the tube window and, finally, the effect of having two different active nuclides present in the same sample.

A number of empirical methods have been devised for the treatment of self-absorption data.[2] In these present investigations, the measured sample activities A_m were expressed in terms of per cent. maximum activity. The maximum activity A_i is defined as the constant activity obtained when a plot of measured activity A_m *versus* surface density x of a series of samples levels off near a surface density equal to the maximum range of the β-particle being considered. The measured activities expressed as per cent. were divided by the corresponding sample surface densities to give per cent. specific activities $a_m = (100A_m/xA_i)$. The values of a_m were then plotted *versus* the surface density.

Apparatus and Materials.—Counting was done with a Nuclear D-34 Geiger tube having a 1.4 mg./cm.² end window, and a Nuclear Instrument and Chemical Corporation Model 163 scalar equipped with an automatic timer. When a heavier window was desired, either a 1.7 or 4.8 mg./cm.² aluminum absorber was placed directly over the tube window. The Geiger tube was mounted in a slotted lucite shelf holder allowing the sample to be placed varying distances from the tube window. A Tracerlab SC-16 Windowless Flow Counter was also employed in some of the experiments. This counter was connected to a Tracerlab P-4 Preamplifier and a Tracerlab SC-2A Scalar.

Sulfur-35 and calcium-45, simple β-emitters with maximum energies of 0.17 and 0.26 mev., respectively, were ob-

(1) Contribution No. 102.

(2) G. K. Schweitzer and B. R. Stein, *Nucleonics*, **7**, No. 3, 65 (1950).

tained from the Oak Ridge National Laboratory. Active H_2SO_4 was prepared by adding the carrier-free sulfur-35 in the form of H_2SO_4 to 0.1 N H_2SO_4. The active $CaCl_2$ solution, containing calcium-45, as received from Oak Ridge, was simply diluted to give an approximately 0.1 N concentration.

The lead and aluminum backings used with certain samples were cut from metal foils having surface densities greater than 200 mg./cm.^{2} The aluminum, copper, zinc and lead sidings were cut from metal foils of surface densities greater than that necessary to give maximum scattering. These sidings were square, of such size that the sample cup touched all four sides, and they extended from the sample shelf to the tube window.

Sample Preparation.—The various samples were prepared by precipitating from solution a given amount of the active ion with an excess of inactive precipitant. The precipitate was filtered, washed twice with distilled water, and then suspended in 95% ethanol. This suspension was introduced into a cylindrical lucite centrifuge tube having as a bottom a detachable stainless steel cup with an internal diameter of 2.4 cm. Centrifugation distributed the solid uniformly and compactly over the bottom of the cup. The supernatant liquid was pipetted off, the cup removed from the tube, and the sample allowed to air dry. By means of a simple calculation, the surface density of the sample was found from the weight of the empty cup, the weight of the cup plus the sample, and the area of the cup bottom.

Calcium, strontium, barium and lead sulfate samples containing calcium-45, and calcium sulfate samples containing both active nuclides were prepared in the above mentioned manner. Calcium carbonate and oxide samples containing calcium-45 were made by igniting calcium oxalate samples at 500 and 900°, respectively, for several hours.

TABLE I

PER CENT. SPECIFIC ACTIVITIES FOR STRONTIUM SULFATE SAMPLES[a]

x, (mg./cm.^{2})	a_m, (cm.^{2}/mg.)	x, (mg./cm.^{2})	a_m, (cm.^{2}/mg.)
0.9	18.6	7.4	11.4
1.7	20.0	9.4	9.6
2.3	19.2	12.2	7.9
3.0	17.0	14.2	7.1
4.2	15.2	19.2	5.1
5.8	13.1		

[a] Samples placed 2.5 cm. from counting tube window.

Experimental Results

Atomic Number of Sample Material.—The effect of changing atomic number of the sample was investigated by measuring the activities of several series of salts containing the same active nuclide with various inactive ions. The experimental specific activities of samples of strontium sulfate (average atomic number of 14.3) are given in Table I, and those for lead sulfate (average atomic number of 21.7) are given in the sixth column of Table II. These data are shown in Fig. 1. Similar trends were noted with the other sulfates and with the calcium samples containing calcium-45. These results show that the effect of the average atomic number on the specific activity is quite pronounced at low surface densities. These effects can be attributed to self-scattering which increases with the atomic number of the sample material.[3]

TABLE II

PER CENT. SPECIFIC ACTIVITIES FOR LEAD SULFATE SAMPLES

		a_m at tube window					a_m 2.5 cm. from window			
							Side scatterer used			
x (mg./cm.^{2})	a_{10} Internal counter	1.4 mg./cm.^{2} window	3.1 mg./cm.^{2} window	6.2 mg./cm.^{2} window	a_m 2.5 cm. from window	a_m 5.0 cm. from window	Al	Cu	Sn	Pb
0.9	26.2	20.8	20.0	19.5	19.6	18.0	19.3	19.5	19.2	19.6
1.3	27.3	21.8	21.1	20.8	20.4	19.1	19.9	19.7	19.6	20.1
1.7	28.0	23.1	21.8	21.4	21.0	19.7	20.8	21.0	20.9	21.4
2.0	29.8	23.7	22.3	21.8	21.5	20.1	21.7	21.5	21.1	21.9
3.0	23.9	19.9	19.5	19.0	18.7	17.8	18.4	18.3	18.8	18.5
3.8	19.6	17.2	17.0	17.0	16.7	16.2	16.2	16.7	17.0	17.1
4.2	16.6	16.0	16.3	16.1	16.0	15.8	16.3	16.7	16.0	16.0
5.9	12.9	13.0	13.0	13.2	13.1	13.3	12.8	12.7	13.0	13.2
6.7	12.2	12.3	12.4	12.0	12.3	12.1	12.4	12.0	12.3	12.1
7.2	12.0	11.8	11.9	11.9	11.8	11.7	11.8	11.4	11.6	11.9
7.6	11.2	11.1	11.2	11.3	11.2	11.2	10.8	11.3	11.1	11.1
8.1	10.4	10.6	10.6	10.2	10.4	10.3	10.1	10.0	10.6	10.8
8.6	10.1	10.1	10.4	10.0	9.9	10.2	10.1	9.9	10.2	10.6
8.9	10.0	9.8	9.9	10.0	10.0	10.0	9.8	9.7	10.0	10.0
10.0	9.4	9.5	9.3	9.5	9.4	9.6	9.4	9.3	9.1	9.5
12.0	8.3	8.1	8.0	8.2	8.0	8.1	8.0	8.1	8.0	8.2
13.5	7.4	7.5	7.1	7.5	7.4	7.3	7.2	7.2	7.1	7.4
14.5	6.9	7.0	6.8	6.9	6.9	6.8	6.9	6.9	6.9	6.9
16.0	6.3	6.2	5.9	6.0	5.9	6.1	5.9	6.0	6.0	5.9
18.2	5.4	5.3	5.3	5.3	5.4	5.3	5.2	5.4	5.4	5.4
20.2	4.9	4.9	4.9	4.9	4.9	4.9	4.9	4.9	4.9	4.9

Atomic Number of the Backing.—A change in the material with which a sample is backed produces a change in the counting rate of low surface density

TABLE III

PER CENT. SPECIFIC ACTIVITIES FOR BARIUM SULFATE SAMPLES MOUNTED ON VARIOUS METALS[a]

Al mount		Steel mount		Pb mount	
x (mg./cm.^{2})	a_m (cm.^{2}/mg.)	x (mg./cm.^{2})	a_m (cm.^{2}/mg.)	x (mg./cm.^{2})	a_m (cm.^{2}/mg.)
1.7	18.0	1.2	19.6	0.9	20.2
3.4	15.7	1.8	20.6	1.6	21.8
5.2	13.3	2.5	19.6	2.5	21.5
6.9	11.8	3.5	16.6	2.9	20.4
8.6	10.2	5.0	14.2	3.5	18.5
10.3	9.2	6.5	12.5	5.3	14.3
12.0	7.9	7.9	12.1	6.4	12.8
13.8	7.1	9.9	9.4	7.5	11.6
15.5	6.4	12.5	7.5	13.3	8.6
17.2	5.8	17.9	5.7	17.3	5.8

[a] Samples placed 2.5 cm. from counting window.

(3) L. E. Glendenin and A. K. Solomon, *Science*, **112**, 623 (1950).

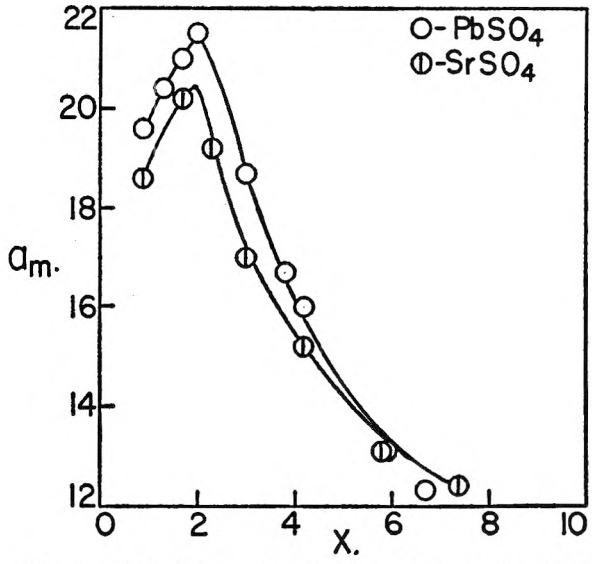

Fig. 1.—Plot of per cent. specific activity *versus* surface density showing the effect of the atomic number of the sample material.

samples. Table III presents specific activity data for barium sulfate samples backed by aluminum, steel and lead, and Fig. 2 is a plot of the values for the aluminum and lead backings. For large samples, those greater than 8 mg./cm.^{2}, the per cent. specific activity is independent of the backing. This is reasonable, since at about this surface density, one would not expect many particles back-scattered by the holder to reach the counting tube. Similar observations were made on other sulfate samples as well as on calcium oxalate and calcium oxide samples. The point of convergence of the two calcium curves was about 11 mg./cm.^{2}

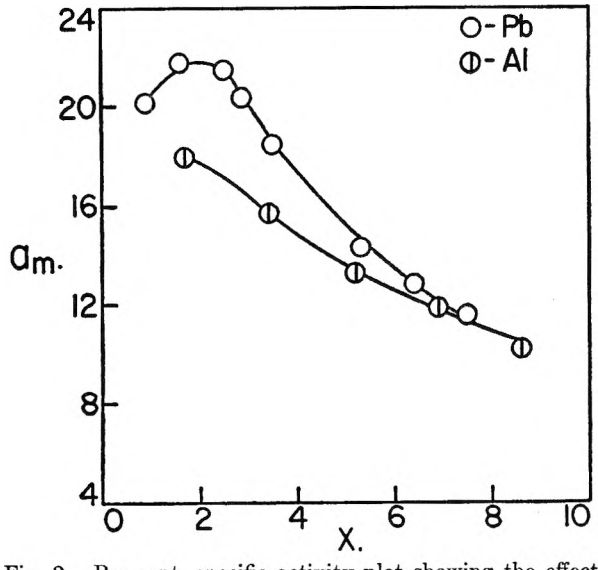

Fig. 2.—Per cent. specific activity plot showing the effect of the sample mount.

Distance.—Variation of the distance from the sample to the counting tube window seems to affect the specific activities to a marked degree, particularly in the low surface density region. In columns three, six and seven of Table II are given experimental data for lead sulfate samples counted at the tube window, and 2.5 cm. and 5.0 cm. from the window. Figure 3 presents these data graphically. It can be seen that as the distance increases the per cent. specific activities of the low surface density samples decrease. The curves converge at a surface density of about 4 mg./cm.^{2} Similar experiments performed with calcium oxalate showed the same trend, with the point of curve convergence being shifted to about 6 mg./cm.^{2} Other active samples, both sulfates and calcium salts, confirmed these results.

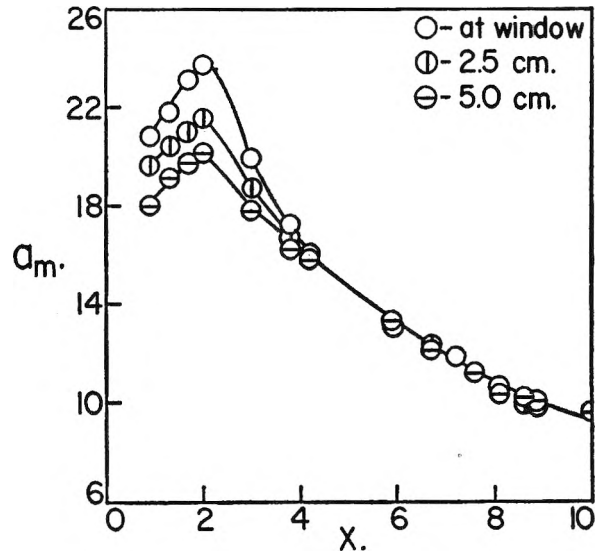

Fig. 3.—Per cent. specific activity plot showing the effect of sample-to-tube distance.

Tube Window Thickness.—Several of the sulfur-35-containing sulfates and calcium oxalate and sulfate labeled with calcium-45 were counted at the tube window with varying window thicknesses. The data obtained for lead sulfate, which is representative, is given in columns three, four and five of Table II. Also given in this table in the second column are specific activity values obtained from the samples by counting them in the internal coun-

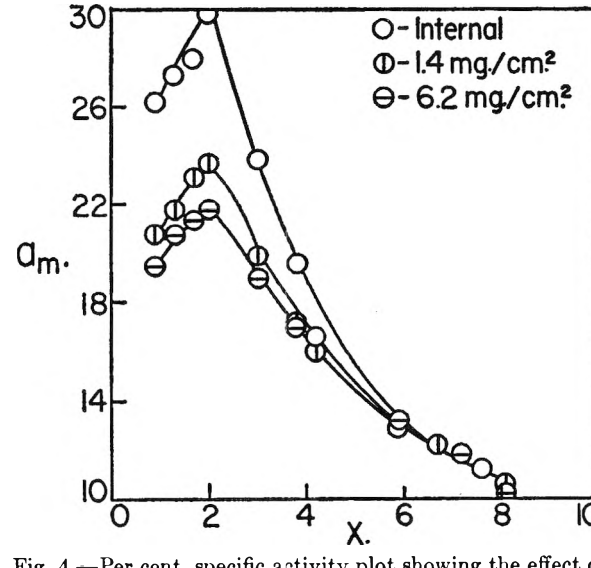

Fig. 4.—Per cent. specific activity plot showing the effect of tube window thickness.

ter. The values are plotted in Fig. 4. Again, a decrease in the specific activities of the low surface density samples as the window thickness increases may be noted. The internal counter curve and the two external counting curves converge at about 6 mg./cm.^{2} for sulfur-35 samples and at about 8 mg./cm.^{2} for calcium-45 samples.

Atomic Number of Siding Material.—In order to determine how the atomic number of the siding material affects the per cent. specific activity values, several series of samples were counted with shields of aluminum, copper, tin and lead placed as was indicated previously. The per cent. specific activities for lead sulfate samples are recorded in Table II, columns eight, nine, ten and eleven. From these, it is seen that a sample has practically the same per cent. specific activity with each of the metal shields showing the per cent. specific activity to be independent of the atomic number of the siding.

Maxima in Curves.—An interesting effect, which was first recorded several years ago,[4] may be noted in all curves. In the low surface density region, the per cent. specific activity does not decrease regularly as surface density increases but exhibits a maximum value at about 2 mg./cm.^{2} for sulfur-35 samples and at about 3 mg./cm.^{2} for calcium-45 samples. This maximum is probably partly due to the non-exponential character of beta-particle absorption at low surface densities.

Mixed Samples.—Table IV presents data for calcium sulfate samples with sulfur-35, with calcium-45, and with both nuclides. Figure 5 indicates that the curve representing the mixed samples falls between those for the samples with only one active nuclide. Other experiments point out that the relative position of the mixed sample curve between the others will be determined by the proportions of the two active nuclides present. In the case as presented in Fig. 5, approximately equal activities were used.

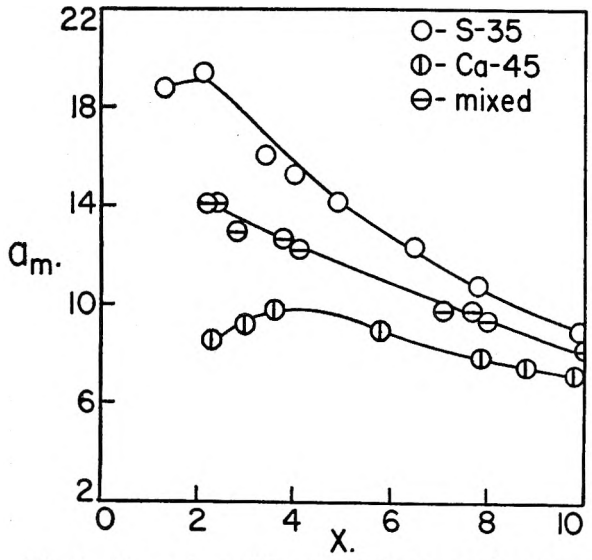

Fig. 5.—Per cent. specific activity plot comparing curves for calcium sulfate containing one active nuclide and containing two active nuclides.

(4) A. K. Solomon, R. G. Gould and C. B. Anfinsen, *Phys. Rev.*, **72**, 1097 (1947).

TABLE IV

PER CENT. SPECIFIC ACTIVITIES FOR CALCIUM SULFATE SAMPLES CONTAINING SULFUR-35, CALCIUM-45, AND BOTH NUCLIDES[a]

With S-35		With Ca-45		With both	
x (mg./cm.^{2})	a_m (cm.^{2}/mg.)	x (mg./cm.^{2})	a_m (cm.^{2}/mg.)	x (mg./cm.^{2})	a_m (cm.^{2}/mg.)
1.3	18.8	2.3	9.6	2.2	14.1
2.1	19.4	3.0	9.2	2.4	14.1
3.4	16.1	3.6	9.8	2.8	13.0
4.0	15.3	5.8	9.0	3.8	12.7
4.9	14.2	7.9	7.9	4.1	12.3
6.5	12.4	8.8	7.5	7.1	9.8
7.8	10.8	9.8	7.2	7.7	9.7
9.9	9.0	11.7	6.6	8.0	9.4
12.9	7.5	12.3	6.4	10.0	8.2
17.8	5.4	15.9	5.4	12.2	7.1
19.3	5.1	20.2	4.6	13.3	6.4
		25.5	3.9	15.4	5.9
				16.2	5.8
				18.0	5.3
				22.4	4.5

[a] Samples placed 2.5 cm. from counting tube window.

Conclusions

A quite widely used method for correcting for self-absorption is the extrapolation of the specific activity curve back to zero surface density. This value is taken as being equal to the true specific activity. This present work has shown that the average atomic number of the sample, the atomic number of the backing, the sample-to-tube distance, and the tube window thickness affect the per cent. specific activities, particularly those of the low surface density samples. These factors make extrapolation to zero surface density somewhat indefinite and subject to variation.

It is recommended that each investigator prepare his own self-absorption correction curves keeping as many variables constant as is possible. Great care should be exercised in comparing the self-absorption data of one investigator with those of another, since sizable variations may arise by slight modification in the above-mentioned factors.

Acknowledgment—This work was performed under the United States Atomic Energy Commission Research Contract No. AT-(40-1)-1058. The authors wish to express their gratitude for this financial assistance.